

**DIFFERENCES IN STRENGTH BETWEEN  
THE GRAIN AND CORIUM LAYERS OF BOVINE LEATHER.**

A thesis submitted for the degree of Doctor of Philosophy

University of Leicester



David O'Leary, BSc (Hons.)

January 1996.

UMI Number: U104981

All rights reserved

INFORMATION TO ALL USERS

The quality of this reproduction is dependent upon the quality of the copy submitted.

In the unlikely event that the author did not send a complete manuscript and there are missing pages, these will be noted. Also, if material had to be removed, a note will indicate the deletion.



UMI U104981

Published by ProQuest LLC 2015. Copyright in the Dissertation held by the Author.  
Microform Edition © ProQuest LLC.

All rights reserved. This work is protected against  
unauthorized copying under Title 17, United States Code.



ProQuest LLC  
789 East Eisenhower Parkway  
P.O. Box 1346  
Ann Arbor, MI 48106-1346



x753966017

### **Acknowledgements.**

I would like to thank my supervisors, Dr. G.E. Attenburrow at The British School of Leather, and Professor M. Blandamer at Leicester University who have offered advice and commented on various aspects of this research.

I would also like to thank Mr A. Landmann at BLC the Leather Technology Centre for assistance with band knife splitting and Mr J.R. O'Leary for useful discussions when developing the software to import Microsoft BitMap images. I am also grateful to Mrs C. Stening-Rees and Dr. J. Snape for their enthusiasm and encouragement.

### Abstract.

Chrome tanned bovine leather comprises two principal strata, the grain and the corium. The tensile strength and specific work of fracture of these two materials was investigated using uniaxial tensile tests and trouser tear tests respectively. Corium material was observed to be intrinsically stronger and tougher than grain material. The greater resistance of corium material to fracture is attributed to the processes of fibre debonding and pull out.

The viscoelastic nature of grain and corium material was investigated by examining differences in strength and toughness over a range of deformation rates. The ultimate tensile properties and the specific work of fracture of both grain and corium material are rate dependent. Energy dissipation during a strain cycle was measured over a range of strain rates and strain levels to determine the bulk hysteresis of grain and corium specimens. The influences of specimen orientation and fatliquor (oil) on strength and toughness are also considered.

The notch sensitivity of grain and corium materials has been scrutinised. Corium material is highly notch insensitive, whereas the fracture of grain material is notably sensitive to the presence of notches. The mechanism of fibre orientation and the phenomenon of fibre independence (or fibre autonomy) are responsible for the notch insensitive fracture behaviour of corium material.

Strain distribution was measured in grain and corium single edge notch specimens. The radius of curvature of the notch was assessed throughout deformation / fracture and local strains at two dimensional levels were measured. Local strains ahead of the advancing crack and the radius of curvature of the crack are considerably higher with corium specimens than with grain specimens.

**Disclaimer.**

This thesis describes original work by David O'Leary which was completed during the period of registration. No part of this work has been submitted for a higher degree at this or any other university.

## Contents.

	<b>Page</b>
<b>List of Tables</b>	viii
<b>List of Figures</b>	ix
<b>Chapter 1</b>	
Introduction.	1
<b>Chapter 2</b>	
Methodology.	7
2.1 Material Acquisition and Preparation.	7
2.1.1 Fatliquoring of Side Leather.	7
2.1.2 Propanone Drying of Side Leather.	8
2.1.3 Splitting of Leather.	9
2.2 Specimen Acquisition and Preparation.	11
2.2.1 Specimen Location.	11
2.2.2 Dimension of Samples.	11
2.2.3 Cutting of Samples.	13
2.2.4 Measurement of Thickness.	13
2.2.5 Marking for Visual Recording.	13
2.3 Mechanical Testing Procedures.	16
2.3.1 Tensile Test Procedure.	16
2.3.2 Strain Cycling Test Procedure.	16
2.3.3 Single Edge Notch Test Procedure.	17
2.3.4 Trouser Tear Test Procedure.	17
2.4 Testing Equipment and Data Acquisition.	18
2.4.1 Environmental System.	18
2.4.2 Force & Stroke Data Acquisition.	18
2.4.3 Visual Data Acquisition.	19
2.4.4 Microscopic Visual Recording of Specimens During Deformation.	22
2.4.5 Grain Surface Examination.	23
2.4.6 Fractography.	23

	<b>Page</b>
2.5 Data Processing and Techniques of Calculation.	25
2.5.1 Accounting for Inertia at the Test Speed of 166.66 mm s <sup>-1</sup> .	25
2.5.2 Tensile Tests.	28
2.5.3 Strain Cycling Tests.	29
2.5.4 Single Edge Notch Tests.	30
2.5.5 Distribution of Strain in the Single Edge Notch Test.	31
2.5.6 Sharpness of the Notch in the Single Edge Notch Test.	33
2.5.7 Trouser Tear Tests.	35
2.5.8 Extension Ratio in the Legs of a Trouser Tear specimen at Tear Propagation.	37
2.6 Chemical Analysis.	39
2.6.1 Determination of Oil Content.	39
2.6.2 Determination of Volatile Matter Content.	40
<b>Chapter 3</b>	
Tensile and Tear Behaviour.	41
3.1 Introduction.	41
3.2 Results.	44
3.2.1 Stress-strain behaviour at a strain rate of 3.33 % s <sup>-1</sup> .	44
3.2.2 Trouser tear tests at a deformation rate of 1.66 mm s <sup>-1</sup> .	51
3.2.3 Ultimate tensile properties and strain rate.	58
3.2.4 Tearing resistance and strain rate.	65
3.2.5 Measurement of the Hysteresis Ratio.	74
3.3 Discussion.	81
3.3.1 Uniaxial Tensile properties.	81
3.3.2 Tearing and the specific work of fracture.	85
3.3.2 (a) Analysis: The specific work of fracture calculation methods.	87
(i) Insignificant leg extension in a linear elastic material.	88
(ii) Significant leg extension in a linear elastic material.	91
(iii) Significant leg extension in an elastic plastic material.	95
3.3.2 (b) The nature of the load-stroke profile during a trouser tear test.	100
3.3.3 Why the corium is tougher than the grain	105
3.3.4 Orientation effects.	114
3.3.4 (a) The effect of specimen orientation on tensile behaviour.	114
3.3.4 (b) The effect of specimen orientation on the specific work of fracture.	117
3.3.5 Fatliquor effects.	119
3.3.6 Strain rate effects.	122

	<b>Page</b>
<b>Chapter 4</b>	
Notch Sensitivity.	126
4.1 Introduction.	126
4.2 Results.	133
4.2.1 Notch sensitivity of grain and corium materials.	133
4.2.2 Mathematical relationship between nominal stress and strain.	138
4.2.3 Analysis of notch sensitivity in terms of the theory of Purslow [1991].	141
4.2.3 (a) Fracture stress of grain material.	141
4.2.3 (b) Fracture strain of grain material.	143
4.2.3 (c) Fracture stress of corium material.	147
4.2.3 (d) Fracture strain of corium material.	150
4.2.4 Strain distribution in single edge notch specimens.	153
4.2.5 Strain distribution in the vicinity of a notch.	166
4.2.6 Radii of curvature in single notch specimens.	177
4.3 Discussion.	183
4.3.1 Estimation of the fracture energy ( $G_0$ ) from single edge notch tests.	183
4.3.2 Notch sensitivity of grain and corium materials.	185
4.3.3 The influence of fatliquor on notch sensitivity.	192
<b>Chapter 5</b>	
5.1 Conclusions.	196
5.2 Industrial consequences of the research.	198
5.3 Suggestions for further work.	200
<b>References</b>	202
<b>Appendix 1</b>	
Process history of wet blue leather.	208
<b>Appendix 2</b>	
The propanone drying process.	210
<b>Appendix 3</b>	
Computer Program listings.	218
A.3.1 Program Inertia.	219
A.3.2 Program Tensile_Test.	225
A.3.3 Program Strain_Cycling_Test.	229
A.3.4 Program Notch_Test.	234
A.3.5 Program Video.	238

	<b>Page</b>
A.3.6 (a) Program Produce_The_Strain_Matrix (entire specimen).	245
A.3.6 (b) Program Produce_The_Strain_Matrix (in vicinity of the notch).	248
A.3.7 Program Ellipse.	251
A.3.8 Program Trouser_Tear_Test.	253
A.3.9 Program Trouser_Tear_Test_Leg_Dimensions.	260
<b>Appendix 4</b>	
Table 3.3 and Table 3.4.	264
<b>Appendix 5</b>	
Derivation of the specific work of fracture from a trouser tear test [Atkins & Mai, 1988].	267
<b>Appendix 6</b>	
Derivation of the theory of notch sensitivity of non linear materials [Purslow, 1991].	274
A.6.1 Notch-Sensitive Case.	275
A.6.2 Notch-Insensitive Case.	279
<b>Appendix 7</b>	
Table A.7.1.	282

### List of Tables.

Table	Title	Page
Table 2.1	Example variables used for the inertia interpolation procedure.	26
Table 3.1	Trouser tear test results (@ 1.66 mm s <sup>-1</sup> & // to backbone).	57
Table 3.2	Trouser tear test results (@ 1.66 mm s <sup>-1</sup> & ⊥ to backbone).	57
Table 3.3	Trouser tear test results for grain material.	260
Table 3.4	Trouser tear test results for corium material.	261
Table 3.5	Trend line equations - toughness versus deformation rate.	72
Table 3.6	The percentage increase in toughness over the range of deformation rates 0.16 mm s <sup>-1</sup> to 166.66 mm s <sup>-1</sup> .	73
Table 3.7	Relationships between hysteresis, strain and strain rate.	76
Table 3.8	Mechanical properties of other flexible and rigid materials.	83
Table 3.9	The specific work of fracture of other flexible and rigid materials.	85
Table 3.10	The diameter of hierarchical fibrous units.	106
Table 3.11	Packing capability throughout the hierarchical fibrous structure.	108
Table 3.12	The surface areas involved in debonding.	109
Table 4.1	Average linear equation for the stress-strain behaviour of FADG, PDG, FADC and PDC.	138
Table 4.2	Predicted and observed values of M for FADG and PDG.	143
Table 4.3	Predicted and observed values of P for FADG and PDG.	144
Table 4.4	Predicted and observed values of s & K <sub>d</sub> ' for FADC and PDC.	151
Table 4.5	Fibre pull out in single edge notch specimens.	180
Table A.2.1	Propanone dehydration vessel dimensions.	211
Table A.2.2	Typical results over three propanone dehydration batch processes.	213
Table A.2.3	Mass balance - Batch 1.	215
Table A.2.4	Mass balance - Batch 2.	216
Table A.2.5	Mass balance - Batch 3.	216
Table A.2.6	Mass balance - Final calculations.	217
Table A.7.1	Estimation of G <sub>c</sub> for FADG, PDG, FADC and PDC material	283

### List of Figures.

<b>Figure</b>	<b>Title</b>	<b>Page</b>
Figure 1.1	Optical micrograph of leather cross section.	2
Figure 2.1	The process treatments for each side of leather.	10
Figure 2.2	Specimen dimensions.	12
Figure 2.3	Visual markings for strain distribution measurement.	15
Figure 2.4	The effect of reducing image detail.	21
Figure 2.5	The geometry of a crack being modelled by an ellipse.	34
Figure 2.6	Typical load-stroke data for a leather trouser tear test.	38
Figure 3.1	Stress-Strain Curves of FADG (12.5 % oil content), PDG, FADC (3.0 % oil content) and PDC specimens (@ 3.33 mm s <sup>-1</sup> & // to backbone).	47
Figure 3.2	Stress-strain curves of FADG (12.5 % oil content), PDG, FADC (3.0% oil content) and PDC specimens (@ 3.33 mm s <sup>-1</sup> & ⊥ to backbone).	50
Figure 3.3	Load-Stroke Curves of FADG (12.5 % oil content), PDG, FADC (3.0% oil content) and PDC Trouser Tear Tests (@ 1.66 mm s <sup>-1</sup> & // to backbone).	55
Figure 3.4	Load-Stroke Curves of FADG (12.5 % oil content), PDG, FADC (3.0% oil content) and PDC Trouser Tear Tests (@ 1.66 mm s <sup>-1</sup> & ⊥ to backbone).	56
Figure 3.5	The effect of strain rate on the breaking stress of FADG (12.5 % oil content), PDG, FADC (3.0% oil content) and PDC tensile specimens.	62
Figure 3.6	The effect of strain rate on the breaking strain of FADG (12.5 % oil content), PDG, FADC (3.0% oil content) and PDC tensile specimens.	63
Figure 3.7	The effect of strain rate on the energy required to rupture FADG (12.5 % oil content), PDG, FADC (3.0% oil content) and PDC tensile specimens.	64
Figure 3.8	The effect of strain rate on the toughness (method 1) of FADG (12.5 % oil content), PDG, FADC (3.0 % oil content) and PDC trouser tear specimens.	68
Figure 3.9	The effect of strain rate on the toughness (method 2) of FADG (12.5 % oil content), PDG, FADC (3.0 % oil content) and PDC trouser tear specimens.	69
Figure 3.10	The effect of strain rate on the toughness (method 3) of FADG (12.5 % oil content), PDG, FADC (3.0 % oil content) and PDC trouser tear specimens.	70

<b>Figure</b>	<b>Title</b>	<b>Page</b>
Figure 3.11	Hysteresis ratio for FADG (12.5 % oil content) at various strain rates and levels.	77
Figure 3.12	Hysteresis ratio for PDG at various strain rates and levels.	78
Figure 3.13	Hysteresis ratio for FADC (3.0 % oil content) at various strain rates and levels.	79
Figure 3.14	Hysteresis ratio for PDC at various strain rates and levels.	80
Figure 3.15	The load-stroke profiles of trouser tear tests.	90
Figure 3.16	Fibre pull out in trouser tear test specimens.	113
Figure 3.17	Fibre direction and the trouser tear test.	118
Figure 4.1	Notch sensitivity.	127
Figure 4.2	Strain energy distribution in notched specimens.	132
Figure 4.3	The dependence of nominal fracture stress on notch length for FADG (8.5 % oil content), PDG, FADC (1.2 % oil content) and PDC specimens.	136
Figure 4.4	The dependence of nominal fracture stress on notch length for FADG (12.5 % oil content), PDG, FADC (3.0 % oil content) and PDC specimens.	137
Figure 4.5	Logarithmic stress strain profiles of grain and corium material.	140
Figure 4.6	The natural log of breaking stress versus the natural log of notch length for FADG and PDG specimens.	142
Figure 4.7	The natural log of breaking strain versus the natural log of notch length for FADG and PDG specimens.	146
Figure 4.8	The natural log of breaking stress versus the natural log of the sample width minus the notch length for FADC and PDC specimens.	149
Figure 4.9	The natural log of breaking strain versus the natural log of the sample width minus the notch length for FADC and PDC specimens.	152
Figure 4.10	Video sequence showing the deformation and fracture of a FADG single notch specimen.	156
Figure 4.11	The strain distribution in a FADG single notch specimen during deformation and fracture.	157

<b>Figure</b>	<b>Title</b>	<b>Page</b>
Figure 4.12	Video sequence showing the deformation and fracture of a PDG single notch specimen.	159
Figure 4.13	The strain distribution in a PDG single notch specimen during deformation and fracture.	160
Figure 4.14	Video sequence showing the deformation and fracture of a FADC single notch specimen.	162
Figure 4.15	The strain distribution in a FADC single notch specimen during deformation and fracture.	163
Figure 4.16	Video sequence showing the deformation and fracture of a PDC single notch specimen.	164
Figure 4.17	The strain distribution in a PDC single notch specimen during deformation and fracture.	165
Figure 4.18	Video sequence showing the deformation and fracture of a FADG single notch specimen.	168
Figure 4.19	The strain distribution in the vicinity of the notch, for a FADG single notch specimen.	169
Figure 4.20	Video sequence showing the deformation and fracture of a PDG single notch specimen.	170
Figure 4.21	The strain distribution in the vicinity of the notch, for a PDG single notch specimen	171
Figure 4.22	Video sequence showing the deformation and fracture of a FADC single notch specimen.	173
Figure 4.23	The strain distribution in the vicinity of the notch, for a FADC single notch specimen.	174
Figure 4.24	Video sequence showing the deformation and fracture of a PDC single notch specimen.	175
Figure 4.25	The strain distribution in the vicinity of the notch, for a PDC single notch specimen.	176

<b>Figure</b>	<b>Title</b>	<b>Page</b>
Figure 4.26	The relationship between radius of curvature and nominal sample strain in single notch specimens.	179
Figure 4.27	Fibre pull out in single notch specimens of grain and corium material.	181
Figure 4.28	A scanning electron micrograph of the surface of a tear propagated from an edge notch in grain material.	182
Figure 4.29	Mechanisms pertaining to the notch insensitive tensile behaviour of corium material.	188
Figure 4.30	Precise determination of the crack tip.	195
Figure A.2.1	A plot of wt% water in the drying solution versus time, over three propanone dehydration batch processes.	214

## Chapter 1

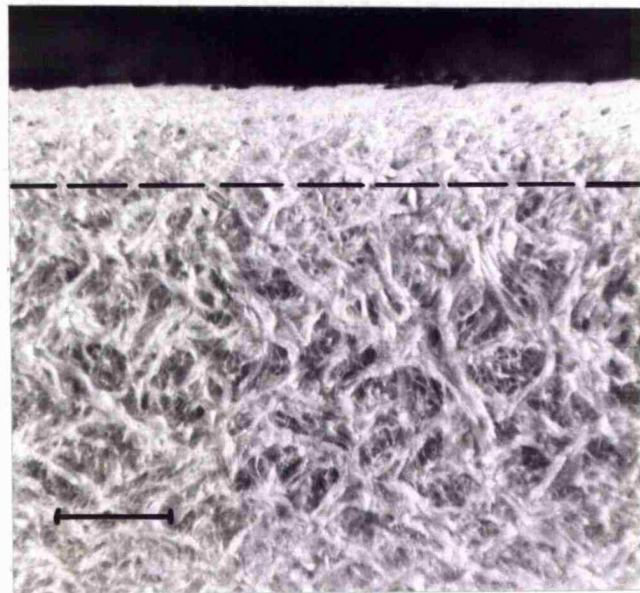
### Introduction.

Leather making involves chemical and mechanical manipulation of animal hides and skins to remove unwanted materials such as hair, epidermis and ground substance while leaving intact the feltwork of collagen fibres that confer structural integrity to the skin. During leather production, the collagen macromolecules are subject to a process of chemical crosslinking (tanning) that provides increased thermal stability and resistance to microbial attack, [Heidemann, 1979]. The unique properties of leather make it ideally suited for use in the manufacture of a variety of products, particularly footwear, [Bailey et al, 1985]. However, leather is also widely used as a quality material for upholstery, clothing, gloves, books, luggage, and footballs.

Microscopic examination of a cross section of bovine leather, even at low magnification, reveals two structurally distinct layers (Figure 1.1). The upper layer, originally closest to the surface of the animal, is called the grain layer and is composed of interwoven collagen fibres of diameter  $< 5 \mu\text{m}$ . The grain layer contains hair follicles. The thicker corium layer, immediately beneath the grain layer, is composed of a feltwork of thicker bundles of fibres (typically of diameter  $\approx 100 \mu\text{m}$ ), [Demsey, 1968]. The boundary between these two layers is not precise and there is a zone, known as the grain-corium boundary, where the collagen fibres progressively reduce in thickness from  $\sim 100 \mu\text{m}$  to  $< 5 \mu\text{m}$ .

Figure 1.1

Low magnification optical micrograph showing the two principal strata of bovine leather.



The grain layer (above the dashed line) and corium layer (below the dashed line).

The Length of the bar is 1 mm.

Whole leather is separated into discrete grain and corium materials by a process known as 'splitting'. Wilson & Kern [1926] and Maeser & Dion [1954] showed that tensile strength of whole leather is significantly higher than the tensile strength of grain material alone. In addition, the loads required to tear grain material are markedly lower than those required to tear full thickness leather in test geometries such as the stitch tear test [Kanagy et al, 1952] and the Bauman tear test (IUP/8) [Mitton, 1964]. However, this early work did not establish any underlying mechanisms responsible for the differences in strength and toughness between the different strata of leather.

Hole et al [1983], showed that during the lasting (stretch forming) operation of shoe making, small cracks can appear in the grain layer. These cracks are detrimental to the appearance, wear and life of shoes. Indeed, this problem was reported as a major shortcoming of leather.

The publications cited above suggest that grain material is generally 'weaker' than corium material. However, differences in strength and the specific work of fracture between grain and corium have yet to be fully characterised. Indeed, fundamental measurements enabling calculation of the specific work of fracture of leather have never been previously carried out. In addition, the reasons for these differences are not understood. By elucidating the principles involved in the relative strength and toughness of grain and corium material, procedures can be developed to increase strength and toughness of grain material.

The process histories of leathers used in the studies discussed above were also not specified. In particular, the presence of fatliquor<sup>1</sup> and its distribution were not reported. Fatliquor significantly alters leather strength [Mattei and Roddy, 1957] and therefore the influence of fatliquor on strength and toughness should, without exception, be taken into account.

The study described in this thesis was aimed at:

- (i) establishing differences in the intrinsic strength and the specific work of fracture between the grain and the corium layers of leather;
- (ii) examining the mechanisms of deformation and specifically fracture of grain and corium materials;
- (iii) relating observations of fracture behaviour to current theories of fracture.

Research on the fracture of materials has had two thrusts in the past few years:

- (i) Both the stress intensity approach and the energy balance approach to fracture mechanics have been successfully applied to many fracture studies. The popularity of fracture mechanics (the stress intensity approach or the energy balance approach) is at least partly due to the lack of need to understand microscopic details of the fracture process [Gerberick & Davidson, 1985].
- (ii) Conversely, the second thrust of fracture research has been to understand

---

<sup>1</sup> The process of fatliquoring is the application of oil-in-water emulsions (the fatliquor) to the leather.

the mechanisms of fracture, i.e. the events which occur as a crack lengthens. This approach requires knowledge of material response as the crack extends and that in turn requires localised measurements. Such measurements generally require complex microscopic techniques in order to determine the response of a material at a crack tip, [Gerberick & Davidson, 1985].

The discipline of fracture mechanics was initially focused exclusively on linear elastic brittle behaviour [Kinloch & Young, 1990]. However, with the successes achieved with linear elastic fracture mechanics, materials for which such an approximation would be invalid became of interest. Indeed, non-linear fracture mechanic techniques have been developed for some circumstances and perhaps the most comprehensive approach to the problem of bulk inelastic, non-linear behaviour is the proposal of a General Theory of Fracture Mechanics [Andrews, 1974, 1980; Andrews & Billington, 1976 and Andrews & Fukahori, 1977].

The experimental approach of this study uses aspects of both fracture mechanics and fracture mechanisms. The experimental work falls into two broad areas, united in the common aims of the study. In chapter 3, 'Tensile and Tear Behaviour', the tensile properties and the specific work of fracture of grain and corium materials are reported and discussed. In addition, the effects of specimen orientation, deformation rate and the presence of oil on tensile and tear properties are examined, as are the influences of strain rate and strain level on the energy dissipating properties of grain and corium materials.

In chapter 4, 'Notch Sensitivity', the differences in (i) the notch sensitivity and (ii) the strain distribution around a notch are evaluated and discussed in terms of recent theories of the fracture behaviour of non-linear materials [Purslow, 1991].

## **Chapter 2**

### **Methodology.**

Differences in strength and toughness between grain and corium layers of bovine leather, were studied using the following procedures and techniques.

#### **2.1 Material Acquisition and Preparation.**

Four commercial chrome-tanned cattle hides were used and their process history is given in Appendix 1. The partially processed leathers (termed wet blue), supplied by a United Kingdom tannery, were separated into two sides by cutting the leather from shoulder to butt along the line of the backbone. Each leather was processed individually.

Initially both sides were subjected to the same washing and neutralization process in an aluminium drum, volume 0.52 m<sup>3</sup> operating at 15 revolutions per minute. At this point one leather side was processed conventionally by fatliquoring and drying. However, the other side was dried (with no addition of oils) by exchanging water with propanone followed by evaporation of the propanone. The treatments for each side of leather are summarised in Figure 2.1.

##### **2.1.1 Fatliquoring of Side Leather.**

Simple air drying of unfatliquored leather (i.e. directly after tannage) leads to an

undesirable degree of interfibre adhesion and produces a material similar in stiffness to plywood. Softness and flexibility are traditionally achieved in the fatliquoring process by the introduction of oils into the leather, [Heidemann, 1993]. An offer of 6% sulphited synthetic ester fatliquor (Remsynol ESI<sup>2</sup>) was used for this process. This type of fatliquor has good emulsifying properties (enabling uniform distribution over the area of the side), is acid stable and provides a deep lubrication through the cross section [Sharphouse, 1983]. Nevertheless, because each side of leather was fatliquored individually, the level and distribution of oil in each batch was not identical and the exact oil content was determined by the method outlined in section 2.6.1.

#### 2.1.2 Propanone Drying of Side Leather.

During the fatliquoring process, uneven deposition of oil through the leather thickness is common. Therefore, potential uncertainty arises in assigning the cause of differences in strength and toughness between discrete leather strata. To avoid this situation and the predicament of excess fibre adhesion without the addition of oils, a propanone dehydration drying technique was devised.

The water content of the wet blue leather was 58.66% on a weight basis. When immersed in propanone, penetration of propanone into the leather occurred. The propanone continued to displace the water in the leather until equilibrium was reached. The drying solution (propanone and water) was replaced with 98%

---

<sup>2</sup>A product of Hodgson Chemicals, Hayes road, Cadishead, Manchester, M44 5BX.

propanone and the batch process repeated until sufficient water had been removed from the leather.

After three batch processes, propanone remaining in the leather was carefully evaporated using a blow heater thereby ensuring the leather did not freeze. Using three batch drying processes, the water content of wet blue leather was reduced to 6% on a wet weight basis. The process specifications and pertinent calculations are summarised in Appendix 2.

### **2.1.3 Splitting of Leather.**

To assess differences in strength and toughness between the grain and the corium, the two layers were separated using a band knife splitting machine<sup>3</sup>. The dried leather was split through the grain-corium boundary, at a depth of approximately 1 mm from the surface of the grain.

---

<sup>3</sup> Located at BLC the Leather Technology Centre, Moulton Park, Northampton.

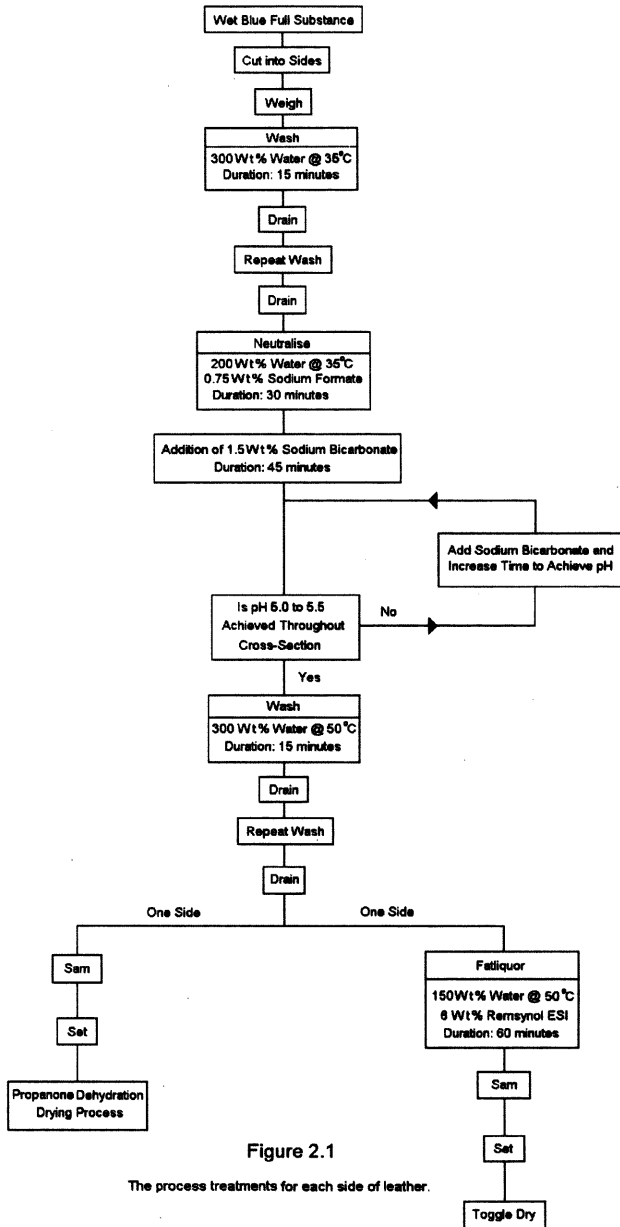


Figure 2.1

The process treatments for each side of leather.

## **2.2 Specimen Acquisition and Preparation.**

### **2.2.1 Specimen Location.**

Two philosophies were adopted in deciding the location of test specimens. Initially, test specimens used for comparative purposes should be nominally identical. Further, areas of rapidly changing composition and areas with a high degree of anisotropy (such as the top of a shoulder, the extremes of a belly and backbone) were avoided.

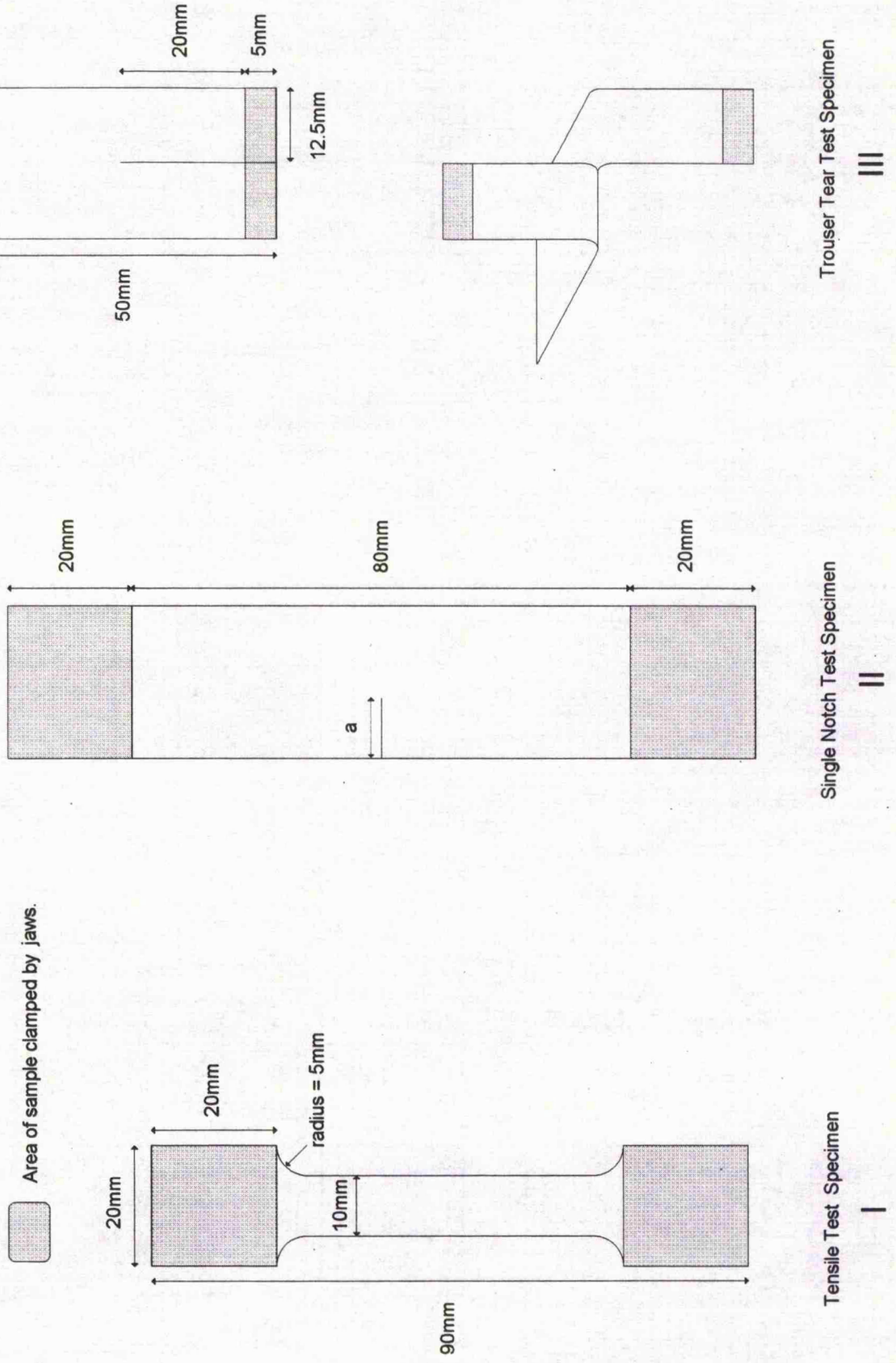
Test specimens used for comparative purposes were cut in the same direction (either parallel or perpendicular to the backbone). When cutting specimens on the same side of a hide, the specimens were cut next to each other over the smallest possible area of material. When cutting specimens on opposite sides of the same hide (i.e. when comparing propanone dried leather with fatliquored air dried leather) sample positions were mirrored across the backbone.

On each side of leather, the sampling area was constrained to a central rectangular region, 1.62 m in a direction parallel to the backbone by 0.82 m perpendicular to the backbone.

### **2.2.2 Dimension of Samples.**

The dimensions of samples for tensile tests, single notch tests and trouser tear tests are shown respectively as (I) (II) & (III) in Figure 2.2.

Figure 2.2. - Specimen Dimensions



### **2.2.3 Cutting of Samples.**

A cutting die of appropriate profile and dimension for each test type was placed normal to the material. The flat surface of the die press moved a fixed distance which ensured that the die was forced through the material and the samples were cut cleanly with straight edges.

### **2.2.4 Measurement of Thickness.**

The thickness of each leather specimen was measured after environmental conditioning, but before initiation of the testing protocol. A dial micrometer gauge measured the thickness following the IUP/4 procedure [Official Methods of Analysis, 1965]. The same contact force, equivalent to  $500 \text{ g m}^{-2}$  was applied to all specimens. The gauge dial was graduated in steps of 0.01 mm and was accurate to this level throughout the range.

### **2.2.5 Marking for Visual Recording.**

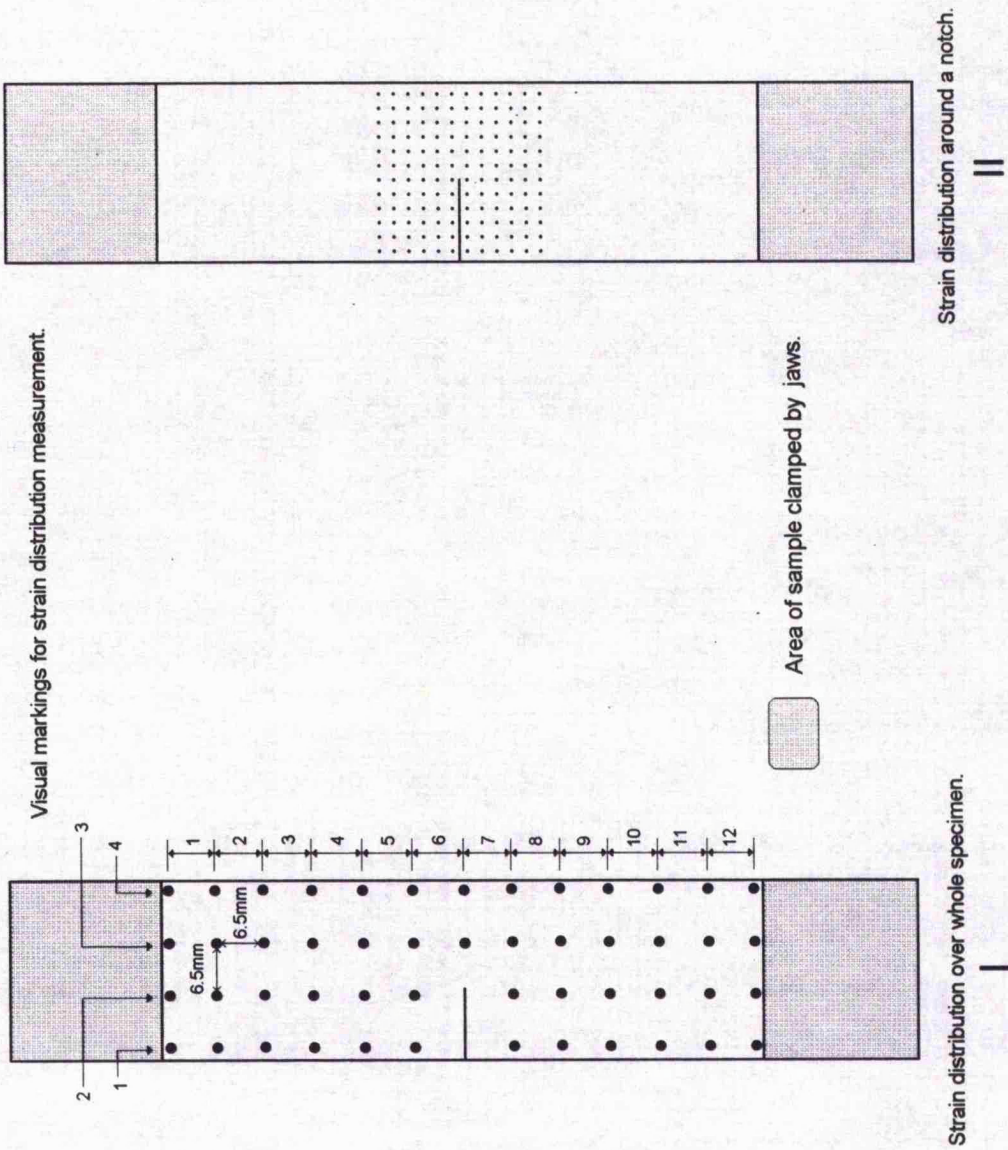
To facilitate measurement of strain distributions, an array of dots was printed on to a single edge notch specimen and straining was visually recorded using an SVHS camera. Two regions of strain distribution were examined, namely strain distribution over a whole sample and strain distribution around a notch.

The former array of dots consisted of four columns by thirteen rows, where each

dot was separated from another by 6.5 mm. In each column, twelve readings of local strain could be calculated between the centre of each dot in its vertical line (Figure 2.3 (I)). For the strain distribution around a notch, the array of dots comprised twelve columns by twelve rows, where the dots were 2 mm apart, (Figure 2.3(II)). From each column of twelve dots, eleven readings of local strain could be calculated between the centre of each dot in its vertical line. Strains transverse to the principal strain axis were not measured.

Markings were also placed on trouser tear test specimens for measurement of extension ratios in the legs. On the front of each sample, (i.e. the grain side) a line was printed across the top of the legs at 90 degrees to the cut. The other line was printed in the same place on the reverse side of the sample; i.e. the flesh side.

Figure 2.3



## **2.3 Mechanical Testing Procedures.**

Deformation and failure resistance in the grain and corium layers of dry leather were measured using uniaxial mechanical testing procedures. In each test, a sample was clamped in the jaws of the tensometer. The separation speed of the jaws, the final distance of jaw separation and the frequency of data collection were entered into the control device.

### **2.3.1 Tensile Test Procedure.**

Dumbbell shaped specimens (Figure 2.2(I)) were strained to rupture at four different rates of  $0.16 \text{ mm s}^{-1}$ ,  $1.66 \text{ mm s}^{-1}$ ,  $16.66 \text{ mm s}^{-1}$  and  $166.66 \text{ mm s}^{-1}$ . Under identical conditions, four tests were carried out in order to take account of any variability of the mechanical properties.

### **2.3.2 Strain Cycling Test Procedure.**

Dumbbell shaped specimens (Figure 2.2(I)) were strained at four different rates (i.e.  $0.16 \text{ mm s}^{-1}$ ,  $1.66 \text{ mm s}^{-1}$ ,  $16.66 \text{ mm s}^{-1}$  and  $166.66 \text{ mm s}^{-1}$ ) to levels of 20% , 40%, 60% and 80% of elongation at break. When the required level of strain was achieved, the strain was immediately reversed at the same speed of application until the upper jaw returned to its original position.

### **2.3.3 Single Edge Notch Test Procedure.**

A notch was cut half way down, and perpendicular to, the left edge of the single edge notch specimens, (Figure 2.2(II)). Notches were cut using a surgical scalpel blade and lengths varied between 0.5 mm and 12.5 mm (half way across the specimen). Samples were strained at a fixed rate,  $1.66 \text{ mm s}^{-1}$ , until complete fracture occurred.

### **2.3.4 Trouser Tear Test Procedure.**

The two legs of a sample were constructed by cutting a length 25 mm from the middle to the base using a surgical scalpel blade. The right leg of the specimen was clamped in the bottom jaw while left leg was bent through  $180^\circ$  and clamped in the top jaw, (Figure 2.2(III)). The specimens were strained at rates of  $0.16 \text{ mm s}^{-1}$ ,  $1.66 \text{ mm s}^{-1}$ ,  $16.66 \text{ mm s}^{-1}$  and  $166.66 \text{ mm s}^{-1}$  over a distance of 45 mm. The strain was then immediately reversed at the same speed of application until the upper jaw returned to its original position. Under identical testing conditions, four tests were carried out.

## **2.4 Testing Equipment and Data Acquisition.**

### **2.4.1 Environmental System.**

For 48 hours immediately preceding testing and during testing, each leather was kept in a room conditioned at  $20 \pm 2^{\circ}\text{C}$  and  $65 \pm 2\%$  Relative Humidity.

### **2.4.2 Force & Stroke Data Acquisition.**

The force and stroke (displacement) data from three classes of test were obtained using either an Instron 1122 universal testing machine or a Dartec M1000/RK hydraulically driven testing machine. Using the Instron 1122, an amplified voltage from a calibrated load cell was recorded, at a frequency of 10 Hz, using a Personal Computer (PC) with a 20 MHz, 80386 processor via a 16 bit A-D converter. The stroke was subsequently calculated as a function of both time and speed of jaw separation. The Dartec M1000/RK operates in a slightly different manner because the load is calculated in real time. In addition, the stroke is also recorded independently and not as a function of time and speed.

On completion of a test using the Instron 1122 tensometer, two columns of data were recorded as an ASCII text file. The first column recorded the time. The second column recorded voltage which was proportional to load. The results from tests using Dartec M1000/RK are also arranged in a two-column ASCII text file. The first column recorded the stroke and the second column recorded the load.

### 2.4.3 Visual Data Acquisition.

For a visual record of specimens during deformation, an SVHS video camera was placed at 90 degrees to the surface of the leather specimen. The camera was placed on a tripod at a horizontal distance of approximately 0.5 m from the specimen. A high intensity studio light ensured sufficient light without shadow. The zoom facility of the camera was used to magnify the image, making sure the important markings on each specimen did not move out of the fixed frame while a specimen was being strained.

For the purpose of visual data acquisition, the notch length of a single notch specimen was fixed at 9 mm. At this notch length, twisting occurred in the leather at the widest section of the opening, thereby obscuring the dot pattern. Therefore, sheets of nonreflective glass were placed 0.5 mm from the back and front of the specimen, thereby 'sandwiching' the sample.

Once a visual recording was complete, quantitative information was obtained by acquiring digitised pictures as a function of time over the duration of the test. A suite of Sony SVHS video editing equipment allowed still images to be produced from a video sequence at time intervals as small as 1/25 th of a second (the limits of conventional video). The still video image was transferred to a video capture card, using a 16 bit half-size ISA card resident within a PC with a 33 MHz, 80486 processor. Using video capture software (VideoSnap by VideoLogic<sup>4</sup>) a digital

---

<sup>4</sup> VideoLogic Limited, Home Park Estate, Kings Langley, Hertfordshire, WD4 8LZ, UK.

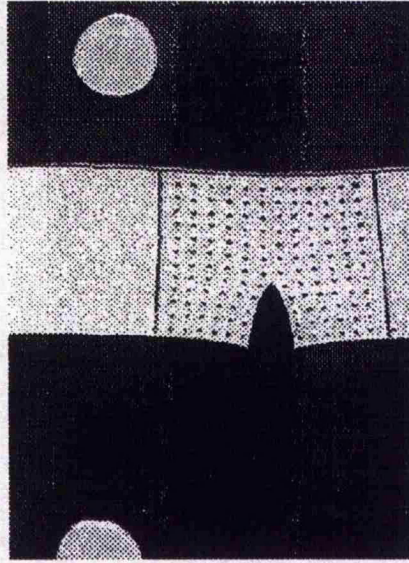
image was obtained using 640 x 480 pixels in a 256 grey shade palette.

Digital images of single notch tests, with both large and small matrices of dots, were acquired at intervals of one second until specimen failure. Each 640 x 480 pixel image was converted from a 256 grey shade palette to a black and white image. The picture detail was reduced so that the image background was entirely white. The area devoid of leather, due to crack opening, was coloured red. A rectangular line of black pixels was drawn around the matrix of dots and the area of crack opening. The only other black pixels present were those constituting the dots.

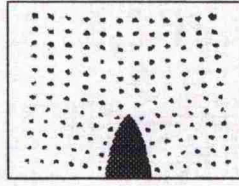
The effect of reducing the image detail in the case of the small area matrix of dots is shown in Figure 2.4. Figure 2.4(I) is the original 256 grey shade palette image. Figure 2.4(II) is the black, white and red image (*note the red appears as grey in this figure.*) These images are stored on disk as 640 x 480 pixel, 16 colour bit map files, ready for data processing.

Four images in each specified trouser tear tests were obtained. Images were obtained before the test commenced, at the point of tear propagation, at maximum stroke conditions and when it became apparent, after reversal of the strain direction, that no load was exerted in the legs of a sample. The image detail was not reduced but instead stored directly on disk as a 640 x 480 pixel, 256 grey shade palette bit map file, ready for data processing.

Figure 2.4  
The effect of reducing image detail.



The original 256 grey shade palette image.



Reduction of image detail.

#### **2.4.4 Microscopic Visual Recording of Specimens During Deformation.**

Detailed visual characteristics of crack initiation and propagation in both the grain and corium, were obtained using a geological microscope. Single notch specimens were strained horizontally using a Hounsfield (W-Type) tensometer. The strain was applied manually using a turning handle which directly separated the jaws of the tensometer. The microscope was positioned on a moving platform directly above a leather specimen with the tip of the notch in centre frame. While a specimen was being strained, the crack initiated and then propagated. The microscope was gently moved so that the tip of the notch remained in frame. Sufficient light for acquisition of visual data was provided by two fibre optically directed halogen light sources.

Throughout the straining of a sample, microscope images were visually recorded using a VHS microscope camera and separate recorder. Magnification of the microscope was set between x80 and x100. Precise magnification levels and dimensions were evaluated, before straining commenced, by recording the calibrated 0.2 mm subsections of a graticule placed on the leather surface. Similarly, the straining of unnotched grain specimens permitted a visual recording of hair follicle distortion in the grain layer. Once the visual recording was complete, digitized pictures were obtained by the technique outlined in section 2.4.3.

#### **2.4.5 Grain Surface Examination.**

A geological microscope directly connected to a 35 mm single lens reflex camera facilitated acquisition of photographic images of the grain surface. The magnification of the microscope was set to approximately  $\times 50$ . Precise magnification levels and dimensions were evaluated by photographing the calibrated 0.2 mm subsections of a graticule, placed on the leather surface.

Subsequent image analysis permitted calculation of hair follicle surface areas and hair follicle density over the grain surface. A digitised version of the image was obtained from a photographic, black and white print of 6 x 4 inches. Each photograph was scanned as a 640 x 480 pixel, 256 grey shade palette image, using a Hewlett Packard ScanJet IIc flat bed scanner and appropriate software. The image was subsequently reduced in detail from 256 grey shade palette to a purely black and white pixel image. These images were stored on disk, as 16 colour bit map files, ready for data processing.

#### **2.4.6 Fractography.**

Fractography is the visual investigation and characterisation of fracture surfaces of a material. Fractographical studies, using an Hitachi S2500 Scanning Electron Microscope (SEM) operated at 10 kV, were carried out on fractured samples of fatliquored air dried grain, propanone dehydrated grain, fatliquored air dried corium and propanone dehydrated corium. The results were in the form of micrographs.

Micrographs of fracture surfaces provide a basis for understanding the fracture process in each layer of leather by visual assessment of properties such as fibre pull out and fracture surface roughness.

## **2.5 Data Processing and Techniques of Calculation.**

The test data were processed using computer programs written in Turbo Pascal 7 on a PC with a 33 MHz, 80486 processor.

### **2.5.1 Accounting for Inertia at the Test Speed of 166.66 mm s<sup>-1</sup>.**

Using a test speed of 166.66 mm s<sup>-1</sup> or greater (on the Dartec testing machine) for tensile tests, strain cycling tests and trouser tear tests, the recorded loads at the two extremes of strain, altered rapidly and were inconsistent with test data at lower speeds. This behaviour was accounted for in terms of the load cell measuring the force necessary to overcome its own inertia. The latter was considerable when the velocity of the moving jaw was 166.66 mm s<sup>-1</sup>. This phenomenon was called an 'inertia glitch.'

In order to remove the inertia glitch from stroke-force data, another test was run with the same levels of maximum jaw separation, speed of jaw separation and rate of data collection, but no sample was clamped in the jaws. At identical recorded levels of jaw separation, the force reading of the test run with no specimen (termed No-Specimen-Test) was subtracted from the force reading of the real test (termed Sample-Test). An estimate of the force required to deform the material was obtained at each recorded level of extension. In other words, the 'inertia glitch' was removed. The program called 'Inertia Glitch' performed this process, (Appendix 3.1).

The program initially reads the stroke-force data for both the No-Specimen-Test and the Sample-Test and places each data set in a separate two dimensional array. The stroke and force data of each test were recorded before jaw separation commenced to ensure complete recording of all data. Hence, the exact starting point of each test was determined by finding six consecutive increases in stroke readings. The stroke and force data prior to this starting point were deleted. Each set of data was normalized to ensure the test began at zero stroke and load by subtracting the starting stroke and load from every reading of stroke and load in the data set.

The maximum stroke in each test was found and the subtraction procedure of the two load values carried out in two sections. The two sections were defined as zero to maximum stroke and maximum to zero stroke. Comparison of the stroke data for these two tests showed the readings of stroke at the same point in time were not identical. Therefore simple subtraction of the No-Specimen-Test load values from the Sample-Test load values was not feasible. Clearly, interpolation of the No-Specimen-Test data was required. The interpolation procedure is explained in steps 1 to 4 using the variables listed in Table 2.1.

Table 2.1

Row Number, n	Sample-Test, mm	Sample-Test, kN	No-Specimen-Test, mm	No-Specimen-Test, kN
1	$mm_{ST1}$	$kN_{ST1}$	$mm_{NST1}$	$kN_{NST1}$
2	$mm_{ST2}$	$kN_{ST2}$	$mm_{NST2}$	$kN_{NST2}$
3	$mm_{ST3}$	$kN_{ST3}$	$mm_{NST3}$	$kN_{NST3}$

Step 1:

In each row of data, the following condition was satisfied,

No-Specimen-Test mm [row n] < Sample-Test mm [row n] < No-Specimen-Test mm [row n + 1]

If the above condition was not satisfied, the row number (n) of the No-Specimen-Test was increased until the condition was satisfied.

Step 2:

Using the No-Specimen-Test stroke and load data from rows (n) and (n + 1) , the equation of a straight line between the two points was obtained as

$$KN = (M \cdot mm) + C \quad [2.1]$$

where  $M = (KN_{NST2} - KN_{NST1}) / (mm_{NST2} - mm_{NST1})$  [2.2]

and  $C = KN_{NST1} - (M \cdot mm_{NST1})$  [2.3]

Step 3:

The constants calculated using equations [2.2] and [2.3] as well as the 'mm' value (row n) from the Sample-Test yielded equation [2.1]. This estimate was subtracted from the kN value (row n) of the Sample-Test to produce data where the inertia glitch was removed in the current row of stroke and force data.

Step 4:

Steps (1) to (3) were repeated, in both sections of data, for each row of stroke and force data.

The stroke and force data of the Sample-Test were stored as an ASCII text file with all inertia glitches removed. At this stage, the data were ready for processing.

### 2.5.2 Tensile Tests.

The raw data from each tensile test were processed to obtain force, extension, stress and strain at the point of specimen rupture and to calculate the energy required to rupture the specimen. The program called 'Tensile Test' performed this process (Appendix 3.2). Initially, the stroke and force data of a requested test file were read and placed in a two-dimensional array. The starting point of the test was determined by finding six consecutive increases in stroke values. The point of rupture was defined as the maximum force value in the sequence of data.

The data were normalized, to ensure the test begins at zero load and stroke, by subtracting the starting stroke and load from every stroke and load in the data set. The energy required to rupture the specimen was calculated by applying Simpson's rule to the stroke and force data. The thickness of the sample was input from the keyboard enabling the calculation of stress. Hence,

$$\text{Stress / MPa} = \frac{\text{force}}{(\text{original thickness}) \times (\text{original width of sample})} \quad [2.4]$$

and strain was calculated as,

$$\text{Strain / \%} = \frac{\text{increase in length}}{\text{original length}} \times 100\% \quad [2.5]$$

Two separate result files were produced and stored on disk. (i) The normalized stroke-force and calculated strain-stress profiles were stored as a four column

ASCII text file. (ii) Test identification and key results of each test were added, as a single row of data, to a tensile test results file. This row of data comprised: test code, sample thickness, force at rupture, extension at rupture, stress at rupture, strain at rupture and the energy required to rupture the specimen.

### 2.5.3 Strain Cycling Tests.

The raw data from each strain cycling test were processed to obtain (i) force, extension, stress and strain at maximum extension of a specimen, (ii) calculate the energy used in straining the material from zero to maximum extension and (iii) the energy returned on unloading a specimen. A hysteresis ratio and immediate set were also calculated. The program called 'Strain Cycling Test' performed these tasks (Appendix 3.3).

Test data were read, test starting points determined, data normalized and stress and strain calculated using the same procedures as used for section 2.5.2. The energy used in straining specimens from zero to maximum extension was calculated by applying Simpson's rule to the stroke and force data over that range of stroke. The energy returned on unloading the specimen was calculated by applying Simpson's rule to the stroke and force data over the range from maximum extension to the level of extension where the load fell to zero. The level of extension at this point was calculated in terms of strain and denoted as immediate set. In addition, the hysteresis ratio of the specimen was calculated using equation [2.6],

$$\beta = (W_i - W_r) / W_i \quad [2.6]$$

$\beta$  is the hysteresis ratio,  $W_i$  is the input energy and  $W_r$  is the recoverable energy.

Two separate files were produced and stored on disk media. The normalized stroke-force and calculated strain-stress cycle profiles were stored as a four column ASCII text file. In addition, test identification and key results of each test were added, as a single row of data, to a strain cycle test results file. This row of data comprised: test code, sample thickness, force at maximum extension, maximum extension, stress at maximum strain, maximum strain, energy used in acquiring maximum extension, energy returned on unloading, hysteresis ratio and the immediate set in the specimen.

#### 2.5.4 Single Edge Notch Tests.

Raw data from each single notch test were used to obtain (i) load, extension, stress and strain at the point of specimen rupture, (ii) the energy required to rupture a specimen and (iii) the energy density of a sample at rupture. The program entitled 'Notch Test' performed these tasks (Appendix 3.4). With few exceptions, this program achieved its objective in the same way as 'Tensile Test' (Section 2.5.2). The energy density at rupture was calculated using equation [2.7].

$$W_R = W_i / (t \times l \times w) \quad [2.7]$$

$W_R$  is the energy density at the point of rupture,  $W_i$  is the input energy density,  $t$  is the average thickness,  $l$  the gauge length of the sample and  $w$  the width of the sample. The dimensions,  $l$  and  $w$  are constant, therefore,

$$W_R = W_i / (0.002 t) \quad \text{J m}^{-3} \quad [2.8]$$

Two separate result files were produced and stored on disk. (i) The normalized stroke-force and calculated strain-stress profiles were output as a four column ASCII text file. (ii) Test identification and key results of each test were added, as a single row of data, to a notch test results file. This row of data comprised: test code, sample thickness, notch length, sample volume, energy required to rupture the specimen, energy density at rupture, force at rupture, extension at rupture, stress at rupture and strain at rupture.

#### **2.5.5 Distribution of Strain in the Single Edge Notch Test.**

The distribution of strain in single edge notch specimens, described in Section 2.4.3, was calculated in two stages.

In the first stage, the coordinates of the centre of each dot were obtained in each digitised picture of both the large and small area matrix of dots in the single notch test series. For each picture, these coordinates were stored in an ASCII text file. The program 'Video' performed this task (Appendix 3.5). The program read a specified bit map image and placed the image on the visual display unit (VDU). A

small, hollow movable image of a box was placed on the screen. This box was moved, using the cursor keys, and was initially located to encompass the top dot of the first column. The 'return' key was pressed and the coordinates of the dot centre recorded. The hollow box was relocated down the column to successive dots and the procedure repeated so that the coordinates of each dot centre in that column were recorded. The hollow box was relocated to the top of the next column and the entire process repeated in successive columns. The coordinates of every dot was stored as a two column ASCII file, in the same order that the coordinate data were collected, i.e. Column(1 to n) [Row(1 to n)].

In the second stage of the data processing, the two column ASCII text file coordinate data were used to calculate local strains between successive, vertically positioned dots. Clearly some movement of the dots transverse to the principal strain axis was inevitable and in such circumstances, local strains (between dot centres) are not measured along the principal strain axis. It was felt that the magnitude and location of local strain variations was the most important consideration. To accurately assess the strain field along the principal strain axis, although possible [Andrews & Fukahori, 1977], was not carried out in this study.

The program 'Produce the Strain Matrix' (Appendix 3.6) uses the x and y coordinates of vertically positioned dots (in the same column of dots) to calculate the distance between dot centres and thus the local strain values.

#### **2.5.6 Sharpness of the Notch in the Single Edge Notch Test.**

The crack opening behaviour of each material was quantified in a series of visually recorded single notch tests. The red coloured areas devoid of leather, due to the crack opening, were read as bitmap images and placed on the screen. The profile of this shape was modelled using the equations of an ellipse, altering the size of the major and minor axes accordingly. The program 'Ellipse' performed this task (Appendix 3.7) and Figure 2.5 illustrates the geometry of such a crack being modelled by an ellipse.

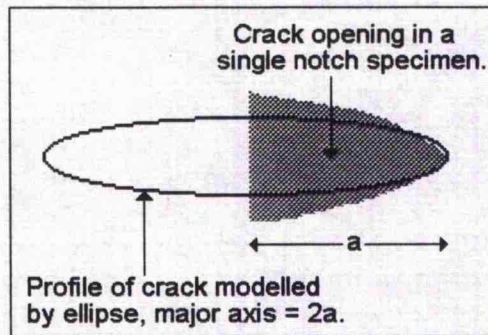


Figure 2.5  
The modelling of crack geometry (performed by program 'Ellipse'.)

### 2.5.7 Trouser Tear Tests.

Raw data from each trouser tear test were processed to obtain, by three separate methods of calculation, the specific work of fracture or toughness. The program 'Trouser Tear Test' (Appendix 3.8) performed this task.

Once the trouser tear test data have been normalised, the stroke-load data have the form shown in Figure 2.6. Point (A) was the point where tearing commences and was found by assessing successive points of maxima in the data from start of the test. Once a maximum had been found, the level of stroke required, after the maximum, to reattain the load value was calculated and called Dist\_A\_to\_C. This process was repeated with successive maxima until the difference in Dist\_A\_to\_C at the current and previous maximum was larger than the mean values of Dist\_A\_to\_C at the current and previous maximum. If the current value of Dist\_A\_to\_C > 0.5 mm this maximum was denoted as the point where tearing commences.

The point of maximum stroke is the point where tearing ceases and is denoted point (B) in Figure 2.6. Point (C) in Figure 2.6 is the point where zero load is achieved during the reversal of the stroke. The plateau tearing force was calculated as the mean reading of load during propagation of the tear and is denoted by the point (P) in Figure 2.6.

The three methods used to calculate the energy required to propagate a crack

through unit area of the material are as follows:

**Method 1.**

Significant leg extension in an elastic-plastic material.

This method enables calculation of the specific work of fracture while also attempting to account for energy dissipated in the legs of an elastic plastic trouser tear specimen. The method is comprehensively discussed in section 3.3.2 (a). Employing this method, the specific work of fracture,  $R_1$  was calculated from Figure 2.6.

$$R_1 = \text{Elastic energy used} / \text{Area cleaved} \quad [2.9]$$

$$R_1 = (\text{Area OABC} - (\text{Area OAD} - \text{Area BCE})) / t \cdot L. \quad [2.10]$$

Where  $t$  is the thickness of a sample and  $L$  is the length of tear in a specimen, measured using vernier callipers.

**Method 2.**

Significant leg extension in an elastic material [Rivlin & Thomas, 1953].

In this method, the energy required to propagate a crack through unit area of material, is called  $R_2$  and calculated as,

$$R_2 = (W_0 A_0 - 2 \lambda F_0) / t \quad [2.11]$$

$W_0$  is the strain energy density in the legs of the test piece,  $A_0$  is the unstressed cross section area of the legs,  $\lambda$  is the extension ratio in the legs at the point of propagation,  $F_0$  is the plateau tearing force and  $t$  is the thickness of the specimen. In Figure 2.6, the point of tear propagation is denoted by point A and the plateau tearing force by point P.

### Method 3.

Insignificant leg extension in an elastic material, [Greensmith & Thomas, 1955].

When very little extension occurs in the legs of the trouser tear specimen, the extension ratio in the legs,  $\lambda \approx 1$  and the energy density in the legs,  $W_0 \rightarrow 0$ . Under these conditions, Equation [2.10] becomes,

$$R_3 = 2 F_0 / t \quad [2.12]$$

### 2.5.8 Extension Ratio in the Legs of a Trouser Tear specimen at Tear Propagation.

To obtain the extension ratio in the legs of the trouser tear specimens ( $\lambda$ ), the bitmap images of the trouser tear test series were analysed. Image processing software (Photofinish<sup>5</sup>) was used to locate the x-y coordinates of each corner of each leg. The changes in surface area and extension ratio of each leg were calculated. The program 'Trouser Tear Test Leg Dimensions' (Appendix 3.9) performed this task.

---

<sup>5</sup> A product the ZSoft Corporation, 450 Franklin Road, Suite 100, Marietta, GA 30067, USA.

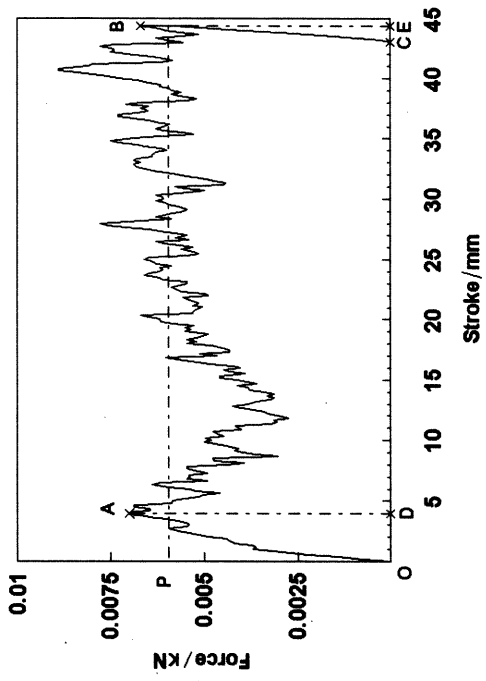


Figure 2.6

Typical load-stroke data for a leather trouser tear test.

## 2.6 Chemical Analysis.

### 2.6.1 Determination of Oil Content.

The IUC/4 procedure [Official Methods of Analysis, 1965] was used to determine the percentage oil content of grain and corium materials. A material was ground to produce a powder and 10 ± 0.1 g of the powder placed in an extraction thimble. Dichloromethane (200 cm<sup>3</sup>) was placed in a flask and the thimble (containing the ground leather) placed in a Soxhlet extractor. The apparatus was arranged so the dichloromethane evaporates, condenses, passes through the ground leather and returns (with the extracted substances) to the flask. Here the dichloromethane was again evaporated and the process repeated approximately fifty times.

The dichloromethane was then distilled from the flask containing the extract and the flask dried in an oven at 102 ± 2 °C for six hours. The oil content is calculated using equation [2.13].

$$\text{Oil Content / \%} = \frac{\text{Mass of extract}}{\text{Mass of original ground leather}} \times 100 \quad [2.13]$$

### 2.6.2 Determination of Volatile Matter Content.

The IUC/5 procedure [Official Methods of Analysis, 1965] was used to determine the percentage volatile matter content (assumed to be extractable water) of grain and corium materials. A material was ground to produce a powder and  $3 \pm 0.01$  g of the powder placed in a crucible. The crucible containing the powder is dried in an oven at  $102 \pm 2^\circ\text{C}$  for six hours, cooled, weighed and returned to the oven. This procedure continued until no further weight reduction occurred.

The percentage of volatile matter is calculated on a wet weight basis, using equation [2.14].

$$\text{Volatile Matter / \%} = \frac{G_1 - G_2}{G_1} \times 100 \quad [2.14]$$

$G_1$  is the weight of the leather powder before drying and  $G_2$  is the weight of the leather powder after drying.

## **Chapter 3**

### **Tensile and Tear Behaviour.**

#### **3.1 Introduction.**

The major aims of this study were to characterize and account for differences in the mechanical behaviour and fracture of the grain and corium layers. The effect of fatliquoring was also considered. Four materials were used, namely fatliquored, air dried grain (FADG), propanone dehydrated grain (PDG), fatliquored, air dried corium (FADC) and propanone dehydrated corium (PDC). In this chapter, the tensile properties and tearing resistance of grain and corium materials over a range of strain rates are reported. The levels of energy dissipation during strain cycling of grain and corium materials were investigated with respect to the level of strain attained and the rate of strain application.

Leather generally exhibits a 'J' shaped stress-strain curve when subject to a uniaxial tensile test [Attenburrow, 1993]. This type of non-Hookean behaviour is shown by other materials of biological origin; eg. arterial tissue [Dorbin, 1978], human skin [Daly, 1966], sea anemone and rat skin [Purslow, 1989a]. Such materials are renowned for high levels of tearing resistance [Vincent, 1982]. Indeed, Gordon [1978] considers the 'J' shaped stress-strain curve an integral factor associated with the high tearing resistance of these materials.

Uniaxial tensile testing of grain and corium specimens, at a specified strain rate

until rupture, enabled characterisation of tensile behaviour. This characterisation included measurement of the stress at rupture, the strain at rupture and the energy required to achieve rupture. In addition the degree of non-linearity and the occurrence of yield points<sup>6</sup> was assessed from inspection of stress-strain profiles. Trouser tear testing of grain and corium specimens, at a specified strain rate, yielded the tearing resistance. Three methods of calculating toughness (outlined in Section 2.5.7) provided tearing resistance in terms of the energy required to cleave a crack of unit area through the material; i.e. the specific work of fracture.

Leather is subject to high strain rates as a consequence of the rapid movement and snagging of shoes / clothing and the high speed lasting of shoes. Leather is also used in situations where the application of loads are slow; eg. for bag straps, belts shoes and clothing. Leather is a viscoelastic material [Whittaker, 1975] and as such, its mechanical properties depend on temperature, time and plasticisers (especially water). Therefore, at constant temperature and moisture content, the rate at which a leather is strained influences its tensile properties. Accordingly, to assess possible differences between grain and corium, the influence of strain rate on tensile and tear properties was examined.

An additional type of non-Hookean behaviour usually demonstrated by viscoelastic materials is apparent when tensile specimens are strained and then unloaded before specimen rupture. Here, the unloading curve is below the loading curve and energy is dissipated in the strain cycle, [Mohsenin, 1980]. However the term

---

<sup>6</sup> As will be discussed later, not all the leather in this work displayed a pure 'J' curve.

hysteresis can only be strictly applied if the material returns to its original strain level after deformation [Kinloch & Young, 1990]. Where residual strain is apparent after a deformation cycle, the material has experienced plastic deformation resulting in permanent set. Practically, true mechanical hysteresis and plastic deformation cannot be differentiated because both processes lead to similar dissipation of energies [Kinloch & Young, 1990].

Andrews [1980] related the apparent fracture resistance of a material ( $K_{Ic}$ ) to the product of a surface free energy term ( $\gamma_0$ ) and a loss function ( $\Phi$ ). The surface free energy term measures the energy required to break unit area of interatomic bonds across the fracture plane. The loss function describes the energy loss processes in the bulk solid and is dependent on strain, crack velocity and temperature. The loss function can be further analysed in terms of the hysteresis ratio ( $\beta$ ). In essence, the loss function equals one, for perfectly elastic materials (where  $\beta=0$ ), and infinity for materials displaying sufficiently large mechanical hysteresis (where  $\beta \rightarrow 1$ ). Accordingly, energy dissipation is very significant when considering the fracture resistance of a material.

Non-linear viscoelastic deformation ensures that the mechanical properties are a function, not only of time, but of the magnitude of stress (or strain) applied [Findley et al, 1989]. Accordingly grain and corium specimens were subject to strain cycling which covered a range of strain levels over a range of strain rates.

## 3.2 Results.

### 3.2.1 Stress-strain behaviour at a strain rate of 3.33 % s<sup>-1</sup>.

Figure 3.1 shows the stress-strain curves of tensile specimens cut in a direction parallel to the backbone. For each material, the stress-strain curves of four separate tensile tests are plotted. The specimens were strained at a rate of 1.66 mm s<sup>-1</sup> (or 3.33 % s<sup>-1</sup>). All specimens were cut over a small region within the official sampling position for bovine leather (IUP/1) [Official methods of Analysis, 1965].

Figures 3.1 (I) and (II) show the stress-strain curves of FADG (12.5 % oil content) and PDG specimens respectively. Both materials display an initial region where straining of the material results in a linear increase in stress. The quasi-linear response occurs between 0 % and 7 % where the modulus of tensile deformation<sup>7</sup> is 10.7 MPa in FADG specimens and 14.5 MPa in PDG specimens.

Beyond this level of strain, the modulus of tensile deformation initially falls to 7.8 MPa in FADG specimens and 9.9 MPa in PDG specimens. The modulus then gradually increases until specimens attain a strain level of  $\approx 43$  % in FADG specimens and  $\approx 34$  % in PDG specimens. Here the modulus attains a constant level of 42.9 MPa in FADG specimens and 44.4 MPa in PDG specimens. Accordingly, further increases in strain induce linear increases in stress until specimen rupture.

---

<sup>7</sup> The modulus of tensile deformation =  $\Delta$  nominal stress /  $\Delta$  nominal strain over a linear (or quasi-linear) region of the stress-strain curve.

The presence of oil in the FADG material appears to raise levels of both fracture stress and fracture strain. Indeed, the average stress level at fracture for the FADG specimens (12.5 % oil content) is  $16.76 \pm 0.61$  MPa compared to  $12.92 \pm 1.05$  MPa for PDG specimens. In addition the average level of strain at rupture for FADG specimens is  $65.08 \pm 0.99$  % compared to  $47.41 \pm 1.99$  % for PDG specimens.

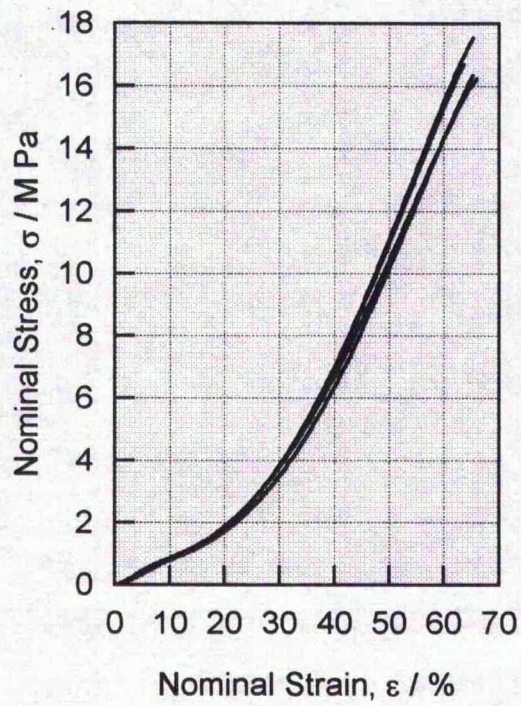
Typical response characteristics demonstrated by FADC (3 % oil content) and PDC specimens during a tensile test are shown in Figures 3.1 (III) and (IV) respectively. Again the tensile specimens were cut in a direction parallel to the backbone. Both corium materials have 'J' shaped stress-strain curves. These curves are characterized by a low modulus at low strain, followed by a region of increasing modulus until a constant modulus is achieved at higher strain levels.

The initial region of low modulus occurs between 0 % and 7 % strain in both FADC and PDC specimens. The modulus of tensile deformation in this strain region is 10.1 MPa for FADC specimens and 10.2 MPa for PDC specimens. The region of increasing modulus occurs between 10 % and 30→40 % strain for both corium materials. Beyond this level of strain, the moduli of tensile deformation remain constant at 84.1 MPa for FADC specimens and 79.5 MPa for PDC specimens. These moduli are noticeably higher than the moduli observed in the corresponding grain material.

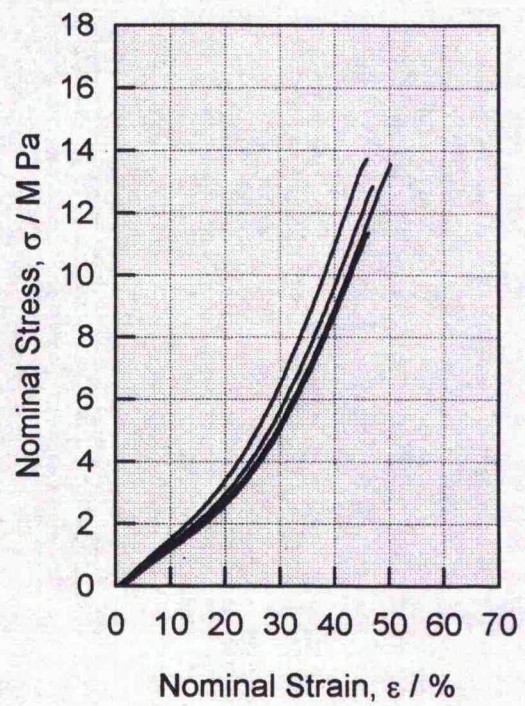
The presence of oil in the corium material has an appreciable effect, increasing the levels of rupture stress and rupture strain. The average stress level at fracture for

the FADC specimens is  $31.27 \pm 1.75$  MPa compared to  $25.01 \pm 0.85$  MPa for the PDC specimens. Further, the average level of strain at rupture for the FADC specimens is  $59.75 \pm 3.59$  % compared to  $51.83 \pm 2.26$  % for PDC specimens. Just before rupture, the stress-strain curves of the FADC specimens turn towards the strain axis and the modulus of tensile deformation is effectively reduced at this point.

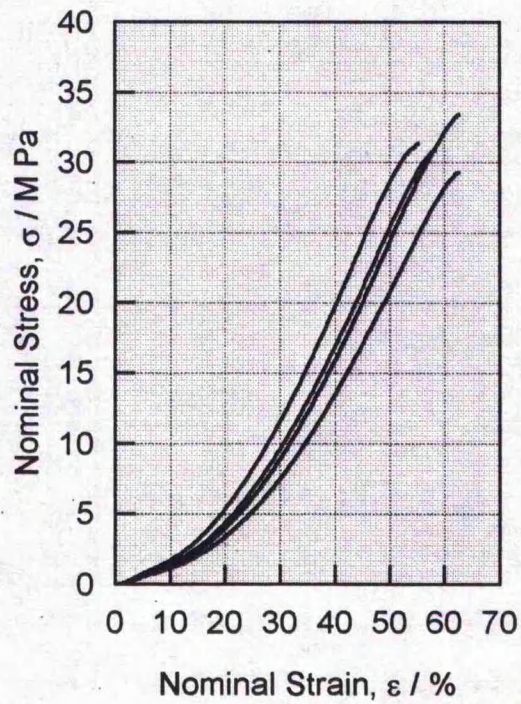
Figure 3.1  
 Stress-Strain Curves of FADG (12.5 % oil content), PDG, FADC (3.0 % oil content) and PDC specimens, **parallel** to the backbone and strained at  $3.33 \text{ mm s}^{-1}$ .



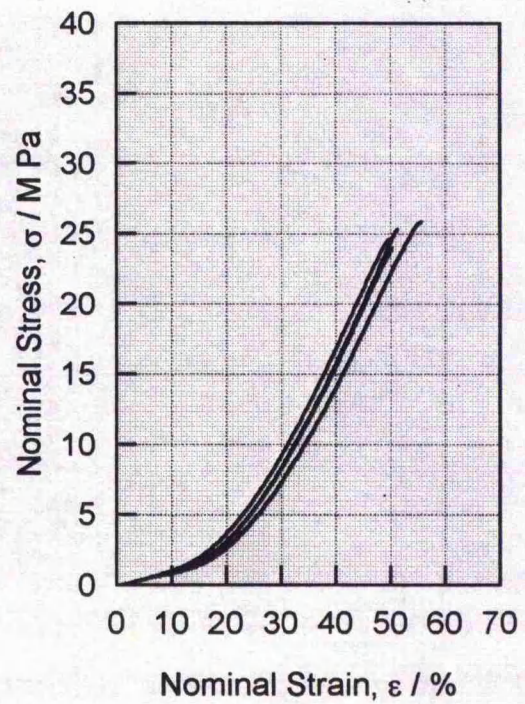
Material = FADG  
 (I)



Material = PDG  
 (II)



Material = FADC  
 (III)



Material = PDC  
 (IV)

The response characteristics of four materials are shown in Figure 3.2. Each graph shows the stress-strain curves of four separate tensile tests and the specimens were cut in a direction perpendicular to the backbone. All specimens were strained at a rate of  $3.33 \text{ \% s}^{-1}$ .

The curves in Figures 3.2 (I) (FADG, 12.5 % oil content) and (II) (PDG) have several points of interest. Between 0 % and 7 % strain, a linear modulus of tensile deformation is again apparent and equal to 7.8 MPa for FADG specimens and 14.6 MPa for PDG specimens. As strains exceed 7 %, the modulus of tensile deformation decreases to 1.1 MPa for FADG specimens and 2.4 MPa for PDG specimens. A non-linear region in the curve is then apparent up to  $\approx 65 \text{ \%}$  in FADG specimens and  $\approx 55 \text{ \%}$  in PDG specimens. At these strain levels, the modulus of tensile deformation has increased to 31.8 MPa in FADG specimens and 35.1 MPa in PDG specimens.

At the point of specimen rupture, the average nominal stress was higher in FADG specimens, at  $12.38 \pm 0.70 \text{ MPa}$  than in PDG specimens where the average breaking stress is  $10.21 \pm 0.73 \text{ MPa}$ . The average strain at rupture was also higher in FADG specimens than in PDG specimens. Indeed, the average strain at rupture was  $86.83 \pm 3.02 \text{ \%}$  in FADG specimens compared with  $65.83 \pm 3.49 \text{ \%}$  in PDG specimens.

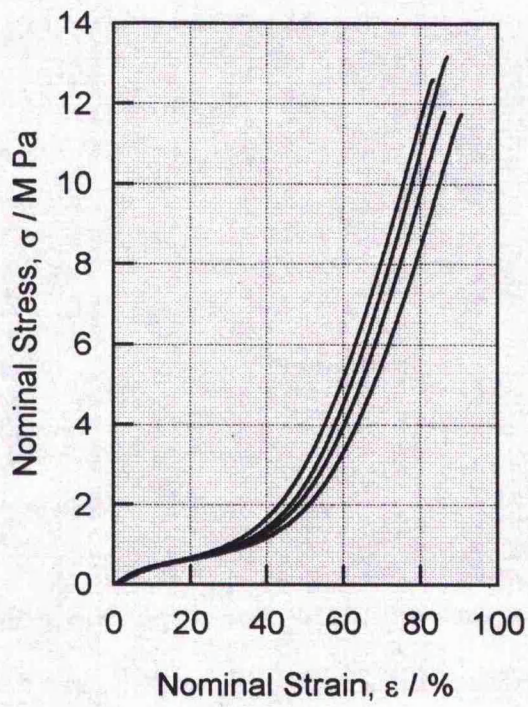
The stress-strain curves of FADC (3.0% oil content) and PDC specimens, (Figures 3.2 (III) and (IV)) differ from the situation where corium specimens are cut parallel

to the backbone (Figures 3.1 (III) and (IV) ). Unlike the 'parallel' specimens the 'perpendicular' specimens do not have a completely 'J' shaped stress-strain curve throughout the strain range. Instead, between 0 % and 7 % strain, the stress-strain curve is linear and has a higher modulus than directly after 7 % strain. The modulus of tensile deformation between 0 % and 7 % strain is 8.1 MPa for the FADC specimens and 8.2 MPa for the PDC specimens.

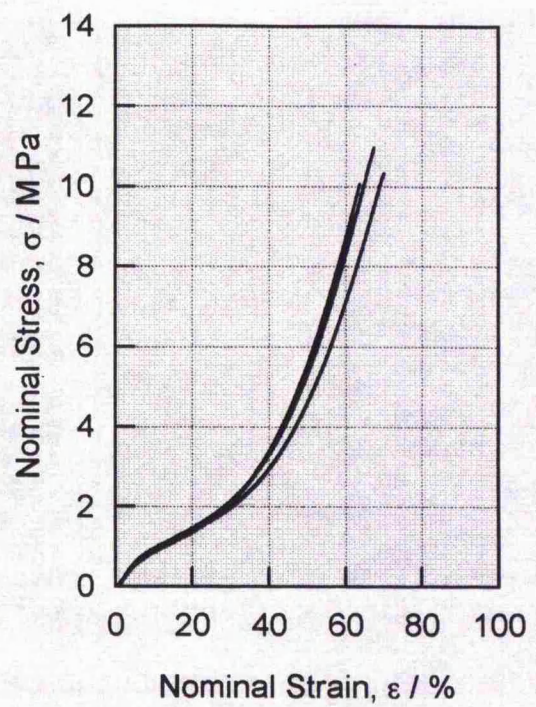
Above 7 % strain, the modulus of tensile deformation falls to around 5.2 MPa in both FADC and PDC specimens. The stress-strain curve is then non-linear. Here, the modulus of tensile deformation steadily increases to a static level of 54.6 MPa at a strain level of 60 % in FADC specimens and 57.7 MPa at 50 % strain in PDC specimens.

The average level of breaking stress in FADC and PDC specimens is  $25.66 \pm 1.07$  MPa and  $23.26 \pm 1.07$  MPa respectively. Thus, specimens cut perpendicular to the back bone (as opposed to parallel to the backbone) withstand a lower level of nominal stress before rupturing. In addition, the average level of strain at rupture in FADC specimens is  $86.50 \pm 5.53$  % and in PDC specimens is  $72.16 \pm 3.43$  %. Hence corium specimens cut perpendicular to the backbone (as opposed to parallel to the backbone) can attain significantly higher levels of strain before rupturing. Before complete fracture of the FADC specimens, the stress-strain curve turns towards the strain axis.

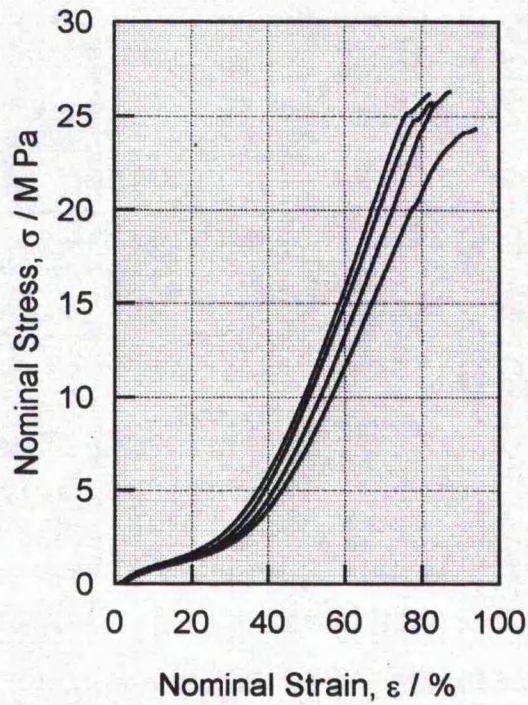
Figure 3.2  
 Stress-strain curves of FADG (12.5 % oil content), PDG, FADC (3.0% oil content) and PDC specimens, **perpendicular** to the backbone and strained  $3.33 \text{ mm s}^{-1}$ .



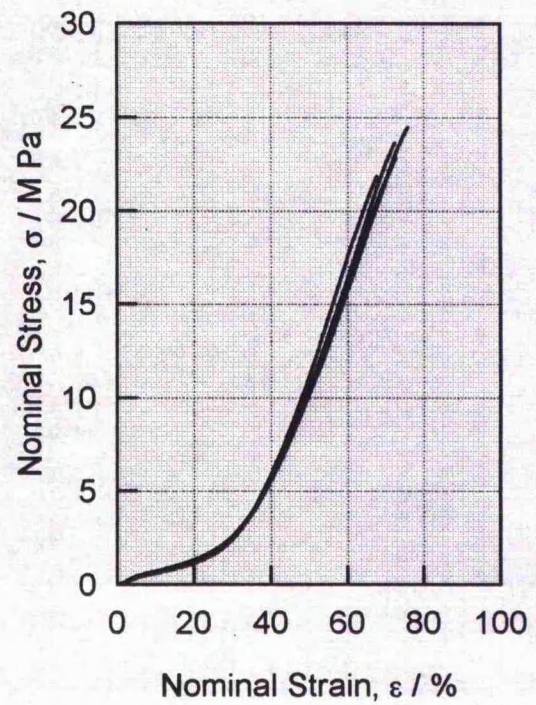
Material = FADG  
 (I)



Material = PDG  
 (II)



Material = FADC  
 (III)



Material = PDC  
 (IV)

### 3.2.2 Trouser tear tests at a deformation rate of 1.66 mm s<sup>-1</sup>.

Typical trouser tear load-stroke profiles are shown in Figures 3.3 (I) and (II) for FADG (12.5 % oil content) and PDG specimens. Figures 3.3 (III) and (IV) show typical curves when FADC (3 % oil content) and PDC trouser tear specimens are tested. The specimens were cut so the notch and advancing tear were parallel to the backbone. All specimens were strained at 1.66 mm s<sup>-1</sup>. Figure 3.4 has the same format as Figure 3.3. However the specimens were cut such that the notch and advancing tear were perpendicular to the backbone.

In all materials and both orientations, the pre-tearing region of each curve reflects the manner in which the load is taken up in the legs of the test piece. Generally, the load rises with one or two very small fluctuations until continuous tearing in the specimen ensues (calculation of this point is outlined in section 2.5.7.) Where the tearing process becomes continuous, fluctuations in load around a plateau are apparent.

The load at the plateau appears higher with corium specimens than with grain specimens. The plateau tearing force is generally higher with fatliquored, air dried specimens than with propanone dehydrated specimens. This is true for both grain and corium materials and is particularly noticeable in specimens cut perpendicular to the backbone.

In all trouser tear tests, the stroke was reversed at a level of 45 mm and the

specimens unloaded. During this period, the load falls rapidly and generally drops to zero before a stroke level of 40 mm. Visual recording of the tests and subsequent measurement of the extension ratio in the legs of the trouser tear specimen, at the point of tear propagation, revealed the extension ratio equals approximately one. This observation justifies the assumptions underlying Equation 2.12, where  $\lambda = 1$  and  $W_o \rightarrow 0$ .

Each test was performed four times with a fresh specimen. Tables 3.1 & 3.2 shows pertinent information regarding direct measurements of specimen thickness, stroke and load at the point of tear propagation, crack area and the extension ratio in the legs of the trouser tear specimens. The tables also report the energy supplied at several stages during stroke application and reversal, as well as three toughness calculations for each material. Table 3.1 reports information regarding specimens of FADG (12.5 % oil content), PDG, FADC (3% oil content) and PDC cut in a direction parallel to the backbone. Table 3.2 has identical format but contains information regarding specimens cut in a direction perpendicular to the backbone.

The results in Tables 3.1 and 3.2 reveal several interesting characteristics:

(i) The three methods produce different estimates of toughness, but all show the same trend. Corium material is significantly tougher than grain. Fatliquored, air dried material is tougher than propanone dehydrated material. However, method (2) predicts the highest toughness while method (1) predicts the lowest toughness.

(ii) The corium material is universally tougher than the respective grain material. The toughness depends on the direction of tear propagation (whether parallel or perpendicular to the backbone) and the presence of oil. In the case of FADG (12.5 % oil content) and FADC (3.0 % oil content) where the tear propagated in a direction parallel to the backbone, the toughness of the corium was 60 % greater than the grain. In the case of PDG and PDC, where the direction of tear propagation was perpendicular to the backbone, the toughness of the corium was 300 % higher than the grain.

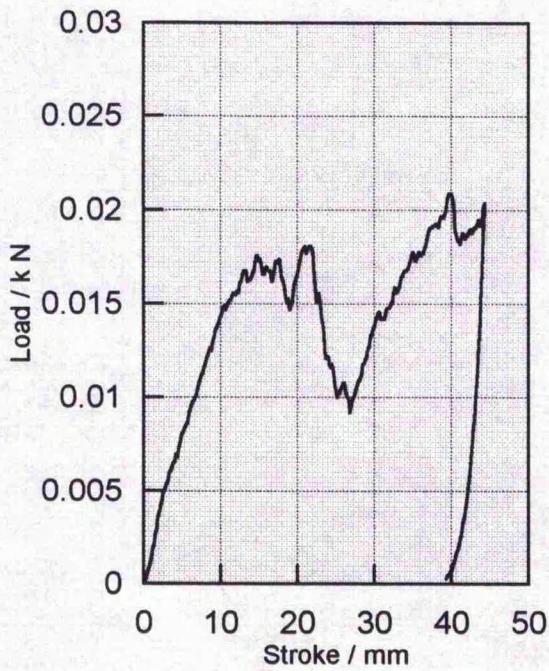
(iii) All three methods of calculating toughness show that oil has a substantial effect on the toughness of both grain and corium materials. In the case of the grain where the tear propagates in a parallel direction to the backbone, the toughness is approximately doubled by the presence of oil at 12.5 %. In this tearing direction, the toughness of the corium is increased by approximately 30 % when oil is present at 3.0 %. However, in the case of the grain where the tear propagates in a direction perpendicular to the backbone, the toughness increases 300 % when 12.5 % oil is present. In this orientation the toughness of the corium is also increased by the presence of 3.0 % oil, but only by around 30 %.

(iv) With grain material, the energy supplied to reach the point where continuous tearing occurs, is substantially higher when oil is present (i.e. FADG as opposed to PDG). Where specimens are cut in a direction parallel to the backbone, the total energy supplied at the point where continuous tearing occurs is 220 % greater in FADG materials than PDG material. This feature was enhanced when the direction

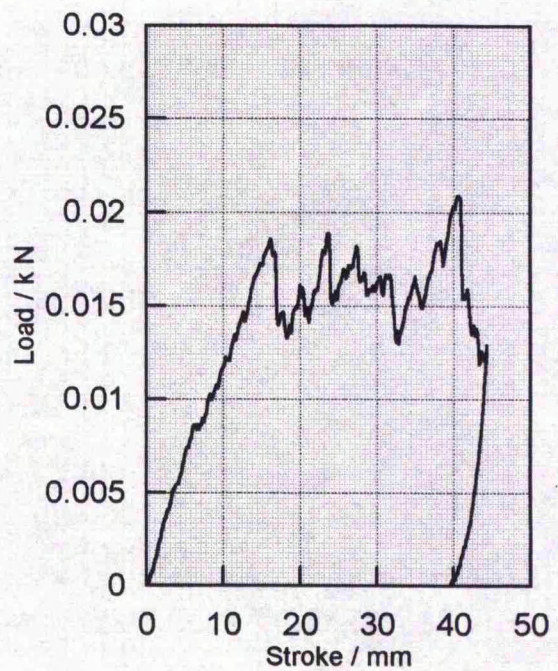
of tear was perpendicular to the backbone. Here, the presence of oil increased this energy by 750 % !

(v) Estimates of the extension ratio, based on visual measurements of the specimen legs at the point of tear propagation are much lower than half the stroke at the point where continuous tear propagation commences (eg  $\frac{1}{2}OD$  in Figure 2.6). These quantities should be equal where continuous tear propagation directly follows tear initiation. Visual measurement of the extension ratio relies on direct observation of the first advancement of the tear. The results indicate some degree of tear occurs prior to gross tear propagation and it is contended that using the visual method, the estimate of the point of continuous tear propagation (and consequently the extension ratio in the legs,  $\lambda$ ) is premature resulting in low estimates of  $\lambda$ .

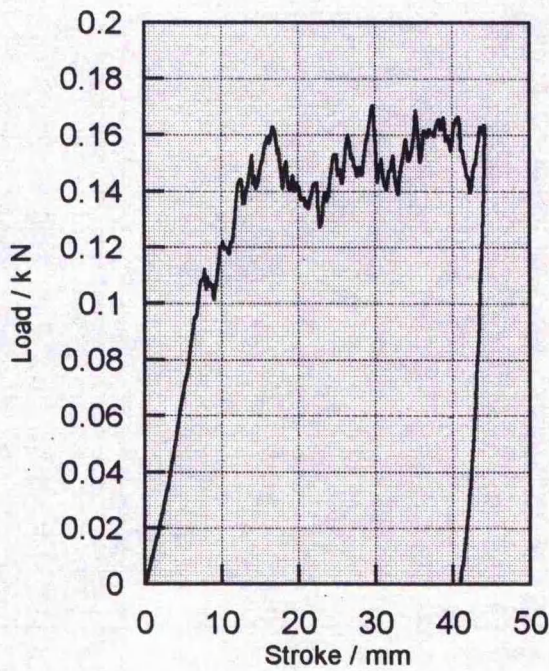
Figure 3.3  
 Load-Stroke Curves of FADG (12.5 % oil content), PDG, FADC (3.0% oil content) and PDC  
 Trousers Tear Tests. Specimens **parallel** to the backbone and strained at  $1.66 \text{ mm s}^{-1}$ .



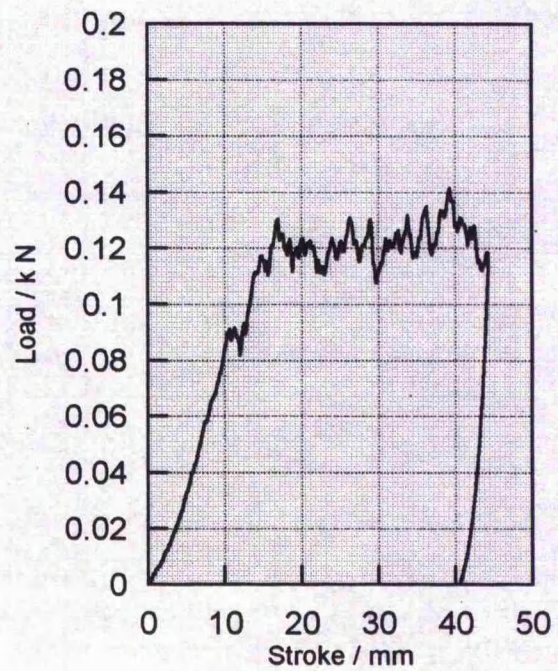
Material = FADG  
 Tear Direction = Parallel to backbone  
 (I)



Material = PDG  
 Tear Direction = Parallel to backbone  
 (II)

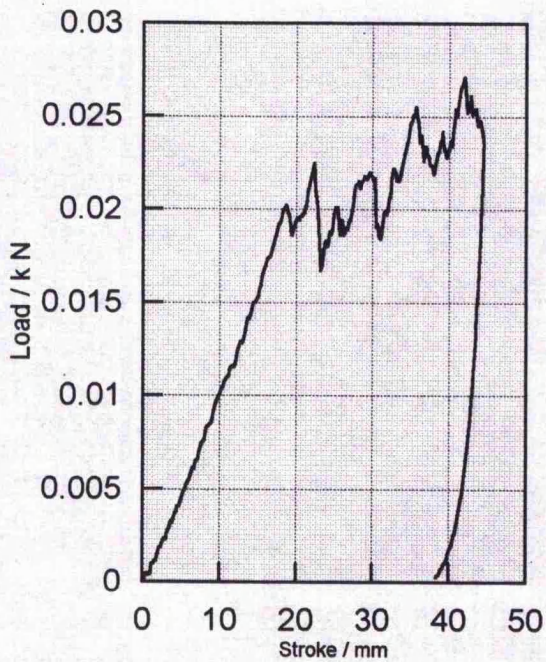


Material = FADC  
 Tear Direction = Parallel to backbone  
 (III)

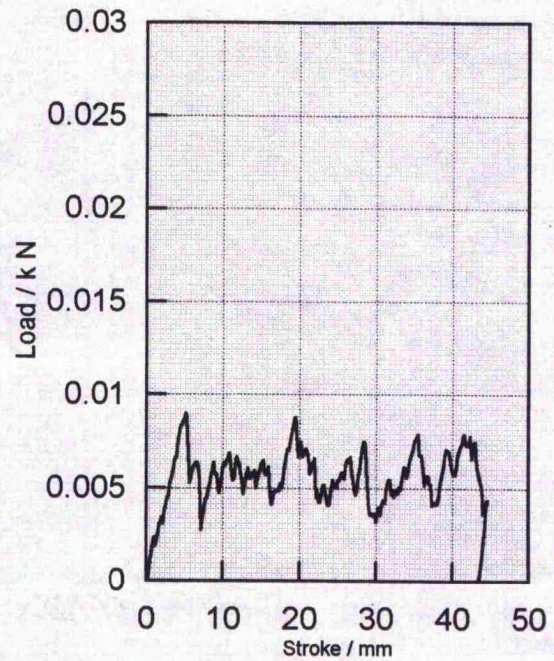


Material = PDC  
 Tear Direction = Parallel to backbone  
 (IV)

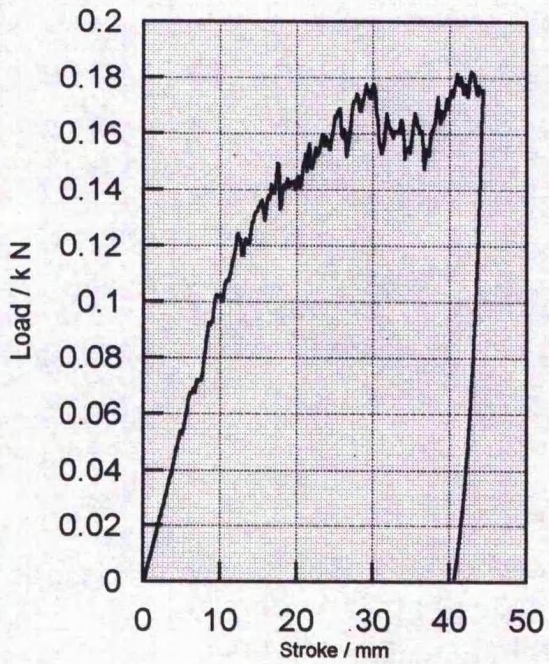
Figure 3.4  
 Load-Stroke Curves of FADG (12.5 % oil content), PDG, FADC (3.0% oil content) and PDC  
 Trouser Tear Tests. Specimens **perpendicular** to the backbone and strained at  $1.66 \text{ mm s}^{-1}$ .



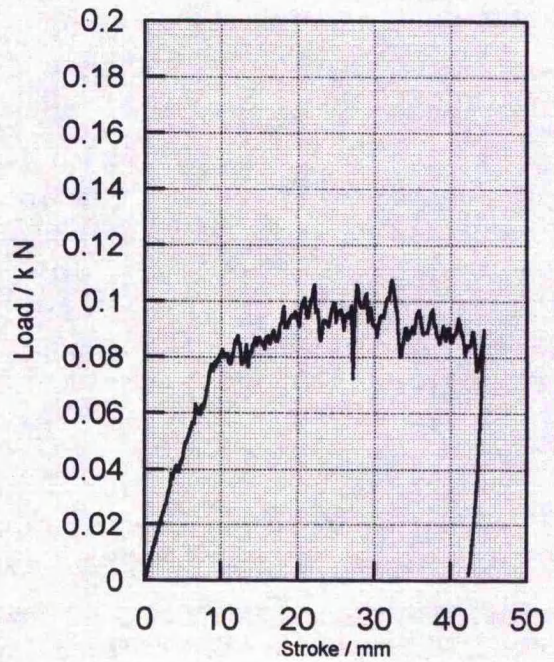
Material = FADG  
 Tear Direction = Perpendicular to backbone  
 (I)



Material = PDG  
 Tear Direction = Perpendicular to backbone  
 (II)



Material = FADC  
 Tear Direction = Perpendicular to backbone  
 (III)



Material = PDC  
 Tear Direction = Perpendicular to backbone  
 (IV)

Table 3.1: Trouser tear test results (Direction of tear propagation parallel to the backbone.)

	FADG	PDG	FADC	PDC
Thickness / mm	0.76 ± 0.12	1.01 ± 0.05	3.42 ± 0.18	4.07 ± 0.06
Length of tear / mm	16.63 ± 1.55	21.25 ± 0.50	17.88 ± 0.48	16.63 ± 0.48
Stroke at continuous tear propagation / mm	12.05 ± 2.67	7.17 ± 1.70	12.32 ± 3.63	16.42 ± 1.83
Load at continuous tear propagation / N	18.19 ± 7.83	10.47 ± 1.31	147.75 ± 28.45	130.29 ± 10.21
Area cleaved / m <sup>2</sup>	1.25x10 <sup>-5</sup> ± 1x10 <sup>-6</sup>	2.16x10 <sup>-5</sup> ± 9x10 <sup>-7</sup>	6.12x10 <sup>-6</sup> ± 2x10 <sup>-7</sup>	6.76x10 <sup>-6</sup> ± 3x10 <sup>-7</sup>
Plateau force / N	20.70 ± 8.13	13.16 ± 1.88	157.75 ± 24.53	125.32 ± 5.72
Energy supplied at continuous tear propagation / J	0.1244 ± 0.0767	0.0391 ± 0.0121	1.0168 ± 0.5888	1.1169 ± 0.1943
Energy supplied at maximum stroke / J	0.7783 ± 0.2815	0.5279 ± 0.0681	6.0025 ± 0.7585	4.5993 ± 0.2327
Energy returned on unloading / J	0.0333 ± 0.0127	0.0068 ± 0.0081	0.1703 ± 0.0193	0.121 ± 0.0142
Energy supplied during continuous tear propagation / J	0.6538 ± 0.2178	0.4888 ± 0.0752	4.9857 ± 0.2269	3.4824 ± 0.2047
Extension ratio in specimen legs at tear initiation	1.11	1.09	1.08	1.05
Toughness (method 1) / J m <sup>-2</sup>	51,853 ± 13,533	22,724 ± 3,741	81,572 ± 3,846	51,490 ± 2,228
Toughness (method 2) / J m <sup>-2</sup>	59,549 ± 16,604	28,251 ± 3,809	99,254 ± 12,001	64,588 ± 2,117
Toughness (method 3) / J m <sup>-2</sup>	53,750 ± 14,966	25,933 ± 3,493	91,875 ± 11,242	61,604 ± 2,028

Table 3.2: Trouser tear tests results (Direction of tear propagation perpendicular to the backbone.)

	FADG	PDG	FADC	PDC
Thickness / mm	0.78 ± 0.05	0.98 ± 0.04	3.80 ± 0.10	4.20 ± 0.06
Length of tear / mm	15.75 ± 0.96	20.75 ± 0.29	16.63 ± 0.48	17.00 ± 0.41
Stroke at continuous tear propagation / mm	18.25 ± 2.44	5.54 ± 0.66	12.85 ± 3.65	11.29 ± 2.16
Load at continuous tear propagation / N	23.35 ± 5.14	6.95 ± 1.89	155.25 ± 65.01	96.34 ± 7.97
Area cleaved / m <sup>2</sup>	1.23x10 <sup>-5</sup> ± 9x10 <sup>-7</sup>	2.03x10 <sup>-5</sup> ± 8x10 <sup>-7</sup>	6.33x10 <sup>-6</sup> ± 3x10 <sup>-7</sup>	7.15x10 <sup>-6</sup> ± 2x10 <sup>-7</sup>
Plateau force / N	21.08 ± 2.11	6.36 ± 0.80	166.75 ± 20.30	106.13 ± 10.25
Energy supplied at continuous tear propagation / J	0.2133 ± 0.0804	0.0251 ± 0.0057	1.0025 ± 0.5319	0.5733 ± 0.1499
Energy supplied at maximum stroke / J	0.7560 ± 0.0874	0.2728 ± 0.0312	6.1875 ± 0.6856	4.0896 ± 0.4092
Energy returned on unloading / J	0.0284 ± 0.0094	0.0035 ± 0.0019	0.2058 ± 0.0584	0.0922 ± 0.0229
Energy supplied during continuous tear propagation / J	0.5427 ± 0.0286	0.2476 ± 0.0316	5.1850 ± 0.3946	3.5163 ± 0.4850
Extension ratio in specimen legs at tear initiation	1.16	1	1.08	1.05
Toughness (method 1) / J m <sup>-2</sup>	44,331 ± 3,226	12,213 ± 1,327	81,913 ± 3,320	49,229 ± 6,898
Toughness (method 2) / J m <sup>-2</sup>	62,668 ± 5,537	12,994 ± 1,232	94,501 ± 9,470	52,920 ± 4,646
Toughness (method 3) / J m <sup>-2</sup>	54,125 ± 4,872	13,000 ± 1,262	87,575 ± 8,870	50,451 ± 4,442

### 3.2.3 Ultimate tensile properties and strain rate.

Breaking stress, breaking strain and the energy supplied to rupture tensile specimens are shown as functions of strain in Figures 3.5, 3.6 and 3.7 respectively. The strain rates used for these tests were 0.33 % s<sup>-1</sup>, 3.33 % s<sup>-1</sup>, 33.33 % s<sup>-1</sup> and 333.33 % s<sup>-1</sup>. All tensile specimens were cut parallel to the backbone.

Figures 3.5, 3.6 and 3.7 graphs (I) and (II) show the response characteristics of the FADG (oil content 12.5 %) and PDG materials respectively. Similarly, the response characteristics of the FADC (oil content 3.0 %) and PDC materials are shown in (III) and (IV). In all graphs, the strain rate axis uses a logarithmic scale.

At each strain rate, four specimens were tested, allowing calculation of relevant averages and standard deviations. All graphs show average values of properties (i.e. breaking stress, breaking strain and energy supplied to rupture the tensile specimens) as well as the appropriate error bars (plus and minus one standard deviation). A trend line through the data and the relevant equation are also shown. The equations are of the form,

$$y = k x^n$$

Here y is the average breaking stress, breaking strain or energy supplied to rupture specimens; k is a constant; x is the percentage rate of deformation per second and n is an exponent where 0 < n < 1.

Figure 3.5 which shows the effect of strain rate on the breaking stress of tensile specimens has several points of interest:

- (i) The average breaking stress of grain specimens is much lower than the average breaking stress of the corium specimens over the range of strain rates examined. This result confirms that the earlier finding obtained at a strain rate of  $3.33 \text{ \% s}^{-1}$ , is applicable over a wide range of strain rates.
- (ii) On increasing the strain rate from  $0.33 \text{ \% s}^{-1}$  to  $333.33 \text{ \% s}^{-1}$ , the average tensile stress at failure of FADG specimens increases 21 %. However, the magnitude of this phenomenon is not repeated by PDG specimens. Here, an increase of only 6 % is predicted by the trend line but the error bars show this conclusion is not statistically significant. In addition, at every strain rate examined, the average breaking stress of grain specimens is at least 35% greater when oil is present in the material (i.e. FADG).
- (iii) Over the range of strain rates examined, the FADC and PDC specimens experience an increase in breaking stress of 25 % and 30 % respectively. Further, the average breaking stress of FADC specimens is at least 10 % greater than PDC specimens at all rates of applied strain.

Relationships between strain rate and breaking strain (Figure 3.6) lead to the following general points:

- (i) The breaking strain of FADG and PDG specimens are only marginally influenced by the rate at which the specimens are strained.
- (ii) The breaking strain attains a maximum of approximately 60 % in FADG specimens and 40 % in PDG specimens. This difference is directly attributed to the presence of oil in FADG specimens. Indeed, the average breaking strain of FADG specimens are the highest observed in the materials studied.
- (iii) In both corium materials, a tangible increase in average breaking strain is observed when the strain rate is increased by a factor of 1000.
- (iv) The breaking strain at all strain rates, is greater in FADC specimens than in PDC specimens which can be directly attributed to the presence of oil in the FADC specimens.

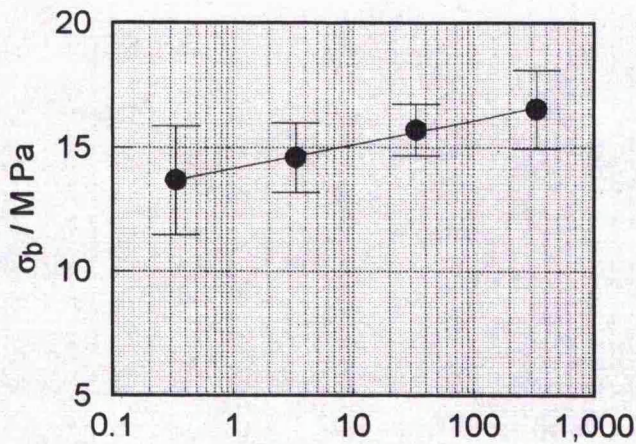
Figure 3.7 shows the effect of strain rate on the energy supplied to rupture tensile specimens. It is important to note that:

- (i) The energy supplied to cause specimen rupture was approximately 8 times higher for corium specimens than for the corresponding grain specimens.

- (ii) On increasing the strain rate from  $0.33 \text{ \% s}^{-1}$  to  $333.33 \text{ \% s}^{-1}$ , the average energy supplied to rupture FADG specimens increased 34 %. However, no discernible rate dependency was observed for PDG specimens. Further, over the range of strain rates examined, the average energy supplied to rupture grain specimens was significantly higher when oil is present in the material (i.e. FADG specimens).
  
- (iii) On increasing the strain rate from  $0.33 \text{ \% s}^{-1}$  to  $333.33 \text{ \% s}^{-1}$ , a 45 % increase in the energy supplied to rupture FADC specimens was apparent. This trend was also observed with the PDC specimens where the energy supplied to cause rupture increased 59 %.

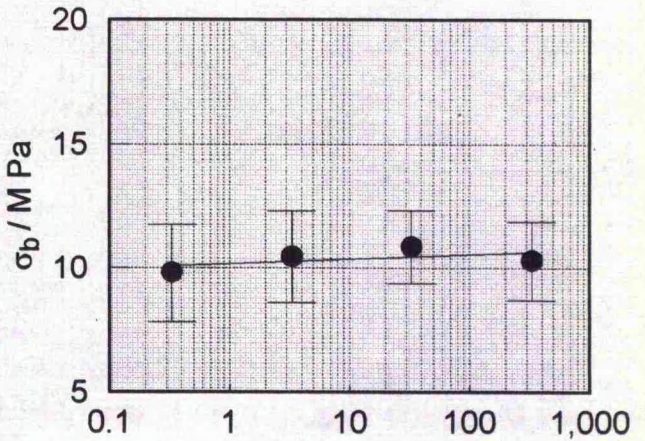
Figure 3.5

The effect of strain rate on the breaking stress of FADG (12.5 % oil content) PDG, FADC (3.0 % oil content) and PDC tensile specimens.



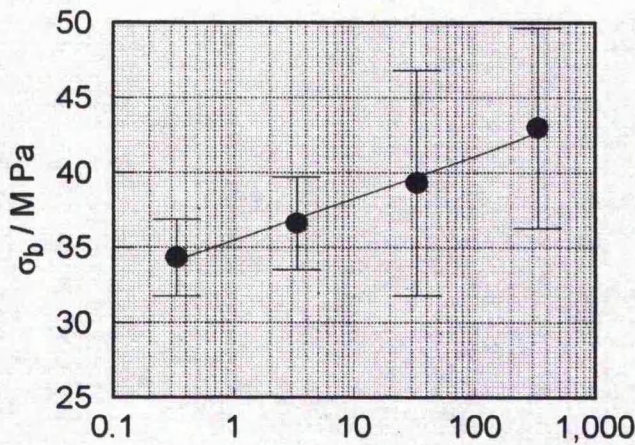
rate, r / % s<sup>-1</sup>  
 $\sigma_b = 14.14 r^{0.028}$

Material = FADG  
(I)



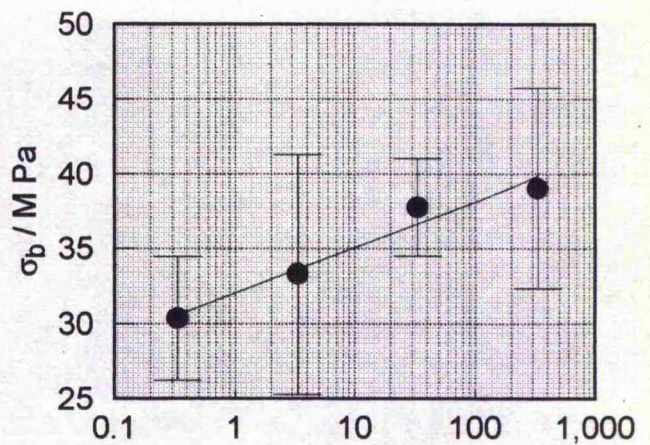
rate, r / % s<sup>-1</sup>  
 $\sigma_b = 10.16 r^{0.008}$

Material = PDG  
(II)



rate, r / % s<sup>-1</sup>  
 $\sigma_b = 35.37 r^{0.033}$

Material = FADC  
(III)

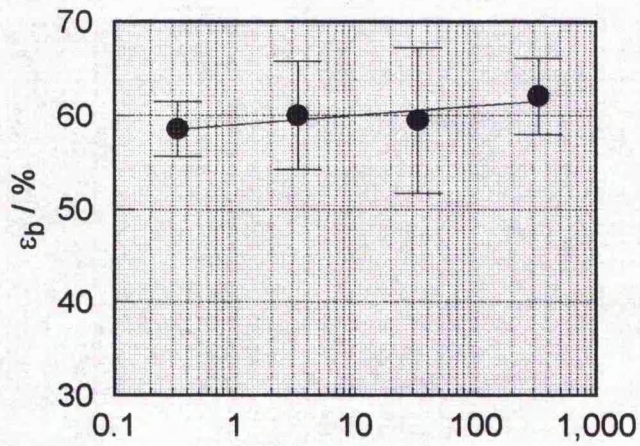


rate, r / % s<sup>-1</sup>  
 $\sigma_b = 31.93 r^{0.038}$

Material = PDC  
(IV)

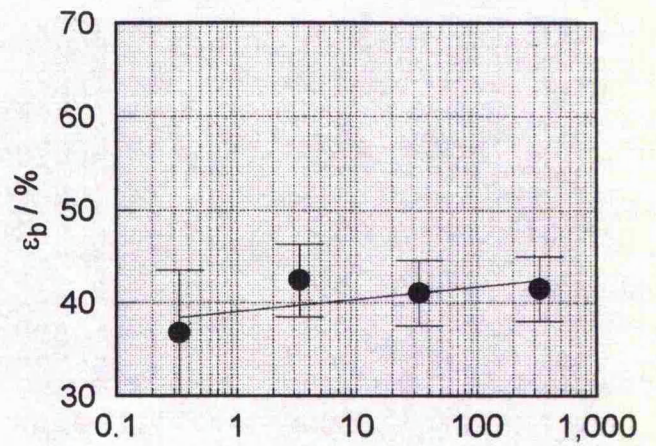
Figure 3.6

The effect of strain rate on the breaking strain of FADG (12.5 % oil content), PDG, FADC (3.0 % oil content) and PDC tensile specimens.



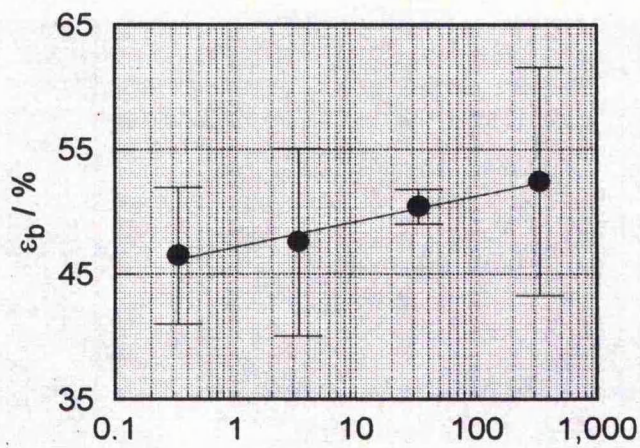
rate,  $r / \% s^{-1}$   
 $\epsilon_b = 59.03 r^{0.007}$

Material = FADG  
(I)



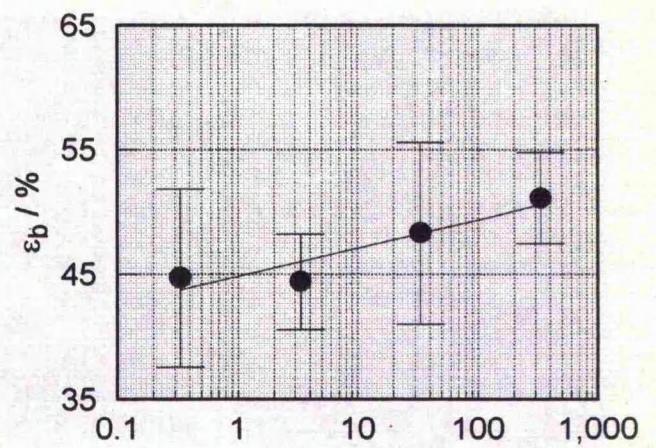
rate,  $r / \% s^{-1}$   
 $\epsilon_b = 39.04 r^{0.014}$

Material = PDG  
(II)



rate,  $r / \% s^{-1}$   
 $\epsilon_b = 47.12 r^{0.018}$

Material = FADC  
(III)

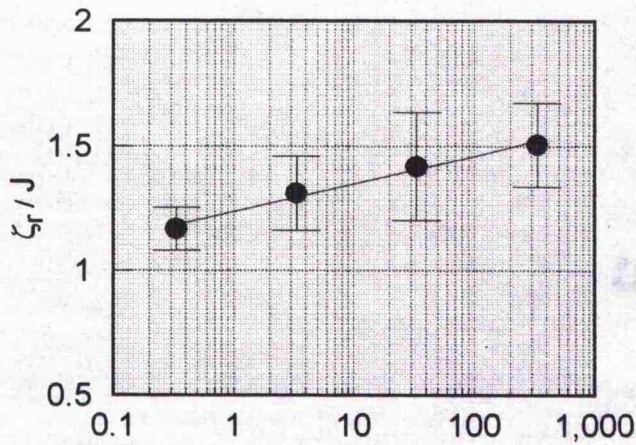


rate,  $r / \% s^{-1}$   
 $\epsilon_b = 44.79 r^{0.021}$

Material = PDC  
(IV)

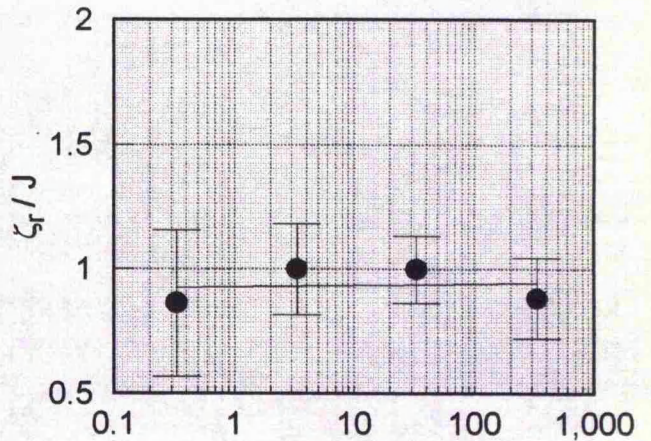
Figure 3.7

The effect of strain rate on the energy required to rupture FADG (12.5 % oil content), PDG, FADC (3.0 % oil content) and PDC tensile specimens.



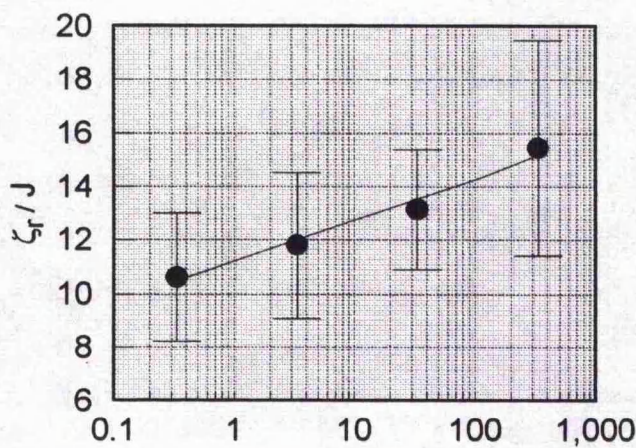
rate,  $r / \% s^{-1}$   
 $\zeta_r = 1.24 r^{0.037}$

Material = FADG  
(I)



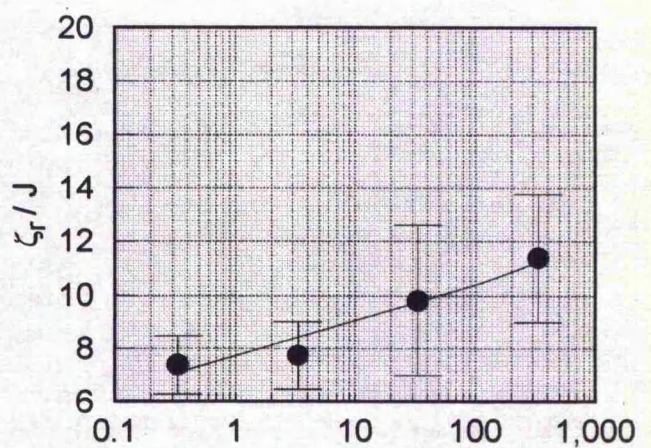
rate,  $r / \% s^{-1}$   
 $\zeta_r = 0.93 r^{0.003}$

Material = PDG  
(II)



rate,  $r / \% s^{-1}$   
 $\zeta_r = 11.13 r^{0.054}$

Material = FADC  
(III)



rate,  $r / \% s^{-1}$   
 $\zeta_r = 7.64 r^{0.067}$

Material = PDC  
(IV)

#### 3.2.4 Tearing resistance and strain rate.

The results of trouser tear tests conducted over a range of deformation rates are reported in this section. The rates of deformation used were  $0.16 \text{ mm s}^{-1}$ ,  $1.66 \text{ mm s}^{-1}$ ,  $16.66 \text{ mm s}^{-1}$  and  $166.66 \text{ mm s}^{-1}$ . At these rates, eight trouser tear specimens were tested. Tear propagation was parallel to the backbone in four specimens and perpendicular to the backbone in four specimens. Visual recording of the tests enabled an assessment of the extension ratio in the legs of a specimen at the point of tear propagation. In each material, one visual measurement of the extension ratio was carried out at all deformation rates in both directions of tear.

The thickness of each specimen was measured before testing and the final length of the tear measured after testing. Hence the area cleaved in each specimen was calculated. Numerical integration of load-stroke information yielded the following information: the energy supplied to the point of continuous tear propagation, the energy returned on unloading the specimen and the energy supplied during continuous tear propagation. Three different methods for calculating the tear resistance (outlined in section 2.5.7) were used to determine the toughness of each specimen.

Accordingly, from each trouser tear test, a profile of results was assembled. The list of data included: (1) the tearing speed, (2) tearing direction, (3) average specimen thickness, (4) length of the tear, (5) stroke at the point of continuous tear propagation, (6) load at the point of continuous tear propagation, (7) the area

cleaved in the specimen, (8) the plateau tearing force, (9) the energy supplied at the point of continuous tear propagation, (10) the energy supplied at maximum stroke, (11) the energy returned when unloading the specimen, (12) the energy supplied during continuous tear propagation, (13) the extension ratio in the legs, (14) toughness (method 1), (15) toughness (method 2), and (16) toughness (method 3).

Under conditions of identical deformation rates and direction of tear propagation, an average and standard deviation was calculated for each item in the results profile. The results are shown in Tables 3.3 and 3.4 which are given in Appendix 4. Table 3.3 summarises the results for FADG (12.5 % oil content) and PDG specimens and Table 3.4 for FADC (3.0 % oil content) and PDC specimens. Both tables contain a large amount of information for calculating, by the three approaches, the intrinsic tear resistance of each material, at each orientation.

To examine the relationship between deformation rate and toughness, as calculated by three approaches, relevant data have been extracted from Appendix 4 (Tables 3.3 and 3.4). The average toughness of each material at each orientation is plotted against the deformation rate on a logarithmic scale in Figures 3.8 to 3.10. Error bars illustrate plus and minus one standard deviation of the average toughness.

For all the graphs in Figure 3.8, method 1 ( $R_1$ ) was used to appraise any changes in toughness over the range of deformation rates examined. All graphs in Figure

3.8 show the relationship between toughness and deformation rate. Within Figure 3.8, the material referred to in each graph (i.e. I to VIII) is as follows:

- (I) & (II) FADG specimens, where the tearing direction is perpendicular to the backbone in (I) and parallel to the backbone in (II).
- (III) & (IV) PDG specimens, where the tearing direction is perpendicular to the backbone in (III) and parallel to the backbone in (IV).
- (V) & (VI) FADC specimens, where the tearing direction is perpendicular to the backbone in (V) and parallel to the backbone in (VI).
- (VII) & (VIII) PDC specimens, where the tearing direction is perpendicular to the backbone in (VII) and parallel to the backbone in (VIII).

This layout is repeated in Figures 3.9 and 3.10. However, in Figure 3.9, the toughness values were those calculated by method 2 ( $R_2$ ). Accordingly, the toughness values in Figure 3.10 were those calculated by method 3 ( $R_3$ ).

Figure 3.8

The effect of strain rate on the toughness (method 1) of FADG (12.5 % oil content), PDG, FADC (3.0 % oil content), PDG, FADC (3.0 % oil content) and PDC trouser tear specimens.

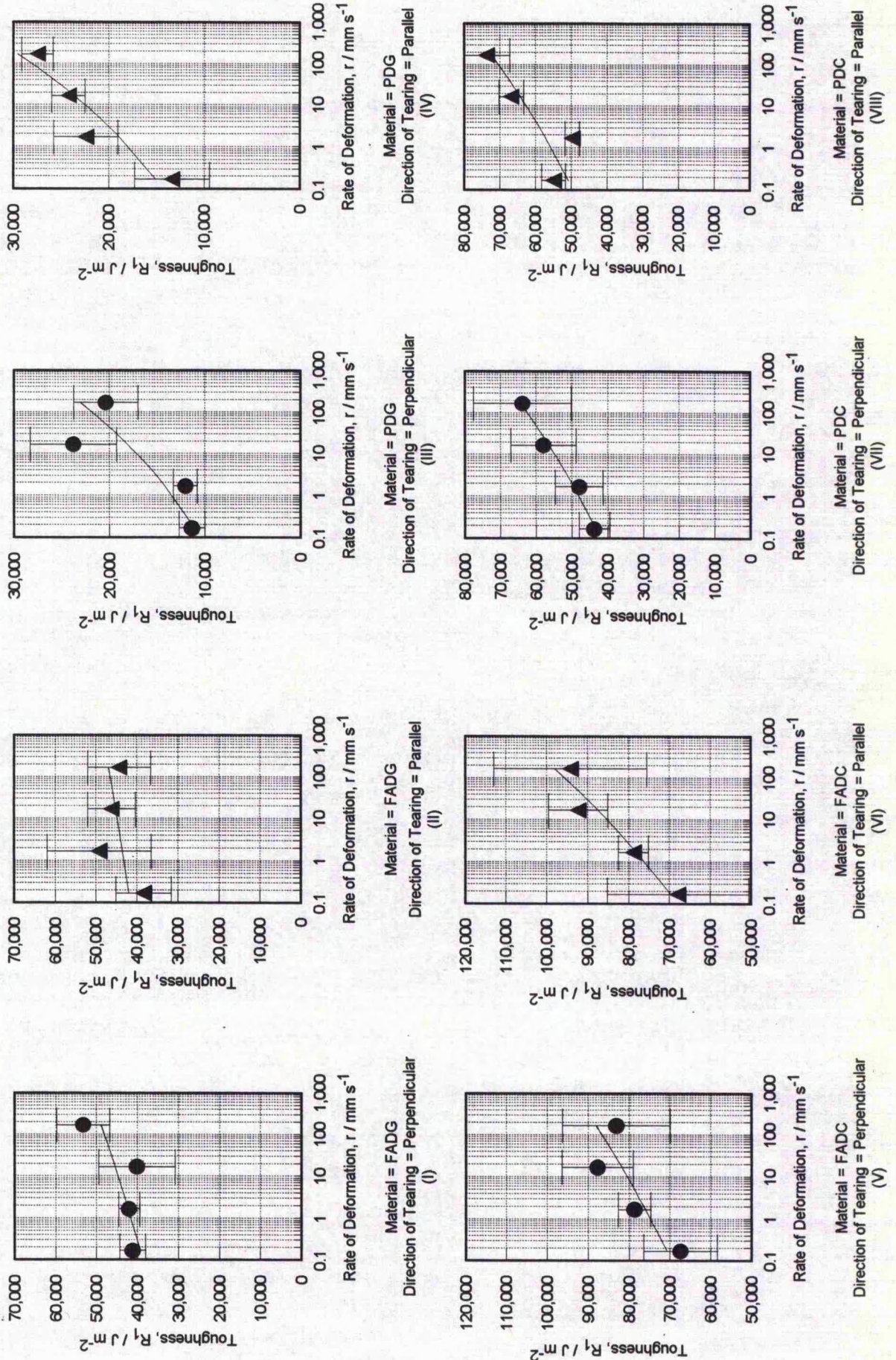


Figure 3.9

The effect of strain rate on the toughness (method 2) of FADG (12.5 % oil content), PDG, FADC (3.0 % oil content), PDG, FADC (3.0 % oil content) and PDC trouser tear specimens.

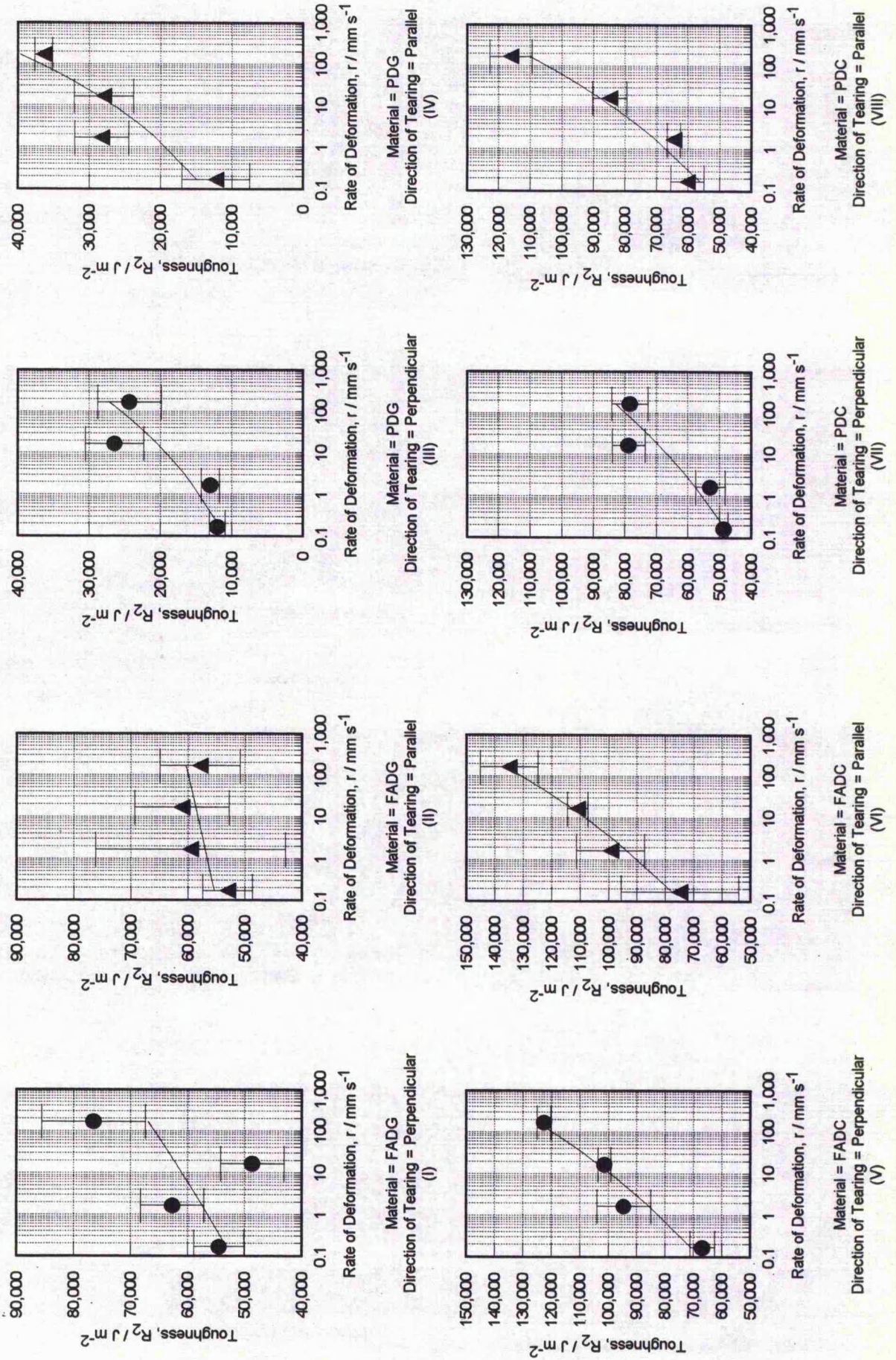
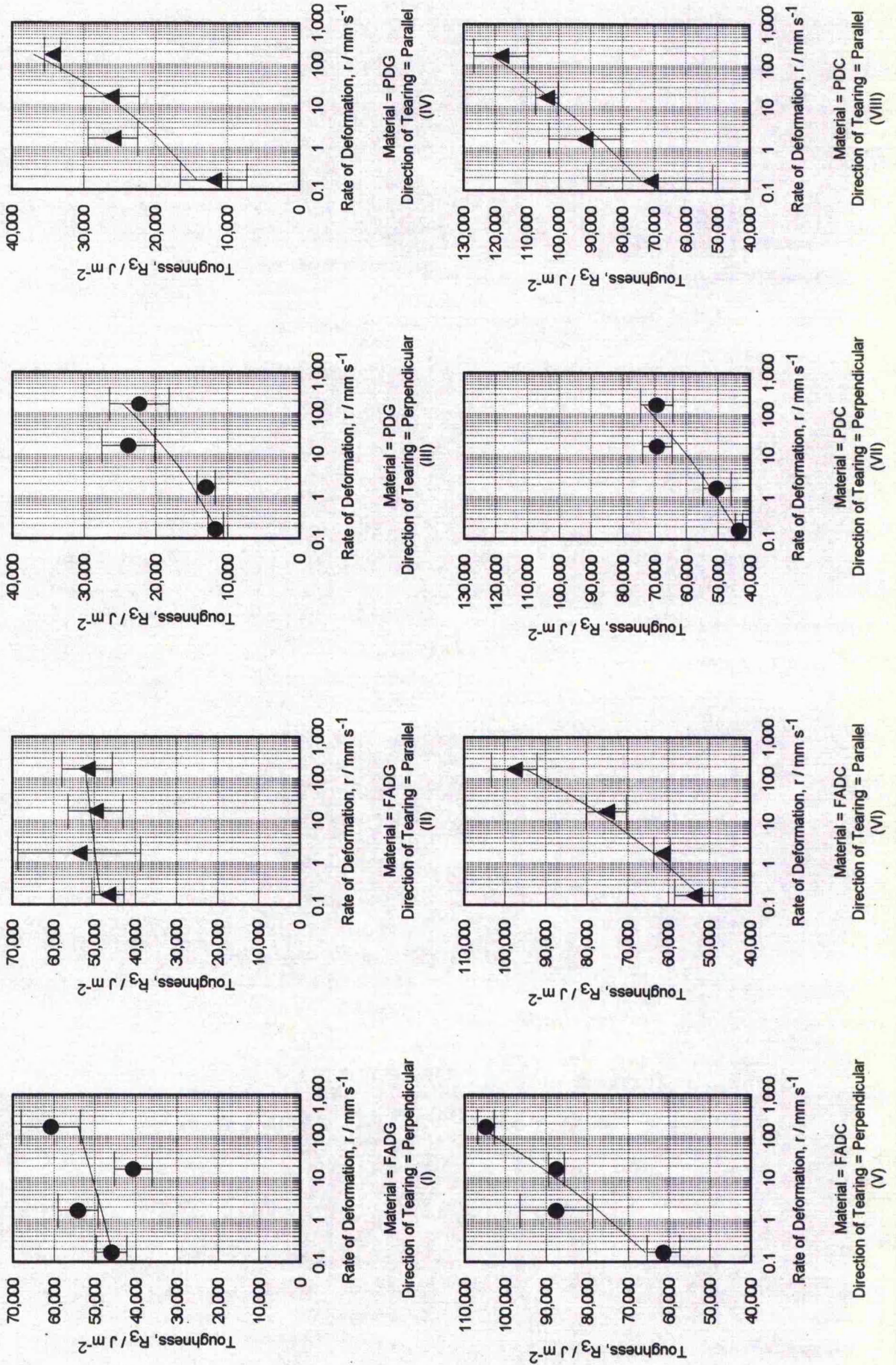


Figure 3.10

The effect of strain rate on the toughness (method 3) of FADG (12.5 % oil content), PDG, FADG (3.0 % oil content) and PDC trouser tear specimens.



Figures 3.8, 3.9 and 3.10 show the relationship between strain rate and toughness as evaluated by three different approaches. From these graphs, three features are immediately apparent:

- (i) The corium specimens are two to four times tougher than the respective grain specimens. This is true for all rates of deformation, regardless of the toughness calculation used, confirming earlier findings at a deformation rate of  $1.66 \text{ mm s}^{-1}$ .
- (ii) Where the material has been fatliquored and air dried as opposed to propanone dehydrated, higher toughness levels are observed. This trend is apparent at all rates of deformation employed in all methods of toughness evaluation.
- (iii) The three methods of calculating toughness do not produce exactly the same results although the trend of increasing toughness with increasing deformation rate is, in general, unaffected by the method of calculation. Estimates of toughness are highest when using method 2. Toughness estimates are slightly lower by using method 3 and slightly lower still by using the calculation techniques of method 1.

Figures 3.8 to 3.10 show a trend line. The equation of each trend line has a power law format. Table 3.5 summarises the equation of the trend line in each graph. Using these equations, the percentage increase in toughness by increasing the rate of deformation from  $0.16 \text{ mm s}^{-1}$  to  $166.66 \text{ mm s}^{-1}$  was calculated. Table 3.6 reports the percentage increase in toughness of each material, in each tearing direction, by all three methods of calculating the toughness.

Table 3.5

Trend Line Equations - Toughness Versus Deformation Rate.

Material	Tearing Direction	Toughness (Method 1)	Toughness (Method 2)	Toughness (Method 3)
FADG	Perpendicular	$R_1 = 41,616 r^{0.0315625}$	$R_2 = 56,525 r^{0.033125}$	$R_3 = 47,845 r^{0.0239063}$
FADG	Parallel	$R_1 = 43,199 r^{0.0160938}$	$R_2 = 56,620 r^{0.0125}$	$R_3 = 49,571 r^{0.0101563}$
PDG	Perpendicular	$R_1 = 13,447 r^{0.105625}$	$R_2 = 14,507 r^{0.123125}$	$R_3 = 14,022 r^{0.110625}$
PDG	Parallel	$R_1 = 17,979 r^{0.0975}$	$R_2 = 19,248 r^{0.14125}$	$R_3 = 18,224 r^{0.13875}$
FADC	Perpendicular	$R_1 = 74,760 r^{0.031875}$	$R_2 = 82,091 r^{0.081875}$	$R_3 = 74,621 r^{0.069375}$
FADC	Parallel	$R_1 = 76,040 r^{0.0496875}$	$R_2 = 89,623 r^{0.081875}$	$R_3 = 60,823 r^{0.08625}$
PDC	Perpendicular	$R_1 = 47,958 r^{0.0571875}$	$R_2 = 55,344 r^{0.079375}$	$R_3 = 50,326 r^{0.074375}$
PDC	Parallel	$R_1 = 55,594 r^{0.05125}$	$R_2 = 66,895 r^{0.0975}$	$R_3 = 84,089 r^{0.07125}$

Table 3.6

The Percentage Increase in Toughness Over The Range of Deformation Rates 0.16 mm s<sup>-1</sup> to 166.66 mm s<sup>-1</sup>.

Material	Tearing Direction	% Increase in R <sub>1</sub> over the range of deformation rates.	% Increase in R <sub>2</sub> over the range of deformation rates.	% Increase in R <sub>3</sub> over the range of deformation rates.
FADG	Perpendicular	24.4 %	25.7 %	18.0 %
FADG	Parallel	11.8 %	9.0 %	7.3 %
PDG	Perpendicular	107.4 %	134.1 %	144.7 %
PDG	Parallel	96.1 %	165.3 %	160.8 %
FADC	Perpendicular	24.6 %	76.1 %	61.5 %
FADC	Parallel	40.9 %	76.1 %	81.5 %
PDC	Perpendicular	48.4 %	73.0 %	67.2 %
PDC	Parallel	42.5 %	96.1 %	63.6 %

### 3.2.5 Measurement of the Hysteresis Ratio.

Stress-strain reversal loops were obtained in the positive stress and strain quadrant using dumbbell specimens of FADG, PDG, FADC and PDC materials. Specimens were strained to 20 %, 40 %, 60 % and 80 % of the elongation at break and the strain was then reversed. This procedure was repeated for various strain rates. A new specimen was used for each experiment and all specimens were cut parallel to the backbone.

In any one material, at a specified strain rate, the upward loop in the stress-strain curve of all specimens should be identical up to the point where the strains are reversed. However, this ideal situation was not apparent when testing the specimens. Indeed, the induced stress at identical levels of strain were not always the same. This phenomena was attributed to the variation in mechanical properties in materials of biological origin including leather, [Maeser, 1960].

Nevertheless, the observed level of hysteresis in each material, at each strain level, at each strain rate can be calculated as outlined in section 2.5.3. The hysteresis data are shown in Figures 3.15 to 3.18 for FADG (12.5% oil content), PDG, FADC (3.0 % oil content) and PDC specimens respectively. In each figure, graphs (I) to (IV) show plots of hysteresis versus the maximum cycle strain at rates of  $0.33 \% s^{-1}$ ,  $3.33 \% s^{-1}$ ,  $33.33 \% s^{-1}$  and  $333.33 \% s^{-1}$  respectively.

The trend curves in each graph are based on a relationship of the form:

$$\beta = K \epsilon^n$$

Where  $\beta$  is the hysteresis ratio,  $K$  is a constant,  $\epsilon$  is the maximum cycle strain and  $0 < n < 1$ . Thus, all materials are assumed to show a rapid increase in hysteresis with strain between zero and 10 % strain, as observed in some non-linear inelastic polymers [Andrews & Fukahori, 1977]. In general, when maximum cycle strains exceed 10 %, successive testing at greater strains achieves only small increases in hysteresis.

The hysteresis values also tend to decrease with increasing strain rate in all materials. The magnitude of hysteresis also varies significantly between the grain specimens and the corium specimens. For example, at a strain rate of  $3.33 \% s^{-1}$ , at 20 % strain, the trend lines predict values of  $\beta = 0.81$  for FADG specimens,  $\beta = 0.78$  for PDG specimens,  $\beta = 0.59$  for FADC specimens and  $\beta = 0.72$  for PDC specimens. The equations of the observed relationship between  $\beta$  and the maximum cycle strain for each material are shown in Table 3.7.

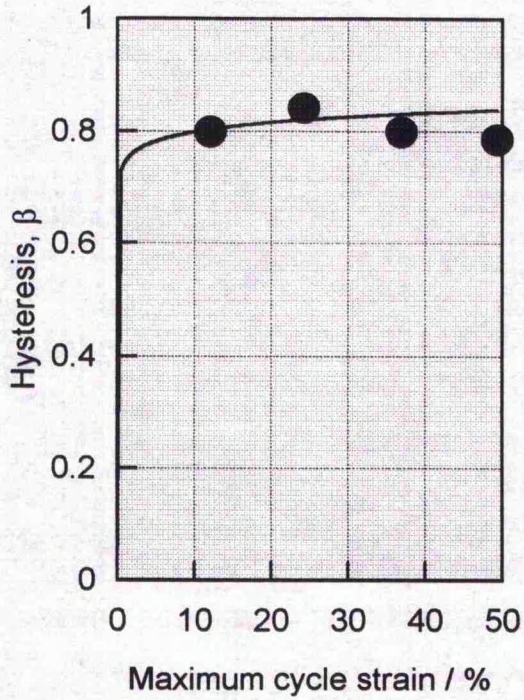
Table 3.7

Relationships between Hysteresis, Strain and Strain rate.

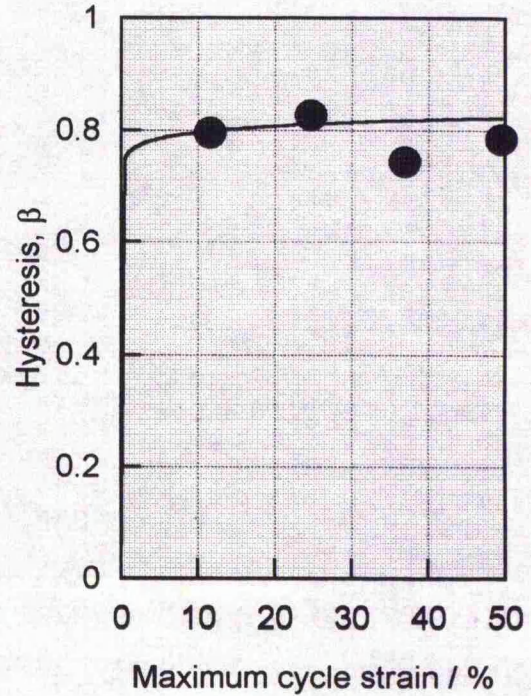
Material	Strain rate = 0.33 % s <sup>-1</sup>	Strain rate = 3.33 % s <sup>-1</sup>	Strain rate = 33.33 % s <sup>-1</sup>	Strain rate = 333.33 % s <sup>-1</sup>
FADG	$\beta = 0.745 \epsilon^{0.03}$	$\beta = 0.760 \epsilon^{0.02}$	$\beta = 0.726 \epsilon^{0.0173438}$	$\beta = 0.453 \epsilon^{0.1275}$
PDG	$\beta = 0.667 \epsilon^{0.05625}$	$\beta = 0.523 \epsilon^{0.13375}$	$\beta = 0.633 \epsilon^{0.070625}$	$\beta = 0.266 \epsilon^{0.31}$
FADC	$\beta = 0.468 \epsilon^{0.09125}$	$\beta = 0.527 \epsilon^{0.04}$	$\beta = 0.476 \epsilon^{0.070625}$	$\beta = 0.259 \epsilon^{0.2425}$
PDC	$\beta = 0.635 \epsilon^{0.03}$	$\beta = 0.675 \epsilon^{0.02}$	$\beta = 0.605 \epsilon^{0.03}$	$\beta = 0.503 \epsilon^{0.03375}$

Figure 3.11

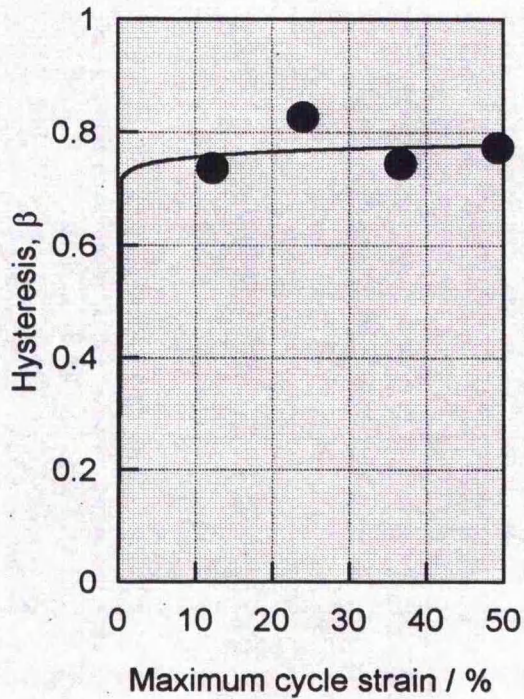
Hysteresis ratio for FADG (12.5 % oil content) at various strain rates and levels.



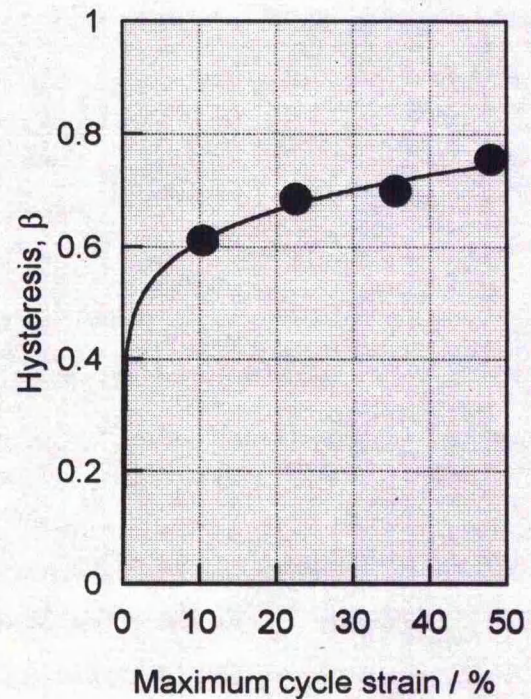
Strain rate = 0.33 % s<sup>-1</sup>  
(I)



Strain rate = 3.33 % s<sup>-1</sup>  
(II)



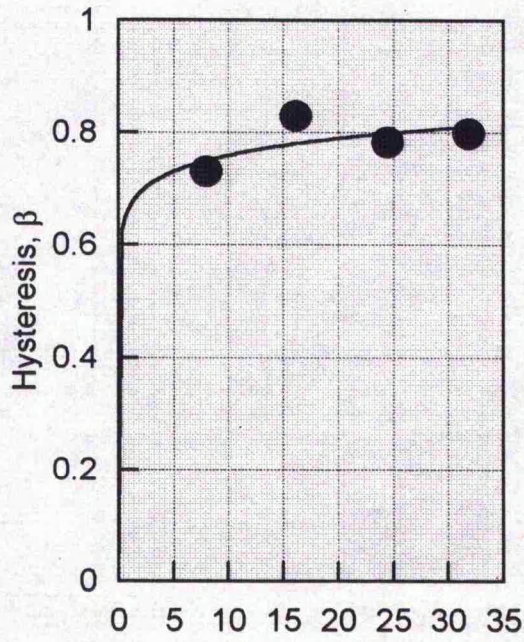
Strain rate = 33.33 % s<sup>-1</sup>  
(III)



Strain rate = 333.33 % s<sup>-1</sup>  
(IV)

Figure 3.12

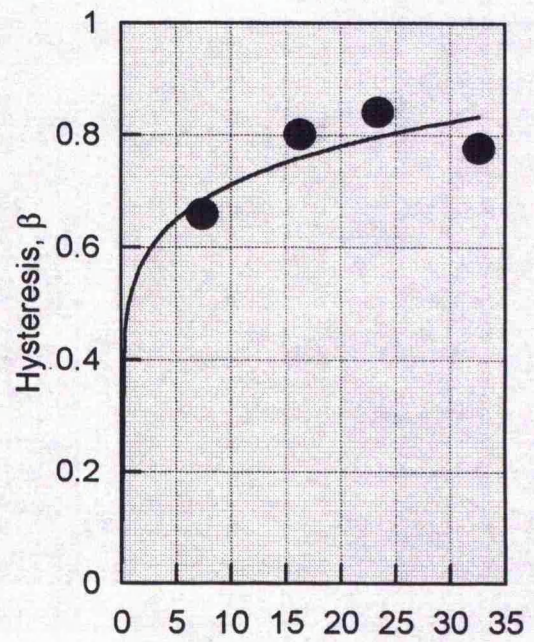
Hysteresis ratio for PDG at various strain rates and levels.



Maximum cycle strain / %

Strain rate = 0.33 % s<sup>-1</sup>

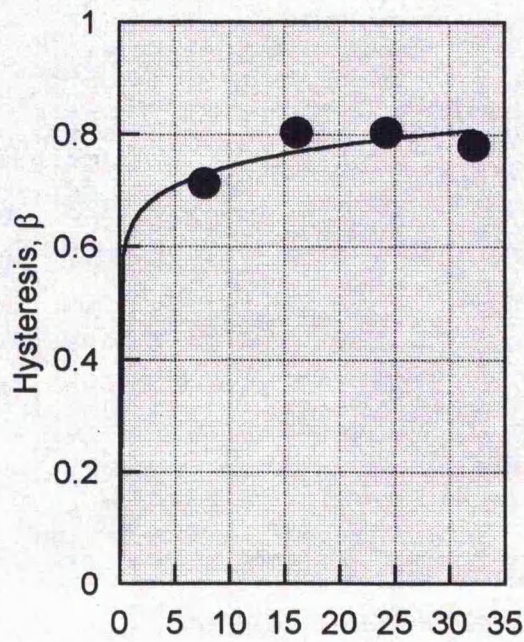
(I)



Maximum cycle strain / %

Strain rate = 3.33 % s<sup>-1</sup>

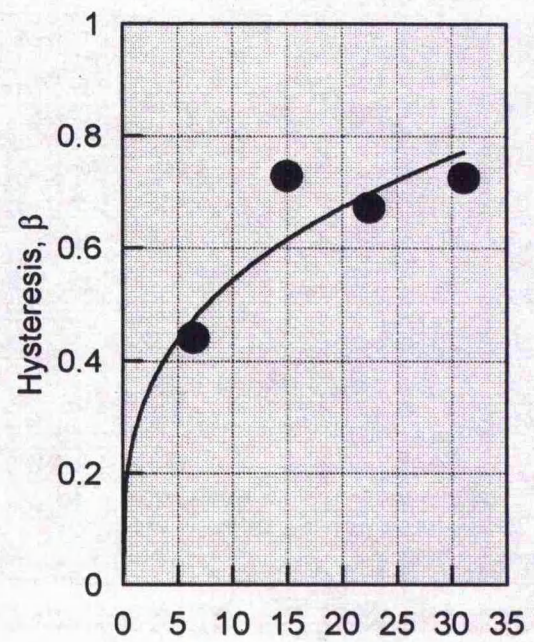
(II)



Maximum cycle strain / %

Strain rate = 33.33 % s<sup>-1</sup>

(III)



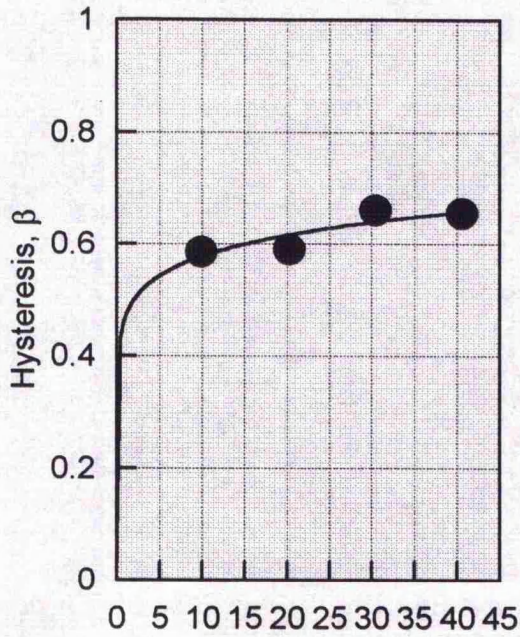
Maximum cycle strain / %

Strain rate = 333.33 % s<sup>-1</sup>

(IV)

Figure 3.13

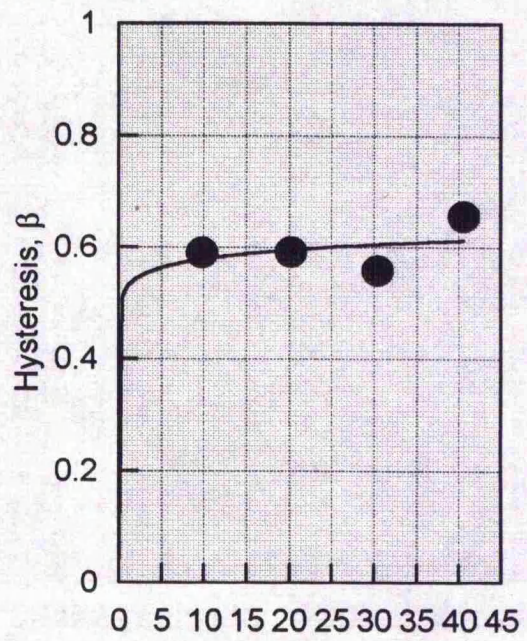
Hysteresis ratio for FADC (3.0 % oil content) at various strain rates and levels.



Maximum cycle strain / %

Strain rate = 0.33 % s<sup>-1</sup>

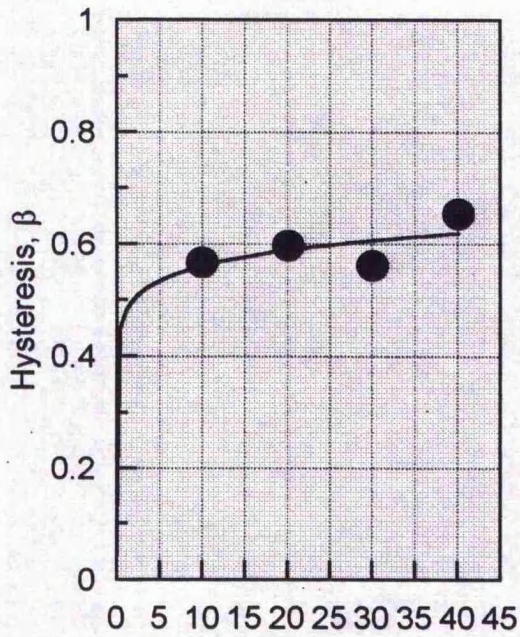
(I)



Maximum cycle strain / %

Strain rate = 3.33 % s<sup>-1</sup>

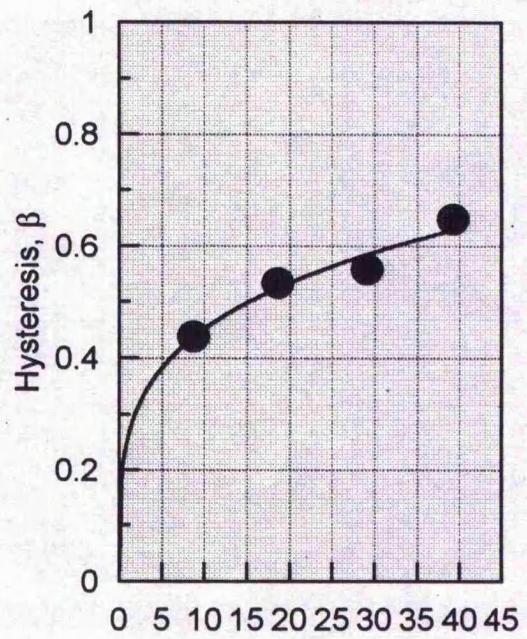
(II)



Maximum cycle strain / %

Strain rate = 33.33 % s<sup>-1</sup>

(III)



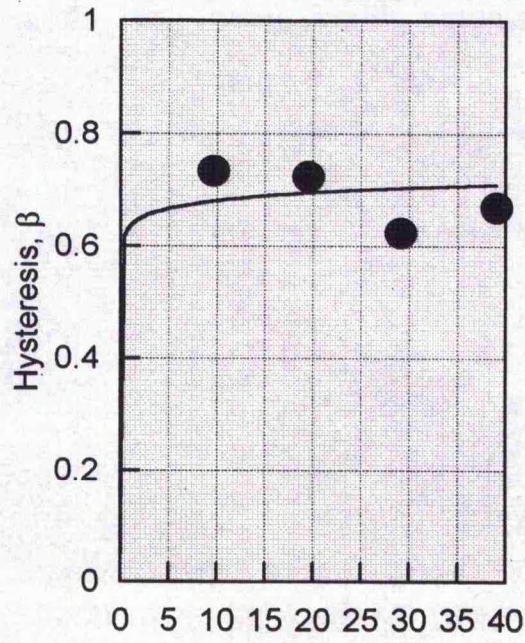
Maximum cycle strain / %

Strain rate = 333.33 % s<sup>-1</sup>

(IV)

Figure 3.14

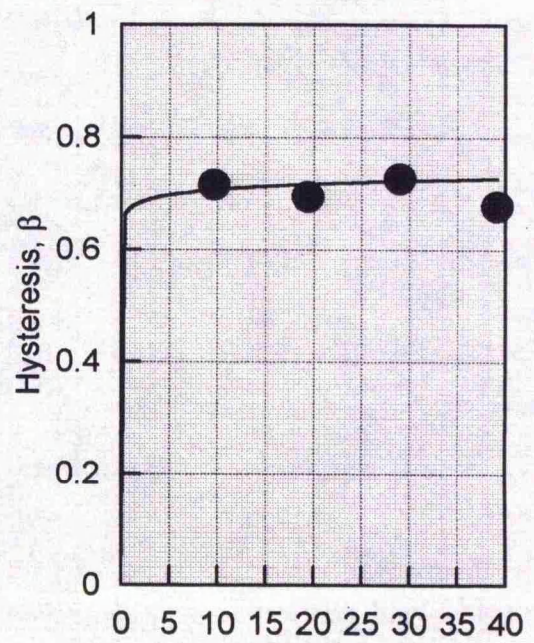
Hysteresis ratio for PDC at various strain rates and levels.



Maximum cycle strain / %

Strain rate =  $0.33 \text{ \% s}^{-1}$

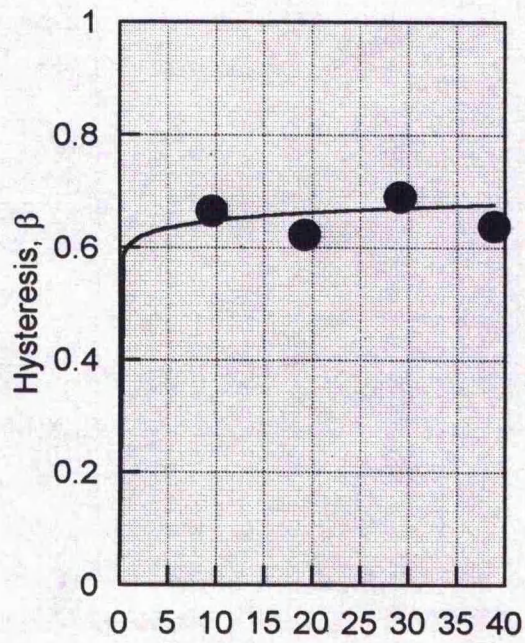
(I)



Maximum cycle strain / %

Strain rate =  $3.33 \text{ \% s}^{-1}$

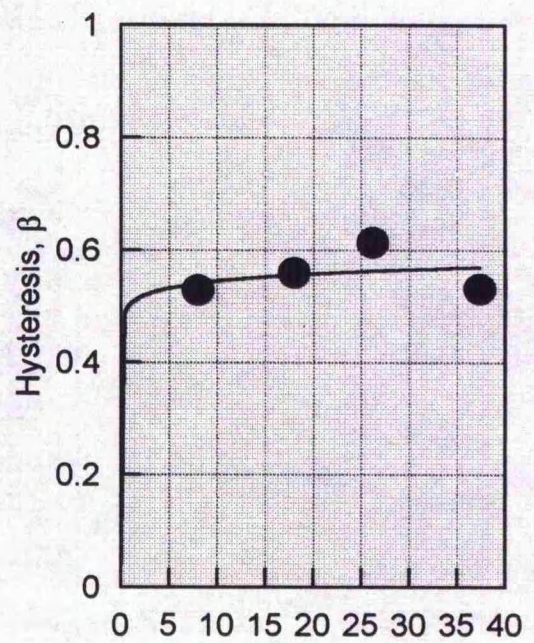
(II)



Maximum cycle strain / %

Strain rate =  $33.33 \text{ \% s}^{-1}$

(III)



Maximum cycle strain / %

Strain rate =  $333.33 \text{ \% s}^{-1}$

(IV)

### **3.3 Discussion.**

In order to discuss differences in mechanical and / or fracture properties between grain and corium materials, it is necessary (due to the differing levels of oil in fatliquored air dried grain and corium) to compare only the propanone dehydrated grain with the propanone dehydrated corium.

#### **3.3.1 Uniaxial Tensile properties.**

Uniaxial tensile tests were used to characterise the four leather materials examined. This characterisation was based on measurements of tensile moduli where the stress-strain curve is quasi-linear, measurement of the nominal stress and strain at rupture and observation of general yielding behaviour.

Maeser and Dion, [1954] evaluated the relationship between thickness and tensile strength of both grain and corium materials. They used lightly fatliquored bovine leather which is comparable to the propanone dehydrated leather (grain and corium) used in this study. The thickness of the grain material employed in this study was approximately 1 mm and the thickness of the corium material was between 3 mm and 4 mm. At these thickness, Maeser and Dion [1954] observe a tensile strength of  $10 \pm 2$  MPa for grain specimens and  $20 \pm 5$  MPa for corium specimens. The tensile strengths of the PDG and PDC materials reported in this study (see section 3.2.1) are therefore consistent with earlier work.

The extension at rupture of full substance bovine leather (adjoined grain and corium) was assessed by Vos and Vlimmeren [1973]. The latter authors focused on the effect of specimen location on tensile properties, over the entire region of a leather side. The percentage elongation at specimen rupture ranged from 35% to 75%, depending on location and orientation of the specimen. The results of section 3.2.1 generally lie within this range. However the fatliquored, air dried grain and corium specimens oriented perpendicular to the backbone rupture at strains up to 20 % higher. The specific effects of both specimen orientation and oil content on tensile properties are discussed later in sections 3.3.4 and 3.3.5 respectively.

At this point, it is appropriate to compare and contrast the tensile properties of grain and corium materials with some other common materials. Accordingly, Table 3.8 shows the tensile modulus, the tensile strength and the ultimate strain % for six common flexible materials, as well as three more rigid materials for comparison. Nevertheless, a level of caution should be adopted because the material properties can change markedly with temperature and strain rate.

Table 3.8

Material	Tensile modulus / MPa	Tensile strength / MPa	Ultimate strain / %	Reference
FADG (12.5 % oil content)	Initial = 11 (/) Final = 43 (/)	17 (/)	65 (/)	Section 3.2
	Initial = 8 (s.) Final = 32 (s.)	12 (s.)	87 (s.)	Section 3.2
FADC (3.0% oil content)	Initial = 10 (/) Final = 84 (/)	31 (/)	60 (/)	Section 3.2
	Initial = 8 (s.) Final = 55 (s.)	26 (s.)	87 (s.)	Section 3.2
Human skin in vitro (female abdomen)	Initial = 0.005 Final = 130	17	65	Daly, [1966]
Silk (cocoon thread)	7,100	600	18	Wainwright et al [1976]
Typical rubber vulcanizate	N/A	1.4	320	Greensmith, [1960]
Polyvinyl acetate / chloride	N/A	30→35	200→400	Higgins, [1977]
Flexible Polyvinyl chloride (PVC)	N/A	7→25	240→380	Higgins, [1977] & Atkins & Mai [1988]
Polyethylene	< 200	12	90→650	Higgins, [1977] & Sinnot, [1991]
Teflon (PTFE)	< 1000	17→25	200→600	Higgins, [1977]
Human nail	4,500	18	14	Duck, [1990]
Mild steel	210,000	430	< 1	Sinnot, [1991]

Human skin, like bovine leather, has a low initial modulus and a final tensile modulus that is significantly higher, indicative of 'J' shaped stress-strain behaviour. However, the initial modulus of human skin is 3 orders of magnitude lower than either grain or corium materials and the final tensile modulus of human skin is 2-3 times higher than observed in either grain or corium materials. Nevertheless, both the tensile strength and the ultimate strain of leather and human skin are comparable.

Details of other flexible materials are also included in the Table 3.8: rubber

vulcanizates (typical application: tyres); polyvinyl acetate / chloride (typical application: upholstery and covering for wires and cables); flexible Polyvinyl chloride (PVC) (typical application: imitation leather cloth); Polyethylene (typical application: plastic bags). In these flexible materials, the tensile strengths are again comparable to grain and corium material. However, the fracture strains of these materials are considerably higher.

The results of section 3.2.1 also show that, for both grain and corium at a nominal strain level of approximately 7%, a kink in the stress-strain curve is observed. At this level of strain the reduction in specimen thickness and/or specimen width is negligible. Thus the nominal stress values are tantamount to the true stress values. Accordingly, it is safe to say that an extrinsic yield point occurs at a nominal strain of approximately 7%.

Directly after the yield point, little or no strain softening in grain or corium specimens is apparent in the respective stress-strain curves. As nominal strains increase, the respective stress-strain curves indicate that grain and corium specimens experience orientation or strain hardening. The profile of these curves are similar to those given by some crystalline polymers and fibre-forming glassy polymers which show a high degree of molecular orientation on drawing. In these materials, the rapid orientation hardening masks any possible strain softening [Kinloch & Young, 1990].

**3.3.2 Tearing and the specific work of fracture.**

The results in section 3.2.2 reveal that the specific works of fracture (or toughness) of the grain and corium, are both high when compared to many metals, polymers and rubbers. Accordingly, the grain can be regarded as a 'tough' material and the corium regarded as an 'exceptionally tough' material. Table 3.9 compares the specific work of fracture (R) for several materials.

Table 3.9

Material	Specific work of fracture, R / kJ m <sup>-2</sup>	Reference
FADG (12.5 % oil content)	40→50	Section 3.2
FADC (3.0 % oil content)	80→90	Section 3.2
Rat skin	20→30	Purslow, [1980]
Rabbit skin	20	Atkins & Mai, [1988]
Medium carbon steel	14	Atkins & Mai, [1988]
Rubber vulcanizates	37 @ slow rates.	Ward, [1983]
Flexible polyvinyl chloride (PVC)	45	Kendall, [1979]
High density polyethylene	33	Kendall, [1979]
Teflon (PTFE)	8	Atkins & Mai, [1988]
Titanium alloys (Ti-6Al-4V)	49	Atkins & Mai, [1988]

The grain material is tougher than many polymers and the corium significantly tougher still. The specific work of fracture of the grain is comparable to rat and rabbit skin. However, the corium is very tough, exceeding the specific work of fracture of titanium alloys.

In discussing the toughness of leather, it is interesting to note (from section 3.2.1), that the stress-strain curve of both grain and corium materials are approximately 'J' shaped. A proposal by Gordon [1978] that materials with a 'J' shaped stress-strain curves are 'more difficult to tear' generated considerable discussion, theoretical analysis and experimental evidence in support of, and in opposition to Gordon's argument [eg Kendall & Fuller, 1987 and Mai & Atkins, 1989]. Gordon [1978] argued that the early horizontal portion of a 'J' shaped curve reflects a lack of shear connectivity in the material. This lack of shear connectivity means it is difficult to concentrate energy into the path of an existing crack and therefore such materials are difficult to tear.

Mai and Atkins [1989] recognised that while many 'J' shaped materials can be easily cut or pierced, the deformation in such conditions is extremely localised. In tests such as the trouser tear test, energy must be fed to the crack site from remotely loaded regions. By testing an elastic material with a 'J' shaped stress-strain curve, significant strains must be achieved in the specimen legs, before the strain energy at the crack site is sufficient to ensure tearing. Accordingly, the materials are 'difficult to tear'.

Leather is based on a biological tissue, skin, which has been chemically modified. The collagen macromolecules have been chemically crosslinked (tanned) to provide increased thermal stability and resistance to microbial attack. Nevertheless, the tearing resistance of biological tissues and leather should be comparable. Purslow [1989a] identified two key factors involved in the tearing resistance of such materials:

- (i) The strain energy stored in the legs of the specimen.
- (ii) The nature of the load-stroke profile during the test.

The strain energy stored in the legs of a trouser tear test specimen can be assessed by considering two regions of the load-stroke profile; (i) the region of pre-tearing and (ii) the region of unloading. In the region of pre-tearing, the specimen legs are being strained and in the region of unloading, the strain is being reversed.

The results of section 3.2.2 show the legs of the trouser tear specimens are subject to some deformation. To assess the most appropriate method(s) for calculating the toughness of these materials, a theoretical analysis is required. The analysis considers the extension of the legs in different material specimens and the consequential affect on each method of calculation. The behaviour of the specimen legs is considered in terms of the strain in the legs, the strain energy density in the legs and the levels of elasticity / plasticity in the legs.

### **3.3.2 (a) Analysis: The specific work of fracture calculation methods.**

The loading-unloading traces for trouser tear tests are generally straight. However, some 'J' shaped behaviour is observed in the loading-unloading regions of corium specimens. Mai and Atkins [1989] assert that if 'J' shaped behaviour is shown in the trouser tear test loading-unloading traces, the toughness of an elastic material is effectively increased. They calculate the specific work of fracture, (R) as,

$$R = 2X_f / t + [2n/(n+1)]/C^{1/n}(X_f/t)^{(n+1)/n}$$

where  $X_f$  is the plateau tearing force,  $t$  is the specimen thickness,  $n$  is the exponent in  $(\sigma = \sigma_0 \epsilon^n)$  to give the non-linear load-stroke behaviour on loading and unloading and  $C = w\sigma_0$  where  $w$  is the width of specimen legs.

However with the materials examined in this study, the numerical value of the expression  $[2n/(n+1)]/C^{1/n}(X_f/t)^{(n+1)/n}$  is insignificant and  $< (1 \times 10^{-5}) \text{ J m}^{-2}$ . Accordingly, it was considered more appropriate to examine linear load-stroke behaviour on loading and unloading the trouser specimens. To examine differences in the three methods of toughness calculation, three different trouser tear test load-stroke profiles are analysed:

- (i) The load-stroke profile of a linear elastic material where the leg extension is insignificant.
- (ii) The load-stroke profile of a linear elastic material where the leg extension is significant.
- (iii) The load-stroke profile of an elastic-plastic material where leg extension is significant.

**(i) Insignificant leg extension in a linear elastic material.**

Where leg extension is insignificant, the loading-unloading sections of the load-stroke trace would be essentially vertical. Indeed, the load stroke profile for a linear elastic material would resemble Figure 3.15 (I) [Mai & Atkins, 1989]. To

calculate the work of fracture by the energy method ( $R_1$ ), the work area, represented by area OABC, is divided by the area of crack produced in the specimen. However, under the conditions shown in Figure 3.15 (I) the following relationships are apparent:

$$\begin{aligned} \text{Crack area} &= \frac{1}{2} \text{Length AB} \cdot t && \text{(where } t \text{ is the specimen thickness)} \\ \text{Area OABC} &= \text{Length AB} \cdot X && \text{(where } X \text{ is the plateau tearing force)} \\ W_0 &\rightarrow 0 && \text{(where } W_0 \text{ is the strain energy density in the legs)} \\ \lambda &\rightarrow 1 && \text{(where } \lambda \text{ is the extension ratio in the legs)} \end{aligned}$$

From Equation 2.9

$$R_1 = \text{Energy Used} / \text{Area Cleaved} \quad [2.9]$$

$$R_1 = \text{Area OABC} / \text{Crack area} \quad [3.1]$$

$$R_1 = \text{Length AB} \cdot X / \frac{1}{2} \text{Length AB} \cdot t \quad [3.2]$$

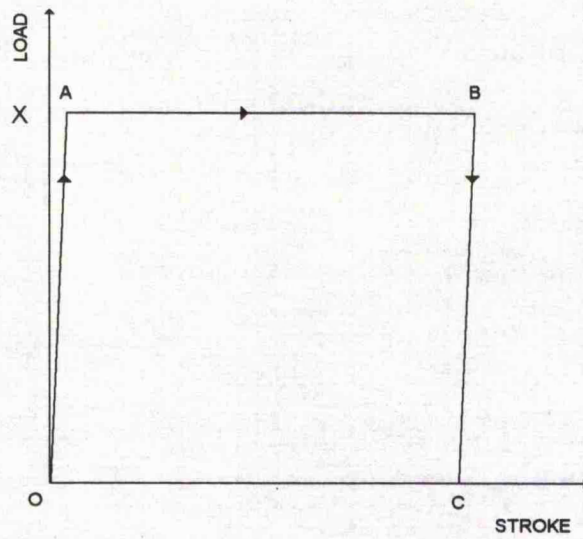
$$R_1 = 2 X / t$$

Therefore  $R_1 = R_3 \quad [3.3]$

Under conditions of linear elasticity where deformation in the specimen legs is insignificant ( $\lambda \rightarrow 1$ ) and negligible strain energy is stored in the legs ( $W_0 \rightarrow 0$ ), the Rivlin and Thomas equation [1953] shown as  $R_2$  in Equation 2.11, reverts to  $2 X / t$ . Therefore  $R_2 \rightarrow R_1$  and  $R_2 \rightarrow R_3$ .

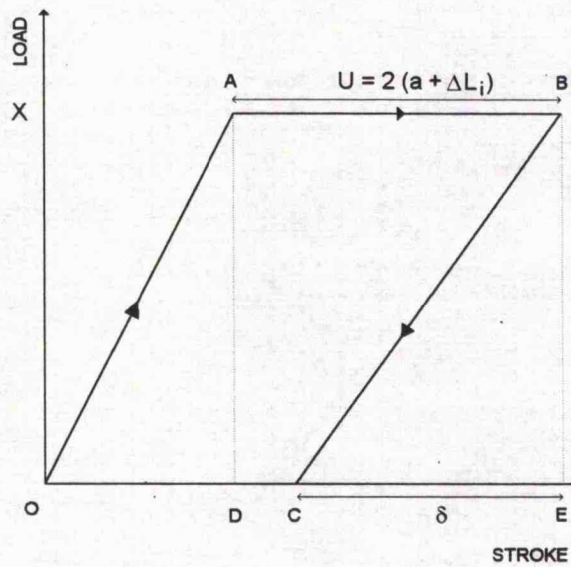
Figure 3.15

The load-stroke profile of trouser tear tests.



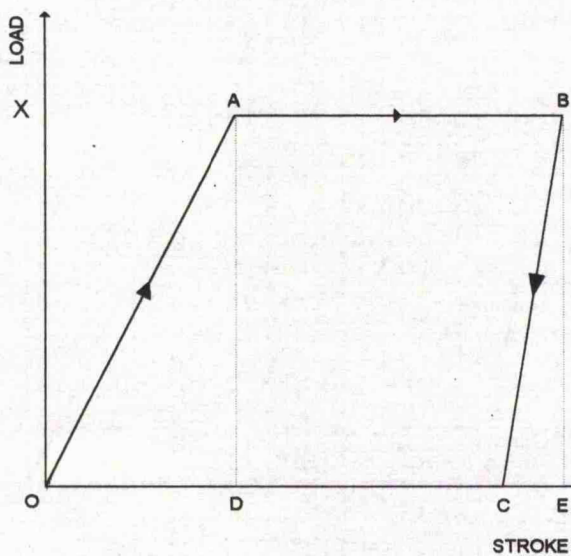
(I)

Loading - Unloading profile where elastic deformation in the legs is insignificant.



(II)

Loading - Unloading profile where linear elastic stretch in the legs is important.



(III)

Loading - Unloading profile where plastic deformation in the legs is important.

**(ii) Significant leg extension in a linear elastic material.**

According to Figure 3.15 (II) the gradient of line AB is greater than the gradient of line BC. At first sight, this seems to imply more energy is returned on unloading than when supplied on loading the specimen legs to ensure tearing. This phenomenon is observed because, as the tear propagates through the specimen, the length of each leg is effectively increasing and therefore the elastically stored strain energy in each leg must also have increased.

Atkins and Mai [1988, p102] analysed the trouser tear test where the specimen legs are linear elastic and can store strain energy. The expression arrived at for the specific work of fracture, using the graphical method of Atkins & Mai [1988], is comprehensively derived in Appendix 5. Using this method, the specific work of fracture (R) is given by equation [3.4].

$$R = X^2 / w t^2 E + 2 X / t \quad [3.4]$$

Examination of equation [3.4] reveals that as the tensile modulus  $E \rightarrow \infty$ , (shown in Figure 3.15 (II)) the specific work of fracture expression reverts to  $R = 2 X / t$ , i.e.  $R_3$ . However, in addition to the assumption of linear elasticity, the other assumptions made in the analysis are strict. In essence, the analysis assumes the tearing force (X), the stress in the growing trouser legs and the strain in the growing trouser legs are constant.

From Table 3.1 and the specimen dimensions, using PDC specimens, it is possible to see the magnitude of the term  $(X^2 / w t^2 E)$  in equation [3.4].

$$X = 125 \text{ N}$$

$$w = 12.5 \times 10^{-3} \text{ m}$$

$$\sigma = (\text{Load at continuous tear propagation} / wt)$$

$$\sigma = 130 / (12.5 \times 10^{-3} \times 4 \times 10^{-3}) = 2.6 \times 10^6 \text{ Pa}$$

$$\epsilon = (\text{Stroke at continuous tear propagation} / 2 \times \text{original leg length})$$

$$\epsilon = 16.42 / 40 = 0.41$$

$$E = \sigma / \epsilon = 2.6 \times 10^6 / 0.41 = 6.34 \times 10^6 \text{ Pa}$$

Therefore, from equation [3.4], in the case of PDC specimens tested at a rate of  $1.66 \text{ mm s}^{-1}$ , where the direction of the tear was parallel to the backbone,

$$R = X^2 / w t^2 E + 2 X / t$$

$$R = 12,323 + 62,500$$

$$R = 74,823 \text{ J m}^{-2}$$

The specific work of fracture,  $R$ , obtained from equation [3.4] is significantly higher than obtained utilising any other method. It would seem that if the material does not comply with the assumptions made in deriving equation [3.4] (i.e. linear elasticity etc), its application becomes dubious. It is contended here that equation [3.4] significantly overestimates the toughness of leather because, in deriving equation [3.4], two non-linear terms are introduced. These terms amplify the disparity in mechanical properties between the fully elastic case and the elastic-plastic case, where significant energy dissipation is observed. As noted in section

3.2.5, leather is highly energy dissipating when deformed. Accordingly, this method of calculating the specific work of fracture was not adopted in this study.

In calculating  $R_2$ , the toughness varies if the strain level and / or strain energy in the specimen legs becomes significant, [Rivlin and Thomas, 1953]. The nature of these variations can be explored by examining equation [2.11]. This equation can be rearranged to produce an expression for  $R_2$  in terms of the plateau tearing force, the strain in the legs and the specimen thickness.

$$\text{From } R_2 = (W_o A_o - 2 \lambda X) / t^8 \quad [2.11]$$

$$\begin{aligned} \text{Where } W_o &= \text{Energy density in specimen legs} \\ W_o &= \text{Area OAD} / (t_t \cdot w_t \cdot l_t) \end{aligned} \quad [3.5]$$

where  $t_t$  is the true thickness of the legs at tear propagation,  $w_t$  is the width of the legs at tear propagation and  $l_t$  is the length of the specimen legs at tear propagation.

$$\begin{aligned} A_o &= \text{Original cross-sectional area of legs} \\ A_o &= (t_o \cdot w_o) \end{aligned} \quad [3.6]$$

where  $t_o$  is the original thickness of the legs and  $w_o$  is the original width of the legs.

---

<sup>8</sup> Equation [2.11] is not identical to the equation derived by Rivlin & Thomas [1953]. However, (t) is required for dimensional correctness.

Equation [2.11] has also been applied by Purslow [1989a] to calculate the toughness of rat skin.

Assuming the thickness and width of specimen legs remain unchanged, i.e.

$t_t \rightarrow t_o$  and  $w_t \rightarrow w_o$  then,

$$W_o A_o = \text{Area OAD} / l_t \quad [3.7]$$

Assuming,

$$\text{Area OAD} = \frac{1}{2} \text{Length OD} \cdot X$$

$$l_t = l_o + \Delta l$$

$$\Delta l = \text{Length OD}$$

Substituting into [3.7],

$$W_o A_o = (\frac{1}{2} \text{OD} \cdot X) / (l_o + \Delta l)$$

$$W_o A_o = (\frac{1}{2} \text{OD} \cdot X) / (l_o + \text{OD})$$

$$W_o A_o = \frac{1}{2} X / (l_o/\text{OD} + \text{OD}/\text{OD})$$

$$W_o A_o = X / 2 (1/\epsilon + 1) \quad [3.8]$$

Taking (  $2 \lambda X$  )

$$2 \lambda X = 2 X (1 + \epsilon)$$

$$2 \lambda X = 2 X + 2 X \epsilon \quad [3.9]$$

Substituting [3.8] and [3.9] into equation [2.11]

$$R_2 \cdot t = W_o A_o - 2 \lambda X$$

$$R_2 \cdot t = X / 2 (1/\epsilon + 1) - [ 2 X - 2 X \epsilon ]$$

$$R_2 \cdot t = 2 X [ (1 / 4(1/\epsilon + 1)) - 1 + \epsilon ]$$

$$\therefore R_2 = 2 X / t \cdot [ (\epsilon / 4(1 + \epsilon)) - 1 + \epsilon ] \quad [3.10]$$

$$R_2 = - R_3 \cdot D \quad [3.11]$$

where  $D = (\epsilon / 4(1 + \epsilon)) - 1 + \epsilon$  [3.12]

Assuming linear elastic deformation in the legs of the specimen and a tear length of  $\frac{1}{2}AB$ , a simplified expression is obtained for  $R_2$  in terms of the plateau tearing force, the specimen thickness and the strain in the legs of the specimen. The toughness expression  $R_2$  of equation [3.10] is dependent on  $2X / t$  (i.e.  $R_3$ ) multiplied by a factor  $D$ . When  $\epsilon \rightarrow 0$  then  $D \rightarrow -1$  and  $R_2 = R_3$ .

**(iii) Significant leg extension in an elastic plastic material.**

A simplified profile of the load-stroke behaviour generally observed in leather is shown in Figure 3.15 (III). It is immediately apparent that, unlike Figure 3.15 (II), the gradient of line CB is greater than the gradient of line OA and this feature is surprising. Under elastic conditions (i.e. Figure 3.15 (II)) the gradient of line CB is less than the gradient of line OA because the leg length increase of the trouser tear specimen ensures the legs are more compliant when the strain is reversed. The fact that the gradient of line CB is greater than the gradient of line OA in Figure 3.15 (III) means that although the specimen legs have become longer, they are actually less compliant instead of more compliant (as would be expected).

The above feature implies that the tensile modulus of the specimen legs has increased as a direct result of strain application. The increase in tensile modulus is attributed to the specimen legs becoming highly oriented as they are strained during the trouser tear test procedure. Accordingly, the legs are subject to a process often described as 'orientation hardening' [Kinloch and Young, 1990].

The energy expended to strain the legs in the pre-tearing region is represented by area OAD. That part of the energy stored elastically in the final length of legs and therefore returned on unloading is represented by area BCE. In the elastic circumstances of Figure 3.15 (II), Area BCE > Area OAD because the length of each leg has increased. Consequently, more energy is returned on unloading the longer legs than is initially supplied to the shorter legs before the tear advances.

However, in the elastic-plastic circumstances of Figure 3.15 (III) where orientation hardening has occurred in the specimen legs, Area BCE  $\ll$  Area OAD. Thus, despite the length increase of each leg, the energy returned on unloading the longer legs is markedly less than the energy initially supplied to the legs before the tear advances.

The Area OAD in Figure 3.15 (III) represents the energy supplied to the original leg lengths before tear propagation. The Area ABCD represents the energy supplied while the specimen is tearing. A portion of this energy is used to propagate the tear and the remaining portion is used, as a result of tear propagation, to sustain sufficient strain energy in the increasing length of each leg. This latter division of energy can be calculated directly under elastic conditions (i.e. Area BCE - Area OAD in Figure 3.15 (II)).

Under elastic-plastic conditions, the Area ABCD still represents the energy supplied while tearing the specimen. Again, a portion of this energy can be attributed to the creation of new surfaces and the remaining portion attributed to sustaining sufficient strain energy in the increasing length of each leg. However, in elastic-

plastic conditions, energy is absorbed in (i) the tearing process itself and (ii) sustaining sufficient strain energy in the legs as the tear propagates. In essence, during tear propagation, supplied strain energy can be divided into four processes:

- (i) Energy is used in the creation of new surface area.
- (ii) Energy is absorbed in the region of the advancing tear.
- (iii) Energy is used to sustain strain energy in the increasing length of each leg as the tear advances.
- (iv) Energy is absorbed when previously unstrained material becomes strained as the length of each leg increases.

Unfortunately, complete energy partition of these four factors is not directly possible from load-stroke data. Nevertheless, it is possible to account for some energy dissipation in calculating the specific work of fracture.

Area BCE (Figure 3.15(III)) represents the energy returned from the increased leg lengths. Clearly, the energy returned from the increased leg length will be greater than the energy returned if the strain in the original leg length were reversed at point A (Figure 3.15 (III)). Thus, in calculating the effective work area, by subtracting Area BCE from OAD, we have completely accounted for the energy absorbed in the legs before tearing occurs as well as some (but not all) of the energy absorbed in process (iv) above.

The effective work area used to create a tear of length,  $l$ , was derived using equation [3.15].

$$\text{Effective work area} = \text{Area OABC} - (\text{Area OAD} - \text{Area BCE}) \quad [3.15]$$

$$\text{Effective work area} = \text{Area OAD} + \text{Area ABCD} - \text{Area OAD} + \text{Area BCE}$$

$$\text{Effective work area} = \text{Area ABCD} + \text{Area BCE} = \text{Area ABED} \quad [3.16]$$

or

$$\text{Effective work area} = \text{Area OABE} - \text{Area BCE} - \text{Area OAD} + \text{Area BCE}$$

$$\text{Effective work area} = \text{Area OABE} - \text{Area OAD} = \text{Area ABED} \quad [3.17]$$

The effective work area in equation [3.15], divided by the created crack area, produces a value of toughness ( $R_1$ ) that 'accounts' for all non-elastic behaviour in the legs of the specimen before tearing commences and some non-elastic behaviour in the legs during tear propagation. Any plastic deformation or hysteresis in the legs of the specimen is an energy dissipating process and separate to the fracture process. By discounting the energy dissipated in deforming the legs, the toughness (calculated by dividing the effective work area by the created tear area) is reduced.

However, intrinsic in the calculation of  $R_2$  and  $R_3$  is the assumption of elasticity. If the material is not elastic, some of the strain energy supplied to the legs in the pre-tearing region is absorbed as either hysteresis or plastic deformation. Accordingly, the transmission of strain energy through the legs is slowed with respect to the applied strain. This process ensures that the strain level and the strain energy supplied to the legs is higher in the region of pre-tear than would be the case if the material were elastic. Calculations of toughness  $R_2$  and  $R_3$  effectively assume that the higher strain in the legs and the greater amount of energy supplied in the pre-tearing region are inherent in the fracture process. Consequently,  $R_2$  and  $R_3$  are higher than  $R_1$ , where any energy dissipation in the pre-tearing region is discounted.

Estimates of the toughness of FADG (12.5 % oil content), PDG, FADC (3.0 % oil content) and PDC specimens are shown in section 3.2.2. The results are in complete accordance with the theoretical analysis in that  $R_1$  predicts the lowest values and  $R_2$  predicts the highest values. The method of calculating  $R_1$  involves separating any energy dissipation (plastic deformation and/or hysteresis) in the legs of the specimen during the pre-tearing region, from energy expended during the tearing process. Consequently  $R_1$  can be thought of as a more authentic assessment of toughness as the condition of elastic behaviour in specimen legs is not intrinsic to the calculation.

However, toughness calculations  $R_2$  and  $R_3$  are useful to highlight the effect of energy dissipation. In particular,  $R_2$  and  $R_3$  highlight that energy dissipation in the specimen legs increases the 'apparent toughness', as measured by the respective methods.

Purslow [1989a], also used these three methods to calculate the specific work of fracture of rat skin. However, he reports (applying the nomenclature of this work) that  $R_1 \approx R_2$  and  $R_3$  is lower. In Purslow's calculation of  $R_1$ , the work expended during the test is calculated as the energy represented by the total area under the load-deflection curve (i.e. the assumption of elasticity is implicit). Accordingly, no account was taken of the energy dissipated in the specimen legs prior to tearing and, as a result, the toughness  $R_1$  is higher.

The remaining factor implicated in the tearing resistance of biological tissues and leather is the nature of the load-stroke profile during tearing. In the next section the tearing behaviour, shown in the load-stroke profiles of grain and corium materials, is discussed.

### 3.3.2 (b) The nature of the load-stroke profile during a trouser tear test.

No published work is concerned specifically with the tearing mechanisms of leather. This point was recognised by Guy and Marriott [1975] who considered the tearing resistance of leather and compared test results from several test geometries. Their most pertinent observation was that the tearing of leather is not catastrophic. Since the leather used in this study is a flexible material, the tearing process of leather can be profitably compared and contrasted with another flexible material, rubber, which has received considerable attention as far as tearing mechanisms are concerned.

The tearing behaviour of elastomers was studied extensively by Greensmith and Thomas, [1955] who classified the tearing of elastomers into two categories: (i) a steady tearing process and (ii) a stick-slip process. A steady tearing process is characterized by the plateau tearing force, the rate of tear propagation remaining essentially constant. A stick-slip process is characterized by regular fluctuations in the plateau tearing force and regular variations in the rate of tear propagation.

An additional category was identified by Stacer et al [1985a]. When testing rubber vulcanizates, these authors recognised two types of slip-stick behaviour, knotty tearing and sawtooth tearing. Knotty tearing is characterized by a tendency for the tear to circle around and propagate for a short period against its original direction, thus creating knots in the specimen. The force response during knotty tearing gradually increases with stroke until a maximum is reached. At this point, the force drops rapidly until a minimum is reached. The phenomena then repeats cyclically throughout the remainder of the test. The force rising to the maximum is associated with creating the knot in the specimen and the rapid drop in force, is

associated with rapid tear propagation. The maxima and minima force values in any one cycle are not necessarily identical to those of any other cycle.

Saw-tooth tearing is also a form of stick-slip tearing where force fluctuations are evident. However, the fluctuations observed in saw-tooth tearing are not as high, and more numerous than those observed with knotty tearing. In addition, the plateau tearing force is not as high as observed with knotty tearing. Differences between knotty and saw-tooth tearing were attributed to the differences in the tear path. Unlike the knotty tearing, the tear path with saw-tooth tearing does not deviate appreciably from the intended path. Additionally, when saw-tooth tearing occurs, no tear growth in any direction, can be observed when the force is rising to a maximum. However, tear tip deformation is usually visible. With both knotty tearing and saw-tooth tearing, the force peaks can be matched with a feature on the surface of the torn specimen after the test.

The tearing resistance of rubber often increases when particulate is added during manufacture. The increase in tear strength can be directly attributed to an enhanced level of energy dissipation, as well as an increase in tear deviation (i.e. knotty tearing), Gent [1978].

Fluctuations in the plateau tearing force of leather are not as severe as those noted in knotty tearing and no regular fluctuation pattern is observable (see Figure 3.4). However, like knotty tearing, the force values at maxima and minima, during a cycle around the plateau tearing force, are not constant throughout the test. Nevertheless no 'knotty' type features are observed in the specimen after the test and the tearing does not appear unstable. Consequently the tearing behaviour observed in leather is perhaps more analogous to the saw-tooth behaviour

described by Stacer et al [1985a]. Unfortunately, a complete analogy is not possible because the numerous force peaks cannot be matched with any distinguishable feature on the surface of the torn specimen after the test.

The force fluctuations observed with leather specimens seem significantly more complex than described by the rubber tearing processes. In tearing both grain and corium specimens a principal irregular trend of tangible force fluctuations is observed. However, contained within each of these discernable maxima and minima are further small but tangible fluctuations.

In rubber specimens, the force fluctuations are attributed to unstable tearing. These instabilities can be traced to viscoelastic processes in the rubbery network, [Stacer and Kelly, 1985b]. However, the tearing of leather does not appear either highly unstable or catastrophic because continuous tearing of the specimen is observed once the tear has initiated and tearing ceases the moment the strain is stopped or reversed. Purslow [1989a] points out that the marked oscillations in the plateau tearing force are common to most biological connective tissues and may have a common cause in that the tear must propagate through a fibrous network of collagen. In addition, the oscillations around a plateau tearing force are observed in paper, where the tear must propagate through a cellulose network of fibres [Corte, 1982].

In light of the factors contributing to the oscillating plateau tearing force in other materials, two factors are responsible for the observed plateau tearing force fluctuations of leather: (i) the network or feltwork of tanned collagen fibres and (ii) the level of energy dissipation observed during tear.

With regard to the initial factor, leather is purported to have a general pattern of inter-weaving fibres [Demsey, 1968]. However in reality, leather is a complex, 3-dimensional, non-woven arrangement of fibres that has no structured repeat units so far as fibre arrangement is concerned. In addition, the fibres in other collagenous materials like aortic media, are known to re-arrange around an advancing tear [Purslow et al, 1984]. Thus, it seems probable this rearrangement will also occur in leather material.

In considering the energy dissipated once continuous tearing ensues, it is important to note the viscoelastic nature of leather during deformation and rupture. Leather shows both hysteresis and plastic deformation during a cycle of deformation (see section 3.2.5). Whilst the tear is propagating, previously unstrained material becomes strained and material currently strained is probably subject to small cyclic deformations. Accordingly, energy is dissipated throughout the tearing process. In light of the oscillating plateau tearing force, energy dissipation is not constant throughout the tear process.

In addition, both the feltwork of tanned collagen fibres and the energy dissipation observed during tear, affect the radius of the tear tip. Consequently, the radius of the tear tip will alter during tear propagation. It therefore seems likely that no variable determining the precise tearing force (at any one point in time) undergoes a regular repetition of values. Indeed, the variables that affect the precise tearing force are probably aperiodic. When considering the non-linear mechanical behaviour of leather, it is probable that the factors influencing the tearing force are non-linear.

Any possible effect of structural re-arrangement, energy dissipation and/or crack

tip sharpness on the precise tearing force are all dynamic because of the nature of the test. The most common types of dynamic systems are differential ones, where the relevant variables change in a smooth or continuous way. This enables the rules governing the changing state of the system to be expressed as differential equations. Accordingly, given the state of the dynamic system at one particular point in time and the evolution equations, it is possible to calculate the state of the system at other points in time. However, if the differential equations contain non-linear expressions, a closed form solution using the equations is not possible.

The study of non-linear dynamic systems that display unstable, aperiodic behaviour is the focus of chaos theory [Kellert, 1993]. In light of this discussion, it seems probable that if all factors pertinent to the tearing of leather could be expressed mathematically, a model that precisely predicts every force fluctuation that is intrinsic to the material's tearing resistance, is unlikely to be achievable.

### 3.3.3 Why the corium is tougher than the grain.

The specific work of fracture, or toughness, is the work required to propagate a crack of unit area through a material. At the most fundamental level, crack propagation involves the splitting apart of two planes of atoms to create two new surfaces. Indeed, the term 'free surface energy' refers to the energy required to separate one plane of atoms from another through unit area of the material. In brittle homogeneous materials like glass, the free surface energy, is a reasonable estimation of the specific work of fracture as no energy absorbing process occurs at the crack tip.

Purslow [1989b] attributes the high toughness of biological materials, such as wood and skin ( $R \approx 10^4 \text{ J m}^{-2}$ ) to structural changes or processes, that occur along or near the path of fracture, and irreversibly absorb much of the supplied strain energy, so making the material tough. Accordingly, differences in the toughness of grain and corium may be attributed to differences in the irreversible processes that occur along or near the fracture path. Such processes are dependent on the mechanical properties of the material's components, their spatial arrangement and the connection between them [Offer et al, 1989].

A significant amount of work has been carried out on the mechanical properties of individual tanned collagen fibres, teased from corium material [eg. Morgan, 1960]. However, individual fibrous units cannot be teased from grain material. Thus, at the present time, it is not possible to clarify differences in the stiffness, breaking strength and breaking strain in the respective components of each

material. Nevertheless, electron microscopy has been used to clarify the hierarchy of tanned collagen, typically found in the corium layer of bovine leather. Five hierarchical fibrous units are reported in corium material; Table 3.10 [Alexander et al, 1993].

Table 3.10.

Unit	Typical diameter
Fibre bundle	60 - 200 $\mu\text{m}$
Fibre	30 - 60 $\mu\text{m}$
Fibril bundle	3 - 6 $\mu\text{m}$
Fibril	0.1 - 0.2 $\mu\text{m}$
Microfibril	10 nm

A typical diameter of the largest fibrous unit in the corium layer is 60 - 200  $\mu\text{m}$ . However, the grain layer is chiefly composed of smaller, highly interwoven collagen fibres, diameter  $\leq 5 \mu\text{m}$  (i.e. of the same diameter as those fibrous units classified as fibril bundles). This is perhaps the most significant structural dissimilarity between the two materials. Accordingly, it is appropriate to associate differences in toughness (between the grain and corium) with the different hierarchical levels of the constituent fibres of each material. In other words, the hierarchy of the constituent fibres in each material affects the fracture process.

In composite materials, the interface between the matrix and the fibres provides the opportunity for energy to be absorbed by the processes of fibre debonding and fibre pull out [Kelly, 1970]. Fibre debonding is defined as the work done in destroying the bond between fibre and matrix [Kelly & Macmillan, 1986]. In the

case of propanone dehydrated grain and corium, there is essentially no matrix. However the feltwork of tanned collagen fibres enable stress and strain transmission during mechanical deformation and so a pseudo matrix can be said to exist.

Fibre pull out occurs when a fibre, large enough to receive stress by shear from the matrix, reaches its fracture stress and fractures ahead of a propagating crack. This situation transpires because the statistical distribution of strength along the fibre length results in fracture at a position remote from the notch tip [Kelly & Macmillan, 1986]. Irreversible work is then expended against friction in pulling the length of fractured fibre through the matrix until it becomes completely liberated. Thus, high levels of fibre pull out in a fracturing material ensure high levels of energy absorption during the fracture process.

In discussing the possible affects of debonding, the findings of Torp et al [1975] are noteworthy. In observing the fracture of tendon, Torp et al described delamination, or dissociation, not only of large fibres from their matrix, but also dissociation of fibrils within larger fibres. Indeed, they concluded that this was a primary fracture mechanism in tendon. In composite materials of brittle fibres in a brittle matrix, the work of debonding is usually less than the work of pull out [Kelly, 1970]. In such composite materials, debonding occurs only between the solid cylindrical fibres and the matrix. Conjecturally, no debonding will occur within the fibre itself.

If debonding occurs at each hierarchical level within the fibre as well as the fibre itself debonding from the matrix, the energy required in the process of debonding is tangibly elevated. Thus, the capacity for energy absorption in the fracture process increases. To estimate maximum possible levels of dissociation in grain and corium materials, it is necessary to examine both the surface area of the largest fibre unit and the surface area of all subsequent hierarchical fibrous units.

The number of cylindrical fibres  $N$ , of radius  $r$ , in a larger fibre of radius  $R$ , with a packing ratio,  $P$  is given by the expression:

$$N = (\pi R^2 / \pi r^2) P \quad [3.18]$$

The packing ratio,  $P$ , expresses the efficiency with which cylindrical elements can be packed into a given space. The most efficient stacking pattern for cylindrical elements is hexagonal. In these conditions 91% of available space can be occupied by hexagonally packed cylindrical elements, thus  $P = 0.91$  [Purslow, 1980].

Using equation [3.18] and the maximum radius of each fibrous unit (from Table 3.10), the number of smaller fibre units within larger fibre units throughout the hierarchy of fibre units is summarised in Table 3.11.

Table 3.11

Number of fibres in a fibre bundle	$(100^2/30^2) \times 0.91$	10
Number of fibril bundles in a fibre	$(30^2/3^2) \times 0.91$	91
Number of fibrils in a fibril bundle	$(3^2/0.1^2) \times 0.91$	819
Number of microfibrils in a fibril	$(0.1^2/0.005^2) \times 0.91$	364

If the surface area involved in debonding the fibre equals the surface area of the cylindrical fibre then the following expression is valid:

$$S.A. = \pi \cdot d \cdot L \quad [3.19]$$

Where S.A. is the surface area involved in debonding, d is the diameter and L is the length of the cylindrical fibre respectively.

Consideration of the debonding process in the corium material, reveals that if the largest fibre unit debonds from the matrix and no other debonding occurs within the fibre, the surface area involved in debonding is  $2 \times 10^{-4} \pi L$ . If the largest fibre unit debonds from the pseudo matrix and debonding also occurs throughout the entire hierarchy of the fibre structure, the following surface areas are involved in debonding.

Table 3.12

Surface area involved in debonding	S.A. x Number units present	Total S.A.
1 fibre bundle	$(200 \times 10^{-6}) \pi L \times 1$	$(2 \times 10^{-4}) \pi L$
the fibres present	$(60 \times 10^{-6}) \pi L \times 10$	$(6 \times 10^{-4}) \pi L$
the fibril bundles present	$(6 \times 10^{-6}) \pi L \times 91$	$(5.46 \times 10^{-4}) \pi L$
the fibrils present	$(0.2 \times 10^{-6}) \pi L \times 819$	$(1.64 \times 10^{-4}) \pi L$
the microfibrils present	$0.01 \times 10^{-6}) \pi L \times 364$	$(3.64 \times 10^{-6}) \pi L$
	Total:	$(15.14 \times 10^{-4}) \pi L$

Thus, within the corium, when debonding one fibre bundle (the largest fibre unit) from the pseudo matrix, assuming that debonding occurs throughout the entire hierarchy of the fibre structure, the total surface area involved in debonding is

elevated to  $(15.14 \times 10^{-4}) \pi L$ .

In considering the grain material (where the largest fibre unit is the size of the fibril bundle) if the largest fibre unit debonds from the pseudo matrix and no other debonding occurs within the fibre, the surface area involved in debonding the largest fibre unit is  $(6 \times 10^{-6}) \pi L$ . However, if total debonding also occurs within the fibre, the surface area involved in debonding the largest fibre unit from the pseudo matrix is elevated to  $(1.74 \times 10^{-4}) \pi L$ .

It is clear that complete dissociation of all fibres into all their sub-fibrous units would not completely occur before macroscopic failure of either grain or corium material. However, whether or not debonding occurs within the largest fibre unit of either material, the surface area involved in debonding the largest fibre unit from the pseudo matrix is always more significant in the corium. Therefore, more energy is likely to be absorbed during the debonding process within the corium. Accordingly, the observed resistance to tear propagation in the corium will be higher than that observed in the grain.

In discussing the possible effects of fibre pull out on the toughness of grain and corium materials, fibre pull out is more significant in corium trouser tear specimens. Figure 3.16 shows a typical trouser tear specimen of grain and corium after test completion. From these and all other trouser tear specimens, two striking features are apparent. First, the length of revealed fibres, pulled from the feltwork, is significantly higher in corium specimens. Second, the diameter of the liberated fibre units is greater in corium specimens.

For fibre pull out to occur, the fibre must fracture ahead of a propagating tear [Kelly & Macmillan, 1986]. Accordingly, fibres ahead of the tear have to be sufficiently large to receive stress by shear from the fibre feltwork to attain fracture stress. Thus, the whole phenomenon of fibre pull out transpires because the statistical distribution of strength, along the length of a fibre, enables fracture at a position remote from the propagating tear. If the statistical distribution of strength along the fibre length can be altered, so as to increase the distance between tangible points of weakness, then assuming the shear stress can still be transmitted over these greater distances, the fibre lengths liberated from the matrix and the energy required to liberate the fibres will both increase.

Notch insensitivity has been extensively examined in various materials; eg meat [Purslow, 1989b] and leaves [Vincent, 1983]. The difference in notch sensitivity of grain and corium material is a major theme of chapter 4. Notch insensitive materials consist of strong fibres oriented perpendicular to the advancing tear in a matrix which is weak in tension [Kelly and Macmillan, 1986]. This being the case, it is probable that some level of internal debonding within a corium fibre bundle, together with its hierarchial internal structure, fulfils the above conditions and consequently fibre bundles may themselves be insensitive to notches.

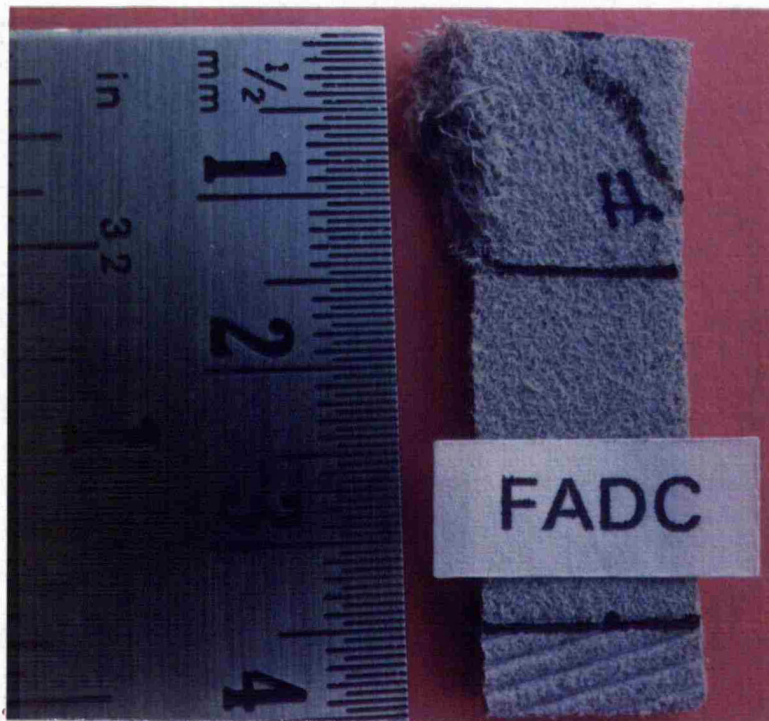
The largest fibre unit of the grain has a lower hierarchical structure than the largest fibre unit of the corium. In addition, the largest fibre unit of the grain cannot achieve the same level of internal debonding as the largest fibre unit of the corium. Therefore, it is less likely that the fibre units of the grain provide the necessary internal structure of a notch insensitive material.

Returning to the corium material, if corium fibre bundles themselves are notch insensitive, then the breaking stress of the fibre bundle is directly proportional (as opposed to more than proportional) to the size of the stress raising statistical defect or flaw. Thus, the size of the irregularity in the fibre bundle must be sufficiently large for the breaking stress to be substantially reduced from its maximum value (i.e. where no flaw or defect is present). Consequently, the strength of the fibre bundle is more evenly distributed along its length. In practical terms, this means larger distances between significant weak points along the length of the fibre unit. As a result, the length of fibre pull out would, and indeed appears to be significantly greater in the case of corium specimens.

In considering the affect of fibre diameter on fibre pull out, it is essential to note that irreversible work is expended against friction in pulling a length of fractured fibre through the feltwork until it is liberated. From Table 3.10, it is clear that the largest fibre unit in the corium is approximately thirty times greater in diameter than the largest fibre unit in the grain. Thus, if the length of fractured fibre being pulled through the feltwork is greater in the corium than the grain, and the diameter of the corium fibre unit is significantly higher, the irreversible work expended against friction in liberating the fibre length must be greater when tearing corium specimens.

Figure 3.16

Fibre pull out in trouser tear test specimens.



#### **3.3.4 Orientation effects.**

In order to consider exclusively the effect of specimen orientation on tensile properties and the specific work of fracture, both parallel and perpendicular orientations of propanone dehydrated grain (PDG) and propanone dehydrated corium (PDC) specimens are compared.

##### **3.3.4 (a) The effect of specimen orientation on tensile behaviour.**

The mechanical properties of full substance bovine leather vary with hide location and the direction in which the testing specimen is cut [Maeser, 1960]. However, the relative orientation effects of separated grain and corium material are not discussed in the literature. The results of section 3.2.1 reveal that by keeping hide location constant, the effect of specimen orientation usually has pronounced effects on the tensile properties of both grain and corium materials.

The differences in strain at rupture, stress at rupture and tensile moduli at rupture of parallel and perpendicular specimens are apparent in the respective nominal stress-strain curves of each material. The approximate 'J' shaped characteristic of full substance leather can be attributed to the progressive orientation of collagen fibres during deformation [Attenburrow, 1992]. Accordingly, differences in the 'J' shaped nominal stress-strain curve are attributed to differences in this progressive orientation of the collagen fibres.

Progressive fibre orientation is dependent upon two factors: (i) initial structural conditions and (ii) fibre restrictions within the feltwork.

Factor (i) is concerned with the initial alignment of fibres (with respect to the direction of strain application) before the material is strained. When the majority of fibres are already aligned in the same direction as the applied strain, they have little scope to orientate towards the strain axis (i.e. they are already aligned in this direction). Hence the fibres themselves are directly strained at low levels of nominal strain. However, if many fibres are aligned in the opposite direction to the applied strain, fibres are able to orientate towards the strain axis. This orientation would ensure higher levels of nominal strain are achieved before deformation occurs by straining the fibres themselves.

(ii) The level of fibre orientation is also dependent on fibre mobility. The mobility of individual fibres within the 3-dimensional feltwork of fibres is restricted by factors such as the level of fibre lubrication, the fibre diameter, the fibre packing density and the subsequent restriction placed on the fibres by the other fibres within the feltwork.

Considering differences in specimens oriented parallel and perpendicular to the backbone, it is probable that the constituent fibres of parallel specimens are already aligned in the same general direction as that of the applied strain, thus the process of fibre orientation is limited. Indeed, the fibres would seem to become aligned to the strain axis at low nominal strains of 30→35%, where a constant tensile modulus is attained. Here it is assumed that further deformation is

associated with straining of the fibres themselves. For specimens oriented perpendicular to the backbone, more fibre orientation seems probable since the non-linearity of the stress-strain curve extends to nominal strain levels of 50→55%.

Furthermore, when approaching rupture, the tensile modulus and the nominal stress levels are higher for parallel specimens than for perpendicular specimens. The modulus observed in parallel specimens, is higher because the strain is being applied to a more oriented network of fibres than is the case for perpendicular specimens. It is important to differentiate between the final level of fibre orientation and the degree of fibre orientation that has occurred. The perpendicular specimens are likely to have experienced more fibre orientation than the parallel specimens, but the network of fibres will not be as highly oriented.

In addition the higher nominal stresses observed in parallel specimens are again likely to be because less actual fibre orientation has occurred. It seems logical that fibre orientation will cause frictional damage to the fibres, and therefore act as a possible stress raiser. More fibre orientation seems apparent in perpendicular specimens, thereby increasing the possibility of fibre damage and reducing tensile strength.

In this respect Kronick & Maleef [1992], when straining whole leather, associated the different acoustic emission signatures with two separate processes; (i) the breaking of inter-fibre adhesions (i.e. the fibres debonding from the pseudo matrix) and (ii) the process of fibre breakage. Although inter-fibre adhesion and the affect of fatliquor and staking have been investigated using acoustic emission techniques [Kronick et al, 1993], the technique has not been used for investigating different

levels of debonding / orientation / fibre damage / fibre breakage, with regard to specimen orientation.

#### **3.3.4 (b) The effect of specimen orientation on the specific work of fracture.**

The specific work of fracture of PDG material is sensitive to specimen orientation. However statistically, orientation has little or no effect on the specific work of fracture of corium material (section 3.2.2). Considering Figure 3.17, when specimens are oriented parallel to the backbone, the general fibre direction is assumed to be in the same direction as the strain axis (represented by the vertical general fibre direction arrow). Under these conditions, the specific work of fracture is higher because conceptually, the tear does not propagate through fibre diameters. Instead, the fibres bridge the advancing tear and are subject to more of a straightforward rupturing process.

When specimens are oriented in a direction perpendicular to the backbone, the general fibre direction is assumed to be nearer ninety degrees to the strain axis (represented by the horizontal general fibre direction arrow). Under these conditions, the specific work of fracture is lower because the tear is able to propagate directly through the feltwork of fibres.

Although directional specific work of fracture is only statistically significant in grain material, it is probable that directional toughness is also a factor in the tearing of corium material. However, it is contended here that directional effects are likely to be masked by the energy dissipation processes of debonding and pull out. This is evident when corium specimens are torn, regardless of orientation.

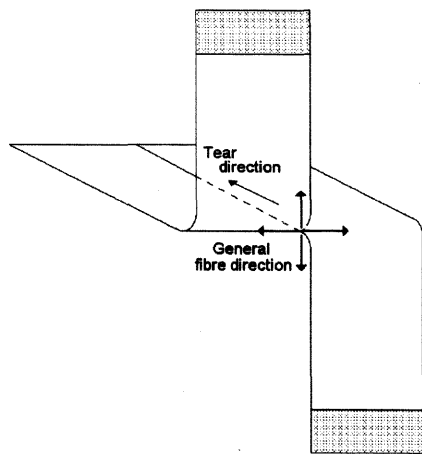


Figure 3.17

Fibre direction and the trouser tear test.

### 3.3.5 Fatliquor effects.

It was not the principal aim of this study to understand the influence of oil addition on the mechanical behaviour of leather. However, oil has a significant influence on the fracture of grain and corium material and we review reasons for its influence. To discuss differences in the tensile and tear properties as a result of a fatliquoring process, we compare the properties of propanone dehydrated material (where no oil is added) with fatliquored, air dried material.

The presence of oil in leather is known to affect the mechanical properties of full substance, chrome tanned bovine leather. Indeed, Mattei and Roddy [1957] used a mixture of sulfated cod oil and raw cod oil to fatliquor at oil levels of 6%, 10%, 15% and 18%. Over this range of oil levels, the tensile strength increased by 42% and the elongation at rupture increased by 34%. These effects were attributed to the increase in 'fibre slippage', i.e. an increase in fibre mobility as a consequence of the higher oil content.

The results show that the mechanical behaviour of grain specimens alter significantly when oil is present. The initial modulus of tensile deformation for FADG specimens is notably lower than PDG specimens (26% lower for specimens with a parallel orientation and 47% lower for specimens with a perpendicular orientation). Thus as a result of the oil's presence, the effective stiffness during initial deformation up to 7% nominal strain is markedly reduced.

Oil in grain material increases the nominal stress at rupture by 30% in parallel specimens and 21% in perpendicular specimens. The nominal strain is also increased by 37% in parallel specimens and 32% in perpendicular specimens. Similar phenomena are observed with corium specimens. However, the percentage increases in equivalent properties are not as pronounced in the corium, presumably because the percentage oil content is not as high.

In discussing why oil leads to these changes in mechanical behaviour, the effects of added oil to grain and corium materials are usefully contrasted with the effects of adding plasticisers to polymers. Plasticisers are added to polymers in order to improve their flow properties [Higgins, 1991]. Two principal groups of plasticisers are used in plastics. The first group, known as primary plasticisers, contain polar groups that neutralise attractive forces between polymer polar groups, and thus reduce the van der Waals attractive forces between adjacent polymer chains. The second group, known as secondary plasticisers, are essentially inert materials without polar groups but which exist, dispersed through the polymer, thereby providing mechanical spacers that separate and so reduce the van der Waals forces of attraction between polymer chains.

The emulsion of synthetic sulphated oil (the fatliquor) is an anionic colloid where large molecules carry a negative charge. After neutralisation, the wet blue leather is slightly acidic and cationic (positively charged). During the fatliquoring process, oil molecules are attracted to leather fibres through the cross section and generally reduce the cationic charge on the leather.

Thus, in the aqueous environment of fatliquoring, the cationic charge on the leather fibres tends to be neutralised by the anionic charge of the fatliquor. Accordingly, in an aqueous environment, the fatliquor can be regarded as a primary plasticiser. However, once dry, the leather becomes hard, crusty and unsuitable for most purposes unless oil is first applied, unless special drying methods are used.

Once dry, both fatliquored and propanone dehydrated grain and corium materials were conditioned at a relative humidity of 65% for at least 48 hours. Accordingly, both fatliquored and propanone dehydrated materials have a moisture content of approximately 14%. Assuming the moisture contents in respective grain and corium materials are comparable, the oil increases the flow characteristics of leather. Accordingly, in a non-aqueous environment, oil is a secondary plasticiser, providing spacers that prevent fibre adhesions as well as providing some lubrication between adjacent fibrous units. Both these processes facilitate higher levels of fibre mobility / orientation.

### 3.3.6 Strain rate effects.

The breaking stress and strain of FADG (12.5 % oil), FADC (3.0 % oil) and PDC materials increase with increasing strain rate. However, despite an abundance of information concerning tensile properties of whole leather strained at a rate of  $1.66 \text{ mm s}^{-1}$  ( $100 \text{ mm min}^{-1}$ ) [eg. Mann et al, 1951], no published work examines the effect of strain rate on the tensile properties of leather. Therefore the strain rate dependent behaviour of similar materials was examined in order to probe the mechanisms responsible for rate sensitivity.

Rat tail tendon (RTT) is a highly oriented, collagen rich connective tissue and, like leather, is sensitive to strain rate. Haut [1983], when assessing age-dependent influences, reported that, at high strain rates the initial yield point of the stress-strain curve is delayed, resulting in higher failure strains at high deformation rates. The rate sensitivity of RTT was, in essence, attributed to the inter-fibrillary matrix of mucopolysaccharides, which help maintain structural integrity of RTT at high strain rates, thereby increasing tensile strength. This explanation could not apply to leather since the inter-fibrillary matrix was removed in the liming process (see Appendix 1.)

The influence of strain rate on tensile properties was also observed in both dry and wet collagen fibres teased from RTT [Arumugam et al, 1992]. Both wet and dry fibres demonstrate that, at higher strain rates, higher stresses are induced at every level of strain. The workers also observed thin broken fibrils dispersed across the fracture surface at slow strain rates whereas thick bundles were observed at

higher strain rates. However, no mechanism relating the viscoelastic properties of the fibres to strain rate sensitive tensile strength was suggested.

The influence of strain rate (and temperature) on the tensile properties of elastomers has been examined by Smith [1958] and extensively reviewed by Ward [1983]. Except at very low strain rates (and high temperatures) where the molecular chains have complete segmental mobility, the fracture process of elastomeric material is dominated by viscoelastic effects.

It is paradoxical that we see no marked change in viscoelasticity (as revealed when examining the hysteresis ratio over a range of strain rates and levels). However, as strain rate increases, the viscoelastic properties of individual fibres may change. Since hysteresis shows little change, the cause of rate dependent rupture of leather must be related to fibre microstructure and energy dissipation in the region of the failure site rather than gross energy dissipation .

The organisation of all the hierarchical fibres of corium material (FADC and PDC) enables an enhanced fibre mobility at higher rates, thereby increasing both rupture stress and strain. The level of fibre mobility is likely to be lower in the grain because of its compact fibrous structure. Accordingly, compact arrangement of fibres also impedes enhancement of fibre mobility at higher strain rates. Thus, the tensile properties of PDG material are essentially independent of strain rate. In section 3.5.1 the presence of oil in grain or corium material was shown to facilitate higher levels of fibre mobility / orientation. Interestingly, oil in grain material (which enables a level of fibre mobility) also promotes a level of strain rate dependency

in terms of the breaking stress and strain.

Subject to fixed rate deformation, leather displays both residual extension and hysteresis [Whittaker, 1975]. The effect of strain level and strain rate on the energy dissipating process during the deformation and fracture of non-linear, inelastic materials is an intrinsic element in the general theory of fracture mechanics [Andrews, 1974]. As such, the relationship between strain level, strain rate and hysteresis of both grain and corium materials is important.

In corroborating the generalized formulation of fracture mechanics in its application to non-linear, flexible, inelastic materials, Andrews & Fukahori [1977] experimentally evaluated a loss function from hysteresis data over a range of strain levels and strain rates. Stress-strain cycling of four materials was carried out at 23 °C. The materials included: styrene-butadiene rubber (SBR), ethylene-propylene-diene rubber (EPDM), plasticised polyvinyl chloride (p-PVC) and low density polyethylene (PE). The hysteresis ratio ( $\beta$ ) increased with strain level and tended to increase with strain rate (although the magnitude of the latter trend is different for each material).

Perhaps not surprisingly, the influence of strain rate and level on hysteresis of the materials studied by Andrews & Fukahori [1977] are not in accordance with the results of section 3.2.5. Both grain and corium materials show a decrease in hysteresis when strain rate is increased. Further, only a small increase in hysteresis is apparent with increasing strain level.

As shown in section 3.2.4, the specific work of fracture increases with increasing deformation rate for both fatliquored, air dried and propanone dehydrated grain and corium materials. In this respect, it is interesting to consider the work of Purslow [1980], who investigated the effect of loading rate on the toughness of rat skin. He discovered that, over the range of strain rates from  $0.08 \text{ mm s}^{-1}$  to  $8.33 \text{ mm s}^{-1}$ , the effect of rate on toughness was not large (the toughness varied, at most, by a factor of two).

Purslow [1980] suggests that viscous losses of energy in trouser tear specimens are not the dominant fracture mechanism of rat skin, but that this mechanism may act in unison with others to produce a tough material. In this study, the effect of deformation rate on the specific work of fracture of the four leather materials has been examined over a larger range of rates ( $0.16 \text{ mm s}^{-1}$  to  $166.66 \text{ mm s}^{-1}$ ). However, increases in toughness observed in this study were not as marked as those observed over a narrower range of rates in rat skin.

Nevertheless, the influence of strain rate on toughness is tangible and attributed to fibre orientation effects in the region of the advancing tear. At low strain rates, the fibres in the path of the advancing tear are subject to orientation forces, but have time to relax and accordingly the degree of orientation in the region of the propagating tear is effectively reduced. At higher rates, the fibres in the path of the advancing tear are subject to orientation forces over short time periods, fibres have no time to relax and consequently orient towards the direction of strain. As discussed in section 3.3.4, fibres oriented in the same direction as the strain in trouser tear specimens (Figure (3.17)) ensure higher values of toughness.

## Chapter 4

### Notch Sensitivity.

#### 4.1 Introduction.

In chapter three, differences in the mechanical behaviour, tensile strength and specific work of fracture of grain and corium materials were established. In order to further understand the reasons for these differences, the notch sensitivities of grain and corium materials are examined in this chapter. The strain distribution around edge notches in grain and corium materials are also analysed.

The concept of notch sensitivity has been discussed by Kelly and Macmillan [1986]. Their analysis indicates that when a material is notch sensitive, the presence of a small crack or notch causes a stress concentration at the tip of a crack. This stress concentration promotes fracture at applied stresses that are very much lower than those required to fracture an unnotched specimen. Examples of materials that lose a large proportion of their strength with only small notches are glass [Griffith, 1920], polymeric materials such as polymethylmethacrylate and polystyrene [Berry, 1972], and biological materials such as fresh potatoes and carrots [Atkins & Mai, 1988].

The effect of a notch in a notch-insensitive material is, again, to reduce the nominal breaking stress. However this reduction is only in direct proportion to the reduction in cross-sectional area as a consequence of the notch presence [Kelly & Macmillan, 1986]. Examples of notch insensitive materials are grass leaves

[Vincent, 1983], rat skin [Purslow, 1980] and meat [Purslow, 1985]. Figure 4.1 illustrates how nominal tensile strength is dependent on notch length for both notch sensitive and notch insensitive materials.

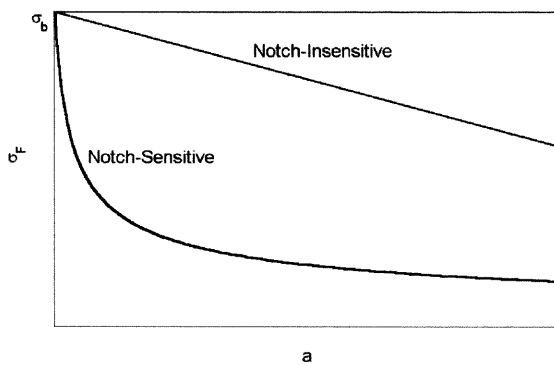


Figure 4.1

The criterion for crack propagation in a notch sensitive material can take one of two forms: (i) the crack will propagate when the stress at its tip reaches some critical value which overcomes the forces of cohesion, as discussed by Kelly & Macmillan [1986], or (ii) the crack will propagate when the energy, released from the body by crack growth, just exceeds the energy required for the creation of the new surfaces of the crack [Griffith, 1920]. Andrews [1980] eloquently illuminates the fact that criterion (i) is more appropriate because criterion (ii) is a necessary, but not sufficient condition for crack propagation, i.e. criterion (ii) implicitly requires criterion (i) to be simultaneously satisfied. However, in practice, the distinction often proves to be rather academic and criterion (ii) is usually the most useful because the detailed stress pattern at the very tip of a crack is almost impossible to ascertain [Andrews, 1980].

Consider a linear elastic plate (loaded at infinity) with an elliptical notch situated mid way down one of its sides. Using criterion (i), the relationship between the applied stress necessary to produce failure and the initial notch length, is described by the equation [4.1], [Kelly & Macmillan, 1986].

$$\sigma_f = \sigma_y / (1 + 2 \sqrt{a/\rho}) \quad [4.1]$$

Where  $\sigma_f$  = applied nominal stress at failure  
 $\sigma_y$  = maximum stress at crack tip  
 $a$  = length of notch  
 $\rho$  = radius of curvature of the notch.

However using criterion (ii), the energy balance approach as originally outlined by Griffith [1920], the relationship between nominal failure stress and notch length (when a sharp crack is placed into one side of a plate loaded at infinity) is given by equation [4.2], [Kinloch & Young, 1990].

$$\sigma_f = (E G_c / \pi a)^{1/2} \quad [4.2]$$

Where  $E$  = Young's Modulus  
 $G_c$  = specific fracture energy

Taking  $(E)$  and  $(G_c)$  as constants in equation [4.2], the relationship between the applied stress necessary to produce failure and the initial notch length for a linear elastic material, may be expressed as,

$$\sigma_f = K a^{-1/2} \quad [4.3]$$

Where K is a constant.

Equations [4.1] to [4.3] describe the relationship between notch length and nominal fracture stress for a linear elastic plate load at infinity. Each equation (assuming the appropriate variables and / or constants are known), shows that the nominal breaking stress falls markedly as notch length increases from zero. Accordingly, Equations [4.1] to [4.3] (showing the dependence of nominal fracture stress on notch length) are those expected to describe a notch sensitive material (Figure 4.1). In the case of a perfectly notch-insensitive material, the nominal applied stress necessary to produce failure falls only gradually with notch length. Indeed, the relationship between nominal fracture stress and notch length is given by equation [4.4], [Kelly & Macmillan, 1986].

$$\sigma_f = \sigma_b (1 - a/w) \quad [4.4]$$

Where  $\sigma_b$  is the nominal breaking stress of an unnotched specimen.

The notch sensitivity of nonlinear elastic materials was considered by Purslow [1991]. Based on the energy balance approach pioneered by Griffith [1920], Purslow implied that notch-insensitive materials have an area to the left of a vertical line through the tip of the notch, which is free of strain energy, (Figure 4.2 (I)). In contrast, a notch sensitive material should have a strain-energy-free-zone confined to a semicircular region around the notch, (Figure 4.2 (II)). The initial

section of Purslow's analysis [1991] uses a power law to describe the stress strain behaviour of unnotched tensile specimens and the non linear behaviour of tensile specimens is described by Equation [4.5]:

$$\sigma = K \epsilon^n \quad [4.5]$$

Where  $\sigma$  = nominal stress  
 $\epsilon$  = nominal strain  
K = constant

When  $n > 1$  the  $\sigma/\epsilon$  curve is 'J' shaped.  
 $n < 1$  the  $\sigma/\epsilon$  curve is 'r' shaped.  
 $n = 1$  the  $\sigma/\epsilon$  curve is linear.

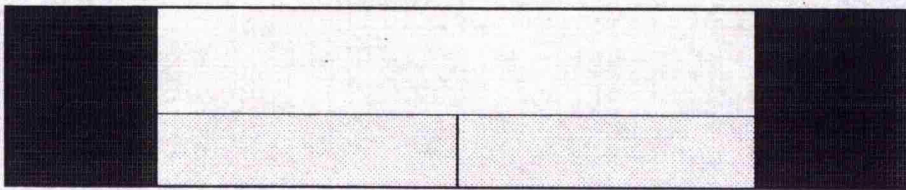
The power law of non-linear ('J' or 'r' shaped) stress-strain behaviour predicts a straight line relationship in a plot of  $\ln(\sigma)$  versus  $\ln(\epsilon)$  [Purslow, 1991]. From equation [4.5],

$$\ln(\sigma) = \ln(K) + n \ln(\epsilon) \quad [4.6]$$

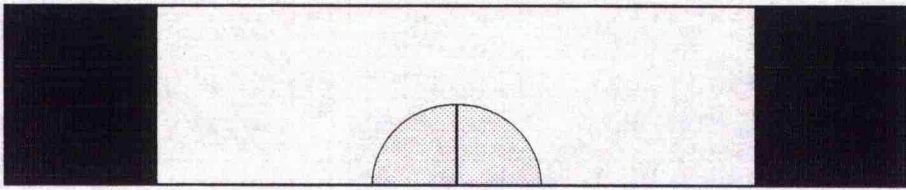
Accordingly, the gradient of the straight line in the above plot is the exponent (n) in Equation [4.5] and the intersection of the line with the stress axis is  $\ln(K)$  in Equation [4.5].

In his analysis, Purslow [1991], uses equation [4.5] as well as estimates of the

distribution of strain energy in single notch specimens and the Griffiths definition of fracture toughness (the partial derivative of the change in strain energy with crack area) to develop several equations. These equations describe the relationships between stress at fracture, strain at fracture and notch length. Comprehensive derivations of these relationships are given in Appendix 6.1 for notch-sensitive materials and in Appendix 6.2 for notch-insensitive materials.



(I) Notch-Insensitive Case.



(II) Notch-Sensitive Case.

Figure 4.2

Strain energy distribution in notched specimens.

Area of sample clamped by jaws.

Strain-Energy-Free-Zones

## 4.2 Results.

### 4.2.1 Notch sensitivity of grain and corium materials.

Figure 4.3 shows four graphs of the format illustrated in Figure 4.1 (i.e. nominal fracture stress versus the initial notch length of single notch samples.) Figures 4.3 (I) and (II) show the notch-sensitive behaviour of FADG (8.5 % oil content) and PDG specimens respectively. The straight line on each graph shows the behaviour predicted for a notch insensitive material (Equation [4.4]). The dark line indicates that the data generally fit a curve with the relationship,

$$\sigma_f = C a^{n'} \quad [4.7]$$

Where  $C = \text{constant}$   
and  $-0.5 < n' < 0$ .

When  $n' = -0.5$  the sensitivity of the material to the presence of a notch accords with Griffith type fracture (Equations [4.2] and [4.3]) and is therefore denoted *completely* notch sensitive. As shown in Figure 4.3 (II) the PDG specimens exhibits a large drop in breaking stress when only small notches are present and indeed, the geometric trend line yields  $n'$  equal to  $-0.50$  signifying *complete* notch sensitivity. Similarly, notched FADG specimens show a marked departure from the line of notch-insensitivity. The geometric trend line for FADG specimens indicates  $n'$  equals  $-0.47$ , demonstrating the degree of notch-sensitivity is very slightly less here than is the case for PDG specimens. It also noticeable from Figures 4.3 (I) and

(II) that the critical crack length of FADG material is in the order of 1 mm, while the critical crack length of PDG material is less than 0.5 mm.

Figures 4.3 (III) and (IV) show the dependence of nominal fracture stress on notch length for FADC (1.2 % oil content) and PDC specimens respectively. Again, the straight line on each graph shows the predicted pattern for a notch insensitive material (Equation 4.4). The dark line indicates that the data generally fit a curve with the relationship,  $\sigma_f = C a^{n'}$  (where  $\frac{1}{2} < n' < 1$ ). Both FADC and PDC material are a great deal less sensitive to the presence of notches than the respective grain material. In fact, both corium materials depart little from the theoretical line of complete notch-insensitivity. However, when comparing the nominal fracture stress of FADC and PDC specimens at identical notch lengths, FADC specimens fracture at applied stress levels approximately 20 % greater than those observed for PDC specimens.

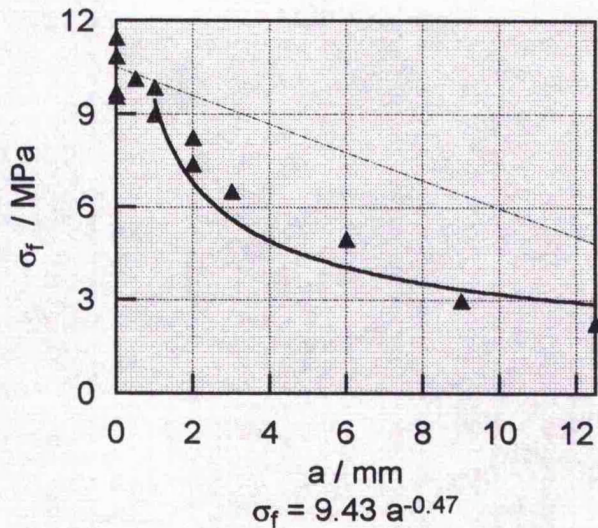
Figure 4.4 has identical format to Figure 4.3. However, Figures 4.4 (I) and (II) show the behaviour of FADG material with the higher oil content of 12.5 % and the PDG control material respectively. From the trend line, where  $n' = -0.5$ , the sensitivity of PDG specimens to the presence of a notch is again in accordance with Griffith type fracture (Equations [4.2] and [4.3]). However, such a high degree of notch sensitivity is not observed with the FADG specimens, where  $n' = -0.313$ . Hence a higher level of oil deposited in the grain layer produces a material with fracture behaviour less sensitive to the presence of notches.

Figures 4.4 (III) and (IV) show the fracture behaviour of FADC (3.0 % oil content)

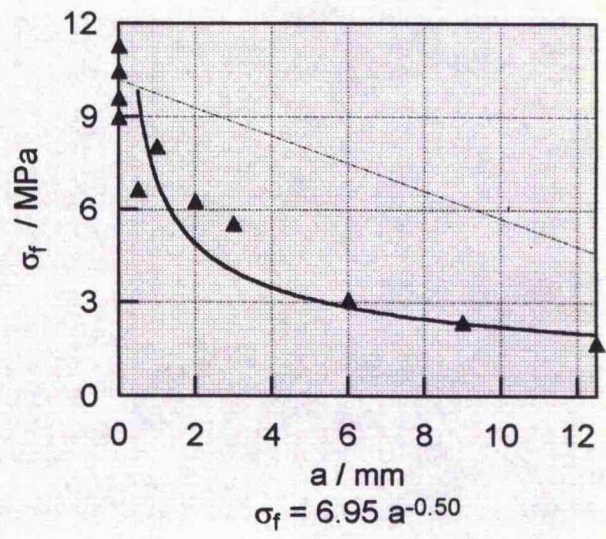
and PDC control material respectively. Perhaps not surprisingly in view of the results shown in Figures 4.3 (III) and (IV), these results indicate a high degree of notch insensitivity. Also, as with Figures 4.3 (III) and (IV), when comparing the results of FADC with the PDC material at identical notch lengths, the trend line signifies that FADC tolerates higher levels of applied stress prior to specimen fracture.

Figure 4.3

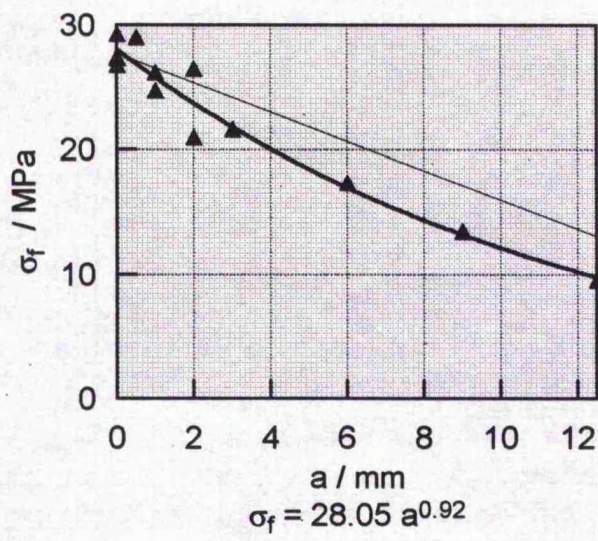
The dependence of nominal fracture stress on notch length for FADG (8.5 % oil content), PDG, FADC (1.2 % oil content) and PDC specimens.



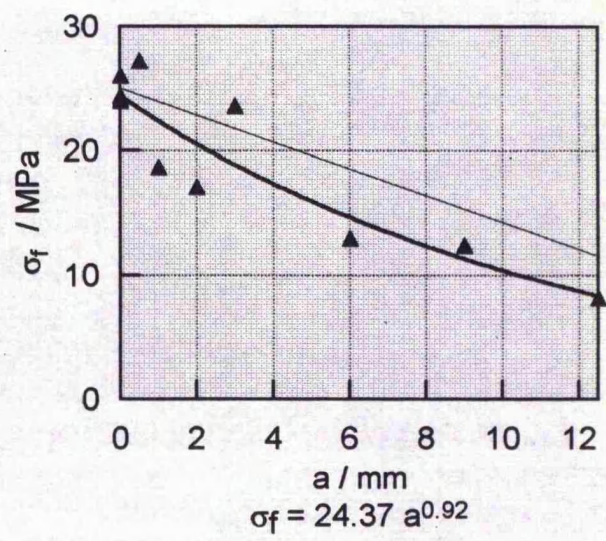
Material = FADG  
(I)



Material = PDG  
(II)



Material = FADC  
(III)

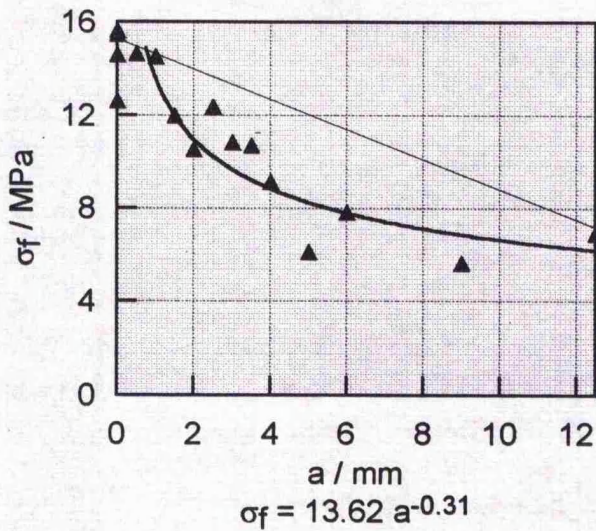


Material = PDC  
(IV)

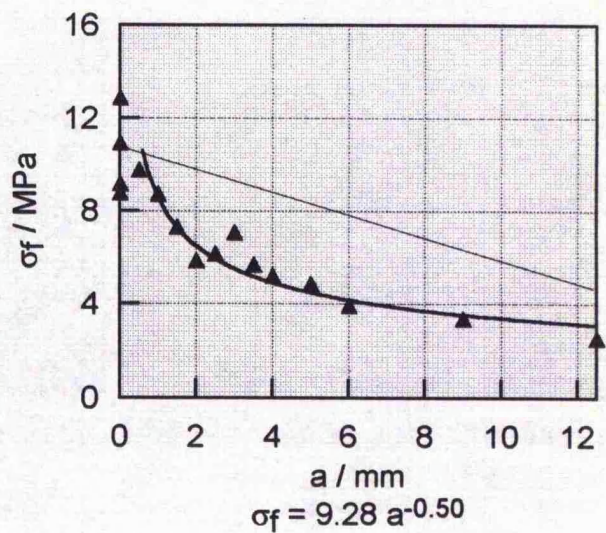
The straight line indicates the expected behaviour of a notch insensitive material.

Figure 4.4

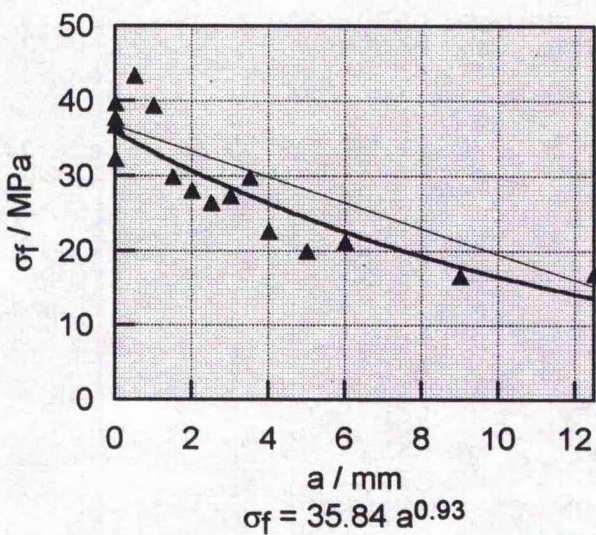
The dependence of nominal fracture stress on notch length for FADG (12.5 % oil content), PDG, FADC (3.0 % oil content) and PDC specimens.



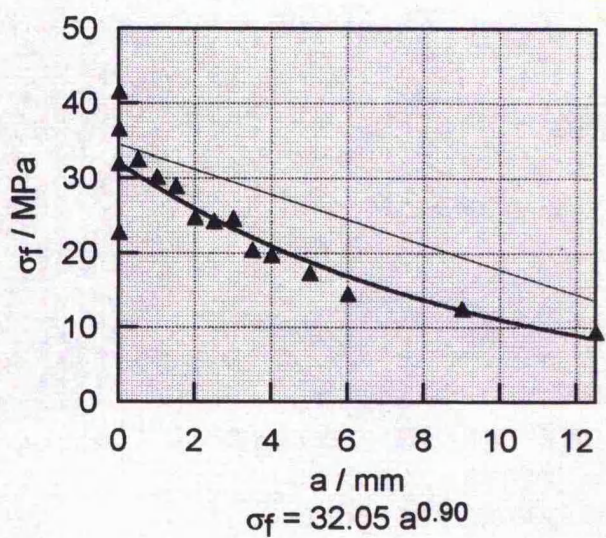
Material = FADG  
(I)



Material = PDG  
(II)



Material = FADC  
(III)



Material = PDC  
(IV)

The straight line indicates the expected behaviour of a notch insensitive material.

#### 4.2.2 Mathematical relationship between nominal stress and strain.

In this section, a relationship between nominal stress and strain for the approximate 'J' shaped stress-strain behaviour of grain and corium material is established. Plots of  $\ln(\sigma)$  versus  $\ln(\epsilon)$  for tensile specimens are shown in Figure 4.5. Figures 4.5 (I) and (II) show four logarithmic stress-strain profiles for FADG (8.5 % oil content) and PDG material respectively. Similarly, Figures 4.5 (III) and (IV) show four logarithmic stress-strain profiles for FADC (1.2 % oil content) and PDC materials respectively.

Table 4.1 records the relationship between nominal stress and strain for each material and the corresponding correlation coefficient ( $r^2$ ). The power model satisfactorily represents the stress-strain curves and the average value of  $r^2 \geq 0.95$  for each material. As expected, the exponent  $n > 1$  in all four materials, this is indicative of the general 'J' shaped stress-strain curve of leather [Attenburrow, 1992]. Nevertheless, agreement is not perfect because there is some departure from a perfect 'J' shaped stress-strain curve in all materials examined, (section 3.2.1).

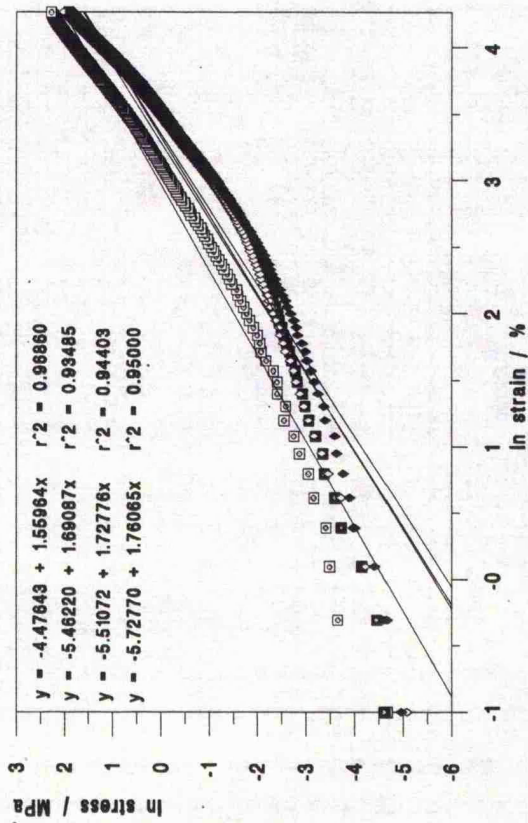
Table 4.1.

Material	Average linear Equation.	$r^2$
FADG	$\ln \sigma = -5.294 + 1.685 \ln \epsilon$	$r^2 = 0.95$
PDG	$\ln \sigma = -2.635 + 1.193 \ln \epsilon$	$r^2 = 0.98$
FADC	$\ln \sigma = -4.183 + 1.845 \ln \epsilon$	$r^2 = 0.98$
PDC	$\ln \sigma = -3.472 + 1.734 \ln \epsilon$	$r^2 = 0.97$

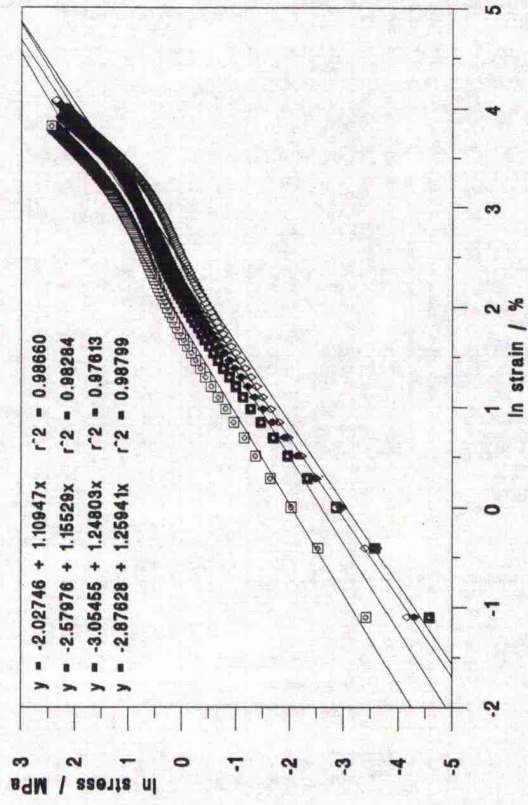
The presence of oil in grain material increases the exponent  $n$ , indicating a move towards a more pronounced 'J' shaped stress-strain pattern. Thus, in the case of PDG material,  $n = 1.193$  as opposed to FADG material (8.5 % oil content) where  $n = 1.685$ , an increase in the exponent  $n$  of 41% due to the presence of oil. A similar, but much less pronounced effect is seen in the corium where, in the case of the PDC material,  $n = 1.734$  compared to the FADC material (1.2 % oil content) where  $n = 1.845$ , an increase in the exponent  $n$  of 6% due to the presence of oil. Both corium layers have a more pronounced 'J' shape than the corresponding grain layers.

Figure 4.5  
Logarithmic stress strain profiles of grain and corium material.

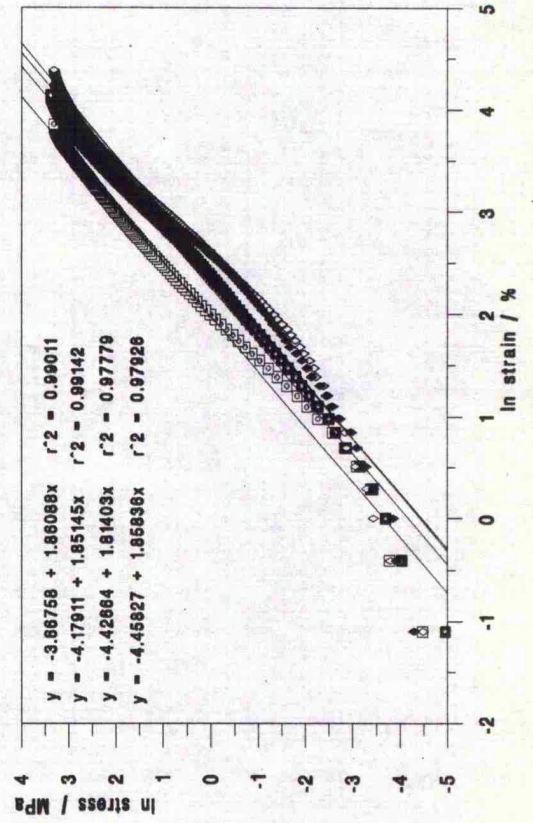
(I) Material = FADG.



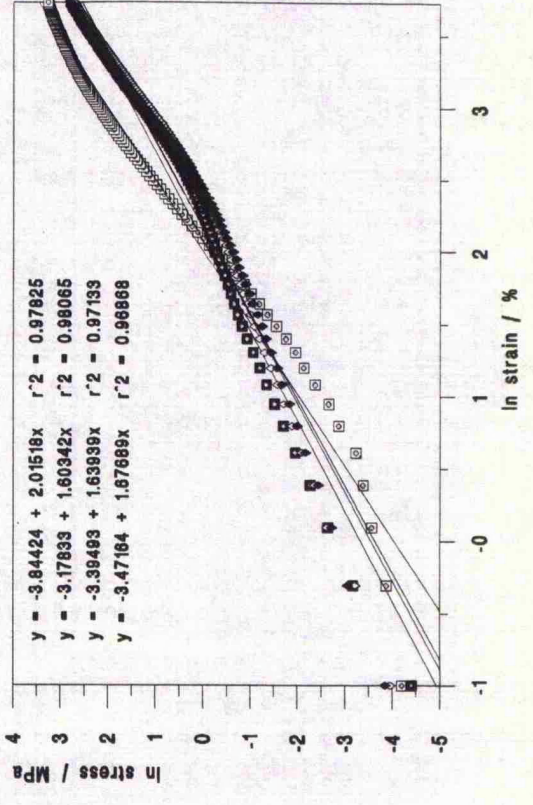
(II) Material = PDG.



(III) Material = FADC.



(IV) Material = PDC.



#### 4.2.3 (a) Fracture stress of grain material.

The derived relationship between fracture stress and notch length for notch-sensitive materials [Purslow, 1991] is,

$$\ln \sigma_f = K_1' - M \ln(a) \quad [4.8]$$

Where  $M = n / n + 1$  [4.9]

As shown in Appendix 6.1

$$K_1' = \text{constant} = n/(n+1) [ \ln(K)/n + \ln(R(n+1) / \pi) ]$$

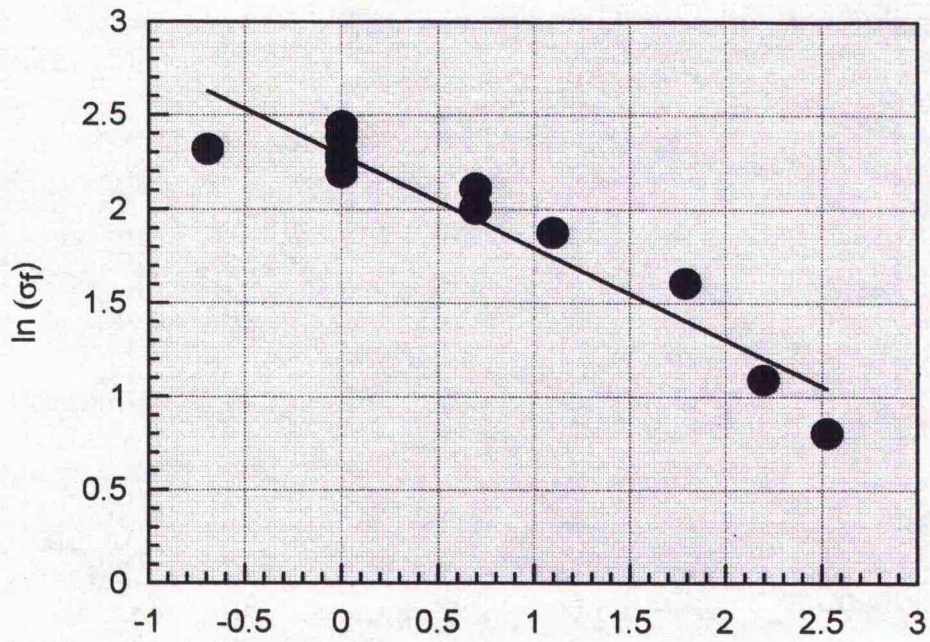
where  $R = - |dU/dA|_U$

and  $K = \sigma / \epsilon^n$

Thus, a plot of  $\ln(\sigma_f)$  versus  $\ln(a)$  in a notch sensitive elastic material should produce a straight line with a gradient equal to  $M$  and an intercept through the ordinate equal to  $K_1'$ . Figures 4.6 (I) and (II) show this format of plot for FADG and PDG material respectively. The linear trend line in each plot and the quoted  $r^2$  values confirm a good fit of the data to an equation having the form of equation [4.8]. Table 4.2 shows a comparison of the variables  $M$  and  $n$ , as predicted from the original stress strain curves, as well as the values of  $M$  observed directly by plotting  $\ln(\sigma_f)$  versus  $\ln(a)$ .

Figure 4.6

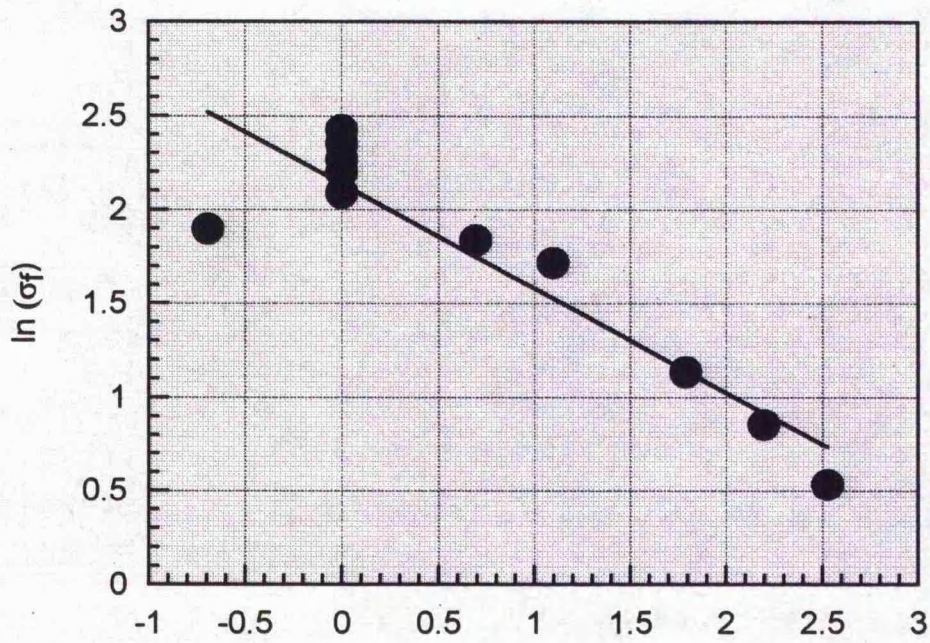
The natural log of breaking stress versus the natural log of notch length for FADG and PDG specimens.



$$\ln(\sigma_f) = 2.29 - 0.49 \ln(a) \quad [r^2 = 0.91]$$

Material = FADG

(I)



$$\ln(\sigma_f) = 2.14 - 0.56 \ln(a) \quad [r^2 = 0.87]$$

Material = PDG

(II)

Table 4.2.

Material	Value of n {obtained from the plot $\ln(\sigma)$ vs. $\ln(\epsilon)$ .}	Predicted value of M {derived from the plot $\ln(\sigma)$ vs. $\ln(\epsilon)$ Equation [4.9]. }	Observed value of M (obtained from the plot $\ln(\sigma_f)$ vs. $\ln(a)$ . }
FADG	1.69	0.63	0.47
PDG	1.19	0.54	0.55

The exponent,  $n$ , describing the stress-strain behaviour of unnotched specimens in Equation [4.6] predicts  $M$  values of 0.63 and 0.54 for the FADG and PDG material respectively. For PDG material, the observed value of  $M$  is in agreement with the predicted value of  $M$ . However for FADG material, the observed value of  $M$  is lower than theoretically predicted. Thus, the theoretical relationship between breaking stress and notch length derived by Purslow [1991], accurately predicts the observed fracture behaviour of single notch PDG specimens but not FADG specimens.

#### 4.2.3 (b) Fracture strain of grain material.

For notch-sensitive materials Purslow [1991], derived the following relationship between fracture strain and notch length.

$$\ln \epsilon_f = K_2' - P \ln(a) \quad [4.10]$$

Where  $P = 1 / n + 1$  [4.11]

As shown in Appendix 6.1

$$K_2' = (1/(n+1)) (\ln (R(n+1)/K\sigma))$$

Thus, a plot of  $\ln (\epsilon_f)$  versus  $\ln (a)$  for a notch sensitive material should produce a straight line with a gradient  $P$  and intercept through the ordinate,  $K_2'$ . Figures 4.7 (I) and (II) show this format of plot for FADG and PDG specimens respectively. The linear trend line in each plot and the quoted  $r^2$  values confirm an acceptable fit of the data to an equation of the form suggested in Equation [4.10]. Table 4.3 shows a comparison of the variables  $P$  and  $n$ , as predicted from the original stress-strain curves, as well as the observed value of  $P$  obtained from a plot of  $\ln (\epsilon_f)$  versus  $\ln (a)$ .

Table 4.3.

Material	Value of $n$ {obtained from the plot $\ln (\sigma)$ vs. $\ln (\epsilon)$ .}	Predicted value of $P$ {derived from the plot $\ln (\sigma)$ vs. $\ln (\epsilon)$ and Equation [4.11]}	Observed value of $P$ {obtained from plot $\ln (\epsilon_f)$ vs. $\ln (a)$ .}
FADG	1.69	0.37	0.16
PDG	1.19	0.46	0.22

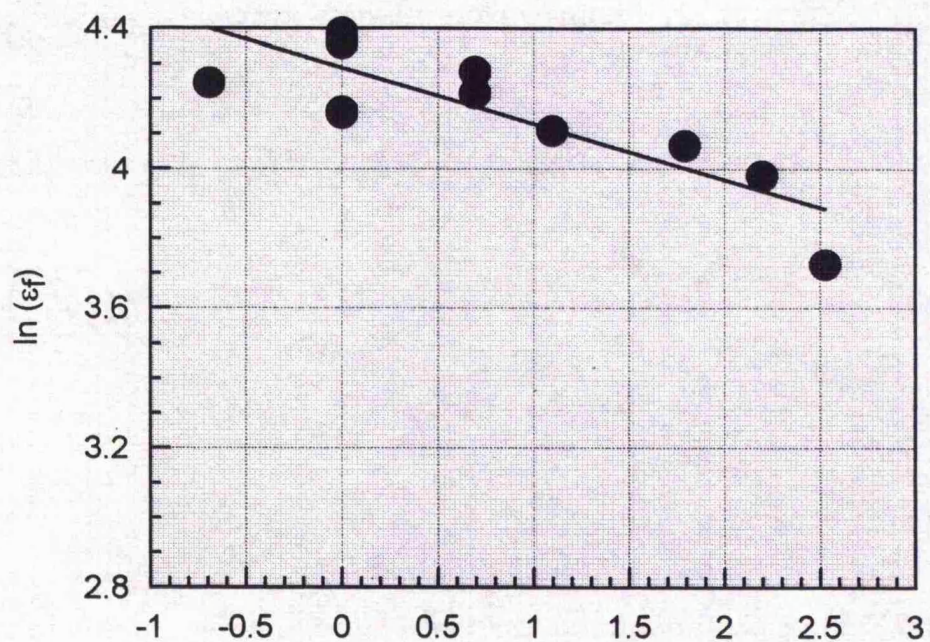
The exponent,  $n$ , describing the stress-strain behaviour of unnotched specimens in Equation [4.6] predicts  $P$  values of 0.37 and 0.46 for FADG and PDG materials respectively. However, observed values of  $P$  for both materials are somewhat lower than theoretical predictions. Thus, it would appear that the theoretical relationship between breaking strain and notch length does not accurately predict the observed behaviour of FADG or PDG single notch specimens.

According to Equation [4.11], when the stress-strain curve of an unnotched tensile specimen is 'J' shaped (in other words the exponent  $n > 1$ ) the value of  $P < 0.5$ . This is indeed the case for both the predicted and observed  $P$  values of each material. However, the predicted fall in breaking strain with increasing notch length is much steeper than actually observed for either FADG or PDG specimens.

Table 4.3 also shows that the breaking strain of both FADG and PDG materials is less sensitive to the presence of a notch than the nominal breaking stress (as predicted for elastic materials with a 'J' shaped tensile behaviour [Purslow, 1991]). In addition, the observed values of  $P$  show that the sensitivity of fracture strain to notch length is lessened by the presence of fatliqor in the grain material.

Figure 4.7

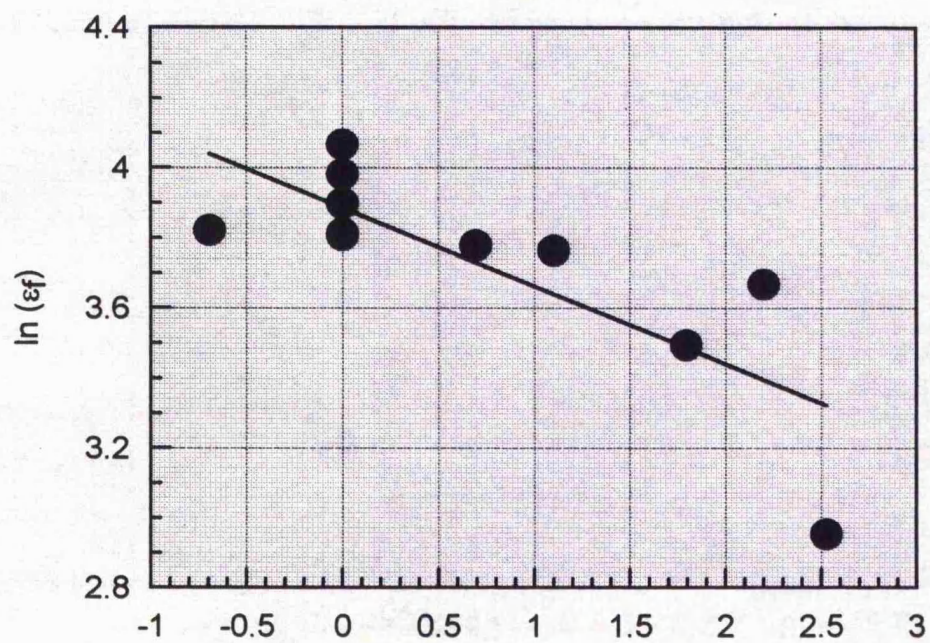
The natural log of breaking stress versus the natural log of notch length for FADG and PDG specimens.



$$\ln(\epsilon_f) = 4.29 - 0.16 \ln(a) \quad [r^2 = 0.71]$$

Material = FADG

(I)



$$\ln(\epsilon_f) = 3.89 - 0.23 \ln(a) \quad [r^2 = 0.62]$$

Material = PDG

(II)

#### 4.2.3 (c) Fracture stress of corium material.

Purslow's approach to notch-insensitive materials [1991] does not lead to a power law between fracture stress, fracture strain and notch length. When deriving the fracture toughness (Appendix 6.2) the supposed nature of the strain-energy-free-zone in a notch insensitive material ensures that the notch length term ( $a$ ) is eliminated. This result is not surprising because, as Equation [4.4] reveals, there is no direct relationship between fracture stress (or strain) and notch length in completely notch-insensitive materials. Nevertheless, a direct relationship does exist between fracture stress and one minus the ratio of notch length to sample width. In other words, for notch insensitive materials, the fracture stress (or strain) is dependent on the width of material remaining in the specimen after the notch has been cut.

For completely notch-insensitive materials, the relationship between fracture stress and notch length can be expressed as,

$$\ln \sigma_f = \ln \sigma_b + \ln (1 - a/W)$$

$$\ln \sigma_f = \ln \sigma_b + \ln [(W - a)/W]$$

$$\ln \sigma_f = \ln \sigma_b + \ln (W - a) - \ln W$$

$$\ln \sigma_f = \ln (\sigma_b / W) + \ln (W - a)$$

$$\text{Hence} \quad \ln \sigma_f = K_3' + q [ \ln (W - a) ] \quad [4.12]$$

$$\text{Where} \quad K_3' = \ln (\sigma_b / W) \quad [4.13]$$

$$\text{and} \quad q = 1 \quad [4.14]$$

Thus, a plot of  $\ln(\sigma_f)$  versus  $\ln(W - a)$  for a notch-insensitive elastic material should produce a straight line with a gradient,  $q$  equal to one and an intercept through the ordinate equal to  $K_3'$ . Figures 4.8 (I) and (II) show plots of  $\ln \sigma_f$  versus  $\ln(W-a)$  for FADC and PDC specimens respectively.

The indication of a completely notch insensitive elastic material is that the value of  $q$  in Equation [4.12] equals one. When this occurs, the value of  $K_3'$  in Equation [4.13] can be rearranged to confirm the breaking stress of unnotched samples. However, the values of  $q$  obtained are 1.57 and 1.59 for FADC and PDC materials respectively, thus indicating some small degree of notch sensitivity. The logarithmic relationships developed in Figures 4.8 (I) and (II) of,

$$\begin{aligned} \ln \sigma_f &= -1.73 + 1.57 \ln(W-a) && \{\text{for FADC specimens}\} \text{ and,} \\ \ln \sigma_f &= -1.94 + 1.59 \ln(W-a) && \{\text{for PDC specimens}\} \end{aligned}$$

or

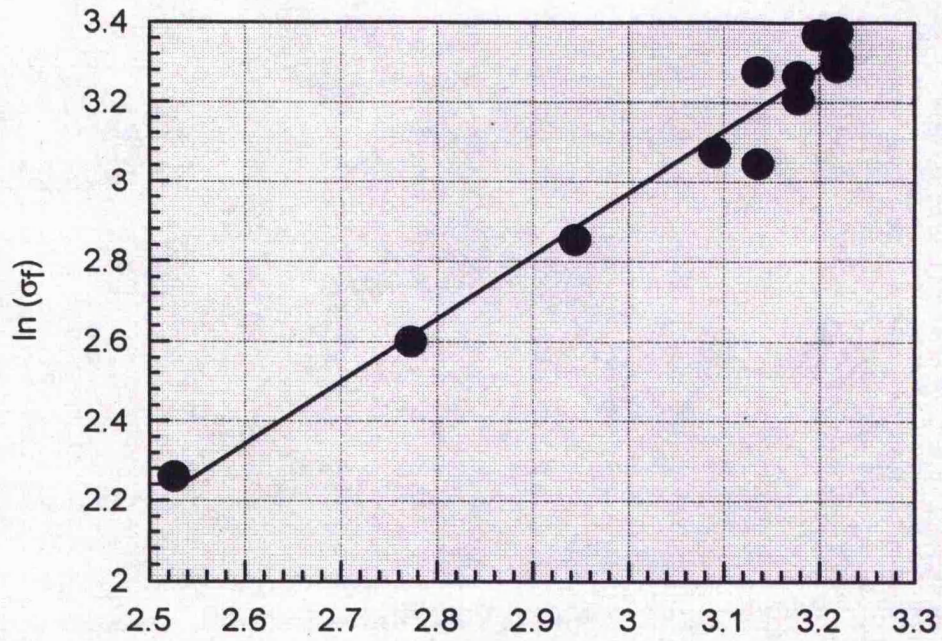
$$\sigma_f = 0.18 (W-a)^{1.57} \quad [4.15]$$

$$\sigma_f = 0.14 (W-a)^{1.59} \quad [4.16]$$

show that breaking stress is a function of  $(W-a)$  (in other words a function of the remaining width in the sample after the notch is cut, and not simply the length of the notch itself). The plots  $(\sigma_f)$  Vs  $(a)$ , for FADC and PDC specimens (Figure 4.3 (III) & (IV)) clearly show the insensitivity of breaking stress to notch length. However, the above analysis and the logarithmic plots yields a relationship between  $(\sigma_f)$  and  $(W - a)$  as opposed to a relationship between  $(\sigma_f)$  and  $(a)$ .

Figure 4.8

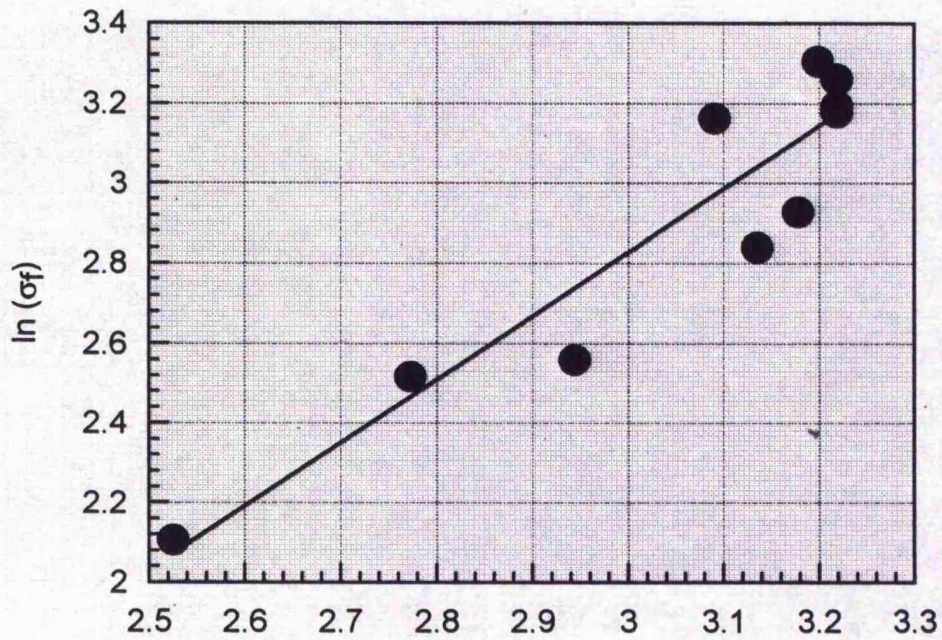
The natural log of breaking stress versus the natural log of the sample width minus the notch length for FADC and PDC specimens.



$$\ln(\sigma_f) = -1.73 + 1.57 \ln(W-a) \quad [r^2 = 0.97]$$

Material = FADC

(I)



$$\ln(\sigma_f) = -1.94 + 1.59 \ln(W-a) \quad [r^2 = 0.88]$$

Material = PDC

(II)

#### 4.2.3 (d) Fracture strain of corium material.

For a completely notch-insensitive, non-linear elastic material, the relationship between fracture strain and notch length is derived in the following manner,

$$\text{From [4.4]} \quad \sigma_f = \sigma_b (1 - a/W) \quad [\text{Kelly \& Macmillan, 1986}]$$

$$\text{From [4.5]} \quad \sigma_f = K \epsilon_f^n \quad [\text{Purslow, 1991}]$$

$$\text{Hence} \quad K \epsilon_f^n = \sigma_b (1 - a/W)$$

$$n \ln (\epsilon_f) = \ln (\sigma_b / K) + \ln [ (W - a)/W ]$$

$$n \ln (\epsilon_f) = \ln (\sigma_b) - \ln (K) + \ln (W - a) - \ln W$$

$$\ln (\epsilon_f) = 1/n \cdot \ln [ \sigma_b / (K W) ] + 1/n [ \ln (W - a) ]$$

$$\text{Hence} \quad \ln (\epsilon_f) = K_4' + s [ \ln (W-a) ] \quad [4.17]$$

$$\text{or} \quad \epsilon_f = e^{K_4'} (W-a)^s \quad [4.18]$$

$$\text{Where} \quad K_4' = 1/n \cdot \ln [ \sigma_b / (K W) ] \quad [4.19]$$

$$\text{and} \quad s = 1/n \quad [4.20]$$

Thus, a plot of  $\ln (\epsilon_f)$  versus  $\ln (W - a)$  for a completely notch-insensitive material produces a straight line with gradient,  $s$  and intercept through the ordinate,  $K_4'$ .

Figures 4.9 (I) and (II) show plots of  $\ln \epsilon_f$  versus  $\ln (W-a)$  for the FADC and PDC specimens respectively and the linear trend is of the form shown in Equation [4.17]. Specifically, the relationships between fracture strain and  $(W - a)$  are:

$$\ln \epsilon_f = 0.64 + 1.09 \ln (W-a) \quad \{\text{for FADC specimens}\} \text{ and}$$

$$\ln \epsilon_f = 2.11 + 0.54 \ln (W-a) \quad \{\text{for PDC specimens}\}.$$

or

$$\epsilon_f = 1.90 (W-a)^{1.09} \quad [4.21]$$

$$\epsilon_f = 8.25 (W-a)^{0.54} \quad [4.22]$$

Using Equations [4.19] and [4.20] it is possible to predict  $K_4'$  and  $s$  for both FADC and PDC, Table 4.4 shows both the predicted and observed values.

Table 4.4

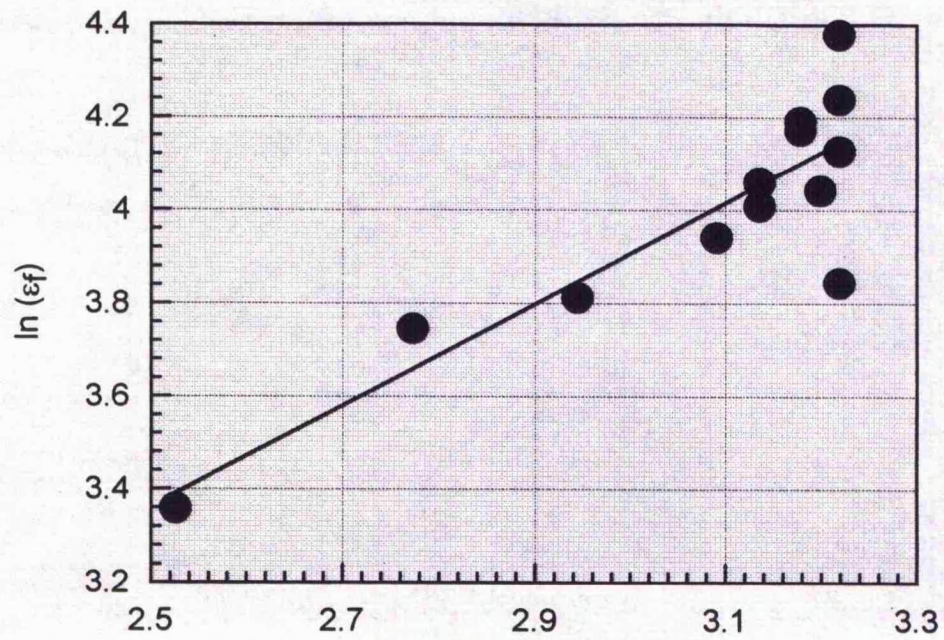
Material	(s) Predicted from Equation [4.20]	(s) Observed	( $K_4'$ ) Predicted from Equation [4.19]	( $K_4'$ ) Observed
FADC	$1/1.85 = 0.54$	1.09	$0.54 \ln [28/(0.015 \times 25)] = 2.33$	0.64
PDC	$1/1.73 = 0.58$	0.54	$0.58 \ln [24.4/(0.031 \times 25)] = 1.99$	2.11

The observed values of  $s$  and  $K_4'$  for PDC specimens agree with predictions. However, some departure from the predicted values of both  $s$  and  $K_4'$  are evident for FADC specimens.

No direct intrinsic relationship exists between notch length ( $a$ ) and nominal breaking strain ( $\epsilon_f$ ) for notch insensitive materials, as apparent from Equation [4.18]. The purpose of the above analysis was to establish a relationship, not between ( $\epsilon_f$ ) and ( $a$ ), but between ( $\epsilon_f$ ) and ( $W - a$ ), i.e. Equation [4.21] and [4.22] for FADC and PDC respectively.

Figure 4.9

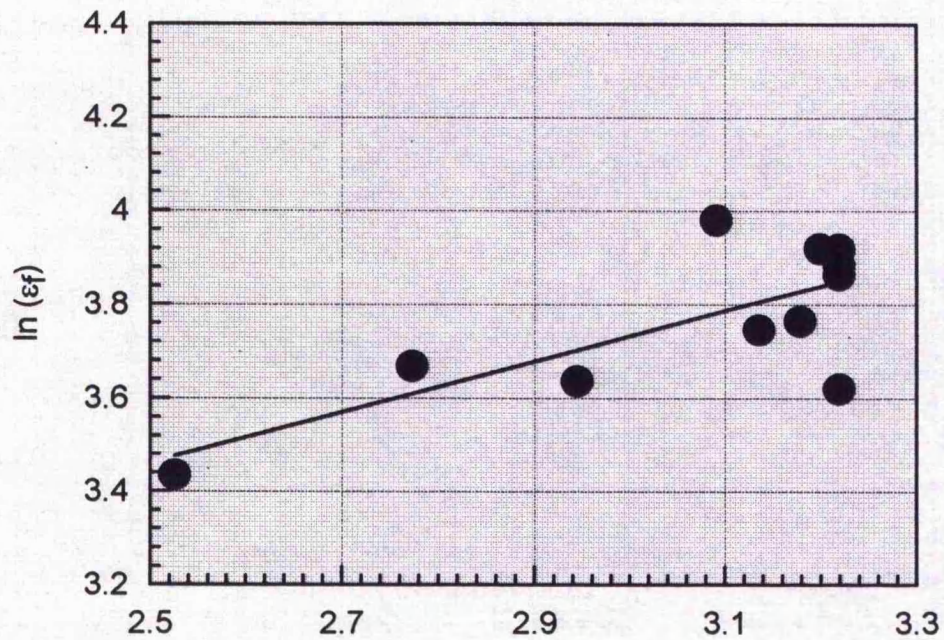
The natural log of breaking strain versus the natural log of the sample width minus the notch length for FADC and PDC specimens.



$$\ln(\epsilon_f) = 0.64 + 1.09 \ln(W-a) \quad [r^2 = 0.77]$$

Material = FADC

(I)



$$\ln(\epsilon_f) = 2.11 + 0.54 \ln(W-a) \quad [r^2 = 0.56]$$

Material = PDC

(II)

#### 4.2.4 Strain distribution in single edge notch specimens.

The theory of notch sensitivity of non-linear materials [Purslow, 1991] associates differences in notch sensitivity of materials to differences in the distribution of strain energy (as illustrated in Figure 3.2). In this respect, it was felt important to obtain a measure of the distribution of strain energy within single edge notch specimens of grain and corium material. To directly measure local stress levels in a notched specimen and produce a map of stress concentration in a material such as leather is an extremely difficult task. However, measurement of local strains (as outlined in section 2.4.3) is a feasible alternative and by measuring local strains throughout a single notch specimen, a strain distribution map can be produced.

Strain energy distribution (as employed by Purslow [1991]) must be differentiated from strain distribution in single edge notch specimens (as used here). Both grain and corium material show non-linear, energy dissipating tensile properties (chapter 3). Accordingly, it would be inappropriate to calculate local strain energies as a function of the local strain and the nominal stress in the specimen (as would be the case for an elastic material). Indeed, to directly measure local strain energies in strained leather would require the measurement of both local stresses and strains.

Nevertheless, a strain distribution map offers a clear indication of the relative magnitude and local topographic variability of deformation within a single edge notch specimen. In essence, the strain distribution map provides a good indication of where strain energy has been distributed within a single edge notch specimen.

Figures 4.10, 4.12, 4.14 and 4.16 show a sequence of video images of FADG (12.5 % oil content), PDG, FADC (3.0 % oil content) and PDC single edge notch specimens at several levels of nominal strain during deformation and fracture. Following each of these figures (i.e. Figures 4.11, 4.13, 4.15 and 4.17) are the 'spectral plots' corresponding to the strain distribution of each image in the preceding figure. Each Spectral plot is a 2-dimensional display of the 3-dimensional array of strain data. The plots are similar to contour plots. However, the strain values (i.e. the Z values in the matrix) are represented by a colourmap fill.

In each plot, there are 4 columns labelled 1 to 4 (left to right) and 12 rows, labelled 1 to 12 (top to bottom) of measured strain values. An inverse-distance weighting algorithm was used to generate the interpolated surface of the colourmap [Stanford Graphics User Guide, 1993 p 505]<sup>9</sup>. Thus, the strain induced between two vertical dots (as illustrated in Figure 2.3 (I)) is represented and referred back to the original grid.

Figure 4.10 shows a sequence of video images during deformation and fracture of a FADG single edge notch specimen (12.5 % oil content). The nominal strain level of the single notch specimen in each image is (I) 8.3 %, (II) 16.6 %, (III) 25.0 %, (IV) 33.3 %, (V) 41.6 % and (VI) 46.4 % (achieved in the last 0.04 of a second before complete sample failure). Figure 4.11 contains six spectral plots, labelled (I) to (VI), that correspond to images (I) to (VI) in Figure 4.10 and show the strain distribution at the same specified nominal strain levels.

---

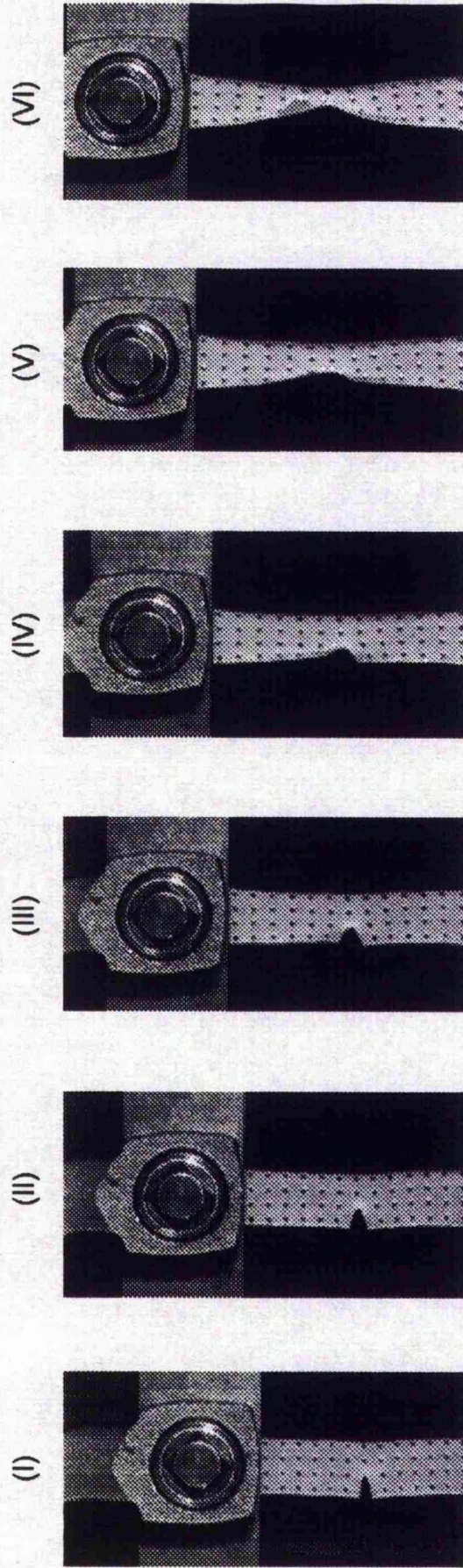
<sup>9</sup> Distributed by Adept Scientific, 6 Business Centre West, Avenue One, Letchworth, Herts, SG6 2HB.

At a sample strain level of 8.3 % in Figure 4.11 (I), much of the area to the left of column number two (indicative of the area to the left of the notch tip in the single edge notch specimen) experiences a low level of strain. However, in columns 3 and 4 (i.e. to the right of the notch on the original grid) at row numbers 5, 6 and 7, an area of higher strain (9 to 13 %) exists. In (II) to (IV), as the nominal strain in the specimen increases, a semi circular region of strain less than 4 % exists around the area of the notch in the original grid.

Additionally, the distance between the first dot above and the first dot below the crack is not indicative of strain as no material is present. Hence the local strain at any such point in the grid is denoted by a zero. In (V) the strain distribution approaches the theoretical distribution of a notch-sensitive material, outlined in Figure 4.2 (II). There is a clear semi-circular region, around the notch, of low strain and higher levels of strain between 40 % and 50 % + in the remainder of the specimen.

Figure 4.11 (VI) is indicative of the strain distribution in the sample in the last 0.04 s before fracture, at a nominal strain level of 46.4 %. The semi-circular region of very low strain has enlarged due to the slow crack growth in the sample and the consequent drop in local strain around the larger notch. However, high levels of local strain distribution (45 to 50 % +) are again noticeable in the surrounding regions.

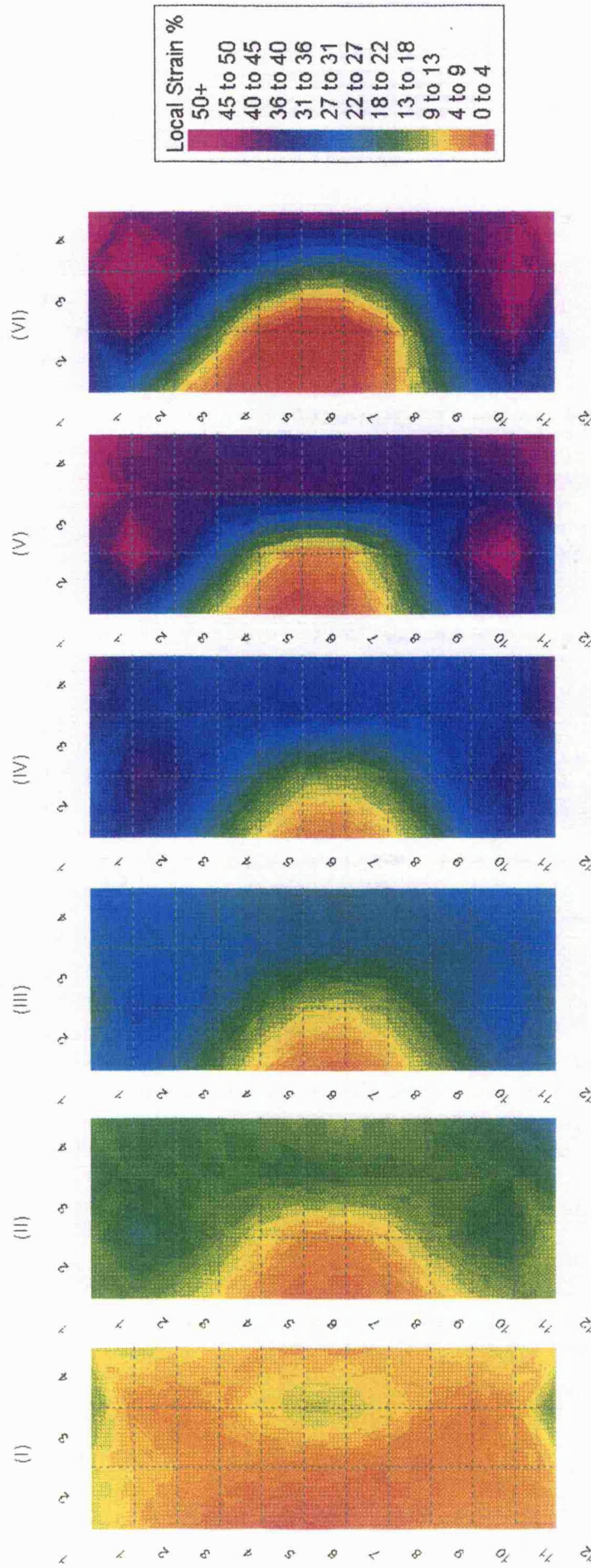
Figure 4.10



Video sequence showing the deformation and fracture of a FADG single notch specimen.

The nominal strain levels are: (I) 8.3 %, (II) 16.6 %, (III) 25.0 %, (IV) 33.3 %, (V) 41.6 %, (VI) 46.4 %.

Figure 4.11

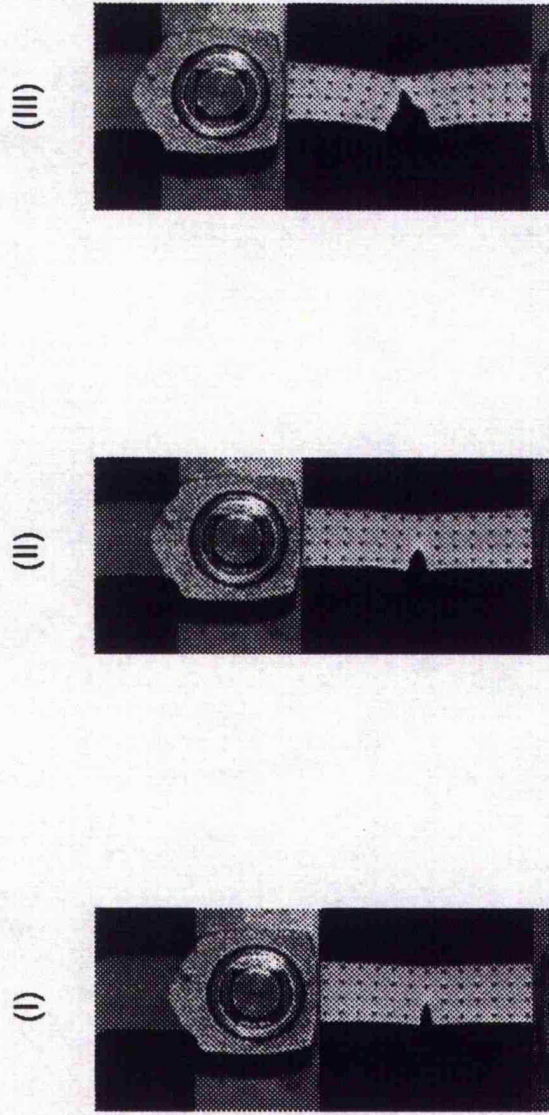


The strain distribution in a FADG single notch specimen during deformation and fracture.

The nominal strain levels are (I) 8.3 %, (II) 16.6 %, (III) 25.0 %, (IV) 33.3 %, (V) 41.6 %, (VI) 46.4 %.

Figure 4.12 shows a sequence of video images of a PDG single notch specimen during deformation and fracture. The nominal strain level in each image is (I) 8.3% (II) 16.6 % and (III) 25.2 % (achieved in the last 0.04 s before complete sample failure). Figure 4.13 contains three spectral plots labelled (I) to (III), showing the strain distribution corresponding to Figure 4.12 (I) to (III) respectively. The PDG specimen fractures at a much lower nominal strain level than the FADG specimen. Figure 4.13 (III) shows that, instead of a clear semi-circular region of low strain around the notch and higher levels of strain (45 to 50 % +) evenly distributed in the remainder of the specimen, only the area ahead of the notch attains anywhere near these levels of local strain (40 to 45 %). At this point the specimen fractures.

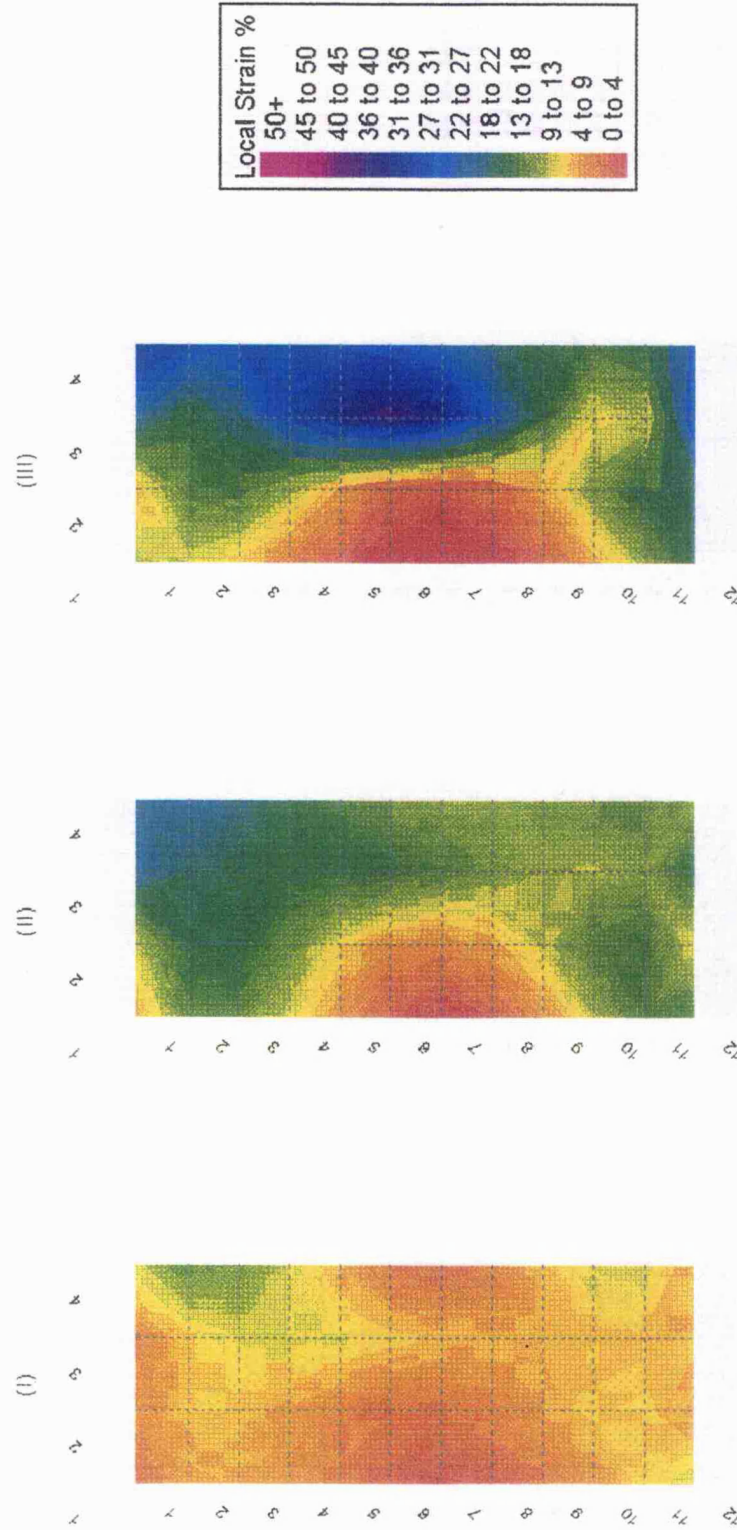
Figure 4.12



Video sequence showing the deformation and fracture of a PDG single notch specimen.

The nominal strain levels are: (I) 8.3 %, (II) 16.6 %, (III) 25.2 %

Figure 4.13



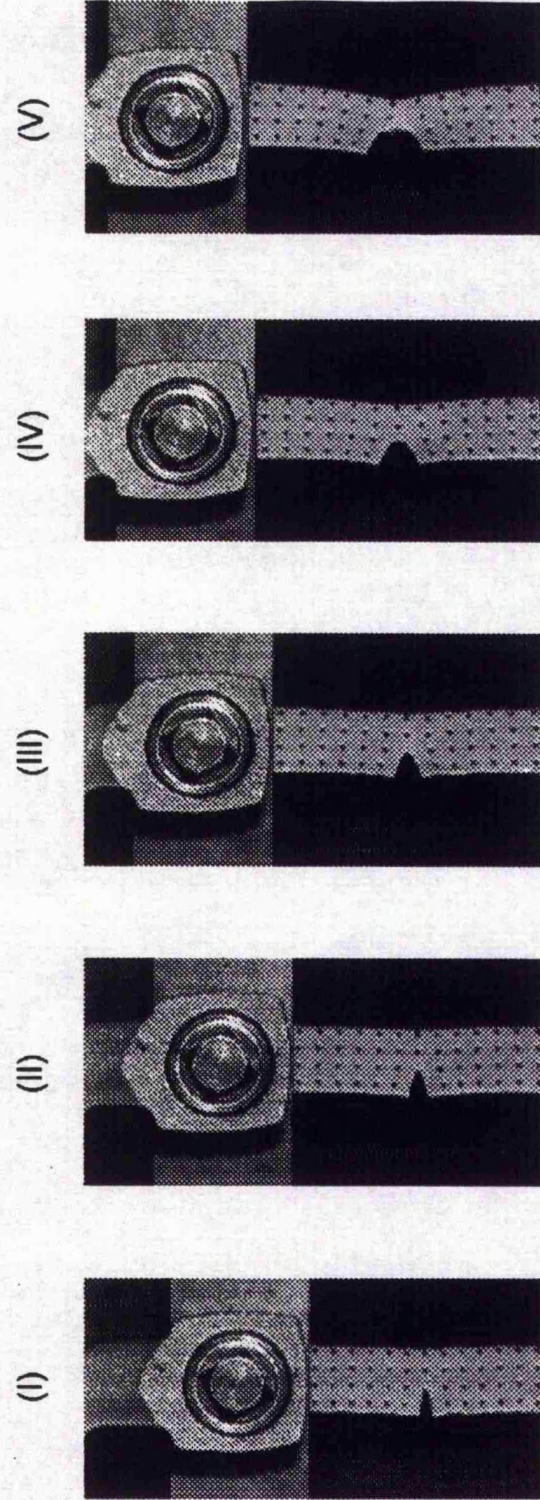
The strain distribution in a PDG single notch specimen during deformation and fracture.

The nominal strain levels are (I) 8.3 %, (II) 16.6 % (III) 25.2 %.

Figure 4.14 shows a sequence of five video images, labelled (I) to (V), and Figure 4.15 shows the corresponding spectral plots that represent the strain distribution in the single edge notch specimen of FADC, during the test. The nominal strain level of the single notch specimen in each image / plot is (I) 8.3 %, (II) 16.6%, (III) 25.0 %, (IV) 33.3 % and (V) 37.0 % (achieved in the last 0.04 s before specimen fracture). From Figure 4.15, as the nominal strain in the sample increases from 8.3 % in (I) to 33.3 % in (IV), the local strains in all areas around the semi-circular region of low strain, increase and remain evenly distributed. However, at a nominal sample strain of 37.0 % in Figure 4.15 (V), a large region of high local strain (50%+) is highly prominent ahead of the notch.

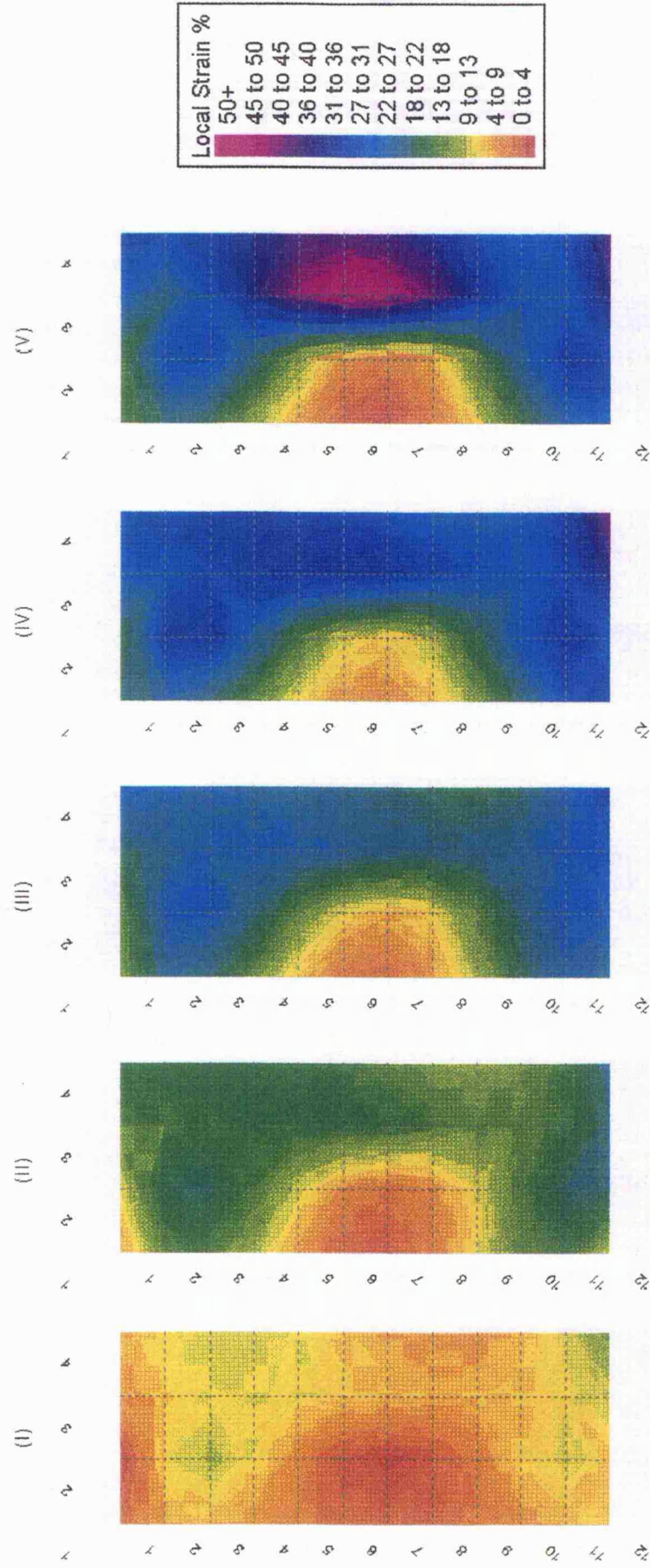
Figure 4.16 is a video sequence of four images labelled (I) to (IV) during the single notch test of PDC material. Figure 4.17 shows the corresponding spectral plots which represent the strain distribution in the specimen, over the duration of the test. The nominal strain level in each image / plot is (I) 8.3 % (II) 16.6 % (III) 25.0 % and (IV) 31.5 % (achieved in the last 0.04 s before complete sample failure). As the nominal strain in the sample increases from 8.3 % in (I) to 25.0 % in (III) a very similar situation to that of the FADC is observed. The local strain in areas around the semi-circular region of low strain, increases and remain evenly distributed. Again the situation just before fracture, shown in Figure 4.17 (IV), indicates a large region of high local strain ahead of the notch of 40 to 45%.

Figure 4.14



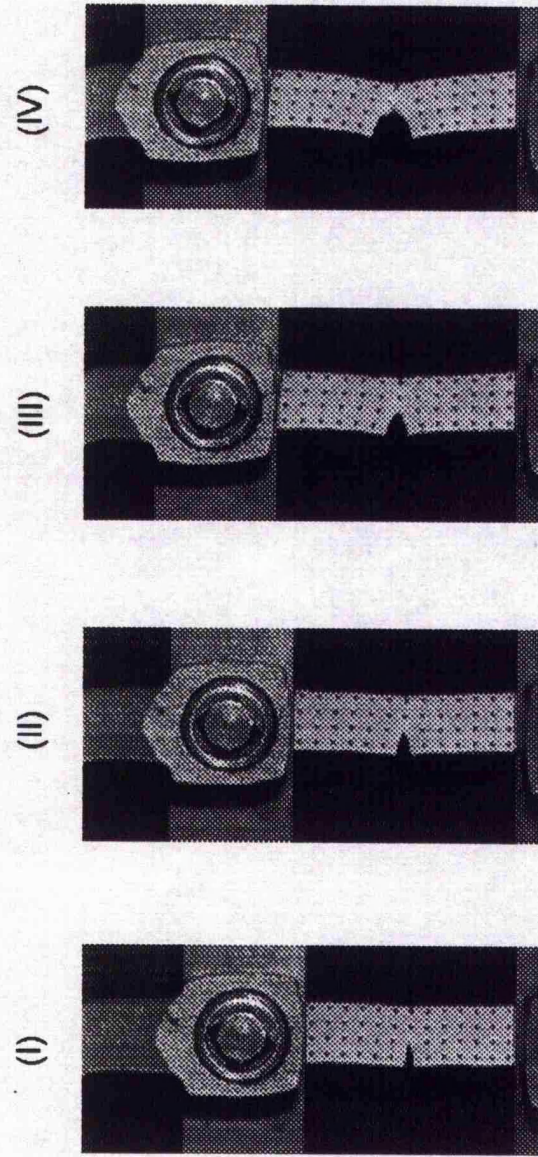
Video sequence showing the deformation and fracture of a FADC single notch specimen.  
The nominal strain levels are: (I) 8.3 %, (II) 16.6 %, (III) 25.0 %, (IV) 33.3 %, (V) 37.0 %.

Figure 4.15



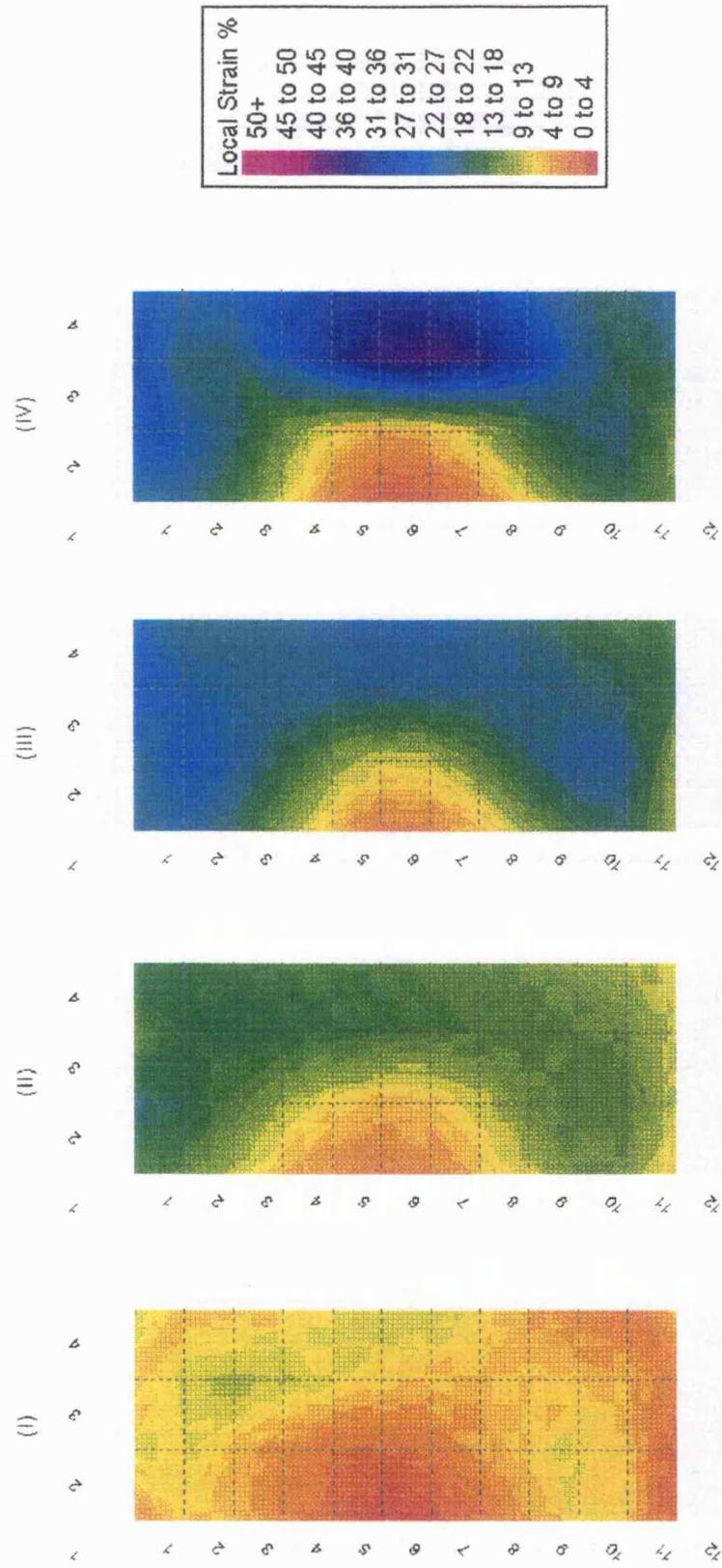
The strain distribution in a FADC single notch specimen during deformation and fracture. The nominal strain levels are (I) 8.3 %, (II) 16.6 %, (III) 25.0 %, (IV) 33.3 %, (V) 37.0 %.

Figure 4.16



Video sequence showing the deformation and fracture of a PDC single notch specimen.  
The nominal strain levels are: (I) 8.3 %, (II) 16.6 %, (III) 25.0 %, (IV) 31.5 %.

Figure 4.17



The strain distribution in a PDC single notch specimen during deformation and fracture.

The nominal strain levels are (I) 8.3 %, (II) 16.6 %, (III) 25.0 %, (IV) 33.5 %.

#### 4.2.5 Strain distribution in the vicinity of a notch.

Figures 4.18, 4.20, 4.22 and 4.24 show a sequence of video images of the deformation and fracture of FADG, PDG, FADC and PDC notched specimens respectively. All images are focused on the area of the specimen in the vicinity of the notch. Figures 4.19, 4.21, 4.23 and 4.25 show a sequence of spectral plots that represent the strain distribution in the vicinity of the notch during deformation and fracture of FADG, PDG, FADC and PDC notched specimens respectively (i.e. they correspond to the images of the previous figure).

The measured area of strain distribution is illustrated in Figure 2.3 (II) and the method used to obtain the strain matrix is outlined in Section 2.5.5. In each spectral plot, there are 12 columns labelled 1 to 12 (left to right) and 11 columns labelled 1 to 11 (top to bottom) of measured strain values. The strain induced between two vertically aligned dots (as illustrated in Figure 2.3 (II)) are represented by a colourmap fill and referred back to the original grid of the strain matrix.

Figure 4.18 shows a sequence of six video images during the deformation and fracture of a FADG specimen. The nominal strain level of the single notch specimen in each image is (I) 8.3 %, (II) 16.6 %, (III) 25.0 %, (IV) 33.3 %, (V) 41.6 % and (VI) 46.4 % (achieved in the last 0.04 s before complete sample failure). Figure 4.19 shows six spectral plots labelled (I) to (VI). These plots show the distribution of strain in the vicinity of the notch and directly correspond to images 4.18 (I) to (VI).

In Figure 4.19, the plots (I) to (V) show how the local strain in the sample builds up to levels of between 45 to 54% to the right of the notch. In addition, at the very tip of the notch, a small area exists where the local strain is between 81 to 90%. In Figure 4.19 (VI) it is evident the crack has propagated and local strains of 90 to 100%+ are apparent at the tip of the crack.

A sequence of four video images and the corresponding spectral plots are shown in Figures 4.20 and 4.21 respectively for a single edge notch specimen of PDG material during deformation and fracture. The nominal strain level of the single edge notch specimen in each image / plot is (I) 8.3 %, (II) 16.6 %, (III) 25.0 %, and (IV) 33.3 %. Figures 4.21 (I) to (III) show how the local strain in the sample builds up to levels of between 18 to 45% to the right of the notch. Additionally, even at the low nominal samples strains in (I) and (II), the local strains measured at the very tip of the notch are significantly higher than the area to the right of the notch tip. In Figure 4.21 (IV) the crack has propagated and local strains of 72 to 90% are apparent at the tip of the crack.

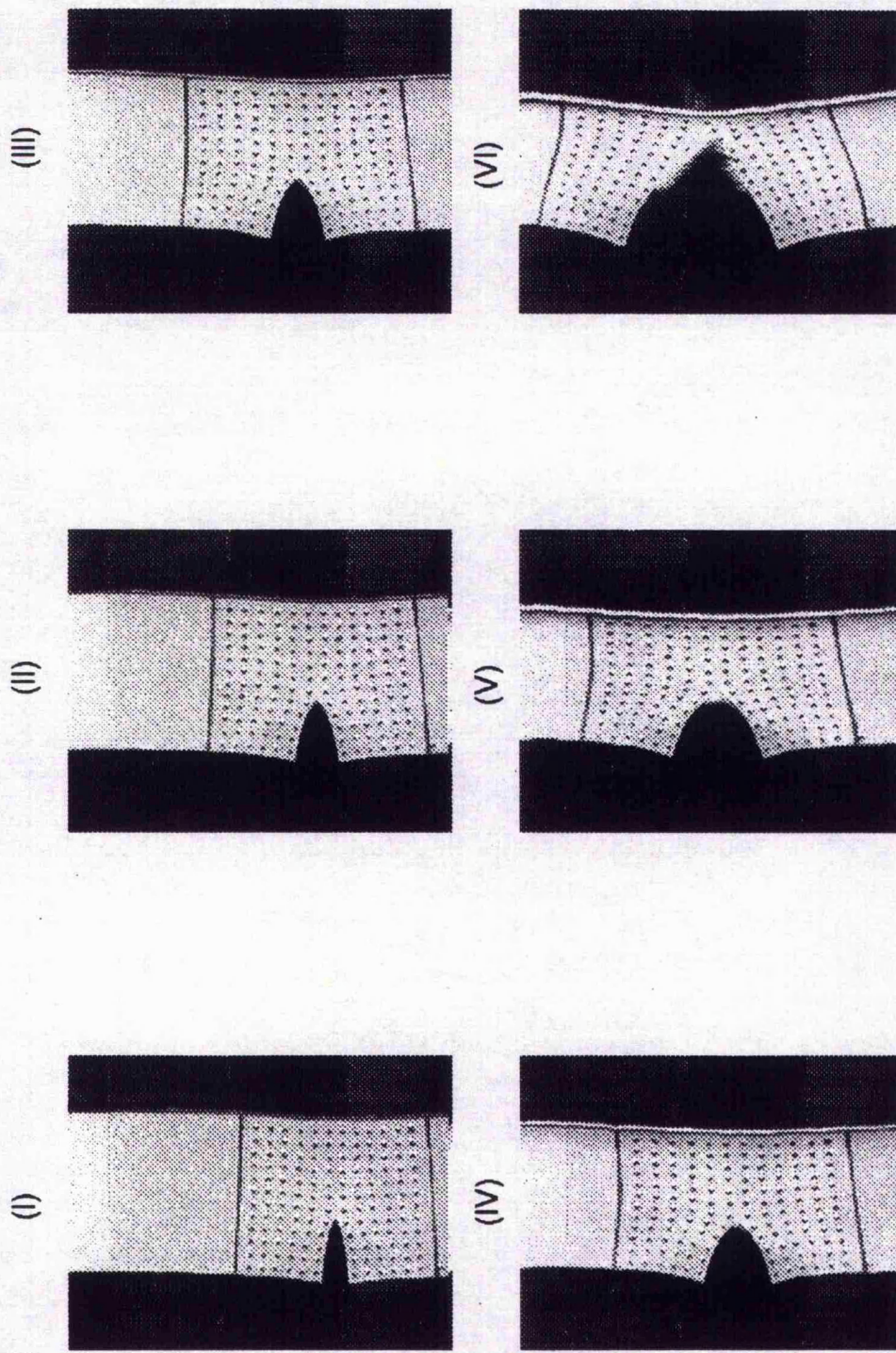
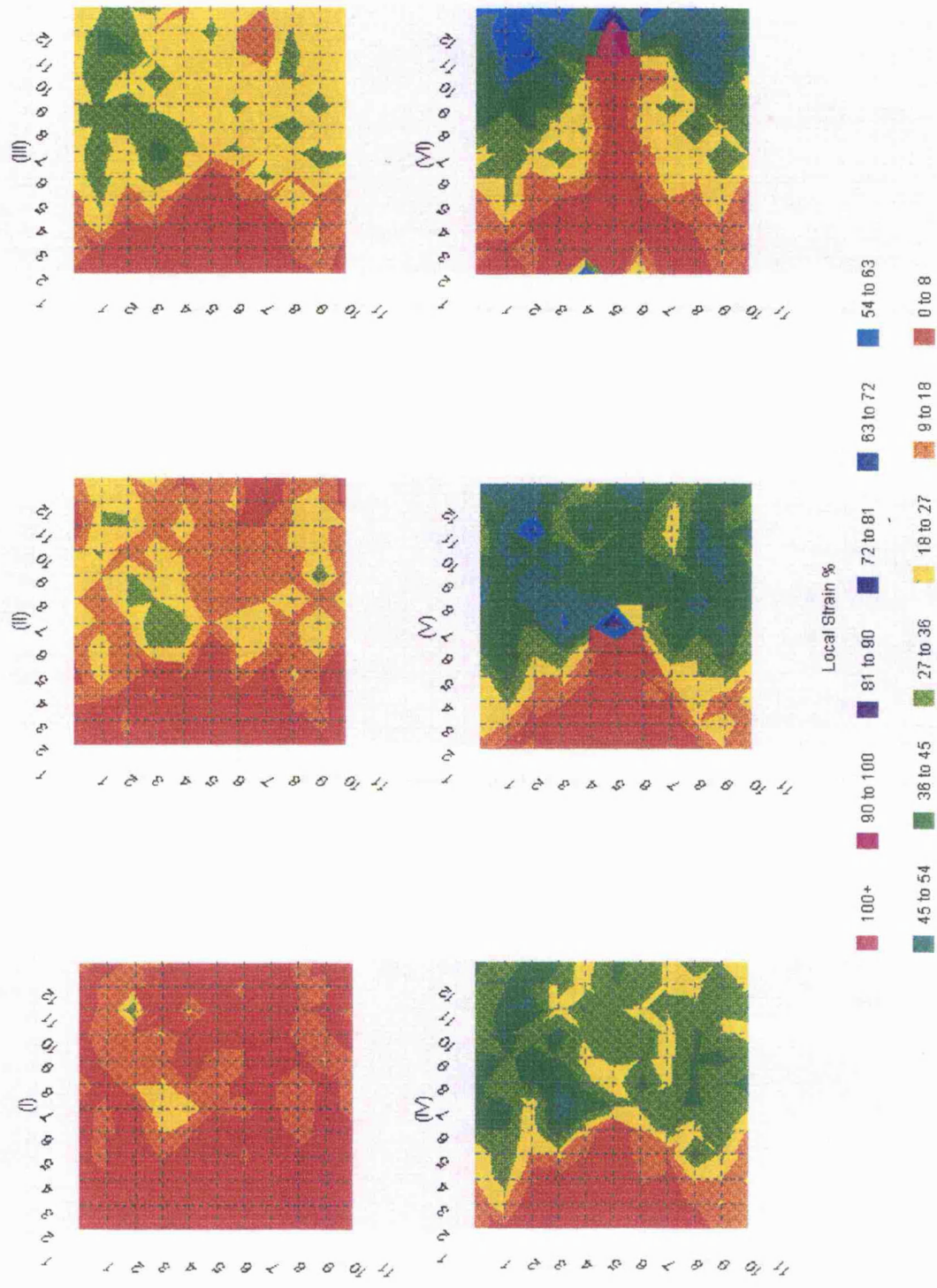


Figure 4.18

Video sequence showing the deformation and fracture of a FADG single notch specimen.

The nominal strain levels are: (I) 8.3 %, (II) 16.6 %, (III) 25.0 %, (IV) 33.3 %, (V) 41.6 %, (VI) 46.4 %.



**Figure 4.19**

The strain distribution in the vicinity of the notch for a FADG single notch specimen

The nominal strain levels are: (I) 8.3 %, (II) 16.6 %, (III) 25.0 %, (IV) 33.3 %, (V) 41.6 %, (VI) 46.4 %.

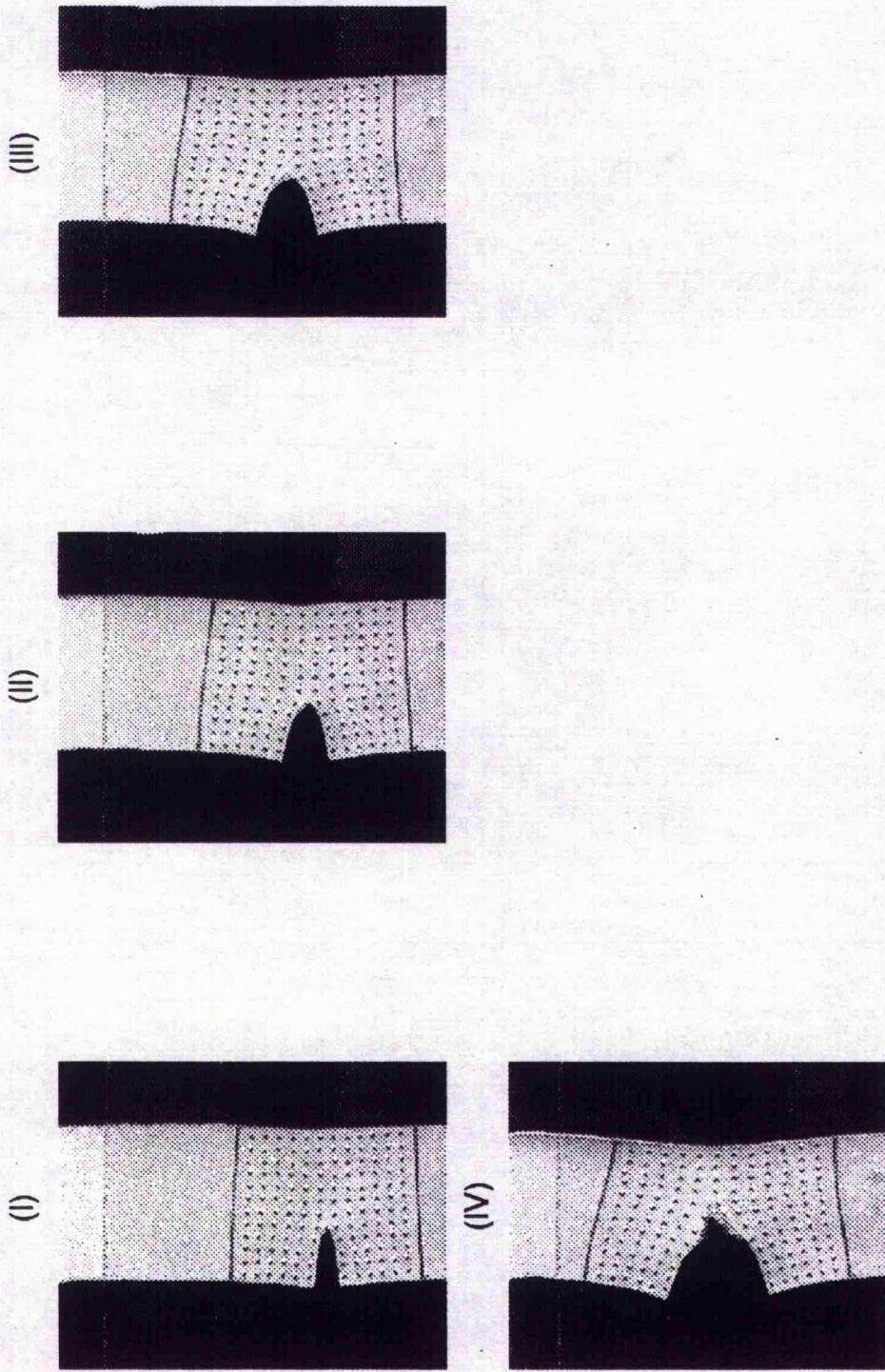


Figure 4.20  
Video sequence showing the deformation and fracture of a PDG single notch specimen.  
The nominal strain levels are: (I) 8.3 %, (II) 16.6 %, (III) 25.0 %, (IV) 33.3 %.

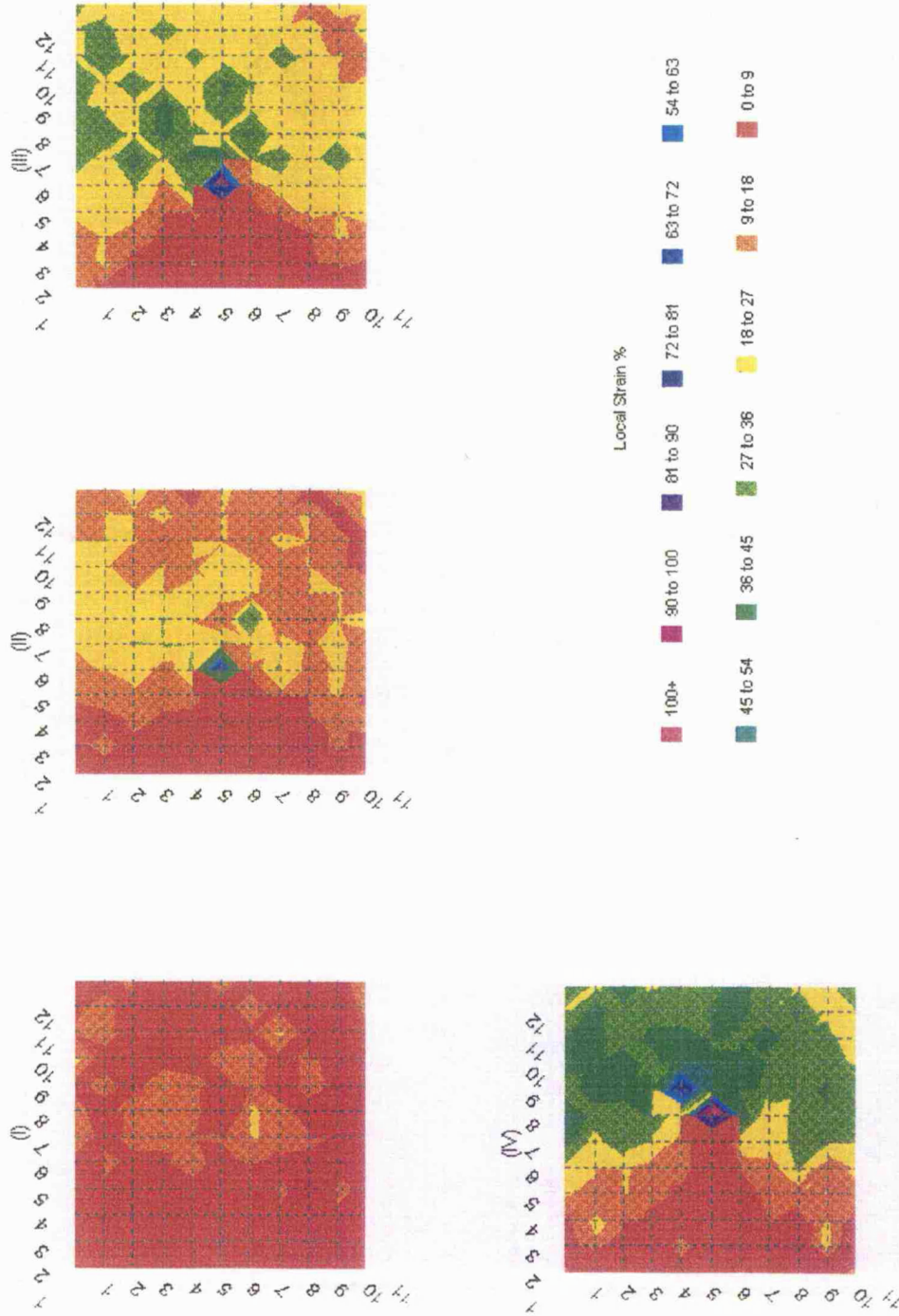


Figure 4.21

The strain distribution in the vicinity of the notch for a PDG single notch specimen  
 The nominal strain levels are: (I) 8.3 %, (II) 16.6 %, (III) 25.0 %, (IV) 33.3 %.

Figure 4.22 shows a sequence of six video images during deformation and fracture of a FADC specimen and Figure 4.23 shows the corresponding six spectral plots. The nominal strain level of the single notch specimen in each image / plot is (I) 8.3%, (II) 16.6 %, (III) 25.0 %, (IV) 33.3 %, (V) 41.6 % and (VI) 46.4 %. Figures 4.23 (I) to (V) show that the local strain in the sample builds up to levels of between 36 and 72% to the right of the notch. In Figure 4.23 (VI) the crack has propagated and a large area of local strains between 181 and 200% + exists at the tip of the crack. In addition, at this sample strain level, a large area to the right of the notch exists where local strains of between 90 and 109% exist.

Finally, Figure 4.24 and 4.25 show a sequence of five images / spectral plots, respectively. These images / plots (labelled (I) to (V)) present the distribution of strain in the vicinity of the notch in a single notch sample of PDC material. The nominal strain level of the single notch specimen in each image / plot is (I) 8.3 %, (II) 16.6 %, (III) 25.0 %, (IV) 33.3 % and (V) 39.5 %. Figures 4.25 (I) to (III) show the local strain in the sample rise to levels of between 18 and 36% to the right of the notch. In (IV) local strains of between 36 and 54% are evident to the right of the notch tip. The local strains at the tip of the notch at this point realise levels of between 145 and 163%. In Figure 4.25 (V) the crack has propagated and maximum local strains of 181 to 200% + are apparent at the tip of the crack.

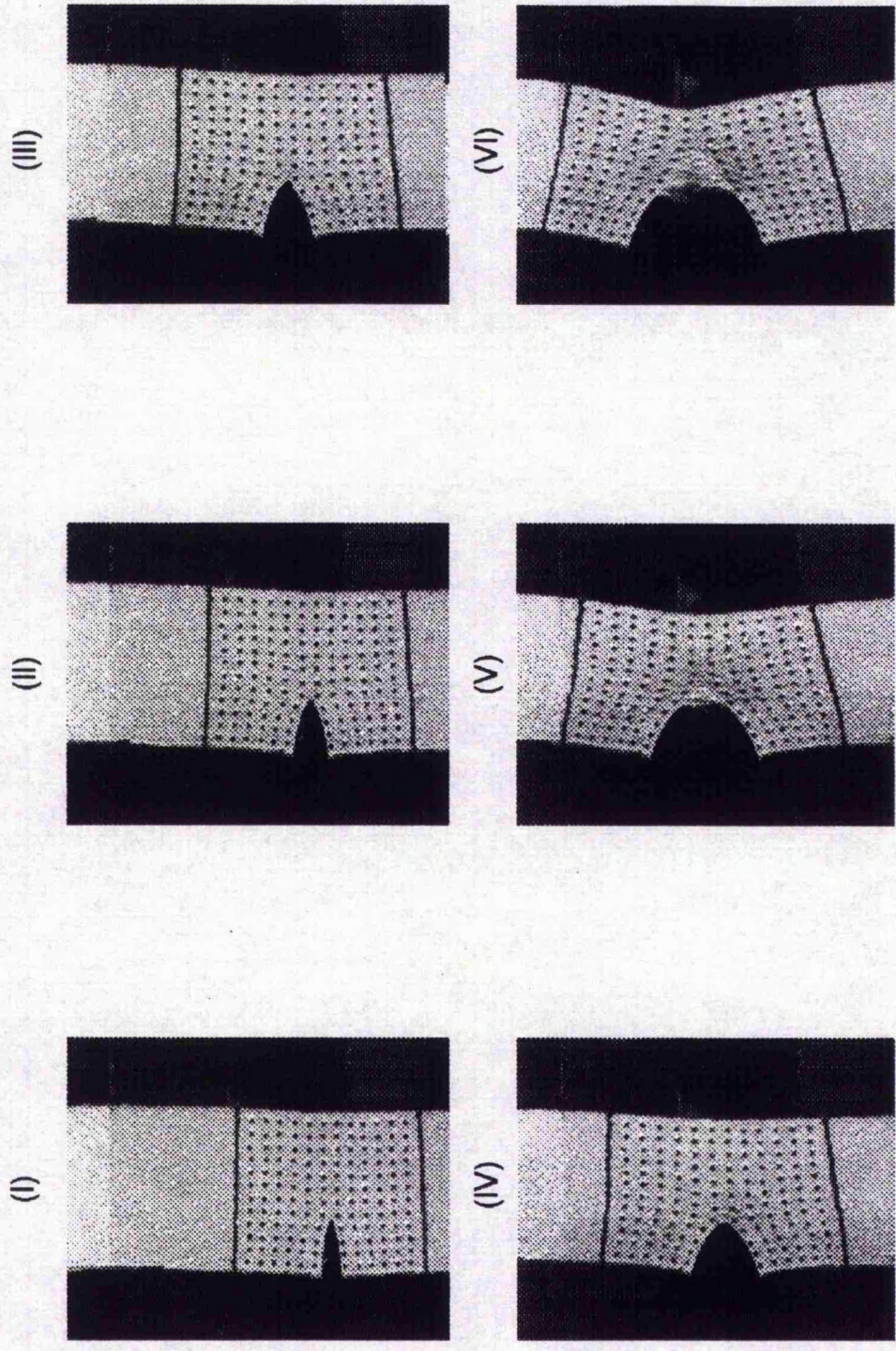


Figure 4.22

Video sequence showing the deformation and fracture of a FADC single notch specimen.  
The nominal strain levels are: (I) 8.3 %, (II) 16.6 %, (III) 25.0 %, (IV) 33.3 %, (V) 41.6 %, (VI) 46.4 %.

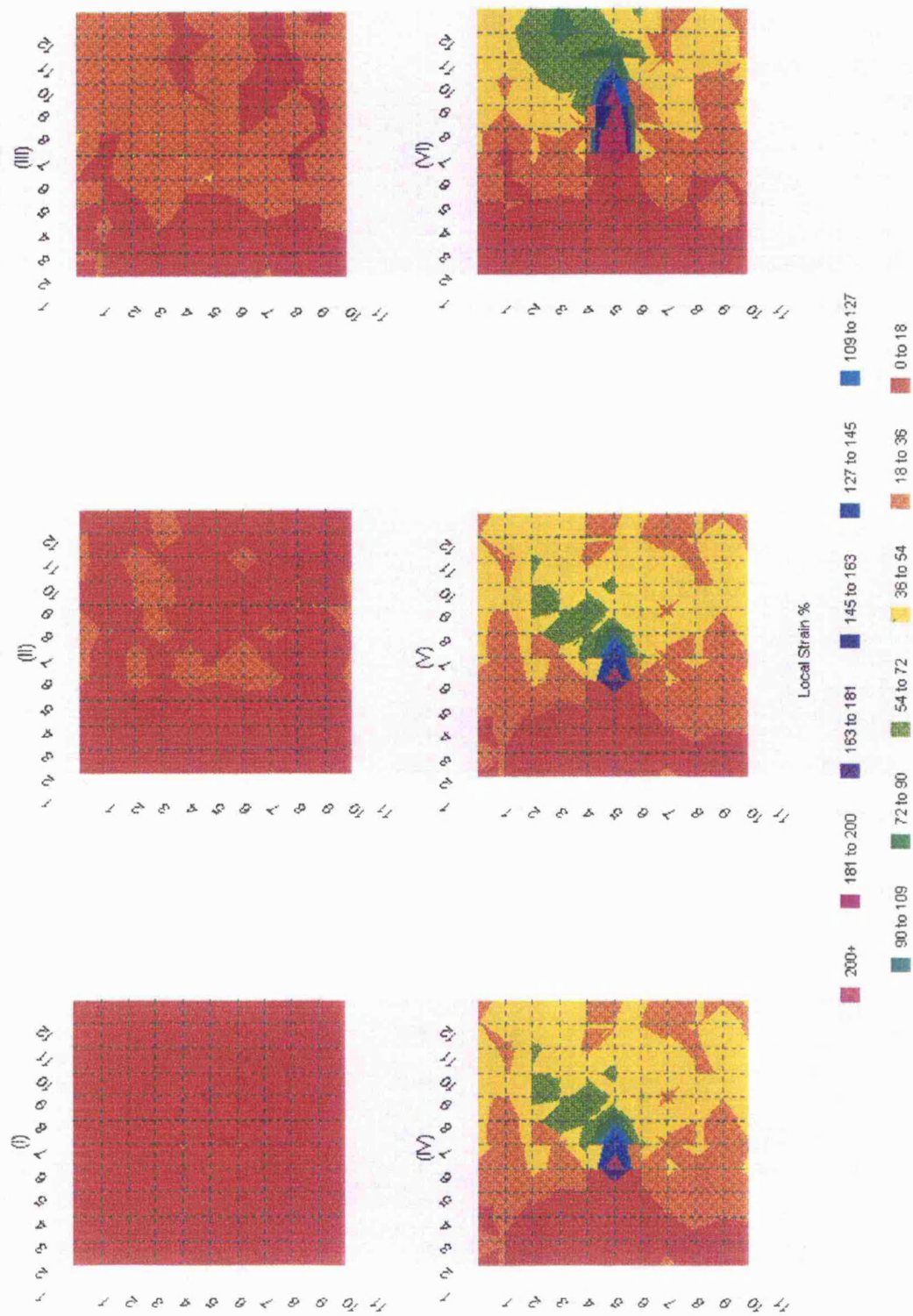


Figure 4.23

The strain distribution in the vicinity of the notch for a FADC single notch specimen

The nominal strain levels are: (I) 8.3 %, (II) 16.6 %, (III) 25.0 %, (IV) 33.3 %, (V) 41.6 %, (VI) 46.4 %.

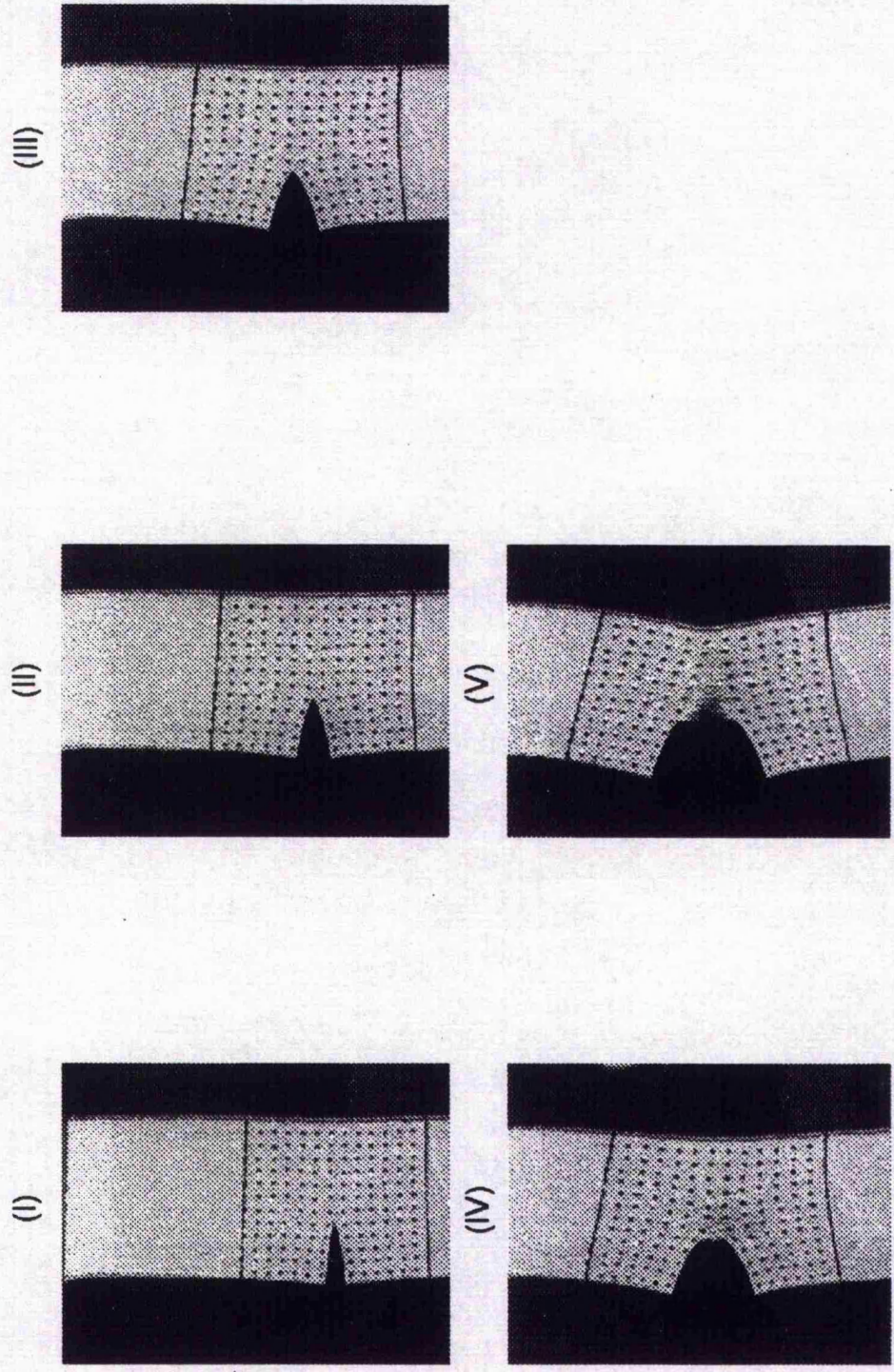


Figure 4.24  
Video sequence showing the deformation and fracture of a PDC single notch specimen.  
The nominal strain levels are: (I) 8.3 %, (II) 16.6 %, (III) 25.0 %, (IV) 33.3 %, (V) 39.5 %.

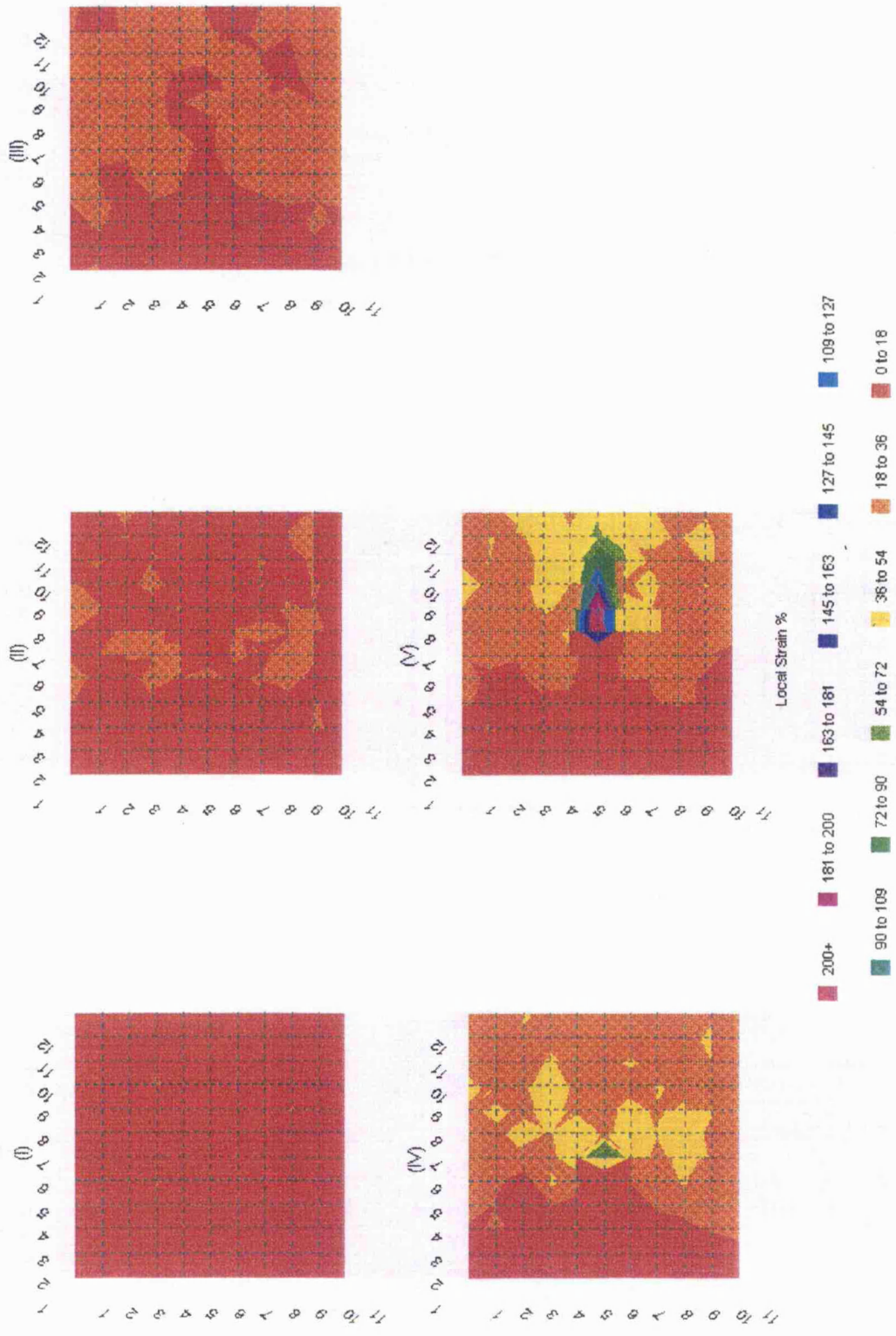


Figure 4.25

The strain distribution in the vicinity of the notch for a PDC single notch specimen  
 The nominal strain levels are: (I) 8.3 %, (II) 16.6 %, (III) 25.0 %, (IV) 33.3 %, (V) 39.5 %.

#### 4.2.6 Radii of curvature in single notch specimens.

The nominal fracture stress of an elastically continuous plate containing an elliptical notch (with a major axis of length,  $a$ ) is given by Equation [4.1]. In this situation, stress concentration depends critically on  $\rho$ , the radius of curvature of the elliptical notch, [Kelly and Macmillan, 1986]. Taking the maximum stress at the crack tip ( $\sigma_c$ ) and the notch length ( $a$ ) to be constant, higher values of radius of curvature ( $\rho$ ) ensure higher levels of nominal stress at failure.

The theory of stress concentration around notches has been developed exclusively for linear elastic materials. Nevertheless it seems reasonable to assume (even in non linear, elastic-plastic materials such as leather) that smaller radii of curvature at the notch tip will be associated with increased stress concentration. It was therefore thought beneficial to examine the tip radii of propagating notches. Accordingly, Figure 4.26 shows the relationships between the radius of curvature of the notch ( $\rho$ ) and the nominal specimen strain ( $\epsilon$  %) for grain and corium single edge notch specimens during deformation and fracture.

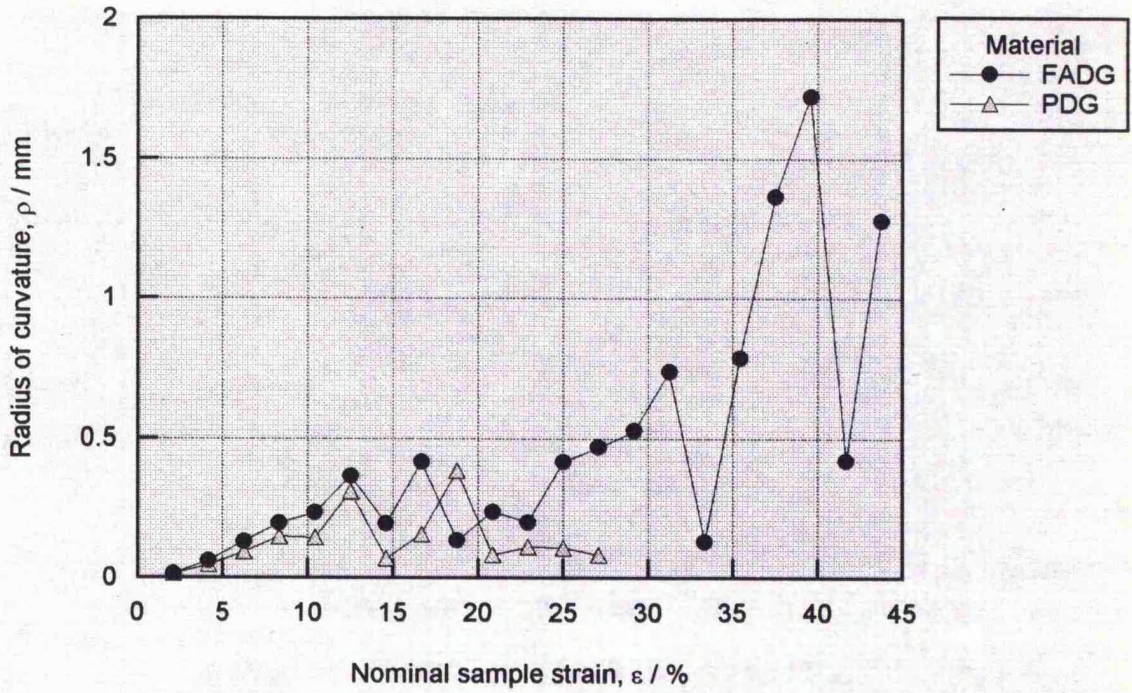
Figure 4.26 (I) shows the relationship between ( $\rho$ ) and ( $\epsilon$  %) in notched FADG and PDG specimens. Some fluctuation is apparent in  $\rho$  for both materials during deformation. However, up to a nominal specimen strain of 23 %,  $\rho$  fluctuates in a similar manner for both FADG and PDG specimens. By increasing nominal strain, the value of  $\rho$  for the PDG specimen remains at approximately 0.15 mm until fracture. However  $\rho$  in the FADG specimen rises to 0.75 mm where slow crack

growth occurs and after some fluctuation in the value of ( $\rho$ ), it attains a maximum of 1.75 mm before fracture.

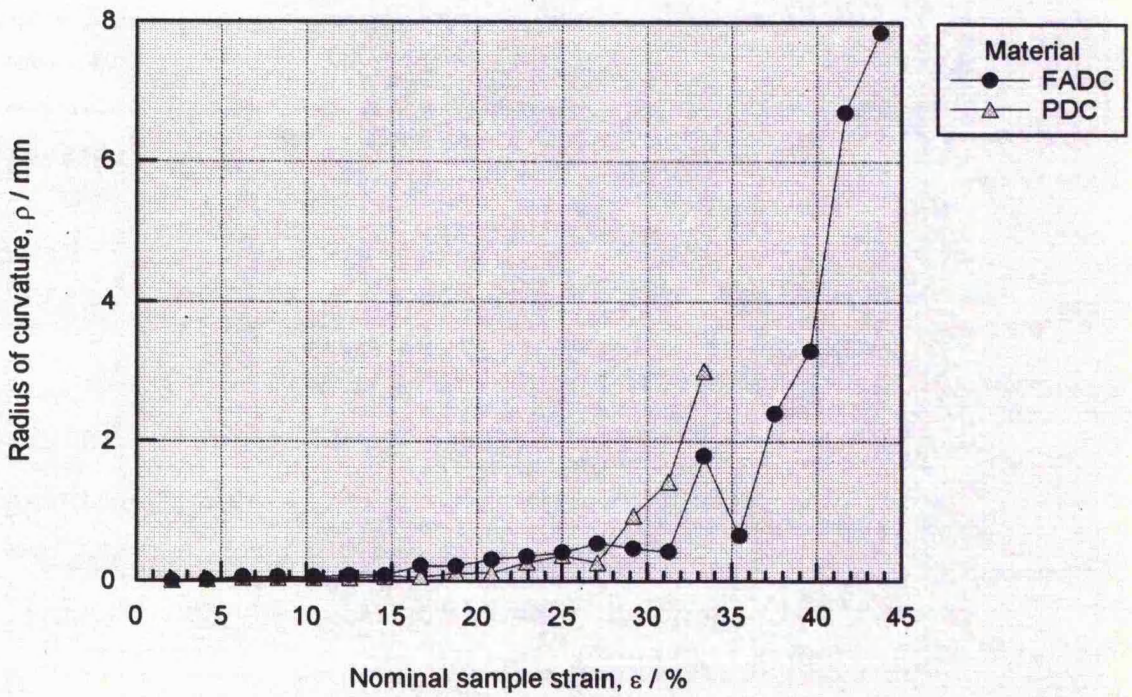
The relationship between ( $\rho$ ) and ( $\epsilon\%$ ) in FADC and PDC specimens is shown in Figure 4.26(II). Here,  $\rho$  rises slowly in both materials up to a nominal strain of 28 %. At this point,  $\rho$  rises to around 3 mm for PDC specimens before fracture. A more marked increase is noticeable in FADC specimens where values of ( $\rho$ ) rise to around 8 mm before the specimen fractures.

Figure 4.26

The relationship between radius of curvature and nominal sample strain in single notch specimens.



(I)



(II)

Figure 4.27 shows FADG, PDG, FADC and PDC single edge notch specimens after complete fracture. Both corium specimens show a considerable level of fibre pull out. However, the grain specimens show very little fibre pull out. Table 4.5 shows the average length of the fibres revealed as a result of the fibre pull out process in the fracture of FADG, PDG, FADC and PDC specimens.

**Table 4.5**

Material.	Range of pull-out lengths.	Average fibre pull-out length.
FADG	0.20 → 0.3 mm	0.25 mm
PDG	0.15 → 0.2 mm	0.18 mm
FADC	0.70 → 1.0 mm	0.85 mm
PDC	0.40 → 0.6 mm	0.50 mm

Figure 4.28 shows a scanning electron micrograph of the surface of a tear propagated from an edge notch in grain material. Figure 4.28 illustrates the existence of a sub-layer in the grain, closest to the outer surface, that is effectively free from fibre pull out.

Figure 4.27

Fibre pull out in single notch specimens of grain and corium material.

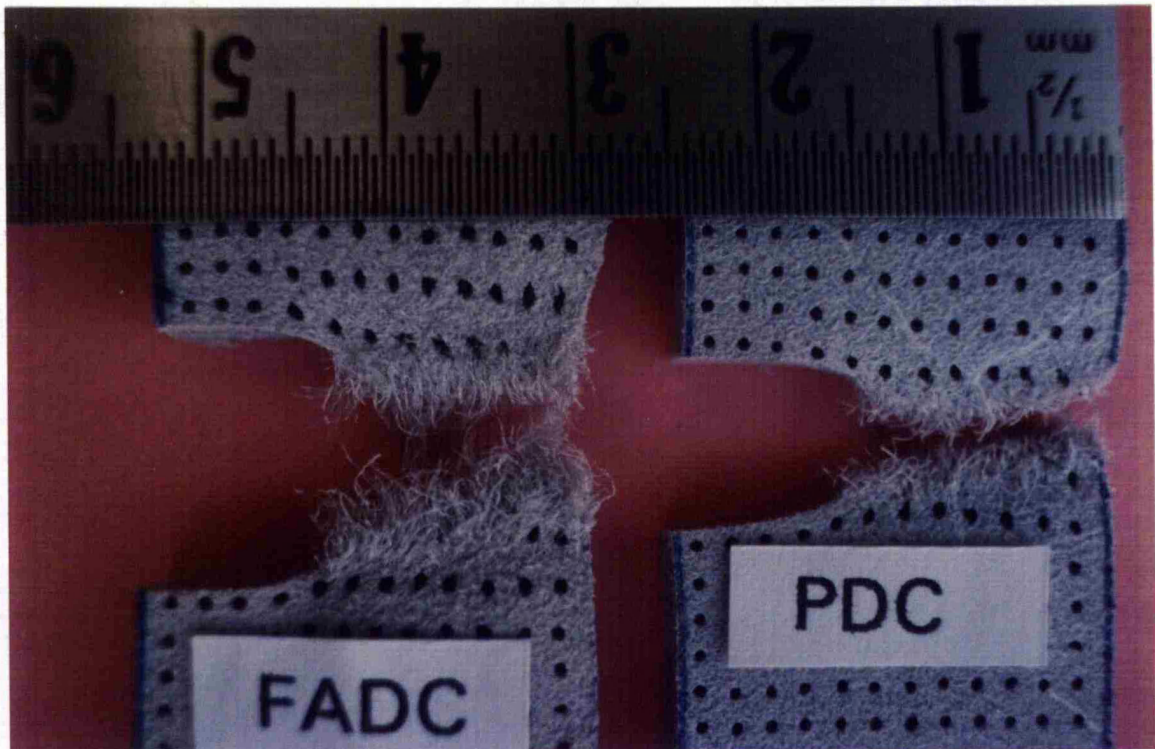
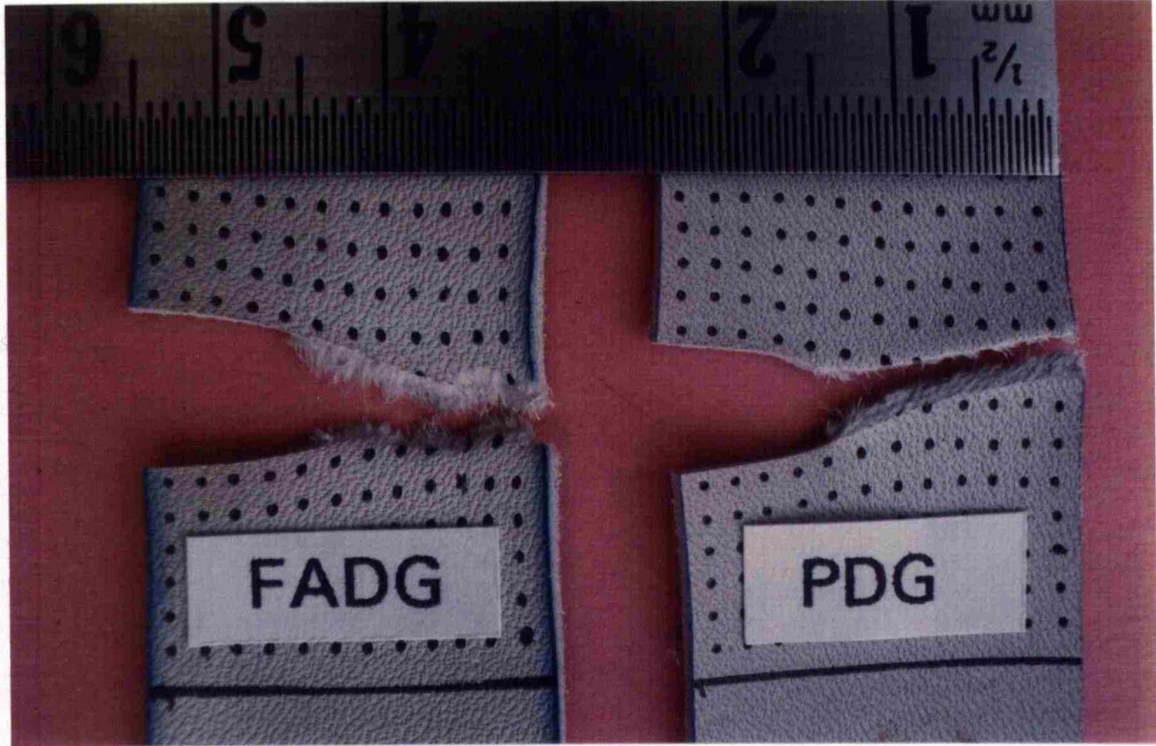
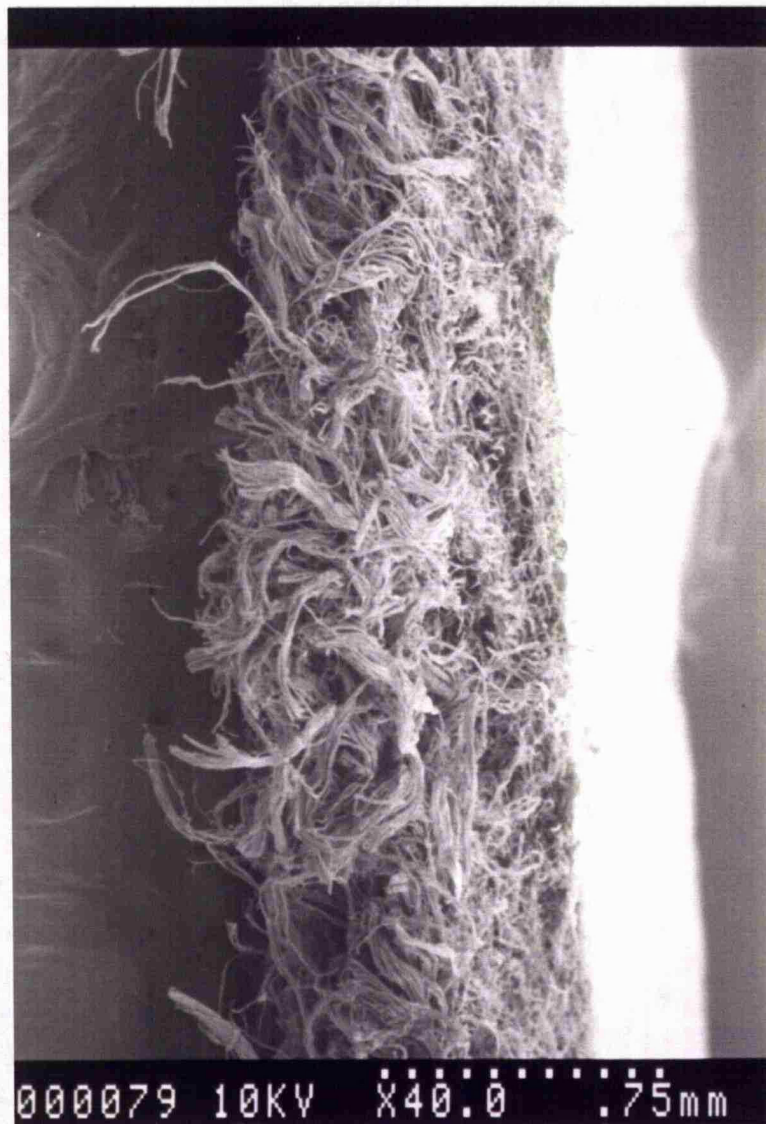


Figure 4.28

A scanning electron micrograph of the surface of a tear propagated from an edge notch in grain material.



### 4.3 Discussion.

#### 4.3.1 Estimation of the fracture energy ( $G_c$ ) from single edge notch tests.

Using the single edge notch test results of Figure 4.4 and Equation [4.2], the fracture energy ( $G_c$ ) can be estimated and compared with the specific work of fracture ( $R$ ) which was calculated using the trouser tear test geometry. Table A.7.1 (Appendix 7) shows the fracture stress and the fracture strain of single edge notch tests with a calculation of  $G_c$  at every notch length. In calculating  $G_c$  for each material, the tensile modulus ( $E$ ) from unnotched tensile specimens (section 3.2.1) was used. The modulus for each material was calculated between 30→40% strain and the strain at fracture (i.e. over a quasi-linear region of the stress-strain curve). Accordingly, the tensile modulus ( $E$ ) was estimated as 42.9 MPa and 44.4 MPa for FADG and PDG material respectively. The tensile modulus for FADC and PDC material was estimated as 84.1 MPa and 79.5 MPa respectively.

The average values of  $G_c \pm$  one standard deviation were calculated over the range of notch lengths for each material. It was found that for FADG specimens  $G_c = 22.4 \pm 9.1 \text{ kJ m}^{-2}$  and  $G_c = 6.7 \pm 1.8 \text{ kJ m}^{-2}$  for PDG specimens. Furthermore, for FADC specimens,  $G_c = 78.9 \pm 9.1 \text{ kJ m}^{-2}$  and  $G_c = 51.4 \pm 9.1 \text{ kJ m}^{-2}$  for PDC single notch specimens.

Estimates of  $G_c$  can be compared with the trouser tear test results (i.e. values of the specific work of fracture,  $R$ ) where the tear propagates in a direction

perpendicular to the backbone (Table 3.2). It can be seen that estimates of  $G_c$  are lower than estimates of  $R$  as calculated by the three separate methods. Nevertheless, the two major trends of Chapter 3 are also demonstrated by estimates of  $G_c$ : (i) the fatliquor is seen to increase the fracture resistance (markedly in the grain) and (ii) the corium material is shown as being 3→4 times tougher than the grain material.

It is also appropriate to consider quantitatively the process of fibre pull out during the fracture of single edge notch specimens (Table 4.5). Fibre pull out contributes to the overall toughness of a material and is a function of several factors including: the nominal length of the fibres pulled from the pseudo matrix; the number of fibres involved during the pull out process and the frictional restraints upon the fibres when being pulled through the pseudo matrix. Clearly the latter two factors are extremely difficult to ascertain with complete certainty. However it is evident from Table 4.5 that the average length of the fibres pulled from the pseudo matrix in corium material is 3→4 greater than the average length of the fibres pulled from the pseudo matrix in the corresponding grain material. This quantitative observation directly correlates with the toughness calculations of chapter 3 where the corium is also 3→4 times tougher than the corresponding grain material. In addition the presence of fatliquor increases the average length of fibres pulled from the pseudo matrix by approximately 40% in grain material and 70% in corium material.

#### 4.3.2 Notch sensitivity of grain and corium materials.

The fracture of PDG material is highly sensitive to the presence of a notch whereas the PDC material is notch insensitive. In a composite material, complete notch insensitivity can be produced by providing an interface parallel to the fibres which is weak in tension. The mechanism proposed by Cook & Gordon [1964], depicts that when a notched specimen is strained, before the fibre fails the induced stress at the crack tip breaks the interface parallel to the fibres, (assuming that the stress to break the interface in tension is considerably less than that required to fracture a fibre). A situation then arises where a crack running transverse to the fibres effectively opens another crack (in the matrix) transverse to itself and runs into it. The stress concentration due to the crack may reduce markedly and notch insensitivity may well result, [Kelly & Macmillan, 1986].

A pseudo matrix can be said to exist in grain and corium material (section 3.3) and as such, the mechanisms suggested to be responsible for notch insensitivity above are entirely feasible. However it is contended that the mechanism of fibre orientation and the phenomenon of fibre independence (or fibre autonomy) are the mechanisms responsible for the notch insensitive behaviour of corium material as opposed to the notch sensitive behaviour of the grain.

In Figure 4.29 (I), a notched specimen of a flexible fibrous material, such as corium, is subject to a nominal strain very much less than the nominal fracture strain. Here, the fibres at the crack tip are subject to a sharp notch and therefore

the highest concentration of stress in the specimen occurs at this point. However, if the fibres at the crack tip are reorienting towards the strain axis, the fibres themselves are not directly strained. Accordingly, even the stress induced in the fibres at the crack tip, is very much less than the fibre fracture stress and the crack will not propagate. Considering this situation in terms of strain energy, the energy density at the crack tip is not sufficient to promote fracture as much of the supplied strain energy has been expended or dissipated in the fibre re-orientation process.

As the material is strained further, the notch 'opens' (Figure 4.29 (II)). In this situation, it is assumed the fibres are physically independent from one another within the material and, as a result of the strain, become markedly orientated transverse to the direction of crack propagation. Here the notch is no longer sharp and possibly the major and minor axis of the elliptical crack seen in (I) have switched. Accordingly, the geometric factors of stress concentration, (i.e.  $(a/\rho)$ ), will have markedly reduced and in essence, the fall in nominal stress at failure, due to the presence of a small notch, is reduced.

Considering this situation in terms of strain energy, the geometry of the notch in Figure 4.29 (II) and the level of physical independency of the fibres, both lead to a well distributed strain energy within the specimen and so high levels of energy density are not significantly focused in one small locality. Accordingly, the energy density in the region of the highly opened crack is not sufficient to promote fracture until heightened levels of nominal stress and strain are attained. Indeed,

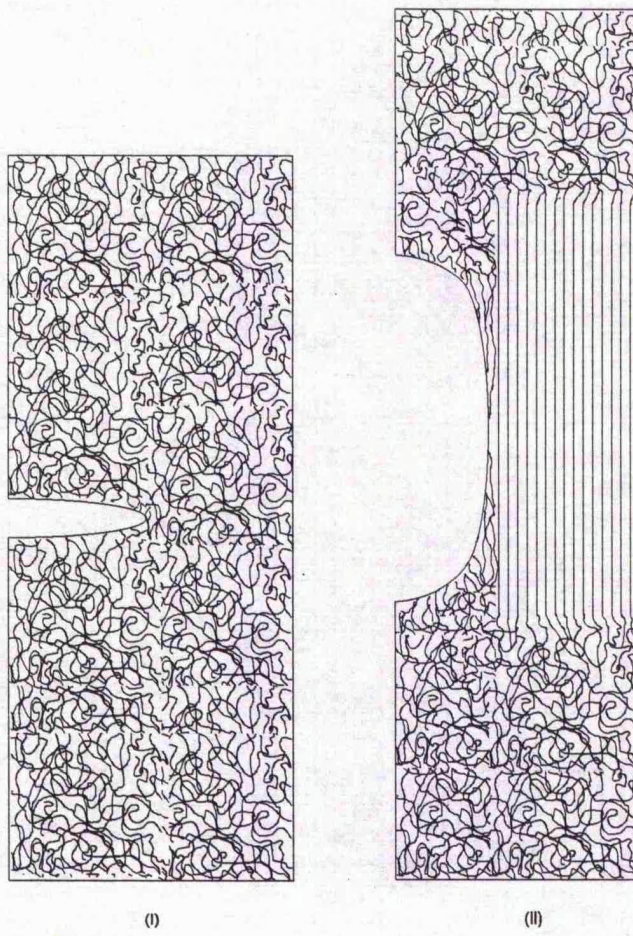
the levels of nominal fracture stress and strain will be comparable to those of an unnotched tensile specimen of width ( $W - a$ ). Under these circumstances the material is defined as notch insensitive.

An analogous situation is seen in lubricated steel wire ropes used for suspension bridges and climbing protection devices. Thin rods of steel are wound together to form a flexible rope-like structure and when in service, are subject to potentially damaging environments. However, fracture of even several constituent thin steel rods within the rope does not appreciably reduce the overall tensile strength because each thin rod has a degree of physical independency from its neighbours (in essence reducing shear connectivity). Accordingly such ropes are notch insensitive.

In section 3.3, higher nominal tensile strains of PDC specimens (compared to PDG specimens) and the more pronounced 'J' shape were attributed to greater levels of fibre orientation. In addition, very high levels of local strain were observed at the tip of the notch in PDC single notch specimens (section 4.2.5). These strain levels are markedly higher than those observed in individual corium fibres, where the nominal strain at fracture occurs between 9 % and 16 % [Mitton, 1945]. This phenomenon, at least in part, can again be attributed to the process of fibre orientation.

Figure 4.29

Mechanisms pertaining to the notch insensitive tensile behaviour of corium material.



Greater fibre orientation in corium material is also evident from the radius of curvature of the notch in single edge notch specimens. The radius of curvature of the notch, just before fracture, in a PDC specimen is 20 times higher than that observed in a PDG specimen, (~3 mm compared to ~ 0.15 mm).

In addition to fibre orientation, it is likely that the largest fibrous units present in corium material have a level of physical independency that is much greater than that of the largest fibrous units present in grain material. Indeed, Attenburrow [1992] postulated that with the coarser structure of the corium, the mean distance between fibre interconnections is greater than in the grain because the grain can maintain some level of tensile strength when split very thin, whereas the corium cannot.

In light of these factors, the mechanisms of fibre orientation and relative fibre independence are responsible for the notch insensitive behaviour in corium material, i.e. the original contention was correct. Indeed, PDC material experiences both a higher level of fibre orientation and greater fibre independence than PDG material. Consequently a higher degree of notch insensitivity is inherent in corium material.

The fracture stress of single edge notch corium specimens is considerably greater than the fracture stress of grain specimens, at all notch lengths. Accordingly, corium material is inherently more resistant to crack propagation than grain material. In addition significantly more fibre pull is evident in corium specimens

than in grain specimens. Both these findings are in accord with the mechanisms underlying the relative weakness of grain material (chapter 3.)

In considering the observed crack advancement in a single edge notch grain specimen, it is important to note that Figure 4.28 illustrates the existence of a sub-layer in the grain material, closest to the outer surface, that is effectively free from fibre pull out. In the video sequence of Figure 4.18 and 4.20, the outer surface of the grain is viewed. It may reasonably be assumed that the observed sharp tip of the tear is formed within this surface sub-layer with any fibre pull out occurring in the under layer that was originally attached to the corium.

In considering the application of Purslow's theory of notch sensitivity of non-linear materials [1991], it has been seen that some departure from theoretical predictions are apparent, particularly for FADG material. When applying his theory to materials with 'r' shaped stress-strain properties, Purslow [1991] observed that nominal fracture stresses and strains were in accordance with predicted values. However, both grain and corium specimens demonstrate 'J' shaped tensile behaviour.

In this respect,  $n > 1$  in Equation [4.5] and therefore  $M > 0.5$  in Equation [4.9]. Accordingly, in Equation [4.7], the value of the exponent  $n' = -M$ , i.e.  $n' < -0.5$ . Where  $n' < -0.5$  a relationship is predicted where the fall in breaking stress with increasing crack length is even more rapid than the behaviour of a brittle material such as glass where  $\sigma_f \propto a^{-1/2}$  [Higgins, 1991]. This level of extreme sensitivity to the presence of a small notch seems an unlikely situation and it would appear,

regardless of the elasticity assumptions, that if the variable  $M > 0.5$ , as a result of a 'J' shaped curve, the theoretical relationship of Equation [4.8] between breaking stress and notch length cannot be realised. Nevertheless, the fracture behaviour of PDG material is highly notch sensitive and in good agreement with the predictions obtained by using the theory of notch sensitivity of non-linear materials. The fracture behaviour of FADG material is less notch sensitive with more pronounced 'J' shaped stress strain behaviour. Accordingly, some departure from theoretical prediction should be expected.

In addition, the theoretical strain distribution for notch-insensitive materials proposed by Purslow [1991] and shown in Figure 4.2 (I) is not apparent in either the FADC or PDC specimens. If this were the case, the complete lengths of column numbers 1 and 2 in Figures 4.15 (V) and 4.17 (IV) would indicate zero strain levels. However in both the FADC and PDC specimens, local strain levels of up to 31% exist in these areas. Accordingly the concept of a notch-insensitive material having a strain energy free region situated to the left of a vertical line drawn through the notch tip is unlikely to apply to corium material as high local strains are evident. Even when considering the hysteresis values of the corium material (section 3.2.5) these significant local strain levels ensure strain energy is distributed within this region of the specimen.

It is contended that the only complete theory enabling the application of fracture mechanics to non-linear, flexible, inelastic materials, such as leather, while also providing some practicable and semi-achievable experimental guidelines is the

theory of General Fracture Mechanics (GFM) [Andrews, 1974,1980; Andrews & Billington, 1976; Andrews & Fukahori, 1977]. The original intention was to test the application of this theory to leather. However, this has not been possible because the crack propagation in single edge notch specimens of corium materials in particular is catastrophic. Accordingly, the measurement of crack velocity (a requirement of GFM) by means of the methods described by Andrews and Fukahori [1977] proved futile.

#### 4.3.3 The influence of fatliquor on notch sensitivity.

The presence of oil in grain material (i.e. FADG material) tangibly reduces the notch sensitivity of the grain at oil contents of 8.5 % and 12.5 %. It has also been seen that the propanone dried corium material is already highly notch insensitive and there is no observable increase in the degree of notch insensitivity as a result of the presence of oil at either 1.2 % or 3.0 %.

The strain distribution maps of FADG and PDG specimens (Figures 4.11 & 4.13) reveal that the oil (present in the FADG single notch specimen) facilitates a more even distribution of local strain than is observed in the PDG specimen. Evidently the effect of the oil is to delay the high levels of local strain, that manifest in the region of the notch tip, by allowing a more even distribution over the whole sample.

As discussed in the previous section, two factors affect the notch sensitivity of

leather material: (i) fibre orientation and (ii) fibre independence. Further, in chapter 3, it was contended that the influence of oil on tensile properties of grain and corium material is twofold. In a non-aqueous environment, the oil is a 'secondary plasticiser' that (i) provides spacers that prevent fibre adhesion and (ii) provides some level of lubrication to the fibres.

By providing spacers that prevent interfibre adhesion, oil promotes heightened levels of fibre independence. Further, by acting as a fibre lubricant, oil also promotes fibre re-orientation by effectively reducing interfibre frictional restrictions. Both these effects can be expected to reduce the notch sensitivity of either grain or corium. Accordingly, reduction in notch sensitivity (i.e. an increase in notch insensitivity) is apparent in grain material at oil content of 8.5 % and a further decrease in notch sensitivity is apparent where the oil content is 12.5 %.

Under conditions of complete notch insensitivity, the condition expressed in Equation [4.4] is authenticated and the maximum degree of notch insensitivity is attained. As noted in the results, the insensitivity of all corium material approaches the case of complete notch insensitivity. Not surprisingly, no further increase in the degree of notch insensitivity is apparent at oil contents of only 1.2 % and 3.0 %.

In both the grain and corium layers, the maximum local strain levels attained during crack propagation are substantially higher when oil is present. Indeed the highest level of recorded local strain during fracture in the FADG specimen is 218 % compared with 88 % in the PDG specimen. This pattern of behaviour is repeated

in the corium layer. Here, the highest level of recorded local strain during fracture in the FADC specimen is 430 % compared with 299 % in the PDC corium specimen.

These local levels of strain are considerably higher than the nominal breaking strain of the single notch sample itself, where a maximum over the four materials of 50% is observed in the FADG specimen. In viscoelastic amorphous elastomers, the rate of elongation at the crack tip is known to be much greater than the rate of elongation of the whole test piece [Gent, 1978]. Hence, it is not unreasonable to also attribute the high local strains at the notch tip to a difference in the rate of elongation between the strain rate at the tip of the notch and the rate of strain application to the specimen as a whole.

Further, it is probable that the high strains ahead of the tear are localised regions of high fibre pull out. They will be of considerably lower density than the rest of the leather and may be, in some respects, similar to crazes in polymers. It is also possible that the real crack tip is obscured by the fibre pull out and that the local strains are being measured in a region which has effectively failed (Figure (4.30)). The higher local strains, observed at the crack tip in fatigued material, are attributed to heightened fibre orientation and increased levels of fibre pull out in the lower density regions of the tip.

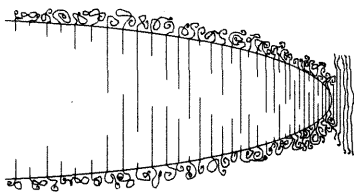


Figure 4.30

Precise determination of the crack tip.

'Where is the tear tip?'

## Chapter 5

### Conclusions and Recommendations.

#### 5.1 Conclusions.

The specific work of fracture of both the grain and corium layers of leather have been assessed through trouser tear testing. The specific work of fracture was calculated using three different methods: method one assumes significant leg extension and that the material is elastic-plastic; method two assumes significant leg extension and that the material is elastic; method three assumes insignificant leg extension and that the material is linearly elastic. Whatever the method of calculation, the corium material is 2 to 4 times tougher than grain material. This is attributed to the higher levels of fibre debonding and pull out in corium material during tear propagation.

Orientation, with respect to the backbone line, influences the ultimate tensile properties of both grain and corium material due to the variable degree of fibre orientation within the bulk specimen. The specific work of fracture of grain material is also sensitive to specimen orientation. This phenomenon is explained by differences in fibre bridging when the tear advances in different orientations. With corium material, any directional effects on the specific work of fracture are masked by energy dissipating process of fibre debonding during tear propagation.

The influence of deformation rate upon the strength and toughness of grain and corium material has been examined. It is contended that the organisation of the

hierarchical fibre structure within corium material enables an enhanced fibre mobility at higher rates, thus elevating stresses and strains at fracture. However, the more compact fibrous structure of the grain material impedes any enhancement of fibre mobility at higher strain rates and rupture stresses and strains are not elevated. The influence of strain rate on the specific work of fracture of grain and corium material is attributed to fibre orientation effects in the region of the advancing tear.

Both grain and corium material display high hysteresis during strain cycling of unnotched specimens. However, these hysteresis values were not observed to alter significantly over the examined range of strain rates and strain levels. The fracture of grain material is highly sensitive to the presence of a notch, whereas corium material is notch insensitive. The mechanism of fibre orientation and the phenomenon of fibre independence (or fibre autonomy) are responsible for the notch insensitivity of corium material. The explanation for notch insensitivity proposed by Purslow [1991], based on strain distribution, is not applicable to corium material.

The presence of oil in grain material reduces the notch sensitivity. It is proposed that this effect is caused by (i) the oil promoting higher levels of fibre independence and (ii) the oil enabling fibre re-orientation by reducing interfibre frictional restrictions. With corium material, higher levels of local strain have been observed at the crack tip during crack propagation and the radius of curvature of such cracks are significantly higher than with grain material. Such phenomena are attributed to localised regions of high fibre pull out in corium material.

## 5.2 Industrial consequences of the research.

In essence, this research has elucidated the principles involved in the relative strength and toughness of grain and corium material so that procedures may be developed to increase the strength and toughness of grain material. However, in addition, aspects of the research have a direct bearing on established leather manufacturing processes, end-user material practices and industry test methods.

- (i) It has been seen that toughness and strength of grain and corium materials are rate sensitive. Indeed, by increasing deformation rates from  $0.16 \text{ mm s}^{-1}$  to  $166.66 \text{ mm s}^{-1}$  a marked increase in both strength and toughness has been observed. The time dependent fracture behaviour of leather will profoundly affect the lasting (stretch forming) operation of shoe making. Clearly if deformation rates during the lasting operation are high, the fracture resistance of the leather material is elevated. Accordingly, crack formation and crack initiation during the lasting operation (which are detrimental to the appearance, wear and life of a shoe) can be reduced or even avoided by increasing the speed of the lasting operation.
  
- (ii) The presence of oil in grain material markedly increases the toughness and strength and reduces notch sensitivity. However (within the range studied) the presence of oil in corium material has little effect on the already highly notch insensitive fracture behaviour and only marginally increases the already high levels of strength and toughness. Accordingly, when fatliquoring full substance bovine leather attention should be paid to

achieving greater oil deposition in the grain layer in order to achieve strength and toughness.

- (iii) Fibre pull out contributes significantly to the fracture resistance of both grain and corium materials. Furthermore, within the grain, there is a sub-layer, closest to the outer surface, which after tearing is effectively free from fibre pull out. Accordingly, thin grain splits (<0.6 mm) maybe expected to be very weak since they are deficient of fibres being pulled from the pseudo matrix during tear propagation. This lack of fibre pull out accounts for the low fracture resistance of thin grain splits. Thus processes that encourage fibre pull out are of significant importance, especially when producing thin grain splits.
- (iv) Fibre independence (or fibre autonomy) is a mechanism that significantly contributes to the greater toughness and notch insensitivity of the corium. If such mechanisms could be enhanced within the grain layer, a significant increase in toughness is likely to result. Accordingly, impregnation of the grain with additional plasticisers or more 'opening up' of the grain layer in the initial liming process, are both processes likely to increase levels of fibre autonomy, thereby increasing toughness and reducing notch sensitivity.
- (v) The intrinsic tearing resistance of leather (as measured via the trouser tear test and calculated in  $\text{J m}^{-2}$ ) is a property of the material itself. Consequently the specific work of fracture (R) is purely indicative of the material's fracture properties. However, current methods to measure the tearing resistance of

leather simply measure the maximum force required to tear a Bauman tear test specimen. Adoption of the trouser tear test procedure and calculation of the specific work of fracture would ensure that an intrinsic fracture property is being estimated and enable a legitimate comparison between materials.

### 5.3 Suggestions for further work.

- (i) Measurement of the crack velocity in the single edge notch specimen orientation will enable application of Andrew's theory of General Fracture Mechanics. The apparent fracture resistance can then be measured in the single notch orientation and broken down into a surface free energy term and an energy loss term.
- (ii) Although this study has dealt with a number of fracture mechanisms pertinent to both grain and corium material, detailed morphological configuration of the collagenous based fibres within leather material and its influence on tearing phenomena are yet to be expressed mathematically.
- (iii) Commercial circumstances often dictate that the 'grain split' be thicker than the grain alone, eg. 1.6 to 1.8 mm. The grain layer of bovine leather is approximately 1 mm thick and therefore if the thickness of the grain split is to be greater than 1 mm, the leather must be split within the corium layer. Consequently, instead of separate grain and corium materials (as used in this study), a grain/corium laminate and a corium material are produced. Further research to examine the mechanical and fracture properties of

bovine leather split at different thickness would enable the development of a laminate theory. A laminate theory would yield the relationship between the thickness of the laminate (i.e. the relative thickness of grain / corium) and the intrinsic strength / toughness of the laminate. In addition such research would enable an estimate of the optimum level at which to split full substance leather in order to obtain specified strength and toughness values for both the grain/corium laminate and the remaining corium layer.

### References.

- Alexander, K.T.W. Covington, A.D. Garwood, R.J. & Stanley, A.M. (1993).  
'The examination of collagen ultrastructure by cryo-scanning electron microscopy.'  
XXII IULTCS Congress Proceedings, Brazil.
- Andrews, E.H. (1974).  
'A generalized theory of fracture mechanics.'  
Journal of Materials Science, 9, 887.
- Andrews, E.H. & Billington, E.W. (1976).  
'Generalized fracture mechanics, Part 2 Materials subject to general yielding.'  
Journal of Materials Science, 11, 1354.
- Andrews, E.H. & Fukahori, Y. (1977).  
'Generalized fracture mechanics - part3. prediction of fracture energies in highly extensible solids.'  
Journal of Materials Science, 12, 1307.
- Andrews, E.H. (1980).  
'The Mechanical Properties of Biological Materials - Fracture.'  
Symposia of the Society for Experimental Biology, 34, 13.
- Arumugam, V. Naresh, M.D. Somanathan, N. & Sanjeevi, R. (1992).  
'Effect of strain rate on the fracture behaviour of collagen.'  
Journal of Materials Science, 27, 2649.
- Atkins, A.G. and Mai, Y.M. (1988).  
'Elastic and plastic fracture.'  
John Wiley & Sons, Chichester.
- Attenburrow, G.E. (1993).  
'The rheology of leather - a review.'  
Journal of the Society of Leather Technologists and Chemists, 77, 107.
- Bailey, D.G. Beuchler, P.R. Everett, A.L. & Fearheller, S.H. (1985).  
'Leather'  
Kirk-Othmer, Concise Encyclopedia of Chemical Technology, Vol 14.
- Berry, J.P. (1972).  
'Fracture of Polymeric Glasses' in 'Fracture - An Advance Treatise.' Vol VII.  
Editor: Liebowitz, H. , Academic Press, New York.
- Cook, J. & Gordon, J.E. (1964).  
'A mechanism for the control of crack propagation in all brittle systems.'  
Proceeding of the Royal Society, London, A282, 508.

- Corte, H. (1982).  
 'Handbook of paper science: science & technology of paper making, paper properties and paper usage.'  
 Editor: Rance, H.F. , Elsevier, London.
- Daly, C.H. (1966).  
 'The biomechanical characteristics of human skin.'  
 PhD Thesis, The University of Strathclyde.
- Demsey, M. (1968).  
 'Leather and light microscopy.'  
 Journal of the American Leather Chemists Association, 63, 666.
- Dorbin, P.B. (1978).  
 'Mechanical properties of arteries.'  
 Physiological Reviews, 58(2), 397.
- Duck, F.A. (1990).  
 'Physical properties of tissue - a comprehensive reference book.'  
 Academic press, London.
- Findley, W.N. , Lai, J.S. & Onatan, K. (1989).  
 'Creep and relaxation of non-linear, viscoelastic materials.'  
 Dover Publications, Inc., New York.
- Gent, A.N. (1978).  
 'Science & Technology of rubber.' (Chapter 10)  
 Academic Press, New York.
- Gerberick, W.W. & Davidson, D.L. (1985).  
 'Measurement of localized deformation by novel techniques.'  
 Metallurgical Society, Pennsylvania, USA.
- Gordon, J.E. (1978).  
 'Structures or why don't things fall down.'  
 Penguin, London.
- Greensmith, H.W. & Thomas, A.G. (1955).  
 'Rupture of rubber III. Determination of tear properties.'  
 Journal of Polymer Science, 18, 189.
- Greensmith, H.W. (1960).  
 'Rupture of rubber. VII. Effect of rate of extension in tensile tests.'  
 Journal of Applied Polymer Science, 3(8), 175.
- Griffith, A.A. (1920).  
 'The phenomenon of rupture and flow in solids.'  
 Philosophical Transactions of the Royal Society London, A221, 163.

- Guy, R. & Marriott, A.G. (1975).  
 'A comparison of two tear tests for leather.'  
 Journal of the society of Leather Technologists and Chemists, 59, 30.
- Haut, R.C. (1983).  
 'Age-dependent influence of strain rate on the tensile failure of rat tail tendon.'  
 ASME Journal of Biomechanical Engineering, 105, 296.
- Heidemann, E (1979).  
 'Fibrous Proteins', p231.  
 Editors: Parry, D.A. & Creamer, L.K. , Academic Press, London.
- Heidemann, E. (1993).  
 'Fundamentals of Leather Manufacturing.'  
 Eduard Roether KG, Darmstadt.
- Higgins, R.A. (1991).  
 'Properties of engineering materials.'  
 Edward Arnold, London.
- Hole, L.G. Tuck-Martin, B.S. & Hale, J. (1983).  
 'The influence of grain structure on grain crack properties of leather.'  
 Journal of the Society of Leather Technologists and Chemists, 63, 98.
- Kanagy, J.R. Leser, W.H. Randall, E.B. Carter, T.J. & Mann, C.W. (1952).  
 'Influence of splitting on the strength of chrome-tanned steer sides.'  
 Journal of the American Leather Chemists Association, 47, 329.
- Kellert, S.H. (1993).  
 'In the wake of chaos.'  
 The University of Chicago Press, Chicago.
- Kelly, A. (1970).  
 'Interface effects and the work of fracture of a fibrous composite.'  
 Proceedings of the Royal Society, London, A319, 95.
- Kelly, A. & Macmillan, N.H. (1986).  
 'Strong Solids.'  
 Clarendon Press, Oxford.
- Kendall, K. (1979)  
 'A fracture energy spectrometer for polymers.'  
 Journal of Materials Science, 14, 1257.
- Kendall, K. & Fuller, K.N.G. (1987).  
 'J-Shaped stress/strain curves and crack resistance of biological materials.'  
 Journal of Physics D - Applied Physics, 20, 1596.

- Kinloch, A.J. & Young, R.J. (1990).  
'Fracture behaviour of polymers.'  
Elsevier Applied Science, London.
- Kronick, P. & Maleef, B. (1992).  
'Nondestructive failure testing of bovine leather by acoustic emission.'  
Journal of the American Leather Chemists Association, 87, 259.
- Kronick, P. Page, A. & Komanowsky, M. (1993).  
'An acoustic emission study of staking and fatliquor.'  
Journal of the American Leather Chemists Association, 88, 178.
- Mann, C.W. Randall, E.B. Mandel, J. Kilduff, T.J. & Charles, A.M. (1951).  
'The sampling of side upper leather.'  
Journal of the American Leather Chemists Association, 46, 248.
- Maeser, M. & Dion, O.J. (1954).  
'The effect of splitting on the tensile properties of leather.'  
Journal of the American Leather Chemists Association, 49, 262.
- Maeser, M. (1960).  
'The effect of hide location and cutting direction on the tensile properties of upper leathers.'  
Journal of the American Leather Chemists Association, 55, 501.
- Mai, Y.W. & Atkins, A.G. (1989).  
'Further comments on j-shaped stress-strain curves and the crack resistance of biological materials.'  
Journal of Physics D - Applied Physics, 22, 48.
- Mattei, V & Roddy, W.T. (1957).  
'Physical properties of leather fatliquored at different oil levels.'  
Journal of the American Leather Chemists Association, 52, 110.
- Mitton, R.G. (1945).  
'Mechanical properties of leather fibres.'  
Journal of the Society of Leather Trades' Chemists, 29, 169.
- Mitton, R.G. (1964).  
'The dependence of tearing load on thickness.'  
Journal of the Society of Leather Technologists and Chemists, 48, 195.
- Mohsenin, N.N. (1980).  
'Physical properties of plant and animal materials.'  
Gordon and Breach, New York.

- Morgan, F.R. (1960).  
 'The mechanical properties of collagen and leather fibres.'  
 Journal of the American Leather Chemists Association, 55, 4.
- Official Methods of Analysis. (1965)  
 The Society Leather Trades' Chemists.  
 Redbourn.
- Offer, G. Knight, P. Jeacocke, R. Almond, R. Cousins, T. Elsey, J. Parsons,  
 N. Sharp, A. Starr, R. & Purslow, P. (1989).  
 'The structural basis of the water-holding, appearance and toughness of meat and  
 meat products.'  
 Food Microstructure, 8, 151.
- Purslow, P.P. (1980).  
 'The toughness of extensible connective tissues.'  
 PhD Thesis, The University of Reading.
- Purslow, P.P. Bigi, A. Ripomonti, A. & Roveri, N. (1984).  
 'Collagen fibre re-orientation around a crack in biaxially stretched aortic media.'  
 International Journal of Biological Macromolecules, 6, 21.
- Purslow, P.P. (1985).  
 'The physical basis of meat texture: observations on the fracture behaviour of  
 cooked bovine.'  
 Meat Science, 12, 39.
- Purslow, P.P. (1989a).  
 'Fracture of non-linear biological materials - some observations from practice  
 relevant to recent theory.'  
 Journal of Physics D-Applied Physics, 22(6), 854.
- Purslow, P. (1989b).  
 'Mechanisms of fracture in meat and meat products.'  
 Editors: Bee, R.D. Richmond, P. & Mingins, E.  
 Food Colloids Special Publication No. 75.
- Purslow, P. (1991).  
 'The notch-sensitivity of non-linear materials.'  
 Journal of Materials Science, 26(16), 4468.
- Rivlin, R.S. & Thomas, A.G. (1953).  
 'Rupture of rubber. 1. Characteristic energy for tearing.'  
 Journal of Polymer Science, 10, 291.
- Sharphouse, J.H. (1983).  
 'Leather Technician's Handbook.'  
 Vernon Lock Ltd., London.

- Sinnot, R.K. (1991).  
'Chemical Engineering, Design (volume 6).'
- Pergamon Press, Oxford.
- Smith, T.L. (1958).  
Journal of Polymer Science, 32, 99.
- Stacer, R.G. Yanyo, L.C. & Kelley, F.N. (1985a).  
'Observations of the tearing of elastomers.'
- Rubber Chemistry and Technology, 58, 421.
- Stacer, R.G. & Kelly, F.N. (1985b).  
'Criteria for unstable tearing of elastomers.'
- Rubber Chemistry and Technology, 58, 924
- Torp, S. Baer, E. & Friedman, B. (1975).  
'Effects of age and mechanical deformation on the ultrastructure of tendon.'
- Structure of Fibrous Biopolymers, p223.  
Sythoff & Noordhoff, Netherlands.
- Wainwright, S.A. Biggs, W.D. Currey, J.D. & Gosline, J.M. (1976).  
'Mechanical Design in Organisms.'
- Edward Arnold, London.
- Ward, I.M. (1983).  
'The Mechanical Properties of Solid Polymers.'
- John Wiley & Sons, Chichester.
- Whittaker, R.E. (1975).  
'The viscoelastic properties of leather and poromerics.'
- Journal of the Society of Leather Technologists and Chemists, 59, 172.
- Wilson, J.A. & Kern, E.J. (1926).  
'Effect of splitting on the tensile strength of leather.'
- Journal of Industrial Engineering Chemistry, 18, 312.
- Vos, A. & Vlimmeren, P.J. van (1973).  
'Topographic differences in physical properties.'
- Journal of the Society of Leather Technologists and Chemists, 57, 93.
- Vincent, J.F.V. (1982).  
'Structural Biomaterials.'
- Macmillan, London.
- Vincent, J.F.V. (1983).  
'The influence of water content on the stiffness and fracture properties of grass leaves.'
- Crop and Forage Science, 38, 107.

**Appendix 1.**

### Process History of Wet Blue Leather.

Initial material = wet salted domestic cattle hide.

Process.	Details.
<b>LIMING</b>	
Dirt soak	200 wt% H <sub>2</sub> O @ 26 °C. Drum for 60 minutes. Drain.
Main soak	170 wt% H <sub>2</sub> O @ 26 °C. Drum for 60 minutes. Drain. Repeat.
Lime	160 wt% H <sub>2</sub> O @ 26 °C. 2.5 wt% sodium sulphide. 5 wt% lime. Drum 90 minutes. Drum for 10 minutes every 30 minutes for 12 hours. Drain.
White lime	150 wt% H <sub>2</sub> O @ 22 °C. 5 wt% lime. Drum 15 minutes. Drum for 10 minutes every 120 minutes for 24 hours. Drain. Empty Drum.
<b>CHROMING</b>	
Wash	90 wt% H <sub>2</sub> O @ 35 °C. Drum 10 minutes. Drain.
Delime	70 wt% H <sub>2</sub> O @ 35 °C. 3 wt% ammonium sulphate. 0.4 wt% sodium metabisulphate. 1 wt% bate. Drum 60 minutes. Drain
Wash	100 wt% H <sub>2</sub> O @ 21 °C. Drum 10 minutes. Drain.
Tan	20 wt% H <sub>2</sub> O @ 21 °C. 6 wt% sodium chloride. 1 wt% sodium formate. Drum 10 minutes. 2.2 wt% sulphuric acid (77%). Drum 120 minutes until pH = 2.9-3.4. 8 wt% chrome powder (42% basic). Drum 60 minutes. 0.5 wt% tanbase. Drum 10 hours whereby pH = 3.6-3.8. Wash. Empty drum.
Sam	Sam & package.

**Appendix 2.**

### The Propanone Drying Process.

Seven litres of propanone were held in a flat bed tray and the sample of leather to be dried was fully immersed in the liquid. The lid of the tray was closed and sealed, using cohesive, propanone resistant tape. A thermometer was also sealed into the lid of the tray to measure the temperature of drying solutions. A small rubber bung in the lid of the tray could be withdrawn and approximately 25 ml of solution removed, placed in a density bottle, weighed and subsequently replaced.

Once a particular batch was complete, the tape was removed, the lid lifted and the propanone replaced quickly. The dimensions of the housing vessel are as in Table A.2.1.

Table A.2.1.

Vessel Measurement	Size
Inside width / m	0.59
Inside height / m	0.08
Inside length / m	0.72
Volume of vessel / m <sup>3</sup>	~ 0.04
Volume of vessel / litre	~ 34

In each drying batch, density measurements of the drying solution are taken over a period of 24 hours.

The density of the acetone in the drying solution as a function of temperature,  $t$ , (where  $0 < t < 54$  °C) was calculated as:

$$\rho_{\text{PROPANONE}} / \text{kg m}^{-3} = \frac{1}{(1.231736956 \times 10^{-3}) (1 + 1.3240 \times 10^{-3}t + 3.8090 \times 10^{-6}t^2 - 0.87983 \times 10^{-9}t^3)}$$

The density of the water in the drying solution as a function of temperature,  $t$ , (where  $0 < t < 33$  °C) was calculated as:

$$\rho_{\text{WATER}} / \text{kg m}^{-3} = \frac{1}{(1 \times 10^{-3}) (1 - 0.06427 \times 10^{-3}t + 8.5050 \times 10^{-6}t^2 - 6.7900 \times 10^{-9}t^3)}$$

The percentage of propanone in the drying solution was calculated as follows:

$$\text{From } x \cdot \rho_{\text{PROPANONE}} + [1 - x] \cdot \rho_{\text{WATER}} = \rho_{\text{DRYING SOLUTION}}$$

$$x = \frac{\rho_{\text{DRYING SOLUTION}} - \rho_{\text{WATER}}}{\rho_{\text{PROPANONE}} - \rho_{\text{WATER}}}$$

$$\text{and } y = (1 - x)$$

Where  $x$  = Wt fraction of propanone in the drying solution.  
Where  $y$  = Wt fraction of water in the drying solution.

Results for three drying batches are shown in Table A.2.2. A plot of (Wt % Water in drying solution) Versus (Time) for each drying batch (Figure A.2.1.) shows most of the water was removed in the first batch and by the third batch, very little water was removed from the leather.

Batch Number	t / min	T / Celsius	Propanone		Water		Weight of Dry		Volume of		Weight of Density Bottle / g + Drying Solution / g		Weight of Drying Solution / g		Drying Solution Density / kg m <sup>-3</sup>		wt % Propanone in Drying Solution		wt % Water in Drying Solution	
			Density / kg m <sup>-3</sup>	Density Bottle / g	Density Bottle / cm <sup>3</sup>	Density Bottle / g	Density Bottle / g	Density Bottle / g	Density Bottle / g	Density Bottle / g	Density Bottle / g	Density / kg m <sup>-3</sup>	Density / kg m <sup>-3</sup>	Density / kg m <sup>-3</sup>	Density / kg m <sup>-3</sup>	Density / kg m <sup>-3</sup>	Density / kg m <sup>-3</sup>			
1	0	16.5	793.7301	988.0509	15.9088	25.4834	36.1927	20.2829	795.9268	98.9301	1.0699									
1	7	16.5	793.7301	988.0509	15.9088	25.4834	36.3346	20.4248	801.4951	96.2181	3.7819									
1	17	16.7	793.5062	988.0186	15.9088	25.4834	36.3640	20.4542	802.6488	95.5513	4.4487									
1	35	17	793.1701	988.9683	15.9088	25.4834	36.4334	20.5236	805.3722	94.0709	5.9291									
1	45	17.3	792.8339	988.9191	15.9088	25.4834	36.4890	20.5792	807.5540	92.8573	7.1427									
1	65	17.8	792.2732	988.8336	15.9088	25.4834	36.5167	20.6069	808.6410	92.0760	7.9240									
1	70	18	792.0487	988.7987	15.9088	25.4834	36.5378	20.6280	809.4680	91.5742	8.4258									
1	108	18.7	791.2625	988.6735	15.9088	25.4834	36.6133	20.7035	812.4317	89.7936	10.2064									
1	173	19.3	790.5679	988.5626	15.9088	25.4834	36.7066	20.7968	816.0929	87.7365	12.2635									
1	241	19.4	790.4754	988.5438	15.9088	25.4834	36.7761	20.8663	818.8202	86.3772	13.6228									
1	306	19.3	790.5879	988.5626	15.9088	25.4834	36.8035	20.8937	819.8654	85.9082	14.0918									
1	371	19.1	790.8129	988.5989	15.9088	25.4834	36.8497	20.9399	821.7083	85.1312	14.8688									
1	421	19.3	790.5879	988.5626	15.9088	25.4834	36.8608	20.9510	822.1439	84.8270	15.1730									
1	1414	19.1	790.8129	988.5989	15.9088	25.4834	36.9441	21.0343	825.4127	83.3484	16.6516									
2	0	18.6	791.3749	988.6917	15.9088	25.4834	36.1384	20.2286	793.7960	98.8322	1.1678									
2	10	18.4	791.5986	988.7277	15.9088	25.4834	36.1792	20.2694	795.3970	98.1666	1.8334									
2	25	18.5	791.4872	988.7097	15.9088	25.4834	36.2254	20.3156	797.2100	97.2384	2.7616									
2	55	18.9	791.0377	988.6389	15.9088	25.4834	36.2381	20.3283	797.7084	96.7868	3.2132									
2	85	19.3	790.5879	988.5626	15.9088	25.4834	36.2670	20.3572	798.8424	96.0310	3.9690									
2	145	19.8	790.0252	988.4677	15.9088	25.4834	36.2752	20.3654	799.1642	95.6156	4.3644									
2	210	20.4	789.3494	988.3508	15.9088	25.4834	36.2845	20.3747	799.5282	95.1283	4.8707									
2	265	20.6	789.1239	988.3112	15.9088	25.4834	36.2878	20.3780	799.6986	94.9640	5.0360									
2	365	20.9	788.7657	988.2511	15.9088	25.4834	36.2894	20.3796	799.7214	94.7792	5.2208									
2	440	21.2	788.4472	988.1903	15.9088	25.4834	36.2986	20.3888	800.0825	94.4526	5.5474									
2	1420	21.2	788.4472	988.1903	15.9088	25.4834	36.2988	20.3900	800.1295	94.4302	5.5698									
3	0	18.5	791.4872	988.7097	14.2269	25.9224	34.8382	20.6113	795.1148	98.2494	1.7506									
3	15	19.3	790.5879	988.5626	14.2269	25.9224	34.8342	20.6073	794.9605	97.8975	2.1025									
3	30	19.4	790.4754	988.5438	14.2269	25.9224	34.8585	20.6316	795.8979	97.3939	2.6061									
3	75	19.8	790.0252	988.4677	14.2269	25.9224	34.8600	20.6331	795.9558	97.1548	2.8452									
3	155	20.3	789.4620	988.3705	14.2269	25.9224	34.8547	20.6278	795.7513	96.9885	3.0105									
3	197	21	788.6729	988.2308	14.2269	25.9224	34.8407	20.6138	795.2113	96.8799	3.1201									
3	312	21.1	788.5601	988.2106	14.2269	25.9224	34.8571	20.6302	795.8439	96.5257	3.4743									
3	395	21.8	787.7689	988.0684	14.2269	25.9224	34.8397	20.6128	795.1727	96.4788	3.5202									
3	1380	21	788.6729	988.2308	14.2269	25.9224	34.8614	20.6345	796.0098	96.4989	3.5011									

Table A.2.2  
Typical results over three propanone dehydration batch processes.

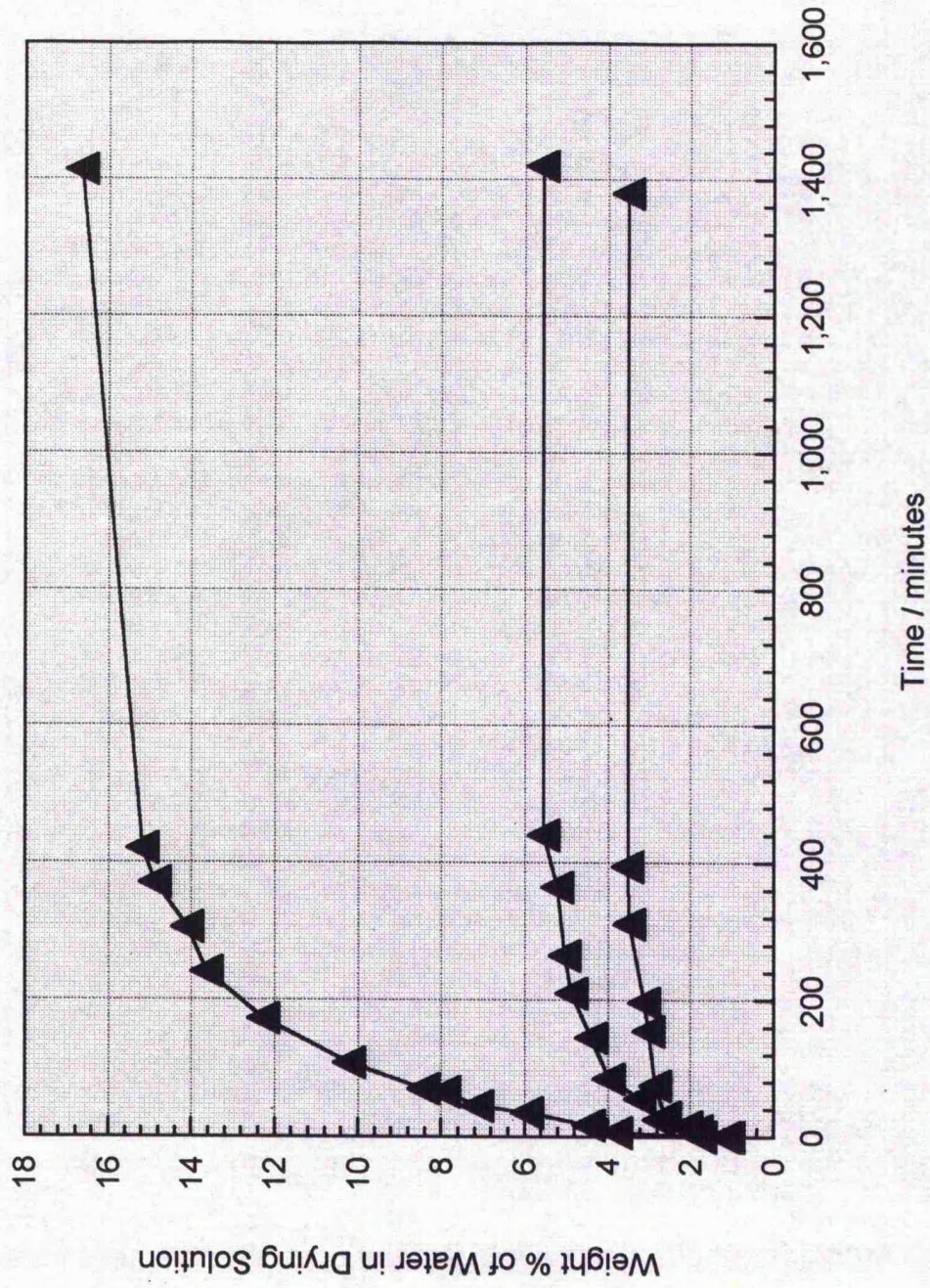


Figure A.2.1

A plot of wt% water in the drying solution versus time, over three propanone dehydration batch processes.

**Calculation of Water Content in Leather (wet weight basis) after Propanone Dehydration.**

If, before propanone dehydration, the total mass and percentage water content (wet weight basis) of the wet blue leather are known, it is possible to calculate a mass balance of water over the entire drying process. These calculations were carried out to determine the final water content in the dried leather on a wet weight basis. The methodology and results of such calculations are given in Tables: A.2.3. to A.2.6.

Table A.2.3.

Batch 1.	Calculation.	Quantity.
Start: volume drying solution		$7 \times 10^{-3}$ m <sup>3</sup>
End: volume drying solution		$4.876 \times 10^{-3}$ m <sup>3</sup>
Start: density drying solution		795.9268 kg m <sup>-3</sup>
End: density drying solution		825.4127 kg m <sup>-3</sup>
Start: mass drying solution	$(795.9268 \times 7 \times 10^{-3})$	5.5714876 kg
End: mass drying solution	$(825.4127 \times 4.876 \times 10^{-3})$	4.0247123 kg
Start: weight % water in drying solution		1.0699 %
End: weight % water in drying solution		16.6516 %
Start: mass of water in drying solution	$(1.0699 \times 10^{-2} \times 5.5714876)$	0.059609345 kg
End: mass of water in drying solution	$(16.6516 \times 10^{-2} \times 4.0247123)$	0.670178993 kg
Water removed from leather over the batch	$(0.670178993 - 0.059609345)$	0.610569648 kg

Table A.2.4.

Batch 2.	Calculation.	Quantity.
Start: volume drying solution		$7 \times 10^{-3}$ m <sup>3</sup>
End: volume drying solution		$5.3008 \times 10^{-3}$ m <sup>3</sup>
Start: density drying solution		793.7960 kg m <sup>-3</sup>
End: density drying solution		800.1295 kg m <sup>-3</sup>
Start: mass drying solution	$(793.7960 \times 7 \times 10^{-3})$	5.556572 kg
End: mass drying solution	$(800.1295 \times 5.3008 \times 10^{-3})$	4.241327 kg
Start: weight % water in drying solution		1.1678 %
End: weight % water in drying solution		5.5698 %
Start: mass of water in drying solution	$(1.1678 \times 10^{-2} \times 5.556572)$	0.064889647 kg
End: mass of water in drying solution	$(5.5698 \times 10^{-2} \times 4.241327)$	0.236233431 kg
Water removed from leather over the batch	$(0.236233431 - 0.064889647)$	0.171343784 kg

Table A.2.5

Batch 3.	Calculation.	Quantity.
Start: volume drying solution		$7 \times 10^{-3}$ m <sup>3</sup>
End: volume drying solution		$6.1504 \times 10^{-3}$ m <sup>3</sup>
Start: density drying solution		795.1148 kg m <sup>-3</sup>
End: density drying solution		796.0098 kg m <sup>-3</sup>
Start: mass drying solution	$(795.1148 \times 7 \times 10^{-3})$	5.5658036 kg
End: mass drying solution	$(796.0098 \times 6.1504 \times 10^{-3})$	4.8957787 kg
Start: weight % water in drying solution		1.7506 %
End: weight % water in drying solution		3.5011 %
Start: mass of water in drying solution	$(1.7506 \times 10^{-2} \times 5.5658036)$	0.097434957 kg
End: mass of water in drying solution	$(3.5011 \times 10^{-2} \times 4.8957787)$	0.171406108 kg
Water removed from leather over the batch	$(0.171406108 - 0.097434957)$	0.073971151 kg

Table A.2.6.

Item.	Calculation.	Quantity.
Total mass of water removed from leather over 3 batches	0.610569648 Kg + 0.171343784 Kg + 0.073971151 Kg	0.85588458 kg
Initial mass of wet blue leather (wet weight basis)		1.6256 kg
Initial percentage water content of wet blue leather (wet weight basis)		58.66 %
Initial mass of water present in wet blue leather (wet weight basis)	$(1.6256 \times 58.66 \times 10^{-2})$	0.95357696 kg
Total mass of water remaining in the leather after drying	$(0.95357696 - 0.85588458)$	0.09769238 kg
Final percentage of water remaining in the leather after drying (wet weight basis)	$\frac{0.09769238}{1.6256} \times 100 \%$	6.00962 %

**Appendix 3.**

### A.3.1 Program Inertia;

{This program removes the inertia glitch.}

{Definition of variable types}

```
var
Counter : integer;
Test_File , A_Line : string;
textfile1 , textfile2 , textfile3 : text;
temp : integer;
mm , KiloNewton : string;
Test_Array : array [1..2 , 1..2000] of real;
No_Sample_Array : array [1..2 , 1..2000] of real;
code : integer;
Last_Row_Test_File : integer;
No_Sample : string;
Last_Row_No_Sample : integer;
Zero_Negative_Numbers : integer;
start_condition : boolean;
Test_Start_Point : integer;
No_Sample_Start_Point : integer;
Rearrange : integer;
Current_Minimum_Different_Alignment , Total_Difference_Alignment : real;
Current_Minimum_Difference_Alignment : real;
First_No_Starts_In_Row : integer;
Adjust_No_Times : integer;
Align : integer;
Adjust_No_Sample_Array : array [1..2000] of real;
File_Output : integer;
mm_real , KiloNewton_real : real;
Output_File_Name : string;
Job_Done : boolean;
Main_Counter : integer;
Maximum_Recorded_mm_Array_Position_Test : integer;
Maximum_mm_Test : real;
mm_Counter : integer;
Maximum_mm_No_Sample : real;
Maximum_Recorded_mm_Array_Position_No_Sample : integer;
Delta_KiloNewton , Delta_mm , C , M : real;
Start_Condition_Integer : Integer;
Subtract_This_Value_KN , Subtract_This_Value_mm : real;
Adjust_Load , Adjust_mm : integer;
Start_Counter : integer;
Rid_Zeros_Condition : boolean;
```

{Read the two data files and place each in a 2-D array}

```
Procedure Read_in_two_files;
begin
{Read in the real test file}
Counter := 1;
writeln ('What is the name of the test file ?');
readln (Test_File);
assign (textfile1 , Test_File);
reset (textfile1);
while not Eof (textfile1) do
begin
readln (textfile1 , A_Line);
temp := pos(chr(9),A_Line);
mm := copy (A_Line,1,(temp-1));
KiloNewton := copy (A_Line,(temp + 1),25);
val (mm , Test_Array [1,counter],code);
val (KiloNewton , Test_Array [2,counter],code);
counter := counter + 1;
if counter = 2000 then writeln ('File too big');
if counter = 2000 then halt;
end;
close (textfile1);
Last_Row_Test_File := (counter -1);
```

```

{Read in no sample test file}
Counter := 1;
writeln ('What is the name of the file with no sample ?');
readln (No_Sample);
assign (textfile2, No_Sample);
reset (textfile2);
while not Eof (textfile2) do
begin
  readln (textfile2, A_Line);
  temp := pos(chr(9),A_Line);
  mm := copy (A_Line,1,(temp-1));
  KiloNewton := copy (A_Line,(temp+1),25);
  val (mm, No_Sample_Array [1,counter],code);
  val (KiloNewton, No_Sample_Array [2,counter],code);
  counter := counter + 1;
end;
close (textfile2);
Last_Row_No_Sample := (counter -1);
end;

{Find the start point for the test array}
Procedure Find_Starting_Point;
begin
  Start_Condition_Integer := 0;
  Counter := 1;
  While Start_Condition_Integer <> 6 do
  begin
    {Note: if we get 6 successive increases in mm, the machine must be moving
    and the test have started.}
    If (Test_Array[1,Counter] < Test_Array[1,Counter+1])
    then Start_Condition_Integer := Start_Condition_Integer + 1;
    If (Test_Array[1,Counter] >= Test_Array[1,Counter+1])
    then Start_Condition_Integer := 0;
    Counter := Counter + 1;
  end;
  Test_Start_Point := Counter - 6;
  writeln ('Test_Start_Point := ',Test_Start_Point);

{Find the start point for the No Sample array}
  Start_Condition_Integer := 0;
  Counter := 1;
  While Start_Condition_Integer <> 6 do
  begin
    {Note: if we get 6 successive increases in mm, the machine must be moving
    and the test have started.}
    If (No_Sample_Array[1,Counter] < No_Sample_Array[1,Counter+1])
    then Start_Condition_Integer := Start_Condition_Integer + 1;
    If (No_Sample_Array[1,Counter] >= No_Sample_Array[1,Counter+1])
    then Start_Condition_Integer := 0;
    Counter := Counter + 1;
  end;
  No_Sample_Start_Point := Counter - 6;

  writeln ('test start row = ',Test_Start_Point);
  writeln ('no sample start row = ', No_Sample_Start_Point);
  readln;
end;

Procedure Push_Rows_To_The_Top;
begin
  {Rearrange the Test_Array}
  Last_Row_Test_File := (Last_Row_Test_File - Test_Start_Point + 1);
  For Rearrange := 1 to Last_Row_Test_File do
  begin
    Test_Array [1,Rearrange] := Test_Array [1,(Test_Start_Point - 1 + Rearrange)];
    Test_Array [2,Rearrange] := Test_Array [2,(Test_Start_Point - 1 + Rearrange)];
  end;
end;

```

```

{Rearrange the No_Sample_Array}
Last_Row_No_Sample := (Last_Row_No_Sample - No_Sample_Start_Point + 1);
For Rearrange := 1 to Last_Row_No_Sample do
  begin
    No_Sample_Array [1,Rearrange] := No_Sample_Array [1, (No_Sample_Start_Point - 1 + Rearrange)];
    No_Sample_Array [2,Rearrange] := No_Sample_Array [2, (No_Sample_Start_Point - 1 + Rearrange)];
  end;
end;

Procedure Adjust_Figures;
begin
{We know that when the test begins, there is in reality NO
load so, we subtract this value of load from the other load readings.
Don't use the last reading of the test for subtraction purposes
because it is NOT zero because the sample is stiff and bending
is occurring, thus producing a negative load.}

{First we'll do the test array}
Subtract_This_Value_KN := Test_Array [2,1]; {Note 1 is the start point because we've pushed the rows up}
Writeln ('First value of force = ',Subtract_This_Value_KN);
For Adjust_Load := 1 to Last_Row_Test_File do
  begin
    Test_Array [2,Adjust_Load] := Test_Array [2,Adjust_Load] - Subtract_This_Value_KN;
  end;
Subtract_This_Value_mm := Test_Array [1,1];
For Adjust_mm := 1 to Last_Row_Test_File do
  begin
    Test_Array [1,Adjust_mm] := Test_Array [1,Adjust_mm] - Subtract_This_Value_mm;
  end;

{Next we'll do the no sample array}
Subtract_This_Value_KN := No_Sample_Array [2,1]; {Note 1 is the start point because we've pushed the rows up}
Writeln ('First value of force = ',Subtract_This_Value_KN);
For Adjust_Load := 1 to Last_Row_No_Sample do
  begin
    No_Sample_Array [2,Adjust_Load] := No_Sample_Array [2,Adjust_Load] - Subtract_This_Value_KN;
  end;
Subtract_This_Value_mm := No_Sample_Array [1,1];
For Adjust_mm := 1 to Last_Row_No_Sample do
  begin
    No_Sample_Array [1,Adjust_mm] := No_Sample_Array [1,Adjust_mm] - Subtract_This_Value_mm;
  end;
end;

Procedure Find_Maximum_mm_Test_Array_Update;
begin
Maximum_mm_Test := Test_Array [1, mm_Counter];
Maximum_Recorded_mm_Array_Position_Test := mm_Counter;
end;

Procedure Find_Maximum_mm_Test_Array;
begin
Maximum_mm_Test := 0;
For mm_Counter := 1 to Last_Row_Test_File do
  begin
    if Test_Array [1, mm_Counter] > Maximum_mm_Test then Find_Maximum_mm_Test_Array_Update;
  end;
end;

Procedure Find_Maximum_mm_No_Sample_Array_Update;
begin
Maximum_mm_No_Sample := No_Sample_Array [1, mm_Counter];
Maximum_Recorded_mm_Array_Position_No_Sample := mm_Counter;
end;

```

```

Procedure Find_Maximum_mm_No_Sample_Array;
begin
Maximum_mm_No_Sample := 0;
mm_Counter := 0;
For mm_Counter := 1 to Last_Row_No_Sample do
begin
if No_Sample_Array [1, mm_Counter] > Maximum_mm_No_Sample then
Find_Maximum_mm_No_Sample_Array_Update;
end;
end;

Procedure Go_Ahead_And_Output;
begin
{Here we have a position where the mm values in the Test_Array lie between
its corresponding row number and the following row number in the No_Sample_
array.
Now we must interpolate (linearly) and obtain the exact mm value in the
No_Sample_Array that fits with the Test_Array, then use the same function
values (ie M & C in Y = MX + C) to alter the force values.
Then subtract the No_Sample_Array force values from the Test_Array force
values and output the mm_real (from the test array) and the KiloNewton_real
into the .adj file}

{M = Delta_KiloNewton / Delta_mm}
Delta_KiloNewton := (No_Sample_Array [2,(First_No_Starts_In_Row + File_Output)]
- (No_Sample_Array [2,(First_No_Starts_In_Row + File_Output - 1)]));

Delta_mm := (No_Sample_Array [1,(First_No_Starts_In_Row + File_Output)]
- (No_Sample_Array [1,(First_No_Starts_In_Row + File_Output - 1)]));

if Delta_mm < > 0 then M := Delta_KiloNewton / Delta_mm;
if Delta_mm = 0 then M := 0;

C := (No_Sample_Array [2,(First_No_Starts_In_Row + File_Output - 1)] -
(M * (No_Sample_Array [1,(First_No_Starts_In_Row + File_Output - 1)]));

KiloNewton_real := (Test_Array [2,Main_Counter]) -
((M * (Test_Array [1,Main_Counter])) + C);

mm_real := Test_Array [1, Main_Counter];

{The output file must have the same format as the input file.}
writeln (textfile3,mm_real,chr(9),KiloNewton_real);

{writeln (textfile3,Test_Array [1,Main_Counter],chr(9),No_Sample_Array [1,(First_No_Starts_In_Row + File_Output -
1)]);}
Main_Counter := Main_Counter + 1;
end;

Procedure Take_Alternative;
begin
writeln ('This may not be accurate as the Max mm reading in the real test is');
writeln ('bigger than in the no sample test, so no interpolation occurs !');
writeln ('Press Return to Continue');
readln;
While Job_Done = False do
begin
Go_Ahead_and_Output;
File_Output := File_Output + 1;
if (Main_Counter = Last_Row_Test_File) OR
(File_Output = Last_Row_No_Sample) then Job_Done := true;
end;
end;
end;

```

```

Procedure Output_mm_KiloNewton_Data;
begin
{Now we know the Test_Array starts @ row 1 & end @ row Last_Row_Test_File}
{We also know that the No_Sample_Array starts @ First_No_Starts_In_Row and
ends @ Last_Row_No_Sample}
{The next step is to subtract the No_Sample_Array load values from the
Test_Array load values and output to the original file .txt}

temp := pos('.',Test_File);
Output_File_Name := copy (Test_File,1,temp);
insert ('adj',Output_File_Name,(temp+1));
writeln ('File will be output under the original test file name with extension .adj , ie ',Output_File_Name);
assign (textfile3,Output_File_Name);
rewrite (textfile3);
File_Output := 1;
Main_Counter := 1;

{Have to check zero to Maximum_mm first then from max mm to 0 mm}
{Here is 0 mm (begining of test) to Max mm}
Job_Done := false;
While Job_Done = false do
begin
if (Test_Array [1, Main_Counter] >=
No_Sample_Array [1,(First_No_Starts_In_Row + File_Output - 1)]) AND
(Test_Array [1, Main_Counter] <=
No_Sample_Array [1,(First_No_Starts_In_Row + File_Output)]) Then
Go_Ahead_and_Output;

if (Test_Array [1, Main_Counter] >
No_Sample_Array [1,(First_No_Starts_In_Row + File_Output - 1)]) AND
(Test_Array [1, Main_Counter] >
No_Sample_Array [1,(First_No_Starts_In_Row + File_Output)]) AND
(File_Output <> Last_Row_Test_File) Then File_Output := File_Output + 1;

if (Test_Array [1, Main_Counter] <
No_Sample_Array [1,(First_No_Starts_In_Row + File_Output - 1)]) AND
(Test_Array [1, Main_Counter] <
No_Sample_Array [1,(First_No_Starts_In_Row + File_Output)]) AND
(File_Output > 1) Then File_Output := File_Output - 1;

if (Test_Array [1, Main_Counter] <
No_Sample_Array [1,(First_No_Starts_In_Row + File_Output - 1)]) AND
(Test_Array [1, Main_Counter] <
No_Sample_Array [1,(First_No_Starts_In_Row + File_Output)]) AND
(File_Output = 1) Then Go_Ahead_and_Output; {ie this is where the data
starts so this is the closest we'll get !!}

if (Main_Counter = Maximum_Recorded_mm_Array_Position_Test) OR
(File_Output = Maximum_Recorded_mm_Array_Position_No_Sample)
then Job_Done := true;

writeln ('Main Counter = ',Main_Counter,' File Output = ',File_Output);
end;

{Here is Max+1 mm to 0 mm}
Main_Counter := Maximum_Recorded_mm_Array_Position_Test + 2;
File_Output := Maximum_Recorded_mm_Array_Position_No_Sample + 2;
writeln ('Test_Array mm = ',Test_Array[1,Main_Counter]);
writeln ('No_Sample_Array mm = ',No_Sample_Array [1,File_Output]);

{Note that in some tests, the No_sample array does not reach the mm value
of Test_Array. In this case, we can't interpolate on the basis of mm, so
just subtract one value from the other !}

Job_Done := false;
If No_Sample_Array [1,File_Output] < Test_Array[1,Main_Counter] then Take_Alternative;

```

```

While Job_Done = false do
begin
if (Test_Array [1, Main_Counter] <=
No_Sample_Array [1,(First_No_Starts_In_Row + File_Output - 1)]) AND
(Test_Array [1, Main_Counter] >=
No_Sample_Array [1,(First_No_Starts_In_Row + File_Output)]) Then
Go_Ahead_and_Output;

if (Test_Array [1, Main_Counter] >
No_Sample_Array [1,(First_No_Starts_In_Row + File_Output - 1)]) AND
(Test_Array [1, Main_Counter] >
No_Sample_Array [1,(First_No_Starts_In_Row + File_Output)])
Then File_Output := File_Output - 1;

if (Test_Array [1, Main_Counter] <
No_Sample_Array [1,(First_No_Starts_In_Row + File_Output - 1)]) AND
(Test_Array [1, Main_Counter] <
No_Sample_Array [1,(First_No_Starts_In_Row + File_Output)])
Then File_Output := File_Output + 1;

{Here we have a situation where the mm in the no sample array have
increased when they should be decreasing ie the cross head is returning.
The only alternative is just to increase the File_Output by one and
send it through all the checkers again !}

if (Test_Array [1, Main_Counter] >
No_Sample_Array [1,(First_No_Starts_In_Row + File_Output - 1)]) AND
(Test_Array [1, Main_Counter] <
No_Sample_Array [1,(First_No_Starts_In_Row + File_Output)])
Then File_Output := File_Output + 1;

if (Test_Array [1, Main_Counter] <=0.01) OR
(No_Sample_Array [1,(First_No_Starts_In_Row + File_Output - 1)] <= 0.01)
then Job_Done := true;

if (Main_Counter = Last_Row_Test_File) OR
(File_Output = Last_Row_No_Sample) then Job_Done := true;

writeln ('Main Counter = ',Main_Counter,' File Output = ',File_Output);
end;

close (textfile3);
writeln ('Procedure is now complete.')
end;

{Main}
Begin
Read_In_Two_Files;
Find_Starting_Point;
Push_Rows_To_The_Top;
Adjust_Figures;
Find_Maximum_mm_Test_Array;
Find_Maximum_mm_No_Sample_Array;
Output_mm_KiloNewton_Data;
Readln;
End.

```

### A.3.2 Program Tensile\_Test;

{This program processes data from the tensile tests}

```
{Definition of variable types}
uses Crt, Dos;
var
The_File : string;
A_Line : string;
txtfile : text; {input file}
textfile : text; {output file}
Resfile : text; {results file}
counter : integer;
mm_KiloNewton_Array : array [1..2, 1..4000] of real;
l : integer;
mm : string;
KiloNewton : string;
temp : integer;
code : integer;
Last_Row : integer;
Maximumforce , Maximum_mm : real;
Maxforcecounter : integer;
Maximum_condition_array_position : integer;
Start_Condition_Integer : integer;
Start_Counter : integer;
Real_Start_Point : integer;
Subtract_This_Value_KN , Subtract_This_Value_mm : real;
Adjust_Load , Adjust_mm : integer;
End_Force_Finder_Condition : boolean;
End_Force_Finder : integer;
Last_Reading_Of_Test : integer;
End_Condition_Integer : integer;
End_Counter : integer;
Calculation : integer;
h : real;
Area_to_Max : real;
Area_to_Relax : real;
File_Output : integer;
Strain , Stress : real;
thickness : real;
Output_File_Name : string;
Rid_Zeros_Condition : Boolean;
Extension : Real;
Force : Real;
Four_times , Two_times : Real;
Final_Adjust : Boolean;

{Read the data file and place in a 2-D array}
Procedure Read_in_File;
begin
counter := 1;
Writeln ('What is the name of the file (Column 1 = mm , Column2 = (KN)');
Readln (The_File);
assign (txtfile, The_File);
reset (txtfile);
while not Eof(txtfile) do
begin
{Read every thing as a string}
readln (txtfile, A_Line);
temp := pos (chr(9),A_Line); {the spacer in this type of text file}
{Now find the X & Y values and put into an array}
mm := copy (A_Line,1,temp-1);
KiloNewton := copy (A_Line,temp+1,25);
Val (mm, mm_KiloNewton_Array[1,counter], code);
Val (KiloNewton, mm_KiloNewton_Array[2,counter], code);
counter := counter + 1;
end;
close (txtfile);
```

```

Last_Row := (counter-1);
end;

Procedure update;
begin
Maximumforce := mm_KiloNewton_Array [2,maxforcecounter];
Maximum_condition_array_position := maxforcecounter;
end;

Procedure Find_Maximum_Force;
begin
Maximumforce := 0;
For maxforcecounter := Real_Start_Point TO Last_Row do
begin
IF mm_KiloNewton_Array[2,maxforcecounter] > Maximumforce THEN update;
end;
end;

Procedure Find_Real_Start_Point;
begin
Start_Condition_Integer := 0;
Start_Counter := 1;
While Start_Condition_Integer <> 6 do
begin
{Note: if we get 6 successive increases in mm, the machine must be moving
and the test have started.}
If (mm_KiloNewton_Array[1,Start_Counter] < mm_KiloNewton_Array[1,Start_Counter+1])
then Start_Condition_Integer := Start_Condition_Integer + 1;
If (mm_KiloNewton_Array[1,Start_Counter] >= mm_KiloNewton_Array[1,Start_Counter+1])
then Start_Condition_Integer := 0;
Start_Counter := Start_Counter + 1;
end;
Real_Start_Point := Start_Counter - 6;
Real_Start_point := Real_Start_Point + 3;
end;

Procedure Adjust_Figures;
begin
{We know that when the test begins, in reality NO load so, we subtract
this value of load from the other load readings. Note that we don't use
the last reading because it is NOT zero because the sample is stiff and
bending is occuring, thus producing a negative load.}

Subtract_This_Value_KN := mm_KiloNewton_Array [2,Real_Start_Point];
writeln ('first value of force = ',Subtract_This_Value_KN);
For Adjust_Load := Real_Start_Point to Last_Row do
begin
mm_KiloNewton_Array [2,Adjust_Load] := mm_KiloNewton_Array [2,Adjust_Load] - Subtract_This_Value_KN;
end;
Subtract_This_Value_mm := mm_KiloNewton_Array [1,Real_Start_Point];
For Adjust_mm := Real_Start_Point to Last_Row do
begin
mm_KiloNewton_Array [1,Adjust_mm] := mm_KiloNewton_Array [1,Adjust_mm] - Subtract_This_Value_mm;
end;

{Now get rid of all zero loads, they are very small and not really there!}
Start_Counter := Real_Start_Point;
Rid_Zeros_Condition := False;
while Rid_Zeros_Condition = False do
begin
IF mm_KiloNewton_Array[2,Start_Counter] < 0 then mm_KiloNewton_Array[2,Start_Counter] := 0;
IF mm_KiloNewton_Array[1,Start_Counter] < 0 then mm_KiloNewton_Array[1,Start_Counter] := 0;
IF Start_Counter = Last_Row then Rid_Zeros_Condition := true;
Start_Counter := Start_Counter + 1;
end;
end;
end;

```

```

Procedure Energy_Used_on_Cycle;
begin
{Calculate area from Real_Start_Point to Maximum_Condition_Array_Position}
{Using Simpsons rule}
Calculation := (Real_Start_Point + 1);
While Calculation <= (Maximum_Condition_Array_Position - 1) do
begin
Four_times := Four_times + (4 * mm_KiloNewton_Array [2, Calculation]);
Calculation := Calculation + 2;
end;
Calculation := (Real_Start_Point + 2);
While Calculation <= (Maximum_Condition_Array_Position - 2) do
begin
Two_times := Two_times + (2 * mm_KiloNewton_Array [2, Calculation]);
Calculation := Calculation + 2;
end;
{Find the distance, h, travelled between each reading by calculating the average}
h := ((mm_KiloNewton_Array [1,Maximum_Condition_Array_Position] - mm_KiloNewton_Array [1,Real_Start_Point])
/ (Maximum_Condition_Array_Position - Real_Start_Point));
Area_to_Max := (h/3) * (mm_KiloNewton_Array [2,Real_Start_Point] +
Four_times + Two_times +
mm_KiloNewton_Array [2,Maximum_Condition_Array_Position]);
{Note KN x mm = Joules}
end;

Procedure Output_Stress_Strain;
begin
writeln('What is the average thickness of the sample in mm?');
Readln (thickness);
thickness := thickness / 1000;
{Sort out name for output file, called the same name but .dat instead of .txt}
temp := pos('.',The_File);
Output_File_Name := copy (The_File,1,temp);
insert ('DAT',Output_File_Name,(Temp+1));
writeln ('Output file name is ',Output_File_Name);
assign (textfile, Output_File_Name);
rewrite (textfile);
writeln (textfile, 'Strain%,MPa,mm,KN');
For File_Output := Real_Start_point to Maximum_Condition_Array_Position do
begin
Strain := (mm_KiloNewton_Array [1,File_Output] / 50{Gauge length}) * 100;
Stress := ((mm_KiloNewton_Array [2,File_Output] * 1000)
/ (thickness{metre} * 0.01{width of sample in metre}))
/ 1000000;{for MPa}
Extension := mm_KiloNewton_Array [1,File_Output];
Force := mm_KiloNewton_Array [2,File_Output];
writeln (textfile, Strain,',',Stress,',',Extension,',',Force);
end;
{Here we make sure the last recorded load / stress is set to zero exactly
as it may be very slightly + or -}
Strain := (mm_KiloNewton_Array [1,Last_Reading_Of_Test] / 50{Gauge length}) * 100;
Stress := 0;
Extension := mm_KiloNewton_Array [1,Last_Reading_Of_Test];
Force := 0;
writeln (textfile, Strain,',',Stress,',',Extension,',',Force);
close (textfile);
end;

Procedure Print_Figures_On_Screen;
begin
Writeln;
Writeln ('Force at Maximum Extension (KN) = ', mm_KiloNewton_Array [2,Maximum_condition_array_position]);
Writeln ('Maximum Extension (mm) = ', mm_KiloNewton_Array [1,Maximum_condition_array_position]);
Writeln ('Stress at Maximum Strain (MPa) = ',((mm_KiloNewton_Array [2,Maximum_condition_array_position] * 1000)
/ (thickness{metre} * 0.01{width of sample in metre})) / 1000000{for MPa});
Writeln ('Maximum Strain (%) = ',(mm_KiloNewton_Array [1,Maximum_condition_array_position] / 50{Gauge
length}) * 100);

```

```

writeln ('Energy to Maximum Extension (J) = ',Area_to_Max);
end;

Procedure Put_Figures_On_Results_File;
begin
Assign (Resfile, 'c:\breakres.txt');
Append (Resfile);
Writeln (Resfile, The_File,chr(9),Thickness,chr(9),
mm_KiloNewton_Array [2,Maximum_condition_array_position],chr(9),
mm_KiloNewton_Array [1,Maximum_condition_array_position],chr(9),
(((mm_KiloNewton_Array [2,Maximum_condition_array_position] * 1000) /
(thickness{metre} * 0.01{width of sample in metre}))
/ 1000000{for MPa}),chr(9),
((mm_KiloNewton_Array [1,Maximum_condition_array_position] / 50){Gauge length}
* 100),chr(9),
Area_to_Max, chr(9));

close (Resfile);
end;

{Main}
Begin
clrscr;
Read_In_File;
Find_Real_Start_Point; {ie where the cross-head is moving}
Find_Maximum_Force;
Adjust_Figures;
Energy_Used_On_Cycle;
Output_Stress_Strain;
Print_Figures_On_Screen;
Put_Figures_On_Results_File;
Readln;
End.

```

### A.3.3 Program Strain\_Cycling\_Test;

{This program processes data from the strain cycling tests}

{Definition of variable types}

```
uses Crt, Dos;
var
The_File : string;
A_Line : string;
txtfile : text; {input file}
textfile : text; {output file}
Resfile : text; {results file}
counter : integer;
mm_KiloNewton_Array : array [1..2, 1..4000] of real;
l : integer;
mm : string;
KiloNewton : string;
temp : integer;
code : integer;
Last_Row : integer;
Maximumforce , Maximum_mm : real;
Maxforcecounter : integer;
Maximum_condition_array_position : integer;
Start_Condition_Integer : integer;
Start_Counter : integer;
Real_Start_Point : integer;
Subtract_This_Value_KN , Subtract_This_Value_mm : real;
Adjust_Load , Adjust_mm : integer;
End_Force_Finder_Condition : boolean;
End_Force_Finder : integer;
Last_Reading_Of_Test : integer;
End_Condition_Integer : integer;
End_Counter : integer;
Calculation : integer;
h : real;
Area_to_Max : real;
Area_to_Relax : real;
File_Output : integer;
Strain , Stress : real;
thickness : real;
Output_File_Name : string;
Rid_Zeros_Condition : Boolean;
Extension : Real;
Force : Real;
Four_times , Two_times : Real;
Final_Adjust : Boolean;

{Read the data file and place in a 2-D array}
Procedure Read_in_File;
begin
counter:= 1;
Writeln ('What is the name of the file (Column 1 = mm , Column2 = KN)');
Readln (The_File);
assign (txtfile, The_File);
reset (txtfile);
while not Eof(txtfile) do
begin
{Read every thing as a string}
readln (txtfile, A_Line);
temp := pos (chr(9),A_Line); {the spacer in this type of text file}
{Now find the X & Y values and put into an array}
mm := copy (A_Line,1,temp-1);
KiloNewton := copy (A_Line,temp+1,25);
Val (mm, mm_KiloNewton_Array[1,counter], code);
Val (KiloNewton, mm_KiloNewton_Array[2,counter], code);
counter:= counter + 1;
end;
close (txtfile);
```

```

Last_Row := (counter-1);
end;

Procedure update;
begin
Maximumforce := mm_KiloNewton_Array [2,maxforcecounter];
Maximum_condition_array_position := maxforcecounter;
end;

Procedure Find_Maximum_Force;
begin
Maximumforce := 0;
For maxforcecounter := Real_Start_Point TO Last_Row do
begin
IF mm_KiloNewton_Array[2,maxforcecounter] > Maximumforce THEN update;
end;
end;

Procedure Find_Real_Start_Point;
begin
Start_Condition_Integer := 0;
Start_Counter := 1;
While Start_Condition_Integer <> 6 do
begin
{Note: if we get 6 successive increases in mm, the machine must be moving
and the test have started.}
If (mm_KiloNewton_Array[1,Start_Counter] < mm_KiloNewton_Array[1,Start_Counter+1])
then Start_Condition_Integer := Start_Condition_Integer + 1;
If (mm_KiloNewton_Array[1,Start_Counter] >= mm_KiloNewton_Array[1,Start_Counter+1])
then Start_Condition_Integer := 0;
Start_Counter := Start_Counter + 1;
end;
Real_Start_Point := Start_Counter - 6;
Real_Start_point := Real_Start_Point + 3;
end;

Procedure Adjust_Figures;
begin
{We know that when the test begins, there is in reality NO
load so, we subtract this value of load from the other load readings. Note
that we don't use the last reading because it is NOT zero because the sample
is stiff and bending is occurring, thus producing a negative load.}

Subtract_This_Value_KN := mm_KiloNewton_Array [2,Real_Start_Point];
writeln ('first value of force = ',Subtract_This_Value_KN);
For Adjust_Load := Real_Start_Point to Last_Row do
begin
mm_KiloNewton_Array [2,Adjust_Load] := mm_KiloNewton_Array [2,Adjust_Load] - Subtract_This_Value_KN;
end;
Subtract_This_Value_mm := mm_KiloNewton_Array [1,Real_Start_Point];
For Adjust_mm := Real_Start_Point to Last_Row do
begin
mm_KiloNewton_Array [1,Adjust_mm] := mm_KiloNewton_Array [1,Adjust_mm] - Subtract_This_Value_mm;
end;
{Now get rid of all zero loads, they are very small and not really there!}
Start_Counter := Real_Start_Point;
Rid_Zeros_Condition := False;
while Rid_Zeros_Condition = False do
begin
IF mm_KiloNewton_Array[2,Start_Counter] < 0 then mm_KiloNewton_Array[2,Start_Counter] := 0;
IF mm_KiloNewton_Array[1,Start_Counter] < 0 then mm_KiloNewton_Array[1,Start_Counter] := 0;
IF Start_Counter = Last_Row then Rid_Zeros_Condition := true;
Start_Counter := Start_Counter + 1;
end;
end;

Procedure Go_Backwards_to_Find_Where_Load_Is_Effectively_Zero;

```

```

begin
End_Condition_Integer := 0;
End_Counter := Last_Row;
writeln (End_Counter);
readln;
While End_Condition_Integer <> 2 do
begin
If (mm_KiloNewton_Array[2,End_Counter] >= mm_KiloNewton_Array[2,(End_Counter-1)])
then End_Condition_Integer := 0;
If (mm_KiloNewton_Array[2,End_Counter] < mm_KiloNewton_Array[2,(End_Counter-1)])
then End_Condition_Integer := End_Condition_Integer + 1;
writeln ('End_Condition_Integer = ',End_Condition_Integer,'End_Counter = ',End_Counter);
End_Counter := End_Counter - 1;
end;
Last_Reading_Of_Test := End_Counter + 2;
end;

Procedure Energy_Used_on_Cycle;
begin
{Calculate area from Real_Start_Point to Maximum_Condition_Array_Position}
{Using Simpsons rule}
Calculation := (Real_Start_Point + 1);
While Calculation <= (Maximum_Condition_Array_Position - 1) do
begin
Four_times := Four_times + (4 * mm_KiloNewton_Array [2, Calculation]);
Calculation := Calculation + 2;
end;
Calculation := (Real_Start_Point + 2);
While Calculation <= (Maximum_Condition_Array_Position - 2) do
begin
Two_times := Two_times + (2 * mm_KiloNewton_Array [2, Calculation]);
Calculation := Calculation + 2;
end;
{Find the distance, h, travelled between each reading by calculating the average}
h := ((mm_KiloNewton_Array [1,Maximum_Condition_Array_Position] - mm_KiloNewton_Array [1,Real_Start_Point])
/ (Maximum_Condition_Array_Position - Real_Start_Point));
Area_to_Max := (h/3) * (mm_KiloNewton_Array [2,Real_Start_Point] +
Four_times + Two_times +
mm_KiloNewton_Array [2,Maximum_Condition_Array_Position]);
{Calculate area from Maximum_Condition_Array_Position to Last_Reading_Of_Test}
{Reset Four-times & Two-times to Zero}
Four_times := 0;
Two_times := 0;
Calculation := Maximum_Condition_Array_Position + 1;
While Calculation <= (Last_Reading_Of_Test - 1) do
begin
Four_times := Four_times + (4 * mm_KiloNewton_Array [2, Calculation]);
Calculation := Calculation + 2;
end;
Calculation := Maximum_Condition_Array_Position + 2;
While Calculation <= (Last_Reading_Of_Test - 2) do
begin
Two_times := Two_times + (2 * mm_KiloNewton_Array [2, Calculation]);
Calculation := Calculation + 2;
end;
Area_to_Relax := (h/3) * (mm_KiloNewton_Array [2,Maximum_Condition_Array_Position] +
Two_times + Four_times +
mm_KiloNewton_Array [2,Last_Reading_Of_Test]);
{Note KN x mm = Joules}
end;

Procedure Output_Stress_Strain;
begin
writeln('What is the average thickness of the sample in mm?');
Readln (thickness);
thickness := thickness / 1000;
{Sort out name for output file, called the same name but .dat instead of .txt}

```

```

temp := pos('.',The_File);
Output_File_Name := copy(The_File,1,temp);
insert('DAT',Output_File_Name,(Temp+1));
writeln('Output file name is ',Output_File_Name);
assign(textfile,Output_File_Name);
rewrite(textfile);
writeln(textfile,'Strain%,MPa,mm,KN');
For File_Output := Real_Start_point to (Last_Reading_Of_Test-1) do
begin
Strain := (mm_KiloNewton_Array [1,File_Output] / 50{Gauge length}) * 100;
Stress := ((mm_KiloNewton_Array [2,File_Output] * 1000)
/ (thickness{metre} * 0.01{width of sample in metre}))
/ 1000000{for MPa}
Extension := mm_KiloNewton_Array [1,File_Output];
Force := mm_KiloNewton_Array [2,File_Output];
writeln(textfile,Strain,',',Stress,',',Extension,',',Force);
end;
{Here we make sure the last recorded load / stress is set to zero exactly
as it may be very slightly + or -}
Strain := (mm_KiloNewton_Array [1,Last_Reading_Of_Test] / 50{Gauge length}) * 100;
Stress := 0;
Extension := mm_KiloNewton_Array [1,Last_Reading_Of_Test];
Force := 0;
writeln(textfile,Strain,',',Stress,',',Extension,',',Force);
close(textfile);
end;

Procedure Print_Figures_On_Screen;
begin
Writeln;
Writeln('Force at Maximum Extension (KN) = ',mm_KiloNewton_Array [2,Maximum_condition_array_position]);
Writeln('Maximum Extension (mm) = ',mm_KiloNewton_Array [1,Maximum_condition_array_position]);
Writeln('Stress at Maximum Strain (MPa) = ',(mm_KiloNewton_Array [2,Maximum_condition_array_position] * 1000)
/ (thickness{metre} * 0.01{width of sample in metre})) / 1000000{for MPa});
Writeln('Maximum Strain (%) = ',(mm_KiloNewton_Array [1,Maximum_condition_array_position] / 50{Gauge
length}) * 100);
writeln('Energy to Maximum Extension (J) = ',Area_to_Max);
writeln('Energy Released on Unloading (J) = ',Area_to_Relax);
Writeln('The Hysteresis Ratio is = ',(Area_to_Max - Area_to_Relax)/Area_to_Max);
Writeln('Immediate Set (e%) = ',(mm_KiloNewton_Array [1,Last_Reading_Of_Test] / 50{Gauge length}) * 100);
end;

Procedure Put_Figures_On_Results_File;
begin
Assign(Resfile,'c:\cycleres.txt');
Append(Resfile);
Writeln(Resfile,The_File,chr(9),Thickness,chr(9),
mm_KiloNewton_Array [2,Maximum_condition_array_position],chr(9),
mm_KiloNewton_Array [1,Maximum_condition_array_position],chr(9),
((mm_KiloNewton_Array [2,Maximum_condition_array_position] * 1000) /
(thickness{metre} * 0.01{width of sample in metre}))
/ 1000000{for MPa}),chr(9),
(mm_KiloNewton_Array [1,Maximum_condition_array_position] / 50{Gauge length}
* 100),chr(9),
Area_to_Max,chr(9),Area_to_Relax,chr(9),
(Area_to_Max - Area_to_Relax)/Area_to_Max,chr(9),
(mm_KiloNewton_Array [1,Last_Reading_Of_Test] / 50{Gauge length} * 100));
close(Resfile);
end;

{Main}
Begin
clrscr;
Read_in_File;
Find_Real_Start_Point; {ie where the cross-head is moving}
Find_Maximum_Force;
Adjust_Figures;

```

```
Go_Backwards_to_Find_Where_Load_Is_Effectively_Zero;  
Energy_Used_On_Cycle;  
Output_Stress_Strain;  
Print_Figures_On_Screen;  
Put_Figures_On_Results_File;  
ReadIn;  
End.
```

### A.3.4 Program Notch\_Test;

{This program processes data from the single notch specimen tests}

```
{Definition of variables}
uses Crt, Dos;
var
The_File : string;
A_Line : string;
txtfile : text; {input file}
textfile : text; {output file}
Resfile : text; {results file}
counter : integer;
mm_KiloNewton_Array : array [1..2, 1..4000] of real;
l : integer;
mm : string;
KiloNewton : string;
temp : integer;
code : integer;
Last_Row : integer;
Maximumforce , Maximum_mm : real;
Maxforcecounter : integer;
Maximum_condition_array_position : integer;
Start_Condition_Integer : integer;
Start_Counter : integer;
Real_Start_Point : integer;
Subtract_This_Value_KN , Subtract_This_Value_mm : real;
Adjust_Load , Adjust_mm : integer;
End_Force_Finder_Condition : boolean;
End_Force_Finder : integer;
Last_Reading_Of_Test : integer;
Calculation : integer;
h : real;
Area_to_Max : real;
Area_to_Relax : real;
File_Output : integer;
Strain , Stress : real;
thickness : real;
Notch_Length : real;
Sample_Volume : real;
Energy_Density : real;
Output_File_Name : string;
Rid_Zeros_Condition : Boolean;
Extension : Real;
Force : Real;
Four_times , Two_times : Real;

{Read the data file and place in a 2-D array}
Procedure Read_in_File;
begin
counter:= 1;
Writeln ('What is the name of the file (Column 1 = mm , Column2 = KN)');
Readln (The_File);
assign (txtfile, The_File);
reset (txtfile);
while not Eof(txtfile) do
begin
{Read every thing as a string}
readln (txtfile, A_Line);
temp := pos (chr(9),A_Line); {the spacer in this type of text file}
{Now find the X & Y values and put into an array}
mm := copy (A_Line,1,temp-1);
KiloNewton := copy (A_Line,temp+1,25);
Val (mm, mm_KiloNewton_Array[1,counter], code);
Val (KiloNewton, mm_KiloNewton_Array[2,counter], code);
counter:= counter + 1;
end;
close (txtfile);
```

```

Last_Row := (counter-1);
end;

Procedure update;
begin
Maximumforce := mm_KiloNewton_Array [2,maxforcecounter];
Maximum_condition_array_position := maxforcecounter;
end;

Procedure Find_Maximum_Force;
{Assume Fracture occurs @ Maximum force}
begin
Maximumforce := 0;
For maxforcecounter := Real_Start_Point TO Last_Row do
begin
IF mm_KiloNewton_Array[2,maxforcecounter] > Maximumforce THEN update;
end;
writeln ('Maximum_condition_array_position = ',Maximum_condition_array_position);
end;

Procedure Find_Real_Start_Point;
begin
Start_Condition_Integer := 0;
Start_Counter := 1;
While Start_Condition_Integer <> 10 do
begin
{Note: if we get 10 successive increases in mm, the machine must be moving
and the test have started.}
If (mm_KiloNewton_Array[1,Start_Counter] < mm_KiloNewton_Array[1,Start_Counter + 1])
then Start_Condition_Integer := Start_Condition_Integer + 1;
If (mm_KiloNewton_Array[1,Start_Counter] >= mm_KiloNewton_Array[1,Start_Counter + 1])
then Start_Condition_Integer := 0;
Start_Counter := Start_Counter + 1;
end;
Real_Start_Point := Start_Counter - 10; {ie the start is the first point where 10 consecutive increases
occur in mm}
writeln ('Real_Start_Point = ',Real_Start_Point);
end;

Procedure Adjust_Figures;
begin
{We know that when the test begins, there is in reality NO
load so, we subtract this value of load from the other load readings. Note
that we don't use the last reading because it is NOT zero because the sample
is stiff and bending is occurring, thus producing a negative load.}

Subtract_This_Value_KN := mm_KiloNewton_Array [2,Real_Start_Point];
writeln ('first value of force = ',Subtract_This_Value_KN);
For Adjust_Load := Real_Start_Point to Last_Row do
begin
mm_KiloNewton_Array [2,Adjust_Load] := mm_KiloNewton_Array [2,Adjust_Load] - Subtract_This_Value_KN;
end;
Subtract_This_Value_mm := mm_KiloNewton_Array [1,Real_Start_Point];
For Adjust_mm := Real_Start_Point to Last_Row do
begin
mm_KiloNewton_Array [1,Adjust_mm] := mm_KiloNewton_Array [1,Adjust_mm] - Subtract_This_Value_mm;
end;
{Now get rid of all zero loads, they are very small and not really there!}
Start_Counter := Real_Start_Point;
Rid_Zeros_Condition := False;
while Rid_Zeros_Condition = False do
begin
IF mm_KiloNewton_Array[2,Start_Counter] < 0 then mm_KiloNewton_Array[2,Start_Counter] := 0;
IF mm_KiloNewton_Array[1,Start_Counter] < 0 then mm_KiloNewton_Array[1,Start_Counter] := 0;
IF Start_Counter = Last_Row then Rid_Zeros_Condition := true;
Start_Counter := Start_Counter + 1;
end;

```

```

end;

Procedure Energy_Used_on_Cycle;
begin
{Calculate area from Real_Start_Point to Maximum_Condition_Array_Position}
{Using Simpsons rule}
Calculation := (Real_Start_Point + 1);
While Calculation <= (Maximum_Condition_Array_Position - 1) do
begin
Four_times := Four_times + (4 * mm_KiloNewton_Array [2, Calculation]);
Calculation := Calculation + 2;
end;
Calculation := (Real_Start_Point + 2);
While Calculation <= (Maximum_Condition_Array_Position - 2) do
begin
Two_times := Two_times + (2 * mm_KiloNewton_Array [2, Calculation]);
Calculation := Calculation + 2;
end;
{Find the distance, h, travelled between each reading by calculating the average}
h := ((mm_KiloNewton_Array [1,Maximum_Condition_Array_Position] - mm_KiloNewton_Array [1,Real_Start_Point])
/ (Maximum_Condition_Array_Position - Real_Start_Point));
Area_to_Max := (h/3) * (mm_KiloNewton_Array [2,Real_Start_Point] +
Four_times + Two_times +
mm_KiloNewton_Array [2,Maximum_Condition_Array_Position]);
{Note KN x mm = Joules}
end;

Procedure Output_Stress_Strain;
begin
Writeln ('What is the average thickness of the sample in mm?');
Readln (thickness);
thickness := thickness / 1000;
Writeln ('What was the initial length of the notch in mm?');
Readln (Notch_Length);
Sample_Volume := (thickness {in metre} * (80/1000) {gauge length in metre}
* (25/1000) {width in metre});
Energy_Density := (Area_to_Max / Sample_Volume); {Joules per cubic metre}
{Sort out name for output file, called the same name but .dat instead of .txt}
temp := post('.',The_File);
Output_File_Name := copy (The_File,1,temp);
insert ('DAT',Output_File_Name,(Temp+1));
writeln ('Output file name is ',Output_File_Name);
assign (textfile, Output_File_Name);
rewrite (textfile);
writeln (textfile, 'Strain%,MPa,mm,KN');
For File_Output := Real_Start_point to Maximum_Condition_Array_Position do
begin
Strain := (mm_KiloNewton_Array [1,File_Output] / 80{Gauge length}) * 100;
Stress := ((mm_KiloNewton_Array [2,File_Output] * 1000)
/ (thickness{metre} * 0.025{width of sample in metre}))
/ 1000000;{for MPa}
Extension := mm_KiloNewton_Array [1,File_Output];
Force := mm_KiloNewton_Array [2,File_Output];
writeln (textfile, Strain,',',Stress,',',Extension,',',Force);
end;
close (textfile);
end;

Procedure Print_Figures_On_Screen;
begin
Writeln;
Writeln ('The File Name = ',The_File);
Writeln ('Thickness (mm) = ',(thickness*1000));
Writeln ('Notch Length (mm) = Notch_Length);
Writeln ('Sample Area (square mm) = ',Sample_Volume);
writeln ('Energy Used (Joules) = ',Area_to_Max);
writeln ('Energy Density (Joules per cubic metre) = ',Energy_Density);

```

```

Writeln ('Force at Fracture (KN) = ',mm_KiloNewton_Array [2,Maximum_condition_array_position]);
Writeln ('Extension at Fracture (mm) = ',mm_KiloNewton_Array [1,Maximum_condition_array_position]);
Writeln ('Stress at Fracture (MPa) = ',((mm_KiloNewton_Array [2,Maximum_condition_array_position] * 1000) /
((thickness){metre} * 0.025{width of sample in metre}))/ 1000000{for MPa});
Writeln ('Strain at Fracture (%) = ',(mm_KiloNewton_Array [1,Maximum_condition_array_position] /
80{Gaugelength})*100);
end;

```

```

Procedure Put_Figures_On_Results_File;
begin
Assign (Resfile, 'c:\notchres.txt');
Append (Resfile);
Writeln (Resfile, The_File,chr(9),(Thickness*1000),chr(9),
notch_Length,chr(9),Sample_Volume,chr(9),
Area_to_Max,chr(9),Energy_Density,chr(9),
mm_KiloNewton_Array [2,Maximum_condition_array_position],chr(9),
mm_KiloNewton_Array [1,Maximum_condition_array_position],chr(9),
(mm_KiloNewton_Array [2,Maximum_condition_array_position] * 1000)
/ ((thickness {metre} * 0.025{width of sample in metre}))
/ 1000000{for MPa},chr(9),
(mm_KiloNewton_Array [1,Maximum_condition_array_position]
/ 80{Gauge length})*100);
close (Resfile);
end;

```

```

{Main}
Begin
clrscr;
Read_in_File;
Find_Real_Start_Point; {ie where the cross-head is moving}
Find_Maximum_Force;
Adjust_Figures;
Energy_Used_On_Cycle;
Output_Stress_Strain;
Print_Figures_On_Screen;
Put_Figures_On_Results_File;
Readln;
End.

```

### A.3.5 Program Video;

{This program processes visual images from the single notch specimen tests}

{The procedure ReadBMP reads a Microsoft windows bitmap (.BMP) file straight into EGA/VGA mapped memory (thereby bypassing the BGI driver interface) This achieves optimum performance at the expense of flexibility.}

```
uses
  Dos,Graph,Crt;
```

```
type
  StatusCode = (BMPOK, BMPOpenError, BMPHeaderReadErr, BMPInfoReadErr,
  BMPImageTooBig, BMPWrongVideo, BMPCompressed, BMPImageReadErr);
```

```
BMPFileheaderRec = record
  bfType : word; { 'BM' }
  bfSize : longint; { size of file in bytes }
  bfRes1 : word; { 0 }
  bfRes2 : word; { 0 }
  bfOffset : longint; { offset in file where bits begin }
end;
BMPInfoheaderRec = record
  biSize : longint; { size of the structure }
  biWidth : longint; { image width in pixels }
  biHeight : longint; { image height in pixels }
  biPlanes : word; { No of colour planes (=1) }
  biBitCnt : word; { colour bits per pixel }
  biCmprsn : longint; { Compression Scheme (=0) }
  biSizlmg : longint; { Number of bitmap bytes }
  biXMetre : longint; { Horizontal resolution pixels/meter }
  biYMetre : longint; { Vertical resolution pixels/meter }
  biClrUsd : longint; { Number of colours used }
  biClrImp : longint; { Important colours }
end;
```

```
var
  Indicator : boolean; { Indicator to detect when a black pixel occurs }
  StartX , StartY : integer; { Scanning X and Y co-ordinates }
  x1, x2, x3, x4 : integer; { x co-ordinates of 4 corners }
  y1, y2, y3, y4 : integer; { y co-ordinates of 4 corners }
  LeatherWidth : integer; { Width of leather }
  LeatherLength : integer; { Length of leather }
  Insidex1, Insidex2, Insidex3, Insidex4 : integer;
  Insidey1, Insidey2, Insidey3, Insidey4 : integer;
  MetIndicator , Endindicator : Boolean;
  MetDotsX , EndDotsX : Integer;
  MetDotsY , EndDotsY : Integer;
  ScanningPositionX, ScanningPositionY : Integer;
  XX, YY,
  Size : word;
  P : Pointer;
  ch : char;
  Terminate : boolean;

  DotX_Array : Array [1..15, 1..15] of integer; { Declare array
  for the position of the X centre of each dot - Assume the maximum
  number of dots is 15 in x direction and 15 in the y direction }

  DotY_Array : Array [1..15, 1..15] of integer; { Declare array
  for the position of the Y centre of each dot - Assume the maximum
  number of dots is 15 in x direction and 15 in the y direction }

  XDots_Counter , YDots_Counter : integer; {Counters for the array
  indicators}

  gd : integer;
  gm : integer;
```

```

GrDriver : integer; { Graphics Driver Id }
GrMode   : integer; { Graphics Mode }
BMPFile  : file;    { Bitmap file variable }
BMPHead  : BMPFileHeaderRec;
BMPInfo  : BMPInfoHeaderRec;
BMPBuff  : array [1..30720] of byte;
GrError  : integer;
BMPStatus: StatusCode;
TurKey   : char;
place    : string;
frame    : string;
Skip     : Boolean;

const
Palette : PaletteType = (size : MaxColors; colors :
(EGABLACK, EGARED, EGAGREEN, EGACYAN, EGABLUE, EGAMAGENTA, EGABROWN, EGADARKGRAY,
EGALIGHTGRAY, EGALIGHTRED, EGALIGHTGREEN, EGAYELLOW, EGALIGHTBLUE, EGALIGHTMAGENTA,
EGALIGHTCYAN, EGAWHITE));

function ReadBMP (Filename : Pathstr; var BMPFile : file) : StatusCode;
var
Nbytes : integer; { Count of actual bytes read }
Status : StatusCode; { Returned status code }
MaxX   : integer;
MaxY   : integer;
X,Y    : integer;
IByte  : integer;
BytesLeft : longint;

Procedure Check_color;
Begin
Skip := False;
if ((BMPBuff[IByte] shr 4) = 15) and ((BMPBuff[IByte] and $F) = 15) then skip := true;
end;

Procedure Put_On_Screen;
Begin
PutPixel (X,Y, BMPBuff[IByte] shr 4);
inc (X);
PutPixel (X,Y, BMPBuff[IByte] and $F);
inc (X);
end;

begin
{ open the file }
Status := BMPPOk;
MaxX := GetMaxX;
MaxY := GetMaxY;
assign (BMPFile, Filename);
reset (BMPFile, 1);
{ read the .BMP file header }
blockread (BMPFile, BMPHead, sizeof(BMPFileHeaderRec), NBytes);
if NBytes <> sizeof(BMPFileHeaderRec) then
Status := BMPHeaderReaderr
else
begin
{ read the bitmap information block and check EGA/VGA compatible }
blockread (BMPFile, BMPInfo, sizeof(BMPInfoHeaderRec), NBytes);
if NBytes <> sizeof(BMPInfoHeaderRec) then
Status := BMPInfoReadErr
else with BMPInfo do
begin
if (biWidth > MaxX + 1) or (biHeight > MaxY + 1) then
Status := BMPImageTooBig
else if biBitCnt <> 4 then
Status := BMPWrongVideo {We can only handle 16-colours }
else if BiCmprsn <> 0 then

```

```

Status := BMPCompressed {We can't handle compression either }
else
begin
seek (BMPFile, BMPHead.BfOffset);

{
Read in and display BMP which is stored arse upwards.
Note that the maximum size of an image is (640x480)/2
(= 153600) bytes allowing 4-bits per pixel.
}
X := 0;
Y := BiHeight-1;
BytesLeft := (BiWidth*BiHeight) div 2;
while (Status = BMPOk) and (BytesLeft <> 0) do
begin
if BytesLeft > 30720 then
begin
BlockRead (BMPFile, BMPBuff, 30720, Nbytes);
if NBytes <> 30720 then
Status := BMPImageReadErr;
end
else
begin
BlockRead (BMPFile, BMPBuff, BytesLeft, Nbytes);
if NBytes <> BytesLeft then
Status := BMPImageReadErr;
end;

for lbyte := 1 to Nbytes do
begin
Check_Color;
if Skip = true then X := X+2;
if Skip = False then Put_On_Screen;
if (X > BiWidth-1) then
begin
X := 0;
dec(Y);
end;
end;
Dec (BytesLeft, Nbytes);
end;
end;
ReadBMP := Status;
end;
end;

procedure ScanningX1y1toX2Y2;
Begin
StartX := 0;
While (StartX <> 639) and (Indicator = False) do
begin
if GetPixel (StartX, StartY) = black then Indicator := True;
PutPixel (StartX, StartY, EGAgreen);
StartX := StartX + 1;
end;
StartX := StartX-1;
end;

procedure ScanningX2Y2toX1Y1;
Begin
StartX := 639;
While (StartX >= 0) and (Indicator = False) do
begin
if GetPixel (StartX, StartY) = black then Indicator := True;
PutPixel (StartX, StartY, EGABlue);

```

```

    StartX := StartX - 1;
  end;
  StartX := StartX + 1;
end;

procedure ScanningX3Y3toX4Y4;
Begin
  StartX := 0;
  While (StartX <> 639) and (Indicator = False) do
  begin
    if GetPixel (StartX, StartY) = black then Indicator := True;
    PutPixel (StartX, StartY, EGAgreen);
    StartX := StartX + 1;
  end;
  StartX := StartX - 1;
end;

procedure ScanningX4Y4toX3Y3;
Begin
  StartX := 639;
  While (StartX >= 0) and (Indicator = False) do
  begin
    if GetPixel (StartX, StartY) = black then Indicator := True;
    PutPixel (StartX, StartY, EGAbblue);
    StartX := StartX - 1;
  end;
  StartX := StartX + 1;
end;

procedure FindBlackPositionX1Y1;
Begin
  { - Find the left corner of the leather
  - Start at pixel (0,0) : scan all x positions at increasing
  values of y
  - The first pixel you come across should be the line x1y1 to x2y2 }
  Indicator := false; {ie set initial indicator to false}
  StartX := 0; {ie set initial x pixel = 0}
  StartY := 0; {ie set initial y pixel = 0}
  ScanningX1Y1toX2Y2;
  while (Indicator = False) and (StartY < 479) do
  Begin
    StartY := StartY + 1;
    ScanningX1Y1toX2Y2;
  end;
  x1 := StartX;
  y1 := StartY;
end;

procedure FindBlackPositionX2Y2;
Begin
  { - Find the top right corner of the leather
  - Start at pixel (639,0) : scan all x positions at increasing
  values of y
  - The first pixel you come across should be the line x2y2 to x1y1 }
  Indicator := false; {ie set initial indicator to false}
  StartX := 639; {ie set initial x pixel = 639}
  StartY := 0; {ie set initial y pixel = 0}
  ScanningX2Y2toX1Y1;
  while (Indicator = False) and (StartY < 479) do
  Begin
    StartY := StartY + 1;
    ScanningX2Y2toX1Y1;
  end;
  x2 := StartX;
  y2 := StartY;
end;

```

```

procedure FindBlackPositionX3Y3;
Begin
{ - Find the bottom left corner of the leather
- Start at pixel (0,479) : scan all x positions at decreasing
values of y
- The first pixel you come across should be the line x3y3 to x4y4 }
Indicator := false; {ie set initial indicator to false}
StartX := 0; {ie set initial x pixel = 0}
StartY := 479; {ie set initial y pixel = 479}
ScanningX3Y3toX4Y4;
while (Indicator = False) and (StartY < > 0) do

Begin
StartY := StartY - 1;
ScanningX3Y3toX4Y4;
end;
x3 := StartX;
y3 := StartY;
end;

```

```

procedure FindBlackPositionX4Y4;
Begin
{ - Find the left corner of the leather
- Start at pixel (639,479) : scan all x positions at decreasing
values of y
- The first pixel you come across should be the line x4y4 to x3y3 }
Indicator := false; {ie set initial indicator to false}
StartX := 639; {ie set initial x pixel = 639}
StartY := 479; {ie set initial y pixel = 479}
ScanningX4Y4toX3Y3;
while (Indicator = False) and (StartY > 0) do
Begin
StartY := StartY - 1;
ScanningX4Y4toX3Y3;
end;
x4 := StartX;
y4 := StartY;
end;

```

Procedure ShowFourCornerCoordinates;

{HERE'S THE SECTION TO WRITE NUMBERS TO THE FILE}

```

var
i : integer; {pseudo x coordinate for array}
j : integer; {pseudo y coordinate for array}
max_i : integer;
max_j : integer;
txtfile : text;
iloop , jloop : integer;

begin
assign (txtfile, place);
rewrite (txtfile);
For iloop := 1 to 12 do
begin
For jloop := 1 to 12 do
begin
writeln (txtfile, DotX_Array[iloop,jloop], ', ',
DotY_Array[iloop,jloop]);
end;
end;
close (txtfile);
end;

```

Procedure WorkOut\_Centre\_and\_Store;  
var

```

CentreX , CentreY : Integer;
Begin
SetColor (Black);
Rectangle (MetDotsX, MetDotsY, EndDotsX, EndDotsY);
CentreX := Trunc(((EndDotsX - MetDotsX)/2) + MetDotsX);
CentreY := Trunc(((EndDotsY - MetDotsY)/2) + MetDotsY);
DotX_Array [XDots_Counter , YDots_Counter] := CentreX;
DotY_Array [XDots_Counter , YDots_Counter] := CentreY;
SetColor (white);
Bar (MetDotsX, MetDotsY, EndDotsX, EndDotsY);
PutPixel (CentreX, CentreY, Black);
end;

```

```

Procedure CollectImage;
Begin
{ Here's where we find the dots and the centre of the dots and put them
in the OnOf_Simple array }
Insidex1 := XX + 1;
Insidex2 := XX + 14;
Insidex3 := XX + 1;
Insidex4 := XX + 14;
Insidex1 := YY + 1;
Insidex2 := YY + 1;
Insidex3 := YY + 14;
Insidex4 := YY + 14;
ScanningPositionX := Insidex1;
ScanningPositionY := Insidex1;
ScanIn_Y_Direction_Meet;
ScanIn_Y_Direction_End;
ScanIn_X_Direction_Meet;
ScanIn_X_Direction_End;
WorkOut_Centre_and_Store;
YDots_Counter := YDots_Counter + 1;
if YDots_Counter > 12 then
begin
YDots_Counter := 1;
XDots_Counter := XDots_Counter + 1;
end;
PutImage(XX, YY, P^, XOrPut); {off}
end;

```

```

Procedure Check_Key;
begin
ch := readkey;
if ord(ch) = 75 then XX := XX-1;
if ord(ch) = 77 then XX := XX+1;
if ord(ch) = 72 then YY := YY-1;
if ord(ch) = 80 then YY := YY+1;
if ord(ch) = 27 then Terminate := true;
if ord(ch) = 13 then CollectImage;
end;

```

```

{Main Program}
begin
writeln ('The file with the frame in is ? ');
readln (frame);
writeln ('The output filename is ?');
readln (place);
GrDriver := DETECT;
InitGraph (GrDriver, GrMode, 'C:\bp\bgi');
SetAllPalette (Palette);
Rectangle (0,0, 15, 15);
Size := ImageSize (XX, YY, (XX + 15), (YY + 15));

```

```
GetMem (P, Size);
GetImage (XX, YY, (XX + 15), (YY + 15), P^);
ClearViewPort;
Bar (0,0,639,479);
BMPStatus := ReadBMP (frame , BMPfile);
FindBlackPositionX1Y1;
FindBlackPositionX2Y2;
FindBlackPositionX3Y3;
FindBlackPositionX4Y4;
XDots_Counter := 1;
YDots_Counter := 1;
XX := x1;
YY := y1;
Repeat
PutImage (XX, YY, P^, XOrPut); {on}
Check_Key;
PutImage(XX,YY,P^, XOrPut); {off}
PutImage(XX,YY,P^, XOrPut); {on}
until Terminate = true;
{turkey := Readkey;}
CloseGraph;
ShowFourCornerCoordinates;
end.
```

### A.3.6. a Program Produce\_The\_Strain\_Matrix;

{This Program Produces the Strain Matrix when examining the strain distribution in a whole single notch specimen.}

Uses Crt, Dos;

```
var
Column_Counter : integer;
Row_Counter : integer;
txtfile : text;
A_Line : string ;
numberstring : string;
number : integer;
temp : integer;
code : integer;
Matrix_Array_Frame0 : array [1..10, 1..30] of integer;
Matrix_Array_temp : array [1..10, 1..30] of integer;
NowFile : string;
Frame_Zero : string;
PresentFrame : string;
Max_R , Max_C : integer;
Strain_Output_File : string;
Rowing , Columning : integer;
Calculation : real;
FileListings : String;
Textfile : text;
cnt : integer;
FrameNames : array [1..30] of string;
Datafiles : array [1..30] of string;
Main_Loop : integer;
Total_Files : integer;

Procedure Read_Frame_Zero;
begin
Column_Counter := 1;
Row_Counter := 1;
assign (txtfile, FrameNames [1]);
reset (txtfile);
while not Eof(txtfile) do
begin
{Read every thing as a string}
readln (txtfile, A_Line);
{Now find the X & Y values and put into an array}
while Length (A_Line) > 1 do
begin
temp := Pos (',',A_Line);
numberstring := copy (A_Line,1,temp-1);
val (numberstring, Matrix_Array_Frame0 [Column_Counter, Row_Counter]
, code);
write (' ',Matrix_Array_Frame0 [Column_Counter, Row_Counter]);
delete (A_Line,1,temp);
Column_Counter := Column_Counter + 1;
if Column_Counter > Max_C then Max_C := Column_Counter;
end;
writeln;
Column_Counter := 1;
Row_Counter := Row_Counter + 1;
if Row_Counter > Max_R then Max_R := Row_Counter;
end;
close (txtfile);
end;

Procedure Read_Particular_Frame;
begin
Column_Counter := 1;
```

```

Row_Counter := 1;
assign (txtfile, FrameNames [Main_Loop]);
reset (txtfile);
while not Eof(txtfile) do
begin
  {Read every thing as a string}
  readln (txtfile, A_Line);
  {Now find the X & Y values and put into an array}
  while Length (A_Line) > 1 do
  begin
    temp:= Pos (',',A_Line);
    numberstring := copy (A_Line,1,temp-1);
    val (numberstring, Matrix_Array_Temp [Column_Counter, Row_Counter]
      , code);
    write (',Matrix_Array_Temp [Column_Counter, Row_Counter]);
    delete (A_Line,1,temp);
    Column_Counter := Column_Counter + 1;

  end;
  Column_Counter := 1;
  writeln;
  Row_Counter:= Row_Counter + 1;

end;
close (txtfile);
end;

```

```

Procedure Work_Out_Strains;
begin
assign (txtfile, Strain_Output_File);
rewrite (txtfile);
writeln (txtfile,'0,1,2,3,4,');
For Rowing := 2 to (Max_R-1) do
begin
write (txtfile, (Rowing-1),',');
For Columning := 2 to (Max_C-1) do
begin
if ((Matrix_Array_Frame0 [Columning,Rowing] > 0 ) and
(Matrix_Array_Frame0 [Columning,(Rowing+1)] > 0) and
(Matrix_Array_Temp [Columning,Rowing] > 0 ) and
(Matrix_Array_Temp [Columning,(Rowing+1)] > 0)) then

calculation:= (((Matrix_Array_Temp [Columning,Rowing] -
Matrix_Array_Temp [Columning,(Rowing+1)]) -
(Matrix_Array_Frame0 [Columning,Rowing] -
Matrix_Array_Frame0 [Columning,(Rowing+1)]) ) /
(Matrix_Array_Frame0 [Columning,Rowing] -
Matrix_Array_Frame0 [Columning,(Rowing+1)]));

if ((Matrix_Array_Frame0 [Columning,Rowing] = 0 ) or
(Matrix_Array_Frame0 [Columning,(Rowing+1)] = 0) or
(Matrix_Array_Temp [Columning,Rowing] = 0 ) or
(Matrix_Array_Temp [Columning,(Rowing+1)] = 0)) then

calculation:=0;
write (txtfile, calculation,',');
end;
writeln (txtfile);
end;
close (txtfile);
end;

```

```

{Main}
Begin

```

```

Max_C := 1;
Max_R := 1;

WriteLn ('Name of the file containing frame names and data output file names?');
readln (FileListings);
assign (textfile, FileListings);
reset (textfile);
cnt := 1;
while not Eof(textfile) do
begin
  {Read every thing as a string}
  readln (textfile, A_Line);
  {Now find the FrameNames & DataFiles and put into an array}
  temp := Pos (';', A_Line);
  FrameNames [cnt] := copy (A_Line, 2, temp-3);
  DataFiles [cnt] := copy (A_Line, temp+2, ((Length(A_Line)-temp)-2));
  writeln (FrameNames [cnt], DataFiles [cnt]);
  cnt := cnt + 1;

end;
Total_Files := cnt-1;
close (textfile);

Read_Frame_Zero;
For Main_Loop := 2 to Total_Files do
begin
  Read_Particular_Frame;
  writeln ('Columns = ', (Max_C-1), ' Rows = ', (Max_R-1));
  Strain_Output_File := (DataFiles [Main_Loop]);
  Work_Out_Strains;
end;

end.

```

### A.3.6. b Program Produce\_The\_Strain\_Matrix;

{This Program Produces the Strain Matrix when examining the strain distribution around a notch.}

```
uses Crt, Dos;

var
Column_Counter : integer;
Row_Counter : integer;
txtfile1 , txtfile2 , txtfile3 : text;
txtfile : text;
A_Line : string ;
numberstring : string;
number : integer;
temp : integer;
code : integer;
cnt : integer;
X_Matrix_Array_Frame0 : array [1..15, 1..15] of integer;
Y_Matrix_Array_Frame0 : array [1..15, 1..15] of integer;
Y_Matrix_Array_temp : array [1..15, 1..15] of integer;
X_Matrix_Array_temp : array [1..15, 1..15] of integer;
FrameNames, DataFiles : array [1..30] of string;
NowFile : string;
Frame_Zero : string;
Present_Frame : string;
Max_R , Max_C : integer;
Strain_Output_File : string;
X , Y : integer;
Calculation : real;
FileListings : String;
Total_Files , Main_Loop : integer;

Procedure Read_Frame_Zero;
begin
assign (txtfile1, Frame_Zero);
reset (txtfile1);
  For Column_Counter := 1 to 12 do
  begin
  For Row_Counter := 1 to 12 do
  begin
  readln (txtfile1, A_Line);
  temp:= Pos (',',A_Line);
  numberstring := copy (A_Line,1,temp-1);
  val (numberstring, X_Matrix_Array_Frame0 [Column_Counter, Row_Counter]
  , code);
  delete (A_Line,1,temp);
  numberstring := copy (A_Line,1,3);
  val (numberstring, Y_Matrix_Array_Frame0 [Column_Counter, Row_Counter]
  , code);
  A_Line := (' ');

  writeln ((' ',Column_Counter,',',Row_Counter,') = (',
  X_Matrix_Array_Frame0 [Column_Counter, Row_Counter],',',
  Y_Matrix_Array_Frame0 [Column_Counter, Row_Counter],')');
  {readln;}
  writeln('hello');
  end;
  end;
close (txtfile1);
end;

Procedure Read_Particular_Frame;
begin
```

```

assign (txtfile2, Present_Frame);
reset (txtfile2);
For Column_Counter := 1 to 12 do
begin
For Row_Counter := 1 to 12 do
begin
readln (txtfile2, A_Line);
temp:= Pos (',',A_Line);
numberstring := copy (A_Line,1,temp-1);
val (numberstring, X_Matrix_Array_temp [Column_Counter, Row_Counter]
, code);
delete (A_Line,1,temp);
numberstring := copy (A_Line,1,3);
val (numberstring, Y_Matrix_Array_temp [Column_Counter, Row_Counter]
, code);
A_Line := ("");
writeln ('',Column_Counter,',',Row_Counter,') = ('',
X_Matrix_Array_temp [Column_Counter, Row_Counter],',',
Y_Matrix_Array_temp [Column_Counter, Row_Counter],');
{readln;}
end;
end;
close (txtfile2);
end;

```

```

Procedure Work_Out_Strains;
begin
Writeln ('Opening for output',Strain_Output_File);
assign (txtfile3, Strain_Output_File);
rewrite (txtfile3);
writeln (txtfile3,'0,1,2,3,4,5,6,7,8,9,10,11,12');
For Y := 1 to 11 do {12 rows of dots so only 11 strains}
begin
write (txtfile3, Y,',');
For X := 1 to 12 do
begin
calculation:= (((Sqrt ((sqr(Y_Matrix_Array_Temp [X,Y] -
Y_Matrix_Array_Temp [X,(Y+1)])) +
(sqr(X_Matrix_Array_Temp [X,Y] -
X_Matrix_Array_Temp [X,(Y+1)]))))
- (Sqrt((sqr(Y_Matrix_Array_Frame0 [X,Y] -
Y_Matrix_Array_Frame0 [X,(Y+1)])) +
(sqr(X_Matrix_Array_Frame0 [X,Y] -
X_Matrix_Array_Frame0 [X,(Y+1)]))))
/ (Sqrt((sqr(Y_Matrix_Array_Frame0 [X,Y] -
Y_Matrix_Array_Frame0 [X,(Y+1)])) +
(sqr(X_Matrix_Array_Frame0 [X,Y] -
X_Matrix_Array_Frame0 [X,(Y+1)]))))
* 100 );
write (txtfile3, calculation,',');
writeln ('',X,',',Y,') = ',calculation);
{readln;}
end;
writeln (txtfile3);
end;
close (txtfile3);
writeln ('Have closed ', Strain_Output_File);
end;

```

```

{Main New}
begin

Writeln ('Name of the file containing frame names and data output file names ?');
readln (FileListings);
assign (textfile, FileListings);
reset (textfile);
cnt := 1;
while not Eof(textfile) do
begin
  {Read every thing as a string}
  readln (textfile, A_Line);
  {Now find the FrameNames & DataFiles and put into an array}
  temp:= Pos (',',A_Line);
  FrameNames [cnt] := copy (A_Line,2,temp-3);
  DataFiles [cnt] := copy (A_Line,temp+2,(Length(A_Line)-temp-2));
  writeln (FrameNames [cnt],DataFiles [cnt]);
  cnt:= cnt + 1;
end;
Total_Files := cnt-1;
close (textfile);

Frame_Zero := FrameNames [1];
Read_Frame_Zero;
For Main_Loop := 2 to (Total_Files) {-1 because already done frame zero} do
begin
  Present_Frame := FrameNames [Main_Loop];
  Read_Particular_Frame;
  Strain_Output_File := (DataFiles [Main_Loop]);
  Work_Out_Strains;
end;
end.

```

### A.3.7 Program Ellipse;

{This program enables the user to model the elliptical crack.}

Uses Crt, Graph;

```
Var
textfile : text;
Data, A_Line, Quick : String;
cnt : integer;
temp : integer;
X, Y_one, Y_two : Array [1..1000] of integer;
Total_Lines_Data : integer;
Code, l : integer;
a, initial_b, b, Y_Centre : integer;
ErrorCode, GraphMode, GraphDriver : integer;
drawer : integer;
X_Centre : integer;
Best_fit_b : integer;
ch : char;
terminate : boolean;
```

Procedure Check\_Key;

begin

ch := readkey;

{This bit alters the size of the ellipse}

if ord (ch) = 75 then a := a - 1;

if ord (ch) = 77 then a := a + 1;

if ord (ch) = 72 then Best\_Fit\_b := Best\_Fit\_b + 1;

if ord (ch) = 80 then Best\_Fit\_b := Best\_Fit\_b - 1;

{This bit alters the centre of the Y coordinates of the ellipse}

if ord (ch) = 45 then Y\_Centre := Y\_Centre + 1;

if ord (ch) = 43 then Y\_Centre := Y\_Centre - 1;

{This bit checks to see if you have completed by pressing escape}

if ord (ch) = 27 then terminate := true;

end;

Procedure Draw\_Notch;

Begin

For Drawer := 1 to Total\_Lines\_Data do

begin

PutPixel (X[Drawer], Y\_one[Drawer], Black);

PutPixel (X[Drawer], Y\_two[Drawer], Black);

end;

end;

Begin

{Here we read the the X, Y pixel data that constitutes the crack profile (done in a previous program)}.

Writeln ('Name of the file containing the X, Y1, Y2 Data?');

readln (Data);

assign (textfile, Data);

reset (textfile);

cnt := 1;

while not Eof(textfile) do

begin

{Read every thing as a string}

readln (textfile, A\_Line);

writeln (A\_Line);

```

{Now find the FrameNames & DataFiles and put into an array}
temp:= Pos (',',A_Line);
Quick := copy (A_Line,1,temp-1);
val (Quick, X [cnt], Code);
if code <> 0 then halt;
delete (A_Line,1,temp);
temp:= Pos (',',A_Line);
Quick := (copy (A_Line,1,temp-1));
val (Quick, Y_one [cnt], code);
if code <> 0 then halt;
Quick := (copy (A_Line,temp+1,((Length(A_Line)-temp))));
val (Quick, Y_two [cnt], code);
if code <> 0 then halt;
{writeln ('x = ',X [cnt], ' y1 = ',Y_one [cnt], ' y2 = ',Y_two [cnt]);}
cnt:= cnt + 1;
end;

Total_Lines_Data := cnt-1;
{writeln (Total_Lines_Data);}

{Here we find the coordinates of the centre and extremes of major/minor
axis of the ellipse}
a := X [Total_Lines_Data] - X [1];
Initial_b := trunc ((Y_two [1] - Y_one [1])/2);
Y_Centre := (Trunc ((Y_two [Total_Lines_Data] - Y_one [Total_Lines_Data])/2))+Y_one [Total_Lines_data];
X_Centre := X [1];

{Here we initialise the graphics interface and draw the ellipse that
approximately fits the notch}
GraphDriver := Detect;
InitGraph (GraphDriver, GraphMode, 'C:\bp\lbg1');
SetColor (EGAWhite);
Bar (0,0,639,479);
Setcolor (EGARed);
FillEllipse (X[1],Y_Centre,a,Best_Fit_b);
Setcolor (EGABlue);
Draw_Notch;

{Here we enable the user to alter the size of the major and minor axis of
the ellipse to enable the best visual fit}
Repeat
Check_Key;
SetColor (EGAWhite);
Bar (0,0,639,479);
Draw_Notch;
Setcolor (EGALightGray);
FillEllipse (X[1],Y_Centre,a,Best_Fit_b);
until terminate = true;

Closegraph;
Writeln ('***** Chosen value of a = ',a,' pixels *****');
Writeln;
Writeln ('***** Chosen value of b = ',Best_Fit_b,' pixels *****');
readln;
end.

```

### A.3.8 Program Trouser\_Tear\_Test;

{This program processes data from the trouser tear tests}

uses Crt, Dos;

{Definition of variable types}

```
var
The_File : string;
A_Line : string;
txtfile : text; {input file}
textfile : text; {output file}
Resfile : text; {results file}
counter : integer;
mm_KiloNewton_Array : array [1..2, 1..4000] of real;
l : integer;
mm : string;
KiloNewton : string;
temp : integer;
code : integer;
Last_Row : integer;
Maximumforce , Maximum_mm : real;
Maxforcecounter : integer;
Maximum_condition_array_position : integer;
Start_Condition_Integer : integer;
Start_Counter : integer;
Real_Start_Point : integer;
Subtract_This_Value_KN , Subtract_This_Value_mm : real;
Adjust_Load , Adjust_mm : integer;
End_Force_Finder_Condition : boolean;
End_Force_Finder : integer;
Last_Reading_Of_Test : integer;
End_Condition_Integer : integer;
End_Counter : integer;
Calculation : integer;
h : real;
Area_to_Max : real;
Area_to_Relax : real;
File_Output : integer;
Output_File_Name : string;
Rid_Zeros_Condition : Boolean;
Extension : Real;
Force : Real;
Four_times , Two_times : Real;
Point_B_Value : real;
j , Point_A , Point_B , Point_C , forcecount , subcount: integer;
Min_To_Max , Dist_A_to_C : array [1..3] of real;
Begina : array [1..3] of integer;
Answer : boolean;
Thickness : real;
Length_Of_Tear : real;
Length_Of_Tear_Graph : real;
Two_F_Upon_t_Calculation_Step : integer;
Total_Force , Plateau_Force : real;
Two_F_Upon_t : real;
Energy_Used , Area_Cleaved_Graph , Area_Cleaved_Sample : real;
Toughness_Area_Cleaved_Graph , Toughness_Area_Cleaved_Sample : real;
Strain_Energy_Density_In_Legs , Unstressed_Cross_Sectional_Area_Legs , Lambda : real;
Tch : real;

Procedure Read_in_File;
begin
counter:= 1;
Writeln ('What is the name of the file (Column 1 = mm , Column2 = KN)');
Readln (The_File);
assign (txtfile, The_File);
reset (txtfile);
```

```

while not Eof(txtfile) do
begin
  {Read every thing as a string}
  readln (txtfile, A_Line);
  temp := pos (chr(9),A_Line); {the spacer in this type of text file}
  {Now find the X & Y values and put into an array}
  mm := copy (A_Line,1,temp-1);
  KiloNewton := copy (A_Line,temp+1,25);
  Val (mm, mm_KiloNewton_Array[1,counter], code);
  Val (KiloNewton, mm_KiloNewton_Array[2,counter], code);
  counter:= counter + 1;
end;
close (txtfile);
Last_Row := (counter-1);
end;

Procedure update;
begin
Maximum_mm := mm_KiloNewton_Array [1,maxforcecounter];
Maximum_condition_array_position := maxforcecounter;
end;

Procedure Find_Maximum_mm;
begin
Maximumforce := 0;
For maxforcecounter := Real_Start_Point TO Last_Row do
begin
IF mm_KiloNewton_Array[1,maxforcecounter] > Maximum_mm THEN update;
end;
Maximumforce := mm_KiloNewton_Array [2,maxforcecounter];
end;

Procedure Find_Real_Start_Point;
begin
Start_Condition_Integer := 0;
Start_Counter := 1;
While Start_Condition_Integer <> 10 do
begin
{Note: if we get 10 successive increases in mm, the machine must be moving
and the test have started.}
If (mm_KiloNewton_Array[1,Start_Counter] < mm_KiloNewton_Array[1,Start_Counter+1])
then Start_Condition_Integer := Start_Condition_Integer + 1;
If (mm_KiloNewton_Array[1,Start_Counter] >= mm_KiloNewton_Array[1,Start_Counter+1])
then Start_Condition_Integer := 0;
Start_Counter := Start_Counter + 1;
end;
Real_Start_Point := Start_Counter - 10; {ie the start is the first point
where 10 consecutive increases
occur in mm}
Real_Start_Point := Real_Start_Point + 3 {the first 3 points are very small
and the mm / KN values are wacky
so we add 3 and start there instead}

end;

Procedure Adjust_Figures;
begin
{We know that when the test begins, there is in reality NO
load so, we subtract this value of load from the other load readings. Note
that we don't use the last reading because it is NOT zero because the sample
is stiff and bending is occurring, thus producing a negative load.}

Subtract_This_Value_KN := mm_KiloNewton_Array [2,Real_Start_Point];
writeln ('first value of force = ',Subtract_This_Value_KN);
readln;
For Adjust_Load := Real_Start_Point to Last_Row do
begin

```

```

mm_KiloNewton_Array [2,Adjust_Load] := mm_KiloNewton_Array [2,Adjust_Load] - Subtract_This_Value_KN;
end;
Subtract_This_Value_mm := mm_KiloNewton_Array [1,Real_Start_Point];
writeln ('first value of mm = ',Subtract_This_Value_mm);
readln;
For Adjust_mm := Real_Start_Point to Last_Row do
begin
mm_KiloNewton_Array [1,Adjust_mm] := mm_KiloNewton_Array [1,Adjust_mm] - Subtract_This_Value_mm;
end;

{Now get rid of all zero loads, they are very small and not really there!}
Start_Counter := Real_Start_Point;
Rid_Zeros_Condition := False;
while Rid_Zeros_Condition = False do
begin
IF mm_KiloNewton_Array[2,Start_Counter] < 0 then mm_KiloNewton_Array[2,Start_Counter] := 0;
IF mm_KiloNewton_Array[1,Start_Counter] < 0 then mm_KiloNewton_Array[1,Start_Counter] := 0;
IF Start_Counter = Last_Row then Rid_Zeros_Condition := true;
Start_Counter := Start_Counter + 1;
end;
end;

Procedure Find_Real_End_Point;
begin
End_Force_Finder_Condition := false;
End_Force_Finder := Maximum_Condition_Array_Position;
While End_Force_Finder_Condition = false do
begin
if (mm_KiloNewton_Array [1,End_Force_Finder]) <= 0.01
then End_Force_Finder_Condition := true;
End_Force_Finder := End_Force_Finder + 1;
end;
Last_Reading_Of_Test := (End_Force_Finder-1);
end;

Procedure Go_Backwards_to_Find_Where_Load_Is_Effectively_Zero;
begin
End_Condition_Integer := 0;
End_Counter := Maximum_Condition_Array_Position + 50; {to avoid inertia}
writeln (End_Counter);
readln;
While End_Condition_Integer <> 2 do
begin
If (mm_KiloNewton_Array[2,End_Counter] >= mm_KiloNewton_Array[2,(End_Counter-1)])
then End_Condition_Integer := 0;

If (mm_KiloNewton_Array[2,End_Counter] < mm_KiloNewton_Array[2,(End_Counter-1)])
then End_Condition_Integer := End_Condition_Integer + 1;

{writeln (mm_KiloNewton_Array[2,(End_Counter)],' < ',mm_KiloNewton_Array[2,(End_Counter+1)]);
readln;}

If (mm_KiloNewton_Array[2,(End_Counter)]) <= 0 then
End_Condition_Integer := End_Condition_Integer + 1;}

writeln ('End_Condition_Integer = ',End_Condition_Integer,'End_Counter = ',End_Counter);
{readln;}
End_Counter := End_Counter - 1;
end;
Last_Reading_Of_Test := End_Counter + 2;
end;

Procedure Collect_Update;
begin
Point_B_Value := mm_KiloNewton_Array [2, j];
Point_B := j;
end;

```

```

Procedure Collect;
begin
While (forcecount < 3) do
begin
While (mm_KiloNewton_Array [2, subcount] < mm_KiloNewton_Array [2, (subcount + 1)]) AND
(subcount < (Maximum_Condition_Array_Position - 1)) do
begin
subcount := subcount + 1;
{writeln ('finding point a, subcount = ',subcount);}
end;

Point_A := subcount;
subcount := subcount + 1;

While (mm_KiloNewton_Array [2, subcount] < mm_KiloNewton_Array [2, Point_A])
AND (subcount < (Maximum_Condition_Array_Position - 1)) do
begin
subcount := subcount + 1;
end;

Point_C := subcount;

{find Point B ie the minimum}

Point_B := Point_A;
Point_B_Value := mm_KiloNewton_Array [2, Point_A];

For j := (Point_A + 1) TO Point_C do
begin
if (mm_KiloNewton_Array [2, j]) < Point_B_Value then Collect_Update;
end;

{calculate mintomax, disatoc}

Min_To_Max [forcecount] := (mm_KiloNewton_Array [2, Point_A] - mm_KiloNewton_Array [2, Point_B]);
Dist_A_to_C [forcecount] := (mm_KiloNewton_Array [1, Point_C] - mm_KiloNewton_Array [1, Point_A]);
Begina [forcecount] := Point_A;

{Add 1 to counter forcecount}
forcecount := forcecount + 1;

end;
end;

Procedure Part_One_Update;
begin
forcecount := forcecount - 1;
Min_to_Max [1] := Min_to_Max [2];
Min_to_Max [2] := 0;
end;

Procedure Part_Two_Update;
begin
forcecount := forcecount - 1;
Dist_A_to_C [1] := Dist_A_to_C [2];
Dist_A_to_C [2] := 0;
end;

Procedure Cant_Be_It;
begin
Answer := False;
Part_Two_Update;
end;

Procedure Find_Where_Tearing_Occurs;
begin

```

```

Answer := False;
while Answer = False do
begin
Collect;
{Note we don't use Min_to_Max here because there is too much fluctuation
in KN readings and so there is an enormous difference in the size of
the glitches upto point_A, so we simply use Dist_A_to_C instead which
seems to work OK.}
IF (ABS(Dist_A_to_C[1] - Dist_A_to_C[2])) > ((Dist_A_to_C[1] + Dist_A_to_C[2]) / 2) Then Answer := True;
IF (ABS(Dist_A_to_C[1] - Dist_A_to_C[2])) < ((Dist_A_to_C[1] + Dist_A_to_C[2]) / 2) Then Part_Two_Update;
IF Dist_A_to_C[2] < 0.5 then Cant_Be_It;
IF subcount >= Maximum_Condition_Array_Position then Answer := true;
end;
{Tearing begins at Point A of the largest mintomax peak}
If Dist_A_to_C[1] > Dist_A_to_C[2] then Point_A := Begina [1];
If Dist_A_to_C[2] > Dist_A_to_C[1] then Point_A := Begina [2];
end;

Procedure Calculate_Toughness_By_Two_F_Upon_t;
begin;
Writeln ('What is the average thickness of the sample in mm ??');
Readln (Thickness);
Writeln ('What is the length of the tear in the sample in mm ??');
Readln (Length_Of_Tear);
For Two_F_Upon_t_Calculation_Step := Point_A to Maximum_Condition_Array_Position do
begin
Total_Force := Total_Force + mm_KiloNewton_Array [2,Two_F_Upon_t_Calculation_Step];
end;
Plateau_Force := (Total_Force / (Maximum_Condition_Array_Position - Point_A)) * 1000; { * 1000 to convert to N}
Two_F_Upon_t := (2 * Plateau_Force) / (Thickness / 1000);
end;

Procedure Calculate_Toughness_By_Energy_Method;
begin
{Calculate area from Real_Start_Point to Maximum_Condition_Array_Position}
{Using Simpsons rule}
Calculation := (Real_Start_Point + 1);
While Calculation <= (Maximum_Condition_Array_Position - 1) do
begin
Four_times := Four_times + (4 * mm_KiloNewton_Array [2, Calculation]);
Calculation := Calculation + 2;
end;
Calculation := (Real_Start_Point + 2);
While Calculation <= (Maximum_Condition_Array_Position - 2) do
begin
Two_times := Two_times + (2 * mm_KiloNewton_Array [2, Calculation]);
Calculation := Calculation + 2;
end;

{Find the distance, h, travelled between each reading by calculating the average}
h := ((mm_KiloNewton_Array [1,Maximum_Condition_Array_Position] - mm_KiloNewton_Array [1,Real_Start_Point])
/ (Maximum_Condition_Array_Position - Real_Start_Point));
Area_to_Max := (h/3) * (mm_KiloNewton_Array [2,Real_Start_Point] +
Four_times + Two_times +
mm_KiloNewton_Array [2,Maximum_Condition_Array_Position]);
{Calculate area from Maximum_Condition_Array_Position to Last_Reading_Of_Test}
{Reset Four-times & Two-times to Zero}
Four_times := 0;
Two_times := 0;
Calculation := Maximum_Condition_Array_Position + 1;
While Calculation <= (Last_Reading_Of_Test - 1) do
begin
Four_times := Four_times + (4 * mm_KiloNewton_Array [2, Calculation]);
Calculation := Calculation + 2;
end;
Calculation := Maximum_Condition_Array_Position + 2;
While Calculation <= (Last_Reading_Of_Test - 2) do

```

```

begin
Two_times := Two_times + (2 * mm_KiloNewton_Array [2, Calculation]);
Calculation := Calculation + 2;
end;
Area_to_Relax := (h/3) * (mm_KiloNewton_Array [2,Maximum_Condition_Array_Position] +
Two_times + Four_times +
mm_KiloNewton_Array [2,Last_Reading_Of_Test]);
{Note KN x mm = Joules}
Energy_Used := Area_to_Max - Area_to_Relax;
Length_Of_Tear_Graph := (((mm_KiloNewton_Array [1, Maximum_Condition_Array_Position]
- mm_KiloNewton_Array [1, Point_A])/2)); {mm}
Area_Cleaved_Graph := (((mm_KiloNewton_Array [1, Maximum_Condition_Array_Position]
- mm_KiloNewton_Array [1, Point_A])/2)/1000) * (Thickness/1000);

Area_Cleaved_Sample := (Length_Of_Tear/1000)*(Thickness/1000);
Toughness_Area_Cleaved_Graph := Energy_Used / Area_Cleaved_Graph;
Toughness_Area_Cleaved_Sample := Energy_Used / Area_Cleaved_Sample;
end;

Procedure Calculate_Toughness_By_Tch;
begin
Writeln ('What is the strain energy density (Wo) is the legs (J/cubic metre)');
Readln (Strain_Energy_Density_In_Legs);
Writeln ('What is the unstressed cross sectional area of the legs (Square metre)');
Readln (Unstressed_Cross_Sectional_Area_Legs);
Writeln ('What is the extension ratio at propagation in the legs, Lambda');
Readln (Lambda);
Tch := -(((Strain_Energy_Density_In_Legs * Unstressed_Cross_Sectional_Area_Legs)
- (2 * Lambda * Plateau_Force)) / (Thickness / 1000));
end;

Procedure Print_Figures_On_Screen;
begin
Writeln;
Writeln('The File = ',The_File);
Writeln('Thickness = ',Thickness); {mm}
Writeln('Length of Tear, Measured = ',Length_Of_Tear); {mm}
Writeln('Length of Tear, Graph = ',Length_Of_Tear_Graph); {mm}
Writeln('Tearing Occurs @ mm = ',mm_KiloNewton_Array[1,Point_A]);
Writeln('Tearing Occurs @ KN = ',mm_KiloNewton_Array[2,Point_A]);
Writeln('Area Cleaved via Graph = ',Area_Cleaved_Graph);
Writeln('Area Cleaved via Sample = ',Area_Cleaved_Sample);
Writeln('Plateau Tearing Force = ',Plateau_Force);
Writeln('Energy Expended to Max mm = ',Area_to_Max); {J}
Writeln('Energy Returned on Unloading = ',Area_to_Relax); {J}
Writeln('Energy Used = ',Energy_Used); {J}
Writeln('Toughness Area Cleaved Graph = ',Toughness_Area_Cleaved_Graph);
Writeln('Toughness Area Cleaved Sample = ',Toughness_Area_Cleaved_Sample);
Writeln('2 F / t = ',Two_F_Upon_t);
end;

Procedure Put_Figures_On_Results_File;
begin
Assign (Resfile, 'c:\tearres.txt');
Append (Resfile);
Writeln (Resfile, The_File,chr(9),Thickness,chr(9),Length_Of_Tear,
chr(9),Length_Of_Tear_Graph,chr(9),mm_KiloNewton_Array[1,Point_A],
chr(9),mm_KiloNewton_Array[2,Point_A],chr(9),Area_Cleaved_Graph,
chr(9),Area_Cleaved_Sample,chr(9),Plateau_Force,chr(9),
Area_to_Max, chr(9),Area_to_Relax,chr(9),Energy_Used,chr(9),
Toughness_Area_Cleaved_Graph,chr(9),Toughness_Area_Cleaved_Sample,
chr(9),Two_F_Upon_t);
close (Resfile);
end;

Procedure Output_Extension_Force_Data;

```

```

Begin
{Sort out name for output file, called the same name but .dat instead of .txt}
temp := pos('.',The_File);
Output_File_Name := copy (The_File,1,temp);
insert ('DAT',Output_File_Name,(Temp+1));
assign (textfile, Output_File_Name);
rewrite (textfile);
writeln (textfile, 'mm,KN');
For File_Output := Real_Start_point to (Last_Reading_Of_Test-1) do
begin
Extension := mm_KiloNewton_Array [1,File_Output];
Force := mm_KiloNewton_Array [2,File_Output];
writeln (textfile, Extension,',',Force);
end;
{Here we make sure the last recorded load / stress is set to zero exactly
as it may be very slightly + or -}
Extension := mm_KiloNewton_Array [1,Last_Reading_Of_Test];
Force := 0;
writeln (textfile, Extension,',',Force);
close (textfile);
end;

{Main}
Begin
clrscr;
Read_in_File;
Find_Real_Start_Point; {ie where the cross-head is moving}
Find_Maximum_mm; {ie where tearing ceases, point z}
Find_Real_End_Point; {ie where mm falls to zero}
Adjust_Figures;
Go_Backwards_to_Find_Where_Load_Is_Effectively_Zero;
forcecount := 1; {an initial variable set to 1 before next procedure}
subcount := Real_Start_Point+30; {an initial variable set to 30 before next procedure}
Find_Where_Tearing_Occurs; {ie point A}
Calculate_Toughness_By_Two_F_Upon_t;
Calculate_Toughness_By_Energy_Method;
Print_Figures_On_Screen;
Put_Figures_On_Results_File;
Output_Extension_Force_Data;
Readln;
End.

```

### A.3.9 Program Trouser\_Tear\_Test\_Leg\_Dimensions;

{This program processes data to calculate the dimensions of the legs in the trouser tear tests}

uses Crt, Dos;

{Definition of variable types}

```
var
X_a, X_b, X_c, X_d : real;
Y_a, Y_b, Y_c, Y_d : real;
Y_q : real;
Line_BC_M_Value , Line_BC_C_Value : real;
Closest_Value : real;
Step_Alone_Line_BC , Current_Step_Alone_Line_X_Value : real;
Line_AQ_M_Value : real;
Length_Aq : real;
Correct_Y_Position_of_q , Correct_X_Position_of_q : real;
Area_Top_Left_Triangle : real;
Area_Bottom_Right_Triangle : real;
Length_AC , Length_BD , Length_AB , Length_CB , Length_CD : real;
The_File : string;
Input_Text_File , Output_Text_File : Text;
A_Line : String [255];
behind_chr9 : string;
Temporary_Position : integer;
Array_Counter : integer;
Instant_Results : Array [1..26] of string;
Go_Do : integer;
Code : integer;
Line_QD_M_Value : real;
Length_qD : real;
Any_Zeros : boolean;
Get_Output_Name : string;
```

Procedure Read\_In\_The\_File;

```
begin
{This Sorts the output file}
Writeln ('Please enter the file name for the OUTPUT file');
Readln (Get_Output_Name);
assign (Output_Text_File,Get_Output_Name);
rewrite (Output_Text_File);
writeln (Output_Text_File,'Picture Code', chr(9),
        'Time of Picture (seconds)',chr(9),
        'Speed of Test mm/s',chr(9),
        'Direction of Tear to Backbone',chr(9),
        'Top Leg Left Length, pix',chr(9),
        'Top Leg Right Length, pix',chr(9),
        'Top Leg Area, sqr pix',chr(9),
        'Bottom Leg Left Length, pix',chr(9),
        'Bottom Leg Right Length, pix',chr(9),
        'Bottom Leg Area, sqr pix');
```

```
{This sorts the input file}
assign (Input_Text_File,The_File);
reset (Input_Text_File);
readln (Input_Text_File,A_Line); {Get rid of top line of writing}
readln (Input_Text_File,A_Line); {Get rid of blank row}
end;
```

Procedure Read\_A\_Line\_Of\_Text;

```
begin
Array_Counter := 1;
Temporary_Position := 1;
readln (Input_Text_File,A_Line);
while Array_Counter < 24 do
begin
```

```

Temporary_Position := pos(chr(9),A_Line);
Behind_chr9 := copy(A_Line,1,Temporary_Position-1);
Instant_Results [Array_Counter] := Behind_chr9;
Delete(A_Line,1,Temporary_Position);
Array_Counter := Array_Counter + 1;
end;
Instant_Results [Array_Counter] := Behind_chr9;
end;

```

```

Procedure Find_Lengths_Of_Lines;
begin
Length_AC := sqrt(sqrt(Y_c-Y_a) + sqrt(X_c-X_a));
Length_BD := sqrt(sqrt(Y_d-Y_b) + sqrt(X_d-X_b));
Length_AB := sqrt(sqrt(Y_b-Y_a) + sqrt(X_b-X_a));
Length_CD := sqrt(sqrt(Y_d-Y_c) + sqrt(X_d-X_c));
end;

```

```

Procedure Update_Top_Left_Triangle;
begin
Closest_Value := abs((-1/Line_BC_M_Value)-Line_Aq_M_Value);
Correct_X_Position_Of_q := Current_Step_Alone_Line_X_Value;
Correct_Y_Position_Of_q := Y_q;
end;

```

```

Procedure Find_Area_Top_Left_Triangle;
begin
Line_BC_M_Value := ((Y_b - Y_c) / (X_b - X_c));
Line_BC_C_Value := (Y_b - (Line_BC_M_Value * X_b));
Length_CB := sqrt(sqrt(Y_b-Y_c) + (sqrt(X_b-X_c)));
Closest_Value := 10000; {ie ridiculously high}
Step_Alone_Line_BC := (X_b - X_c)/1000;
Current_Step_Alone_Line_X_Value := X_c;
While Current_Step_Alone_Line_X_Value < X_b do
begin
Y_q := ((Line_BC_M_Value * Current_Step_Alone_Line_X_Value) + Line_BC_C_Value);
{Here there is a possibility of division by zero to give infinite M
Hence we must account for it}
If (Current_Step_Alone_Line_X_Value - X_a) <> 0 then
Line_AQ_M_Value := ((Y_q - Y_a) / (Current_Step_Alone_Line_X_Value - X_a));
If (Current_Step_Alone_Line_X_Value - X_a) = 0 then
Line_AQ_M_Value := 10000; {ie ridiculously high near infinity}
If abs((-1/Line_BC_M_Value) - Line_AQ_M_Value) < Closest_Value then Update_Top_Left_Triangle;
Current_Step_Alone_Line_X_Value := Current_Step_Alone_Line_X_Value + Step_Alone_Line_BC;
end;

```

```

{Here we find length Aq}
Length_Aq := sqrt((sqrt(Correct_Y_Position_of_q - Y_a) +
(sqrt(Correct_X_Position_of_q - X_a)));
Area_Top_Left_Triangle := 0.5 * Length_CB * Length_Aq;
writeln('Area_Top_Left_Triangle = ',Area_Top_Left_Triangle);
end;

```

```

Procedure Update_Bottom_Right_Triangle;
begin
Closest_Value := abs((-1/Line_BC_M_Value)-Line_QD_M_Value);
Correct_X_Position_Of_q := Current_Step_Alone_Line_X_Value;
Correct_Y_Position_Of_q := Y_q;
end;

```

```

Procedure Find_Area_Bottom_Right_Triangle;
begin
Line_BC_M_Value := ((Y_b - Y_c) / (X_b - X_c));
Line_BC_C_Value := (Y_b - (Line_BC_M_Value * X_b));
Length_CB := sqrt(sqrt(Y_b-Y_c) + (sqrt(X_b-X_c)));
Closest_Value := 10000; {ie ridiculously high}
Step_Alone_Line_BC := (X_b - X_c)/1000;
Current_Step_Alone_Line_X_Value := X_c;

```

```

While Current_Step_Alone_Line_X_Value < X_b do
begin
Y_q := ((Line_BC_M_Value * Current_Step_Alone_Line_X_Value) + Line_BC_C_Value);
{Here there is a possibility of division by zero to give infinite M
Hence we must account for it}
If (Current_Step_Alone_Line_X_Value - X_d) <> 0 then
Line_QD_M_Value := ((Y_q - Y_d) / (Current_Step_Alone_Line_X_Value - X_d));
If (Current_Step_Alone_Line_X_Value - X_d) = 0 then
Line_QD_M_Value := 10000; {ie ridiculously high near infinity}
If abs((-1/Line_BC_M_Value) - Line_QD_M_Value) < Closest_Value then Update_Bottom_Right_Triangle;
Current_Step_Alone_Line_X_Value := Current_Step_Alone_Line_X_Value + Step_Alone_Line_BC;
end;

{Here we find length Aq}
Length_qD := sqrt ((sqr(Correct_Y_Position_of_q - Y_d)) +
(sqr(Correct_X_Position_of_q - X_d)));
Area_Bottom_Right_Triangle := 0.5 * Length_CB * Length_qD;
writeln ('Area_Bottom_Right_Triangle = ',Area_Bottom_Right_Triangle);
end;

Procedure Call_3_Routines;
begin
Find_Lengths_Of_Lines;
Find_Area_Top_Left_triangle;
Find_Area_Bottom_Right_Triangle;
end;

{Main}
begin
clrscr;
Writeln ('Trouser Tear Dimensions Program. ');
Writeln ('What is the file name? ');
Readln (The_File);
Read_In_The_File;
For Go_Do := 1 to 32 do
begin
Read_A_Line_Of_Text;
Val (Instant_Results [5], X_a, Code);
Val (Instant_Results [7], X_b, Code);
Val (Instant_Results [9], X_c, Code);
Val (Instant_Results [11], X_d, Code);
Val (Instant_Results [6], Y_a, Code);
Val (Instant_Results [8], Y_b, Code);
Val (Instant_Results [10], Y_c, Code);
Val (Instant_Results [12], Y_d, Code);
{Here we check that none of the x,y variables are zero,
if they are then we don't call the 3 routines.}
Any_Zeros := False;
If X_a = 0 then Any_Zeros := true;
If X_b = 0 then Any_Zeros := true;
If X_c = 0 then Any_Zeros := true;
If X_d = 0 then Any_Zeros := true;
If Y_a = 0 then Any_Zeros := true;
If Y_b = 0 then Any_Zeros := true;
If Y_c = 0 then Any_Zeros := true;
If Y_d = 0 then Any_Zeros := true;
If Any_Zeros = False then Call_3_Routines;
If Any_Zeros = True then write (Output_Text_File,Instant_Results [1],
chr(9),Instant_Results [2],
chr(9),Instant_Results [3],
chr(9),Instant_Results [4],
chr(9),'0',chr(9),'0',chr(9));

{here we must output results of the top leg}
If Any_Zeros = False then write (Output_Text_File,Instant_Results [1],
chr(9),Instant_Results [2],
chr(9),Instant_Results [3],

```

```

chr(9),Instant_Results [4],
chr(9),Length_AC,
chr(9),Length_BD,
chr(9),
(Area_Top_Left_Triangle + Area_Bottom_Right_Triangle));

```

```

Val (Instant_Results [13], X_a, Code);
Val (Instant_Results [15], X_b, Code);
Val (Instant_Results [17], X_c, Code);
Val (Instant_Results [19], X_d, Code);
Val (Instant_Results [14], Y_a, Code);
Val (Instant_Results [16], Y_b, Code);
Val (Instant_Results [18], Y_c, Code);
Val (Instant_Results [20], Y_d, Code);

```

```

{Here we check that none of the x,y variables are zero,
if they are then we don't call the 3 routines.}

```

```

Any_Zeros := False;
If X_a = 0 then Any_Zeros := true;
If X_b = 0 then Any_Zeros := true;
If X_c = 0 then Any_Zeros := true;
If X_d = 0 then Any_Zeros := true;
If Y_a = 0 then Any_Zeros := true;
If Y_b = 0 then Any_Zeros := true;
If Y_c = 0 then Any_Zeros := true;
If Y_d = 0 then Any_Zeros := true;

If Any_Zeros = False then Call_3_Routines;
If Any_Zeros = True then writeln (Output_Text_File,chr(9),'0',
chr(9),'0',
chr(9),'0');
{here we must output results of the bottom leg}
If Any_Zeros = False then writeln (Output_Text_File,chr(9),
Length_AC, chr(9),
Length_BD, chr(9),
(Area_Top_Left_Triangle +
Area_Bottom_Right_Triangle));

```

```
end;
```

```
Close (Output_Text_File);
end.
```

**Appendix 4.**

Material	FADG											
Testing Speed / mm s <sup>-1</sup>	0.166666	1.666666	16.666666	166.666666	1666.666666	16666.666666	166666.666666	1666666.666666	16666666.666666	166666666.666666	1666666666.666666	16666666666.666666
Tearing Direction	Perpendicular	Parallel										
Thickness / mm	0.78 ± 0.05	1.56 ± 0.10	3.12 ± 0.20	6.24 ± 0.40	12.48 ± 0.80	24.96 ± 1.60	49.92 ± 3.20	99.84 ± 6.40	199.68 ± 12.80	399.36 ± 25.60	798.72 ± 51.20	1597.44 ± 102.40
Length of Tear / mm	11.83 ± 0.75	23.66 ± 1.50	47.32 ± 3.00	94.64 ± 6.00	189.28 ± 12.00	378.56 ± 24.00	757.12 ± 48.00	1514.24 ± 96.00	3028.48 ± 192.00	6056.96 ± 384.00	12113.92 ± 768.00	24227.84 ± 1536.00
Stroke at continuous tear propagation / mm	22.52 ± 2.83	45.04 ± 5.66	90.08 ± 11.32	180.16 ± 22.64	360.32 ± 45.28	720.64 ± 90.56	1441.28 ± 181.12	2882.56 ± 362.24	5765.12 ± 724.48	11530.24 ± 1448.96	23060.48 ± 2897.92	46120.96 ± 5795.84
Load at continuous tear propagation / kN	0.018375 ± 0.008874	0.03675 ± 0.017748	0.0735 ± 0.035496	0.147 ± 0.070992	0.294 ± 0.141984	0.588 ± 0.283968	1.176 ± 0.567936	2.352 ± 1.135872	4.704 ± 2.271744	9.408 ± 4.543488	18.816 ± 9.086976	37.632 ± 18.173952
Average Cleaved / m <sup>2</sup>	0.000062 ± 0.000003	0.000124 ± 0.000006	0.000248 ± 0.000012	0.000496 ± 0.000024	0.000992 ± 0.000048	0.001984 ± 0.000096	0.003968 ± 0.000192	0.007936 ± 0.000384	0.015872 ± 0.000768	0.031744 ± 0.001536	0.063488 ± 0.003072	0.126976 ± 0.006144
Plateau Force / N	18.18 ± 2.4	36.36 ± 4.8	72.72 ± 9.6	145.44 ± 19.2	290.88 ± 38.4	581.76 ± 76.8	1163.52 ± 153.6	2327.04 ± 307.2	4654.08 ± 614.4	9308.16 ± 1228.8	18616.32 ± 2457.6	37232.64 ± 4915.2
Energy supplied at continuous tear propagation / J	0.1854 ± 0.024	0.3708 ± 0.048	0.7416 ± 0.096	1.4832 ± 0.192	2.9664 ± 0.384	5.9328 ± 0.768	11.8656 ± 1.536	23.7312 ± 3.072	47.4624 ± 6.144	94.9248 ± 12.288	189.8496 ± 24.576	379.6992 ± 49.152
Energy supplied at maximum stroke / J	0.5844 ± 0.062	1.1688 ± 0.124	2.3376 ± 0.248	4.6752 ± 0.496	9.3504 ± 0.992	18.7008 ± 1.984	37.4016 ± 3.968	74.8032 ± 7.936	149.6064 ± 15.872	299.2128 ± 31.744	598.4256 ± 63.488	1196.8512 ± 126.976
Energy returned on unload / J	0.02 ± 0.0044	0.04 ± 0.0088	0.08 ± 0.0176	0.16 ± 0.0352	0.32 ± 0.0704	0.64 ± 0.1408	1.28 ± 0.2816	2.56 ± 0.5632	5.12 ± 1.1264	10.24 ± 2.2528	20.48 ± 4.5056	40.96 ± 9.0112
Energy supplied during continuous tear propagation / J	0.3771 ± 0.0279	0.7542 ± 0.0558	1.5084 ± 0.1116	3.0168 ± 0.2232	6.0336 ± 0.4464	12.0672 ± 0.8928	24.1344 ± 1.7856	48.2688 ± 3.5712	96.5376 ± 7.1424	193.0752 ± 14.2848	386.1504 ± 28.5696	772.3008 ± 57.1392
Extension ratio in specimen legs	1.18 ± N/A											
Toughness (method 1) / J m <sup>-2</sup>	41185 ± 3137	82370 ± 6274	164740 ± 12548	329480 ± 25096	658960 ± 50192	1317920 ± 100384	2635840 ± 200768	5271680 ± 401536	10543360 ± 803072	21086720 ± 1606144	42173440 ± 3212288	84346880 ± 6424576
Toughness (method 2) / J m <sup>-2</sup>	54529 ± 4411	109058 ± 8822	218116 ± 17644	436232 ± 35288	872464 ± 70576	1744928 ± 141152	3489856 ± 282304	6979712 ± 564608	13959424 ± 1129216	27918848 ± 9184384	55837696 ± 36768768	111675392 ± 73537536
Toughness (method 3) / J m <sup>-2</sup>	49590 ± 3707	99180 ± 7414	198360 ± 14828	396720 ± 29656	793440 ± 59312	1586880 ± 118624	3173760 ± 237248	6347520 ± 474496	12695040 ± 948992	25390080 ± 1897984	50780160 ± 3795968	101560320 ± 7591936
Material	POG											
Testing Speed / mm s <sup>-1</sup>	0.166666	1.666666	16.666666	166.666666	1666.666666	16666.666666	166666.666666	1666666.666666	16666666.666666	166666666.666666	1666666666.666666	16666666666.666666
Tearing Direction	Perpendicular	Parallel										
Thickness / mm	1.08 ± 0.08	2.16 ± 0.16	4.32 ± 0.32	8.64 ± 0.64	17.28 ± 1.28	34.56 ± 2.56	69.12 ± 5.12	138.24 ± 10.24	276.48 ± 20.48	552.96 ± 40.96	1105.92 ± 81.92	2211.84 ± 163.84
Length of Tear / mm	20 ± 0.41	40 ± 0.82	80 ± 1.64	160 ± 3.28	320 ± 6.56	640 ± 13.12	1280 ± 26.24	2560 ± 52.48	5120 ± 104.96	10240 ± 209.92	20480 ± 419.84	40960 ± 839.68
Stroke at continuous tear propagation / mm	5.2 ± 1.88	10.4 ± 3.76	20.8 ± 7.52	41.6 ± 15.04	83.2 ± 30.08	166.4 ± 60.16	332.8 ± 120.32	665.6 ± 240.64	1331.2 ± 481.28	2662.4 ± 962.56	5324.8 ± 1925.12	10649.6 ± 3850.24
Load at continuous tear propagation / kN	0.00519 ± 0.001014	0.01038 ± 0.002028	0.02076 ± 0.004056	0.04152 ± 0.008112	0.08304 ± 0.016224	0.16608 ± 0.032448	0.33216 ± 0.064896	0.66432 ± 0.129792	1.32864 ± 0.259584	2.65728 ± 0.519168	5.31456 ± 1.038336	10.62912 ± 2.076672
Average Cleaved / m <sup>2</sup>	0.000026 ± 0.000012	0.000052 ± 0.000024	0.000104 ± 0.000048	0.000208 ± 0.000096	0.000416 ± 0.000192	0.000832 ± 0.000384	0.001664 ± 0.000768	0.003328 ± 0.001536	0.006656 ± 0.003072	0.013312 ± 0.006144	0.026624 ± 0.012288	0.053248 ± 0.024576
Plateau Force / N	6.13 ± 0.82	12.26 ± 1.64	24.52 ± 3.28	49.04 ± 6.56	98.08 ± 13.12	196.16 ± 26.24	392.32 ± 52.48	784.64 ± 104.96	1569.28 ± 209.92	3138.56 ± 419.84	6277.12 ± 839.68	12554.24 ± 1679.36
Energy supplied at continuous tear propagation / J	0.0152 ± 0.00171	0.0304 ± 0.00342	0.0608 ± 0.00684	0.1216 ± 0.01368	0.2432 ± 0.02736	0.4864 ± 0.05472	0.9728 ± 0.10944	1.9456 ± 0.21888	3.8912 ± 0.43776	7.7824 ± 0.87552	15.5648 ± 1.75104	31.1296 ± 3.50208
Energy supplied at maximum stroke / J	0.2588 ± 0.0383	0.5176 ± 0.0766	1.0352 ± 0.1532	2.0704 ± 0.3064	4.1408 ± 0.6128	8.2816 ± 1.2256	16.5632 ± 2.4512	33.1264 ± 4.9024	66.2528 ± 9.8048	132.5056 ± 19.6096	265.0112 ± 39.2192	530.0224 ± 78.4384
Energy returned on unload / J	0.0375 ± 0.0018	0.075 ± 0.0036	0.15 ± 0.0072	0.30 ± 0.0144	0.60 ± 0.0288	1.20 ± 0.0576	2.40 ± 0.1152	4.80 ± 0.2304	9.60 ± 0.4608	19.20 ± 0.9216	38.40 ± 1.8432	76.80 ± 3.6864
Energy supplied during continuous tear propagation / J	0.2578 ± 0.035	0.5156 ± 0.070	1.0312 ± 0.140	2.0624 ± 0.280	4.1248 ± 0.560	8.2496 ± 1.120	16.4992 ± 2.240	32.9984 ± 4.480	65.9968 ± 8.960	131.9936 ± 17.920	263.9872 ± 35.840	527.9744 ± 71.680
Extension ratio in specimen legs	1.03 ± N/A											
Toughness (method 1) / J m <sup>-2</sup>	11340 ± 1332	22680 ± 2664	45360 ± 5328	90720 ± 10656	181440 ± 21312	362880 ± 42624	725760 ± 85248	1451520 ± 170496	2903040 ± 340992	5806080 ± 681984	11612160 ± 1363968	23224320 ± 2727936
Toughness (method 2) / J m <sup>-2</sup>	12000 ± 1103	24000 ± 2206	48000 ± 4412	96000 ± 8824	192000 ± 17648	384000 ± 35296	768000 ± 70592	1536000 ± 141184	3072000 ± 282368	6144000 ± 564736	12288000 ± 1129472	24576000 ± 2258944
Toughness (method 3) / J m <sup>-2</sup>	11875 ± 1078	23750 ± 2156	47500 ± 4312	95000 ± 8624	190000 ± 17248	380000 ± 34496	760000 ± 70000	1520000 ± 139904	3040000 ± 279808	6080000 ± 559616	12160000 ± 1119232	24320000 ± 2238464

Table 3.3

Trousers tear test results for grain material

Material	FADC	FADC	FADC								
Testing Speed / mm s <sup>-1</sup>	0.166666	1.66666	16.66666	166.6666	1666.666	16666.66	166666.6	1.66666	16.66666	166.66666	1666.6666
Testing Direction	Perpendicular	Parallel	Parallel	Parallel	Parallel						
Thickness / mm	3.68 ± 0.14	3.68 ± 0.1	3.43 ± 0.02	3.68 ± 0.07	3.68 ± 0.02516	3.68 ± 0.05	3.68 ± 0.05	3.8 ± 0.12	3.42 ± 0.16	3.54 ± 0.14	3.83 ± 0.07
Length of Tear / mm	16.63 ± 0.48	16.63 ± 0.48	14.75 ± 0.29	16.5 ± 0.82	15.88 ± 3.14	15.88 ± 3.14	15.88 ± 3.14	18.5 ± 0.41	17.88 ± 0.46	18.25 ± 0.5	18.5 ± 0.41
Stroke at continuous tear propagation / mm	9.04 ± 3.83	12.85 ± 3.65	13.15 ± 3.36	15.88 ± 3.14	15.88 ± 3.14	15.88 ± 3.14	15.88 ± 3.14	8.37 ± 0.75	12.32 ± 3.63	10.75 ± 2.18	18.15 ± 3.64
Load at continuous tear propagation / kN	0.66875 ± 0.020265	0.15225 ± 0.06501	0.129 ± 0.026387	0.19225 ± 0.026516	0.19225 ± 0.026516	0.19225 ± 0.026516	0.19225 ± 0.026516	0.1655 ± 0.037683	0.14775 ± 0.026453	0.15975 ± 0.068344	0.2275 ± 0.02624
Average Cleaved / m <sup>2</sup>	0.000571 ± 0.000001	0.000633 ± 0.000003	0.000506 ± 0.000012	0.000684 ± 0.000039	0.000684 ± 0.000039	0.000684 ± 0.000039	0.000684 ± 0.000039	0.000704 ± 0.000023	0.000612 ± 0.000021	0.000645 ± 0.000024	0.000649 ± 0.000027
Plateau Force / N	112 ± 6.16	166.75 ± 20.3	150 ± 2.71	203.26 ± 0.5	203.26 ± 0.5	203.26 ± 0.5	203.26 ± 0.5	135.75 ± 38.7	157.75 ± 24.53	183.5 ± 11.9	232.75 ± 15.95
Energy supplied at continuous tear propagation / J	0.3114 ± 0.2521	1.0025 ± 0.5318	0.8621 ± 0.4225	1.688 ± 0.5446	1.688 ± 0.5446	1.688 ± 0.5446	1.688 ± 0.5446	0.4444 ± 0.1382	1.0168 ± 0.588	0.6707 ± 0.2701	2.1333 ± 0.791
Energy supplied at maximum stroke / J	4.3025 ± 0.3172	6.1875 ± 0.6656	5.995 ± 0.124	7.375 ± 0.759	7.375 ± 0.759	7.375 ± 0.759	7.375 ± 0.759	5.3575 ± 1.4025	6.0025 ± 0.7565	7.0875 ± 0.4319	8.6375 ± 0.4332
Energy returned on untear / J	0.142 ± 0.0194	0.2058 ± 0.0584	0.283 ± 0.0383	0.3628 ± 0.0495	0.3628 ± 0.0495	0.3628 ± 0.0495	0.3628 ± 0.0495	0.1363 ± 0.1025	0.1703 ± 0.0183	0.2575 ± 0.0463	0.4228 ± 0.0581
Energy supplied during continuous tear propagation / J	3.6491 ± 0.5152	5.185 ± 0.3946	4.4388 ± 0.44	5.2942 ± 0.6625	5.2942 ± 0.6625	5.2942 ± 0.6625	5.2942 ± 0.6625	4.7746 ± 1.2356	4.9587 ± 0.2289	5.6563 ± 0.5964	6.0814 ± 0.6989
Extension ratio in specimen legs	1.08 ± N/A	1.08 ± N/A	1.16 ± N/A	1.17 ± N/A	1.17 ± N/A	1.17 ± N/A	1.17 ± N/A	1.05 ± N/A	1.08 ± N/A	1.07 ± N/A	1.14 ± N/A
Toughness (method 1) / J m <sup>-2</sup>	67397 ± 9014	81913 ± 3320	67720 ± 8965	83095 ± 13224	83095 ± 13224	83095 ± 13224	83095 ± 13224	67861 ± 17371	81572 ± 3446	82310 ± 7332	94209 ± 18735
Toughness (method 2) / J m <sup>-2</sup>	66789 ± 4360	84501 ± 8470	101388 ± 2186	122534 ± 2328	122534 ± 2328	122534 ± 2328	122534 ± 2328	74778 ± 20668	86254 ± 12001	116228 ± 3560	134904 ± 10187
Toughness (method 3) / J m <sup>-2</sup>	61375 ± 4065	87675 ± 8870	87475 ± 1853	104750 ± 2082	104750 ± 2082	104750 ± 2082	104750 ± 2082	71250 ± 19555	91875 ± 11542	103750 ± 3594	118250 ± 8817
Material	PDC	PDC	PDC								
Testing Speed / mm s <sup>-1</sup>	0.166666	1.66666	16.66666	166.6666	1666.666	16666.66	166666.6	0.166666	1.66666	16.66666	166.66666
Testing Direction	Perpendicular	Parallel	Parallel	Parallel	Parallel						
Thickness / mm	4.15 ± 0.18	4.2 ± 0.06	3.82 ± 0.14	4.38 ± 0.12	4.38 ± 0.12	4.38 ± 0.12	4.38 ± 0.12	4.34 ± 0.15	4.07 ± 0.06	3.93 ± 0.05	4.41 ± 0.11
Length of Tear / mm	16 ± 0.82	17 ± 0.41	15 ± 0.41	16.38 ± 0.25	16.38 ± 0.25	16.38 ± 0.25	16.38 ± 0.25	16.38 ± 0.83	16.83 ± 0.48	16 ± 0	15.75 ± 0.65
Stroke at continuous tear propagation / mm	11.61 ± 2.78	11.28 ± 2.16	18.28 ± 8.62	12.36 ± 7.2	12.36 ± 7.2	12.36 ± 7.2	12.36 ± 7.2	9.97 ± 4.26	16.42 ± 1.83	14.77 ± 3.1	16.25 ± 2.64
Load at continuous tear propagation / kN	0.078498 ± 0.011018	0.068343 ± 0.007971	0.134737 ± 0.017172	0.13275 ± 0.033945	0.13275 ± 0.033945	0.13275 ± 0.033945	0.13275 ± 0.033945	0.077144 ± 0.034831	0.132087 ± 0.010208	0.132823 ± 0.030761	0.208344 ± 0.011684
Average Cleaved / m <sup>2</sup>	0.000659 ± 0.000011	0.000715 ± 0.000002	0.000587 ± 0.000012	0.000718 ± 0.000003	0.000718 ± 0.000003	0.000718 ± 0.000003	0.000718 ± 0.000003	0.000711 ± 0.000003	0.000676 ± 0.0000025	0.000628 ± 0.000009	0.000695 ± 0.000012
Plateau Force / N	86.62 ± 3.14	106.13 ± 10.25	135.83 ± 10.88	162 ± 7.62	162 ± 7.62	162 ± 7.62	162 ± 7.62	116.49 ± 7.57	125.32 ± 5.72	147.66 ± 9.48	215.35 ± 6.69
Energy supplied at continuous tear propagation / J	0.4027 ± 0.1754	0.5733 ± 0.1469	1.1868 ± 0.44651	1.0254 ± 1.0049	1.0254 ± 1.0049	1.0254 ± 1.0049	1.0254 ± 1.0049	0.404 ± 0.3755	1.1169 ± 0.1943	0.6965 ± 0.3788	1.7845 ± 0.362
Energy supplied at maximum stroke / J	3.3809 ± 0.133	4.0886 ± 0.4082	4.7812 ± 0.2082	5.7825 ± 0.1759	5.7825 ± 0.1759	5.7825 ± 0.1759	5.7825 ± 0.1759	4.4258 ± 0.2546	4.6983 ± 0.2327	5.2824 ± 0.2787	7.3023 ± 0.1649
Energy returned on untear / J	0.0775 ± 0.0053	0.0622 ± 0.0029	0.1781 ± 0.038	0.186 ± 0.0135	0.186 ± 0.0135	0.186 ± 0.0135	0.186 ± 0.0135	0.1178 ± 0.0199	0.121 ± 0.0142	0.1832 ± 0.0357	0.4003 ± 0.0757
Energy supplied during continuous tear propagation / J	2.6089 ± 0.2584	3.5183 ± 0.485	3.4041 ± 0.5831	4.5881 ± 0.6307	4.5881 ± 0.6307	4.5881 ± 0.6307	4.5881 ± 0.6307	3.8038 ± 0.3332	3.4828 ± 0.2047	4.1987 ± 0.2673	5.1175 ± 0.4387
Extension ratio in specimen legs	1.12 ± N/A	1.05 ± N/A	1.14 ± N/A	1.13 ± N/A	1.13 ± N/A	1.13 ± N/A	1.13 ± N/A	1.12 ± N/A	1.05 ± N/A	1.13 ± N/A	1.19 ± N/A
Toughness (method 1) / J m <sup>-2</sup>	43747 ± 4255	46228 ± 6886	57885 ± 9103	63775 ± 13726	63775 ± 13726	63775 ± 13726	63775 ± 13726	54887 ± 3558	51480 ± 2228	66786 ± 3470	73713 ± 624
Toughness (method 2) / J m <sup>-2</sup>	48857 ± 1327	52620 ± 4446	78823 ± 5287	78387 ± 5770	78387 ± 5770	78387 ± 5770	78387 ± 5770	60184 ± 5284	64588 ± 2117	84884 ± 5473	118075 ± 6830
Toughness (method 3) / J m <sup>-2</sup>	43477 ± 1184	50451 ± 4422	66235 ± 4616	66275 ± 5133	66275 ± 5133	66275 ± 5133	66275 ± 5133	55749 ± 4726	61604 ± 2028	76192 ± 4871	97724 ± 5569

Table 3.4

Trouser tear test results for colium material

**Appendix 5.**

Using the graphical approach of Atkins and Mai [1988] the following derives the specific work of fracture of a linear elastic material where the specimen legs store strain energy. Assuming that,

$L_0$  = Original length of each leg before test commences, and

$\delta_1$  = Stretch in each leg before tearing commences.

Once tearing commences, if the strain is reversed, the unloaded current length of each leg is denoted as  $a$ . This length will clearly be greater than  $L_0$ . The increase in length from  $L_0$  to  $a$  (denoted  $\Delta L_i$ ) can only be attributed to the tear advancing through the specimen as we are referring to the unloaded current leg length and the material is linear elastic. Clearly, the current length of each leg is dependent on both the original length before testing commences and the increase in length due to the tear advancing, thus

$$a = L_0 + \Delta L_i \quad [A5.1]$$

Assuming,

$\delta$  = the stretch in each leg while the specimen is tearing and,

$L_A$  = the actual length of each leg while the specimen is tearing (including the stretch),

$$L_A = a + \delta \quad [A5.2]$$

The trouser tear specimen has two legs and therefore the total leg length while the specimen is tearing is expressed as

$$2 L_A = 2 (a + \delta) \quad [A5.3]$$

It is clear that unless  $L_0 = 0$ , the original length of the legs affects equations [A5.1] and [A5.2]. Indeed, as the displacement or stroke ( $U$ ), is zero when the test commences it is not strictly correct to assume that,

$$U = 2 (a + \delta) \quad [A5.4]$$

However, the displacement can be defined by the expression,

$$U = 2 (L_A - L_0) \quad [A5.5]$$

Using equation [A5.1] and [A5.2],

$$\begin{aligned} U &= 2 (a + \delta - L_0) \\ U &= 2 (L_0 + \Delta L_i + \delta - L_0) \\ U &= 2 (\Delta L_i + \delta) \end{aligned} \quad [A5.6]$$

In other words, the displacement is the sum of the '*unloaded current leg length increase*' ( $\Delta L_i$ ) in each leg and the total stretch in each leg ( $\delta$ ).

If the tearing load is denoted as  $X$ ,  $w$  is the leg width, and  $t$  is the specimen thickness, the stress in the legs ( $\sigma$ ) is expressed as,

$$\sigma = X / w t \quad [A5.7]$$

Assuming a constant tensile modulus ( $E$ ) in the legs, the strain ( $\epsilon$ ) can be expressed as,

$$\epsilon = X / (E w t) \quad [A5.8]$$

The elastic strain can also be expressed as,

$$\epsilon = \delta / a \quad [A5.9]$$

rearrangement and substitution gives the expression,

$$\delta = (X a) / (E w t) \quad [A5.10]$$

For a quasi-static increment of crack propagation in a body, containing an existing crack of area  $A$ , being loaded by a pair of self equilibrating external forces,  $X$ , with associated displacements  $U$ ,

$$X dU = d\Lambda + J dA \quad [A5.11]$$

Where  $\Lambda$  is the elastic strain energy of a cracked body and  $J = R =$  the specific

work of fracture during equilibrium fracture [Atkins and Mai, 1988]. Assuming the elastic energy in the specimen legs is shown by the expression,

$$\left( \frac{1}{2} X \delta \right) \times 2 \text{ legs} = X \delta$$

and substituting [A5.6] into [A5.11], we have

$$X d[2 (\Delta L_i + \delta)] = d[X \delta] + R dA \quad [A5.12]$$

Using the product rule,

$$X d[2 (\Delta L_i + \delta)] = X d(\delta) + \delta d(X) + R dA \quad [A5.13]$$

Dividing both sides of equation [A5.13] by  $d(A)$  we have

$$X d[2\Delta L_i + 2\delta] / d(A) = X d(\delta) / d(A) + \delta d(X) / d(A) + R dA / d(A)$$

or

$$2X d(\Delta L_i) / d(A) + 2X d(\delta) / d(A) = X d(\delta) / d(A) + \delta d(X) / d(A) + R \quad [A5.14]$$

Considering the factor,  $d(\Delta L_i) / d(A)$ , i.e. the rate of change of leg length with leg area, it is apparent that leg area,  $A = a.t$ , thus

$$1/t = a/A. \quad [A5.15]$$

Accordingly  $d(\Delta L_i) / d(A) = 1/t$  and therefore,

$$\begin{aligned} 2 X / t + X d(\delta) / d(A) &= \delta d(X) / d(A) + R \\ X d(\delta) / d(A) - \delta d(X) / d(A) &= R - 2 X / t \\ X d(\delta) / d(A) - \delta d(X) / d(A) &= (t R - 2 X) / t \end{aligned} \quad [A5.16]$$

By dividing both sides of [A5.16] by  $X^2$ , we arrive at the expression

$$[ X d(\delta) / d(A) - \delta d(X) / d(A) ] / X^2 = (t R - 2 X) / t X^2 \quad [A5.17]$$

Applying the quotient rule to [A5.17]

$$\begin{aligned} d/d(A) (\delta/X) &= (t R / t X^2) - (2 X / t X^2) \\ d/d(A) (\delta/X) &= R / X^2 - 2 / t X \end{aligned} \quad [A5.18]$$

From [A5.8],  $X = \epsilon w t E$ .

From [A5.9],  $\delta = \epsilon a$ .

Thus,

$$\delta / X = a / (w t E) \quad [A5.19]$$

From [A5.15],  $a = A / t$  and substituting into [A5.19] we arrive at the expression,

$$\delta / X = A / (w t^2 E) \quad [A5.20]$$

Substituting [A5.20] into [A5.18],

$$d/d(A) (A / (w t^2 E) ) = R / X^2 - 2 / t X$$

$$1 / w t^2 E = R / X^2 - 2 / t X$$

Rearranging for R,

$$R / X^2 = 1 / w t^2 E + 2 / t X$$

$$R = X^2 / w t^2 E + 2 X^2 / t X$$

$$R = X^2 / w t^2 E + 2 X / t$$

[A5.21]

**Appendix 6.**

### A6.1 Notch-Sensitive Case.

U = total strain energy in shaded volume of specimen Figure 4.2 (II)

$$U = \int_0^{\epsilon_f} \sigma \cdot d\epsilon \cdot \text{shaded volume in Figure 4.2 (II)}$$

#### Strain Energy

From  $\sigma = K \epsilon^n$

$$U = \int_0^{\epsilon_f} K \epsilon^n \cdot d\epsilon \cdot \text{shaded volume in Figure 4.2 (II)}$$

$$U = K \int_0^{\epsilon_f} \epsilon^n \cdot d\epsilon \cdot \text{shaded volume in Figure 4.2 (II)}$$

$$U = K [1/(n+1) \cdot \epsilon_f^{n+1}] \cdot \text{shaded volume in Figure 4.2 (II)}$$

$$U = K \cdot (\epsilon_f^{n+1}/n+1) \cdot t(WL - (\pi/2) a^2) \quad [A6.1]$$

#### Fracture Toughness

$$R = - |dU/dA|_U$$

$$A = a \cdot t$$

$$\therefore R = - 1/t \cdot d/da (U)$$

Substitute from [A6.1]

$$R = - 1/t \cdot d/da [ K \cdot (\epsilon_f^{n+1}/n+1) \cdot t(WL - (\pi/2) a^2) ]$$

$$R = - 1/t \cdot d/da [ (K \cdot (\epsilon_f^{n+1}/n+1) \cdot t W L) - (K \cdot (\epsilon_f^{n+1}/n+1) \cdot t (\pi/2) a^2) ]$$

$$R = - 1/t [ - 2 K (\epsilon_f^{n+1}/n+1) t (\pi/2) a ]$$

$$R = K (\epsilon_f^{n+1}/n+1) \pi a \quad [A6.2]$$

### Failure Strain

Taking R as a constant,

$$\begin{aligned}\epsilon_f^{n+1} &= R (n+1) / K \pi a \\ \epsilon_f &= [ R (n+1) / K \pi a ]^{1/n+1}\end{aligned}\quad [A6.3]$$

Taking R, K and  $\pi$  as constants

$$\epsilon_f \propto [(n+1) / a]^{1/n+1}$$

In a linear material,  $n = 1$ ,  $\epsilon_f \propto (2 / a)^{1/2}$ , ie  $\epsilon_f \propto \sqrt{2} a^{-1/2}$

### Failure Stress

From  $\sigma = K \epsilon_f^n$

$$\epsilon_f^n = \sigma_f / K$$

$$[\epsilon_f^n]^{n+1/n} = [\sigma_f / K]^{n+1/n}$$

$$\epsilon_f^{n+1} = [\sigma_f / K]^{n+1/n}$$

Substituting into Equation [A6.2]

$$R = K [ \epsilon_f^{n+1} / (n+1) ] \pi a$$

$$R = K [ (\sigma_f / K)^{n+1/n} / (n+1) ] \pi a$$

$$R(n+1) / K \pi a = [ \sigma_f / K ]^{n+1/n}$$

$$[ R(n+1) / K \pi a ]^{n/n+1} = \sigma_f / K$$

Hence,

$$\begin{aligned}
 \sigma_f &= K [ R(n+1) / \pi a ]^{n/n+1} \\
 \sigma_f &= K^{n/n} \cdot K^{-n/n+1} [ R(n+1) / \pi a ]^{n/n+1} \\
 \sigma_f &= K^{n/n^2+n} [ R(n+1) / \pi a ]^{n/n+1} \quad [A6.4]
 \end{aligned}$$

Taking R, K and  $\pi$  as constants

$$\sigma_f \propto [ (n+1) / a ]^{n/n+1}$$

In a linear material,  $n = 1$ ,  $\sigma_f \propto (2/a)^{1/2}$ , ie  $\sigma_f \propto \sqrt{2} a^{-1/2}$ , and thus the theory is in agreement with linear elastic fracture mechanics.

#### Log - Log Relationship between $\sigma_f$ and a

From Equation [A6.4],

$$\begin{aligned}
 \sigma_f &= K^{n/n^2+n} [ R(n+1) / \pi a ]^{n/n+1} \\
 \therefore \ln \sigma_f &= \ln K^{n/n^2+n} + \ln [ R(n+1) / \pi a ]^{n/n+1} \\
 \ln \sigma_f &= [ \ln K (n/n(n+1)) ] + [ \ln [ R(n+1) / \pi a ] \cdot n/n+1 ] \\
 \ln \sigma_f &= [ \ln K (n/n(n+1)) ] + n/n+1 [ \ln R(n+1) - \ln (\pi a) ] \\
 \ln \sigma_f &= [ \ln K (n/n(n+1)) ] + [ (n/n+1)(\ln R(n+1)) - (n/n+1)(\ln (\pi a)) ] \\
 \ln \sigma_f &= [ \ln K (n/n(n+1)) ] + [ (n/n+1)(\ln R(n+1)) - (n/n+1)(\ln \pi + \ln a) ] \\
 \ln \sigma_f &= [ \ln K (n/n(n+1)) ] + [ (n/n+1)(\ln R(n+1)) - (n/n+1)(\ln \pi) - (n/n+1)(\ln a) ] \\
 \ln \sigma_f &= \ln K (n/n(n+1)) + [ (n/n+1)(\ln R(n+1) - (\ln \pi)) ] - (n/n+1)(\ln a) \\
 \ln \sigma_f &= \ln K (n/n(n+1)) + [ (n/n+1)(\ln (R(n+1) / \pi)) ] - (n/n+1)(\ln a) \\
 \ln \sigma_f &= n/(n+1) [ \ln(K)/n + \ln (R(n+1) / \pi) ] - (n/n+1)(\ln a) \quad [A6.5]
 \end{aligned}$$

$$K_1' = n/(n+1) [ \ln(K)/n + \ln(R(n+1)/\pi) ] = \text{constant.}$$

$$M = n / n+1$$

Hence,

$$\ln \sigma_f = K_1' - M \ln(a)$$

Log - Log Relationship between  $\epsilon_f$  and a

From Equation [A6.3],

$$\epsilon_f = [ R(n+1) / K \pi a ]^{1/n+1}$$

$$\therefore \ln \epsilon_f = 1/(n+1) \cdot \ln [ R(n+1)/K \pi a ]$$

$$\ln \epsilon_f = 1/(n+1) \cdot \ln [ R(n+1) - \ln(K \pi a) ]$$

$$\ln \epsilon_f = 1/(n+1) \cdot [ \ln R(n+1) - \ln(K) - \ln(\pi) - \ln(a) ]$$

$$\ln \epsilon_f = (1/(n+1)) (\ln(R(n+1)/K\pi)) - (1/(n+1)) (\ln(a)) \quad [A6.6]$$

$$K_2' = (1/(n+1)) (\ln(R(n+1)/K\pi)) = \text{constant.}$$

$$P = 1 / n+1$$

Hence,

$$\ln \epsilon_f = K_2' - P \ln(a)$$

### A6.2 Notch-Insensitive Case.

U = total strain energy in shaded volume of specimen Figure 4.2 (I)

$$U = \int_0^{\epsilon_f} \sigma \cdot d\epsilon \cdot \text{shaded volume in Figure 4.2 (I)}$$

#### Strain Energy

From  $\sigma = K \epsilon^n$

$$U = \int_0^{\epsilon_f} K \epsilon^n \cdot d\epsilon \cdot \text{shaded volume in Figure 4.2 (I)}$$

$$U = K \int_0^{\epsilon_f} \epsilon^n \cdot d\epsilon \cdot \text{shaded volume in Figure 4.2 (I)}$$

$$U = K [1/(n+1) \cdot \epsilon^{n+1}] \cdot \text{shaded volume in Figure 4.2 (I)}$$

$$U = K \cdot (\epsilon_f^{n+1}/n+1) \cdot Lt (W - a) \quad [A6.7]$$

#### Fracture Toughness

$$R = - |dU/dA|_U$$

$$A = a \cdot t$$

$$\therefore R = - 1/t \cdot d/da (U)$$

Substitute from [A6.7]

$$R = - 1/t \cdot d/da [ K \cdot (\epsilon_f^{n+1}/n+1) \cdot Lt (W - a) ]$$

$$R = - 1/t \cdot [ - K \cdot (\epsilon_f^{n+1}/n+1) \cdot (L t a) ]$$

$$R = K L \cdot (\epsilon_f^{n+1}/n+1) \quad [A6.8]$$

### Failure Strain

Taking R as a constant,

$$\begin{aligned}\epsilon_f^{n+1} &= R (n+1) / K L \\ \epsilon_f &= [ R (n+1) / K L ]^{1/n+1}\end{aligned}\quad [A6.9]$$

Taking R, K and L as constants

$$\epsilon_f \propto (n+1)^{1/n+1}$$

In a linear material,  $n = 1$ ,  $\epsilon_f \propto \sqrt{2}$ , ie  $\epsilon_f \propto \text{constant}$ .

### Failure Stress

From  $\sigma = K \epsilon_f^n$

$$\epsilon_f^n = \sigma_f / K$$

$$[ \epsilon_f^n ]^{n+1/n} = [ \sigma_f / K ]^{n+1/n}$$

$$\epsilon_f^{n+1} = [ \sigma_f / K ]^{n+1/n}$$

Substituting into Equation [A6.8]

$$R = K L [ (\sigma_f / K)^{n+1/n} / n + 1 ]$$

$$R(n+1) / KL = (\sigma_f / K)^{n+1/n}$$

$$[ R(n+1) / KL ]^{n/n+1} = \sigma_f / K$$

Hence,

$$\begin{aligned}\sigma_f &= K [ R(n+1) / KL ]^{n/n+1} \\ \sigma_f &= K^{n/n} \cdot K^{-n/n+1} \cdot [ R(n+1) / L ]^{n/n+1} \\ \sigma_f &= K^{n/n^2+n} \cdot [ R(n+1) / L ]^{n/n+1}\end{aligned}\quad [A6.10]$$

Taking R, K and L as constants

$$\sigma_f \propto (n+1)^{n/n+1}$$

**Appendix 7.**

Material	Thickness / mm	Notch Length / mm	Fracture Stress / MPa	Fracture Strain / %	Estimate of $G_c$ / kJ m <sup>-2</sup>
FADG	0.75	0.00	14.61	52.32	N/A
FADG	0.79	0.00	15.48	58.94	N/A
FADG	0.76	0.00	15.64	63.88	N/A
FADG	0.82	0.00	12.63	64.94	N/A
FADG	0.95	0.50	14.66	58.61	7.87
FADG	0.87	1.00	14.53	56.67	15.45
FADG	0.94	1.50	11.98	51.45	15.76
FADG	0.87	2.00	10.54	45.64	16.27
FADG	0.97	2.50	12.37	53.11	27.99
FADG	1.10	3.00	10.85	50.63	25.88
FADG	0.93	3.50	10.72	45.21	29.44
FADG	0.94	4.00	9.15	44.37	24.52
FADG	1.02	5.00	6.12	31.13	13.73
FADG	0.88	6.00	7.84	42.93	27.02
FADG	0.90	9.00	5.64	40.02	20.95
FADG	0.97	12.50	6.93	40.85	43.93
PDG	1.01	0.00	12.88	44.21	N/A
PDG	1.01	0.00	10.94	36.74	N/A
PDG	1.01	0.00	9.20	45.70	N/A
PDG	0.95	0.00	8.80	43.01	N/A
PDG	1.10	0.50	9.79	35.60	3.39
PDG	1.16	1.00	8.73	35.57	5.39
PDG	1.08	1.50	7.33	32.79	5.70
PDG	1.12	2.00	5.88	27.19	4.89
PDG	1.06	2.50	6.17	28.54	6.74
PDG	1.10	3.00	7.08	28.35	10.64
PDG	1.08	3.50	5.70	25.40	8.05
PDG	1.04	4.00	5.22	26.01	7.70
PDG	1.04	5.00	4.86	23.97	8.37
PDG	1.15	6.00	3.94	22.71	6.59
PDG	1.05	9.00	3.39	19.64	7.30
PDG	1.11	12.50	2.55	16.85	5.76
FADC	3.00	0.00	36.70	37.67	N/A
FADC	3.23	0.00	39.70	45.98	N/A
FADC	3.58	0.00	37.75	54.01	N/A
FADC	2.94	0.00	32.33	52.67	N/A
FADC	3.40	0.50	43.37	36.67	35.13
FADC	3.81	1.00	39.41	35.17	58.01
FADC	3.99	1.50	29.89	33.33	50.06
FADC	3.82	2.00	28.07	32.51	58.84
FADC	3.46	2.50	26.41	31.27	65.14
FADC	3.13	3.00	27.32	26.59	83.63
FADC	3.15	3.50	29.84	33.82	116.41
FADC	3.66	4.00	22.61	28.12	76.36
FADC	3.93	5.00	19.96	27.90	74.38
FADC	3.86	6.00	21.24	26.97	101.14
FADC	3.58	9.00	16.61	21.45	92.70
FADC	2.59	12.50	16.99	30.29	134.73
PDC	3.58	0.00	32.05	43.01	N/A
PDC	2.26	0.00	41.64	39.67	N/A
PDC	2.88	0.00	36.63	47.65	N/A
PDC	3.19	0.00	22.86	47.36	N/A
PDC	3.71	0.50	32.53	34.79	20.91
PDC	3.74	1.00	30.23	37.52	36.10
PDC	3.48	1.50	28.99	36.88	49.82
PDC	3.10	2.00	24.80	32.10	48.62
PDC	2.83	2.50	24.29	32.30	58.29
PDC	3.78	3.00	24.64	29.70	71.94
PDC	2.82	3.50	20.52	29.28	58.23
PDC	2.96	4.00	19.81	27.92	62.00
PDC	3.36	5.00	17.35	28.76	59.47
PDC	3.72	6.00	14.56	28.36	50.27
PDC	3.74	9.00	12.58	24.58	56.25
PDC	2.70	12.50	9.49	24.79	44.52

Table A.7.1. Estimate of  $G_c$  for FADG, PDG, FADC and PDC material.